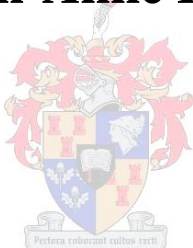


The Structural Analysis of Imidazole- Functionalised Metallocycles

By

Leigh-Anne Loots



*Thesis presented in partial fulfilment of the requirements for
the degree Doctor of Philosophy*

at

the University of Stellenbosch

Supervisor: Prof. Leonard J. Barbour
Faculty of Science
Department of Chemistry & Polymer Science

March 2012

DECLARATION

By submitting this thesis/dissertation electronically, I declare that the entirety of the work contained therein is my own, original work, that I am the sole author thereof (save to the extent explicitly otherwise stated), that reproduction and publication thereof by Stellenbosch University will not infringe any third party rights and that I have not previously in its entirety or in part submitted it for obtaining any qualification.

March 2012

ACKNOWLEDGEMENTS

First and foremost I would like to thank my supervisor, Len Barbour, for introducing me to a fascinating field of research and helping me to learn the many tools of the trade. Giving me the freedom to explore a world of possibilities and providing numerous opportunities for me throughout my postgraduate career to learn from him and other high-rated scientists.

To the Supramolecular Materials Research group which has been my academic family over the past few years and has fostered my learning in a comfortable and supportive environment. Special mention must be made to Malcolm Applewhite, Anneli Heyns, Storm Potts, Sean Robinson and Helene Wahl for their much appreciated support, friendship and entertainment.

To the Harry Crossley Foundation and the National Research Foundation (NRF) of South Africa for financial support.

And last, but certainly not least, my friends and family for their endless love and support

ABBREVIATIONS

ASU	Asymmetric Unit
CHCl ₃	Chloroform
CIF	Crystallographic Information File
CSD	Cambridge Structural Database
D _{calc}	Calculated Density
DCM	Dichloromethane
DDQ	Dichloro Dicyano Quinone
DMSO	Dimethyl Sulfoxide
EtOAc	Ethyl Acetate
EtOH	Ethanol
M _r	Molecular Mass
MeCN	Acetonitrile
MeOH	Methanol
NMR	Nuclear Magnetic Resonance
PXRD	Powder X-ray Diffraction
TGA	Thermal Gravimetric Analysis
TLC	Thin Layer Chromatography
SCD	Single-Crystal X-ray Diffraction
Z	Number of formula units in the unit cell
δ	Chemical Shift (in ppm)
α	angle between the <i>b</i> and <i>c</i> axes
β	angle between the <i>a</i> and <i>c</i> axes
γ	angle between the <i>a</i> and <i>b</i> axes
θ	angle of X-ray incident beam
ρ	Density

PUBLICATIONS

- "A simple and robust method for the identification of pi-pi packing motifs of aromatic compounds" *CrystEngComm*, 2012, **14**, 300-304
- A Rudimentary Method for Classification of $\pi\cdots\pi$ Packing Motifs in Aromatic Molecules and Cocrystals – to be published as a chapter in the book *Frontiers of Crystal Engineering Vol. III: The Importance of pi-pi Interactions in Crystal Engineering*
- Manuscript in preparation: Concomitant crystallisation of topological isomers of a copper(II)-based metallocycle

CONFERENCES

ISIC 12 – XII International Seminar on Inclusion Compounds , Stellenbosch, South Africa,
4-9 April 2009
Poster Presentation – Hydrogen-Bonded Rings or Chains? The Conundrum
Presented by Single-Crystal Diffraction Alone

ABSTRACT

The primary objective of this study was to synthesise novel metallocyclic compounds and analyse their crystal structures. To this end seven novel imidazole-functionalised ligands were synthesised and reacted with a variety of transition-metal halide salts. In addition to this study a new, simple, yet robust methodology for the analysis of $\pi\cdots\pi$ packing motifs in aromatic molecules is described.

Seventeen homeotypic metallocyclic compounds were obtained with a ligand containing a dimethoxyphenyl spacer between imidazole functionalities. These compounds form reliably from a number of solvent systems involving acetonitrile and they all include acetonitrile molecules as part of their host assembly. In each case a second guest molecule is enclosed within the walls of the metallocycles. These compounds are compared by means of thermal analysis, calculated powder X-ray diffraction patterns as well as crystal packing similarity calculations.

Metallocycles prepared from a phenanthrene-based ligand form an unprecedented infinite $\pi\cdots\pi$ stack, which induces the assembly of an infinite catenane. This catenane forms concomitantly with its topological isomer, which consists of unlinked metallocycles. The intermolecular interactions responsible for the two topologically unique structures were investigated.

Finally, a further twelve metallocycles were prepared from four novel imidazole-functionalised ligands and their structures were analysed for any similarities and/or differences. A few of these crystals showed the release of solvent guest molecules as single-crystal to single-crystal transformations.

OPSOMMING

Die primêre doel van hierdie studie was om nuwe metallosiklieseverbindings te sintetiseer en hul kristalstrukture te ontleed. Vir hierdie doel is sewe nuwe imidasool-gefunksionaliseerde ligande gesintetiseer en gereageer met 'n verskeidenheid van oorgangsmetaalhaliedsoute. In hierdie studie word 'n nuwe, eenvoudige, maar robuuste metode vir die ontleding van $\pi\cdots\pi$ verpakkingmotiewe in aromatise molekules beskryf.

Sewentien homeotipiese metallosiklieseverbindings is verkry met 'n ligand met 'n dimetoksifeniel spasieerder tussen imidasool funksionaliteite. Hierdie verbindings vorm op betroubare wyse vanuit 'n aantal oplosmiddelsisteme wat asetonitriël behels en almal sluit asetonitriël molekules as deel van hul gasheer samestelling in. In elke geval is 'n tweede gasmolekule ingesluit binne die mure van die metallosiklieseverbindings. Hierdie verbindings is deur middel van termiese analise, berekende poeier X-straaldiffraksie patrone, sowel as kristalverpakking gelykvormigheidsberekeninge vergelyk.

Metallosiklieseverbindings wat voorberei is vanaf 'n phenanthrene-gebaseerde ligand, vorm 'n uitsonderlike oneindige $\pi\cdots\pi$ verpakking, wat die samestelling van 'n oneindige katenaan tot gevolg het. Hierdie katenaan vorm saam met sy topologiese isomeer, wat bestaan uit ongekoppelde metallosiklieseverbindings. Die intermolekulêre interaksies wat verantwoordelik is vir die twee topologies unieke strukture word ondersoek.

Ten slotte, was 'n verdere twaalf metallosiklieseverbindings uit vier voorheen onbekende imidasool-gefunksionaliseerde ligande voorberei en hul strukture is vir enige ooreenkomste en/of verskille ontleed. 'n Paar van hierdie kristalle ondergaan die vrystelling van die oplosmiddelmolekules as 'n enkel-kristal na enkel-kristal omsetting.

TABLE OF CONTENTS

Title Page	i
Declaration.....	ii
Acknowledgements.....	iii
Abbreviations.....	iv
List of Publications, Conference Proceedings	v
Abstract.....	vi
Opsomming.....	vii
Table of Contents.....	viii
Atom Colours.....	xiii

CHAPTER 1 Introduction

1.1 Introduction.....	1-2
1.2 Supramolecular chemistry	1-2
1.3 Crystal Engineering	1-3
1.4 Self-Assembly and Recognition	1-3
1.5 Inclusion Compounds	1-4
1.6 Isostructurality	1-5
1.7 Chemical Topology.....	1-6
1.8 Solvates and Solvatomorphism.....	1-8
1.9 Supramolecular Interactions	1-8
1.9.1 Coordinative Bonds.....	1-9
1.9.2 The Hydrogen Bond	1-9
1.9.3 π -Acceptors	1-10
1.9.4 Van der Waals Interactions	1-11

1.9.5	Lone-pair $\cdots\pi$ Interactions	1-12
1.10	Aspects of this Study	1-12
1.11	References.....	1-18

CHAPTER 2 Analytical Methods and Techniques

2.1	Single-Crystal X-ray Diffraction (SCD).....	2-2
2.2	Powder X-ray Diffraction (PXRD).....	2-3
2.3	Thermogravimetric Analysis (TGA).....	2-3
2.4	Computer Packages:.....	2-4
2.4.1	MSRoll	2-4
2.4.2	Cambridge Structural Database (CSD)	2-4
2.4.3	Mercury	2-5
2.4.4	CrystalExplorer	2-5
2.4.5	PLATON – SQUEEZE	2-7
2.5	Solution NMR.....	2-8
2.6	Ligand Design.....	2-8
2.7	Note on Nomenclature	2-10
2.8	References	2-11

CHAPTER 3 A Rudimentary Method for Classification of $\pi\cdots\pi$ Packing

Motifs for Aromatic Molecules

3.1	Introduction.....	3-2
3.2	Theoretical Models	3-3
3.3	$\pi\cdots\pi$ Interactions	3-5
3.4	Structure Prediction and Comparisons.....	3-7
3.5	$\pi\cdots\pi$ Interactions in Heteroaromatic Molecules.....	3-8

3.6	$\pi\cdots\pi$ Interactions in Cocrystals	3-13
3.7	Summary	3-17
3.8	References	3-18

CHAPTER 4 Isostructurality in Metalloccycles

4.1	Introduction	4-2
4.2	The Host Assembly	4-4
4.3	Dichloromethane Solvate	4-12
4.4	Chloroform Solvates	4-14
4.5	Benzene Solvates	4-16
4.6	MC1 _{Dioxane}	4-19
4.7	MC1 _{Acetone}	4-23
4.8	MC1 _{EtOH}	4-25
4.9	MC1 _{MeCN}	4-27
4.10	Copper-Based Metalloccycles	4-31
	4.10.1 MC11 _{DCM}	4-31
	4.10.2 MC11 _{CHCl3}	4-36
	4.10.3 MC11 _{Vac}	4-38
4.11	Further Analysis and Discussion	4-41
4.12	Thermogravimetric Analysis	4-43
4.13	Powder X-ray Diffraction Analysis	4-46
4.14	Isostructurality Calculations	4-49
4.15	General Discussion	4-53
4.16	Experimental	4-56
4.17	References	4-61

CHAPTER 5 Chemical Topology of Concomitant Metallo-cycles

5.1	Introduction.....	5-2
5.2	Topology.....	5-4
5.3	Results.....	5-6
5.3.1	An Infinite [<i>n</i>]catenane (1).....	5-6
5.3.2	The Prime Link – Disconnected Metallo-cycles (2).....	5-11
5.4	Discussion and Concluding Remarks	5-15
5.5	Experimental.....	5-18
5.6	References.....	5-20

CHAPTER 6 Structural Analysis of Imidazole-Functionalised Metallo-cycles

6.1	Introduction.....	6-2
6.2	Results.....	6-3
6.2.1	Structures obtained with a 9,10-dihydrophenanthrene spacer	6-3
6.2.1.1	MC21 _{Benz}	6-3
6.2.1.2	MC22.....	6-7
6.2.1.3	MC23.....	6-14
6.2.2	Structures obtained with 2-Methylimidazole Coordinating Groups	6-20
6.2.2.1	MC24.....	6-20
6.2.2.2	MC24 _{Vac}	6-23
6.2.2.3	MC25.....	6-24
6.2.2.4	MC26.....	6-26
6.2.3	Structures obtained with a terphenyl spacer.....	6-29
6.2.3.1	MC27.....	6-29
6.2.3.2	MC27 _{CCl4}	6-32
6.2.3.3	MC27 _{Vac}	6-36

6.2.3.4	MC28.....	6-39
6.2.3.5	MC29.....	6-42
6.3	Discussion and Concluding Remarks	6-44
6.4	Experimental.....	6-47
6.5	References.....	6-53

CHAPTER 7 Summary and Concluding Remarks

References.....	7-5
-----------------	-----

APPENDICES CD

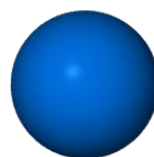
Structure files: .res and .cif Files

Publications and Posters

ATOM COLOURS



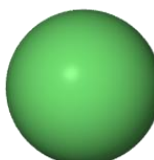
Carbon



Cobalt



Oxygen



Copper



Nitrogen



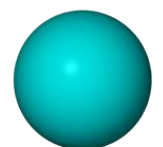
Zinc



Hydrogen



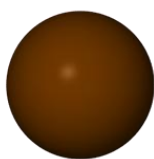
Iodine



Cadmium



Chlorine



Bromine

CHAPTER 1

INTRODUCTION

“and what is the use of a book,’ thought Alice, ‘without pictures or conversation?”

— *Lewis Carroll, Alice in Wonderland*

“What would the properties of materials be if we could really arrange the atoms the way we want them?...I can hardly doubt that when we have some control of the arrangement of things on a small scale we will get an enormously greater range of possible properties that substances can have, and of different things that we can do.” – Richard P. Feynman, *From the Bottom Up*, American Physical Society Lecture, Caltech, Dec 29, 1959

1.1 INTRODUCTION

This introductory chapter serves to acquaint the reader with a few concepts addressed during the study that follows. Although the field of supramolecular chemistry is still regarded as a relatively young area of chemistry, there has been much progress in the past few decades. Much of this work is out of the scope of this particular study and therefore only a brief overview of the relevant topics will be discussed here.

1.2 SUPRAMOLECULAR CHEMISTRY

Nobel Laureate Jean-Marie Lehn eloquently defined supramolecular chemistry as ‘chemistry beyond the molecule’.¹ However, it was the work of Pepinsky² and later by Schmidt³ that first introduced the concepts of this field of ‘chemistry of the non-covalent bond’.⁴ Species held together by noncovalent interactions between two or more covalently bound molecules or ions are known as ‘supermolecules’.⁵ Others have described this area of research as taking an holistic view of materials, where the whole is greater than the sum of its parts, such that the properties of a material are the result of a compromise between many smaller components.^{6,7} To appreciate and comprehend what constitutes the whole, it is necessary to deconstruct it into its individual components. For the supramolecular chemist this can be likened to playing with Lego, making use of a variety of building blocks that can assemble to form complicated structures and can just as easily be broken down into individual parts, i.e. in a “reversible reaction.”⁵ It is through this act of “play” that one is able to understand how things work.

Supramolecular chemistry, while rooted in chemistry, is a highly collaborative and therefore interdisciplinary field that draws on the expertise of physicists, theoreticians and computational modellers, crystallographers, inorganic and solid-state chemists, synthetic organic chemists, biochemists and biologists,⁴ all seeking to create new materials or comprehend complicated biological processes. As such, supramolecular chemistry goes beyond just the synthesis of novel materials but also delves into understanding the principles that govern the formation and function of these materials. This includes the elucidation of the interactions between the molecules as well as how these interactions can be manipulated. The accumulation and implementation of this information to construct solid-state materials is referred to as “crystal engineering”.

1.3 CRYSTAL ENGINEERING

Crystal engineering is a sub-division of supramolecular chemistry that explores interactions within crystalline solids and endeavours to apply this knowledge to the rational design of novel materials.⁵ According to Desiraju, crystal engineering is “*the understanding of intermolecular interactions in the context of crystal packing and in the utilisation of such understanding in the design of new solids with desired physical and chemical properties*”.⁷ This endeavour typically involves three steps: 1) study of the intermolecular interactions, 2) study of the packing modes, 3) study of the crystal properties and their fine-tuning with deliberate variations in the packing.⁷ The examination of recurring patterns of interactions in systematic studies of known structures is the cornerstone of crystal engineering and the discoveries from these studies may be used to make general predictions about expected crystal structure features.⁵ Therefore, crystal engineering encompasses the investigation of interaction geometries and energies from a theoretical and/or crystallographic perspective, the synthesis of crystals (both exploratory and by design), and the investigation of the structures and properties of the crystalline products.⁸ It can also be regarded as a field that considers crystals as synthetic targets. The development of these target materials is appealing owing to the properties, functions and applications that they may possess. Examples include porous materials for gas separations, polar materials for non-linear optical applications, materials with tailored magnetic and photophysical properties that may be useful in electronic technologies and so forth.⁸ The foundations of crystal engineering lie in the concepts of molecular recognition and self-organisation. Recognition events between complementary molecular fragments give rise to the organisation of molecules in the solid state.⁹

1.4 SELF-ASSEMBLY AND RECOGNITION

Self-assembly is the basis upon which complex matter is formed and the mechanisms are generally complicated. Supramolecular self-assembly concerns the spontaneous association of either a few or many components to create a larger, aggregate species through the formation of reversible (noncovalent) interactions.^{5,10} Structures that ‘self-organise’ can be designed to do so by selecting suitable components and interactions for supramolecular synthesis, and this is considered self-assembly by design.¹¹ Therefore, to obtain a supramolecular target by means of self-assembly, the chemist is required to design molecules containing complementary functionalities since there is no direct control over the assembly process. The use of weak, noncovalent interactions in self-assembly has the distinct advantage in that these interactions are usually reversible and therefore the chemical system ultimately rearranges to the most thermodynamically stable product.^{5,12} This ability to rearrange suggests that these

systems have the capacity to self-correct, which is an obvious advantage in biological systems.¹² The possibility for supramolecular systems to form under kinetic rather than thermodynamic control, however, should not be overlooked.

Metal-ligand interactions are among the most widely employed intermolecular interactions in synthetic self-assembly processes, primarily owing to their lability and high-degree of directionality.⁵ Exploiting the fact that metal-ions have well-defined and predictable coordination environments, they can be coupled with rigid ligands to lend pathways towards predictable self-assemblies.⁵

Molecular recognition processes rely on a number of factors for the assembly of a solid-state structure, including hydrogen bonding between molecular functional groups, complementary geometry of molecules i.e. humps fit into bumps and other directing factors (e.g. $\pi\cdots\pi$ interactions).

1.5 INCLUSION COMPOUNDS

Sir Humphry Davy was the first to record the discovery of host-guest compounds in 1811¹³ when he came upon the chlorine hydrate by bubbling chlorine into cool water. Further studies of inclusion compounds date back to the last century and pertain to hydroquinone,^{14,15} cyclodextrin inclusion compounds,¹⁶ Dianin's compound,^{17,18} urea inclusion compounds¹⁹ and later zeolites^{20,21} and metal-organic frameworks.²²⁻²⁵

Powell⁴ was the first to propose a formal definition of supramolecular cage-like host-guest structures, which he termed '*clathrates*'. These inclusion compounds comprise two or more components that associate without ordinary chemical connections, but rather through complete enclosure of one set of molecules (guests) in a suitable structure formed by another (host).^{4,25}

The host compounds can be separated into two distinct classes according to the topological relationship between the guest and host (Figure 1.1).^{4,26} The class designated as cavitands is described as host molecules that completely enclose guest molecules within intramolecular cavities, and they can exist both in solution and the solid state.^{4,5,27} Examples of this class include cyclodextrins, cyclophanes, calixarenes, cavitands, cryptands and various carcerands.²⁶ Conversely, '*clathrands*' or '*intercalates*' are lattice inclusion compounds. In other words the hosts pack in such a manner as to leave cavities, channels or layers in the crystal structure and various guest molecules are accommodated in these interstitial spaces. Clathrands typically exist only in the solid state.^{4,27}

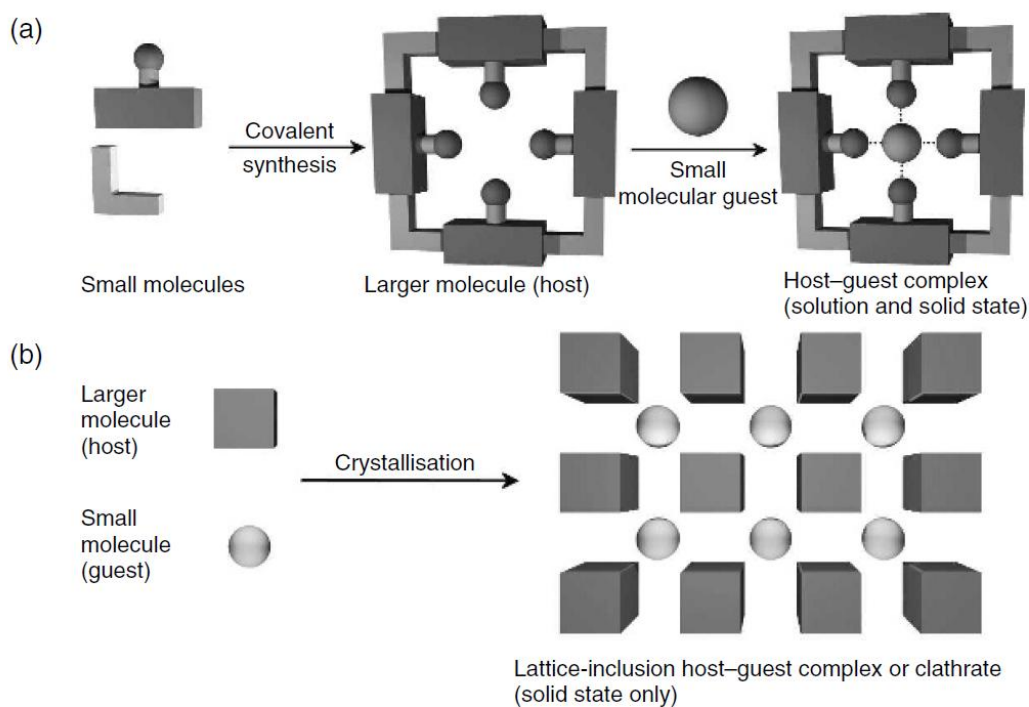


Figure 1.1 The two classes of inclusion compounds: (a) host-guest complexation; (b) lattice inclusion. Figure modified from reference 5

For some inclusion compounds it is possible to remove the included guest from the structure to leave the undisturbed host framework (apohost), which is then capable of taking up another guest. In other instances, the removal of the guest molecules results in a rearrangement, or collapse, of the host framework, and these inclusion compounds thus require the presence of the guest during crystallisation. This is referred to as guest-induced host assembly (template effect).⁶

1.6 ISOSTRUCTURALITY

It was Mitscherlich²⁸ (1819) who introduced the term ‘*isomorphous*’ to describe two crystals having the same external morphologies. However, external morphologies of crystals do not necessarily confer any information about the microscopic arrangements of the compounds. The concept of isostructurality in crystals pertains to the identical or near identical packing arrangements of chemically unique compounds. This term is typically used in the description of two organic molecules that share the same three-dimensional packing arrangement of geometrically similar structural units in two different crystals²⁹ and thus crystallise in identical space groups. These characteristics suggest that the two structures are virtually superimposable.²⁹ Inclusion compounds that form part of an isostructural series provide the opportunity to study structure and property relationships owing to the constancy of the host arrangement.²⁹ Recognition of isostructural compounds is most convenient by powder X-ray diffraction techniques where the patterns of two isostructural compounds are closely correlated. Intensity peak positions in the diffractograms of two isostructural compounds

often coincide owing to similar atomic lattice positions in the crystals.²⁹ Any discrepancies in the peak intensities of the two diffractograms can be attributed to the different guest molecules included within the host assemblies.²⁹ Kálmán has been at the forefront of investigations of isostructurality in crystals and is responsible for the development of various descriptors (or indices) with which isostructurality in organic compounds can be quantified.²⁹ The reader is referred to the work of Kálmán^{30,31} and co-workers for a more comprehensive explanation of these descriptors, or to the discussion in *Chapter 4* for a more brief explanation.

Isostructurality can appear in a number of classes of inclusion compounds. Often the formation of an isostructural series is brought about by the inherent stability of the host frameworks. However, isostructurality may also arise in structures of clathrates where the host is only stable with the inclusion of a guest molecule.²⁹ Examples of isostructural inclusion compounds include, but are certainly not limited to, the classes of Hofmann clathrates,^{32,33} Werner complexes³⁴ and cyclodextrins.³⁵

1.7 CHEMICAL TOPOLOGY

For centuries, people have been fascinated with knots, links and entanglements. Entanglements have been the subject for many graphical artists and have a rich history and symbolism in Irish, Islamic and Chinese cultures.³⁶ Much of the fascination in present day society is related to the aesthetic beauty of the various intricate designs and chemists have been intrigued by the possibilities of designing and synthesising materials with these same complex architectures.

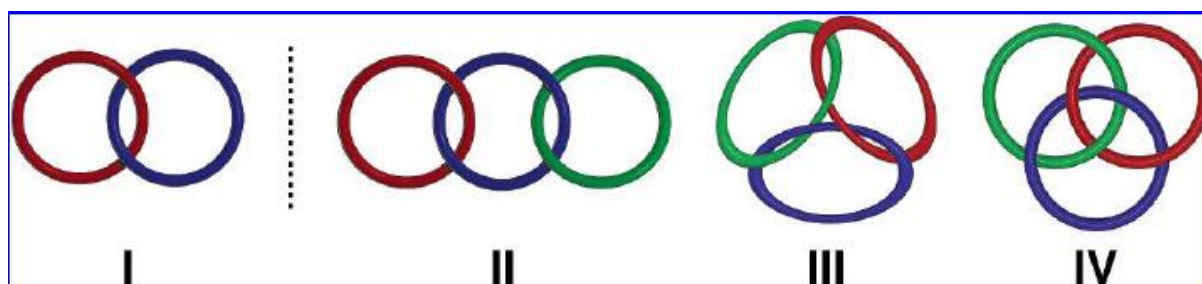
Topology is best known as a branch of mathematics associated with graph theory. Low-dimensional topology can also be connected to areas of molecular biology and chemistry. The idea of chemical topology first appeared in a seminal paper by Frisch and Wasserman in the early 1960's.³⁷ In the arena of supramolecular chemistry, topology refers to the connectivities of molecular entities. Two species are considered to be topologically connected if the two components are mechanically linked. These two components are not chemically linked but rather threaded through or around one another to form a single entity.⁵ In other words, these species are topologically nontrivial and the uncoupling of the two components requires the breaking of a chemical bond.⁵

Adopting the ideas of mathematical graph theory, molecular systems can be reduced to their simplest representations, which are known as molecular graphs. The molecular graph is a simplistic line-diagram depicting the connectivity of a molecule or molecular species.⁵ So the molecular graph of a simple macrocycle would be represented as a planar circle. The molecular graph of a nontrivial entanglement, however, cannot be represented as a planar

graph. For a number of chemically nontrivial species composed of interlinking components, the unlinked components are regarded as topological isomers of the nontrivial entity. Topological isomers are thus defined as compounds that have the same covalent connectivity but are topologically distinct and the interconversion of these components cannot occur without the breaking of chemical bonds.

Interlinking components are also known to form chiral products, particularly in knots, even when utilising non-chiral starting materials. Such chirality is known as topological chirality and, analogous to the topological isomers, there is the possibility of topological stereoisomers in this chiral species.

The fascination surrounding such systems, from a chemical perspective, stems from two sources. First, and most simply, because they are aesthetically pleasing and represent a significant synthetic challenge. Secondly, and more importantly, many interlocking structures have been shown to have interesting physical properties or the potential for them, specifically in the field of nanoscale machines and molecular electronic devices.^{5,36,38}



Scheme 1.1: Simple representation of topologically interlinked architectures: (I) [2]catenane, (II) [3]catenane and the stereoisomers of a trefoil knot (III and IV). Reproduced from reference 39.

Mechanically interlinked assemblies can be divided into three main classes: rotaxanes, catenanes and knots (Scheme 1.1). Rotaxanes are molecular assemblies in which a linear component is mechanically threaded through one or more cyclic molecules with the ends of the linear components terminated with bulky groups to prevent unthreading of the structure.⁴⁰ Pseudorotaxanes (also known as molecular threads) are formed by threading a cyclic species onto a separate extended linear component. Thus they are similar to rotaxanes, but the linear component does not have bulky termini to prevent unthreading.⁴⁰

Stoddart once referred to catenanes as ‘looping the loop’.⁴¹ Catenanes are defined as supramolecular systems consisting of cyclic components, not necessarily identical, that are mechanically linked, being held in an analogous fashion to the links in a chain.⁴¹ The components of the chains are usually held together by mutual association via one or more non-covalent interactions.⁴¹ Further discussion on catenanes can be found in *Chapter 5* of this text. The reader is also referred to the reviews published by Sauvage for a more comprehensive overview of the topics of chemical topology and entanglements.^{36,42,43}

1.8 SOLVATES AND SOLVATOMORPHISM

When molecules of the solvent of crystallisation become entrapped in the crystal lattice, we refer to the solid adduct as a solvate.⁴⁴ In these instances, the larger component is referred to as the “*host*” and the incorporated guest is often termed the “*guest*”.⁴⁴

Solvates are usually stabilised as a result of improved packing or more favourable intermolecular interactions, induced by the inclusion of solvent molecules. Certain, often bulky, molecular shapes favour the inclusion of solvent guests to facilitate an organised periodic packing arrangement. Because these molecules often require solvent molecules to fill any void spaces in the formation of a crystal, there is the possibility that they may have the capacity to include various guests such that these solvates bear some resemblance to one another. If two solvates are similar in that they comprise the same components but appear in differing stoichiometric ratios of host to guest, the term ‘*pseudopolymorphs*’ has been suggested.⁴⁵ ‘*Solvatomorphism*’ is recommended for the description of solvates that include different guests while the host remains constant.⁴⁵ Taking this one step further, it has been proposed that ‘*solvatopolymorphs*’ are compounds with different crystal modifications of the given solvate i.e. the same guest molecule.⁴⁵ These last three terms are relatively new in the nomenclature and are still under scrutiny by the crystal engineering community.

1.9 SUPRAMOLECULAR INTERACTIONS

Typically intermolecular interactions can be classed as medium-range or long-range. The isotropic, or medium-range forces, are responsible for the molecular shape and size of the individual molecules as well as close packing, whereas intermolecular orientations and functions are determined by anisotropic, long-range forces.^{26,46}

Noncovalent interactions represent the energies that hold the supramolecular species together. They are considerably weaker than covalent interactions (Table 1.1), but often act in a cooperative manner to stabilise supramolecular complexes.

Table 1.1 Strength scale of different intermolecular interactions and hydrogen bonds.⁴⁷

Interaction Type	Energy (kcal·mol ⁻¹)	Example
Very strong H bonds	15-40	O–H...O ⁻ , F–H...F ⁻
Coordinative bonds	20-45	M–N, M–O
Strong Hydrogen bonds	5-15	O–H...O, N–H...O
Weak hydrogen bonds	1-4	C–H...O, O–H...π
van der Waals interactions	0.5-2	CH ₃ ...CH ₃ , CH ₃ ...Ph
Heteroatom interactions	1-2	N...Cl, I...I, Br...Br
π–stacking	2-10	Ph...Ph, nucleobases

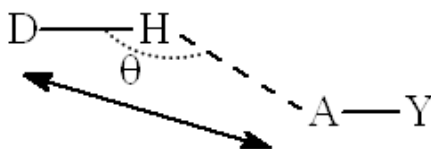
1.9.1 COORDINATIVE BONDS

The coordinative bond is a weak covalent (ion-dipole) interaction that is considered relatively labile. Coordinative bonds exist between metal cation acceptors and electron-pair donor atoms, usually a ligand molecule with a nitrogen or oxygen donor.⁴⁸ Coordinative bonds are weaker than the conventional covalent bonds, but they are considerably stronger and offer greater directionality compared to the weaker intermolecular interactions (Table 1.1). In addition, the diversity of available transition-metals and binding ligands provides greater versatility owing to the different coordination geometries available.⁴⁹

1.9.2 THE HYDROGEN BOND

The hydrogen bond has drawn much attention in the area of crystal engineering and there are many reviews delineating the nature of the hydrogen bond.⁵⁰⁻⁵⁴ Although Pimentel and McClellan first proposed a definition for the hydrogen bond that includes borderline donors and acceptors,⁵⁴ it was Pauling who provided a more expansive definition. He said that “*under certain conditions an atom of hydrogen is attracted by rather strong forces to two atoms, instead of only one, so that it may be considered to be acting as a bond between them*”.⁵⁴ Further restrictions have been implemented. However, the most accepted definition of a hydrogen bond is that ‘*a hydrogen bond exists where there is evidence that it exists*’.⁹ The hydrogen bond is considered a robust and specific interaction in the supramolecular context, owing to its strength and directional nature as well as the frequency with which it occurs.⁵³

These intermolecular interactions can be classified into very strong, strong and weak hydrogen bonds, according to strength and directionality (Table 1.2). A simple two-centred D–H···A hydrogen bond, as shown in Scheme 1.2, tends towards linearity with θ values in the range 150-180°.²⁶ Contact distances between interacting atoms D and A that are less than the sum of the van der Waals radii are characteristic of strong hydrogen bonds.



Scheme 1.2 Definition of the hydrogen bond of the type D–H···A–Y.⁵³

Table 1.2 Some properties of strong, moderate, and weak hydrogen bonds; adapted from a table in *The Weak Hydrogen Bond in Structural Chemistry and Biology*.⁵⁴ The numerical data are guiding values only.⁵⁰

	Very Strong	Strong	Weak
Interaction type	Strongly covalent	Mostly electrostatic	Electrostatic /dispersive
Bond Energy / -kcal·mol ⁻¹	15-40	4-15	<4
Examples	[F...H...F] [N...H...N] ⁺	O – H...O = C O – H...O – H	C – H...O O – H...π
Bond lengths / Å			
H...A	1.2–1.5	1.5–2.2	2.0–3.0
Lengthening of D – H / Å	0.08–0.25	0.02–0.08	<0.02
D – H versus H...A	D – H ≈ H...A	D – H < H...A	D – H ≪ H...A
D...A / Å	2.2–2.5	2.5–3.2	3.0–4.0
Bonds shorter than van der Waals radii	100%	Almost 100%	30-80%
directionality	Strong	moderate	Weak
Bond angles, θ /°	170-180	>130	>90
Effect on crystal packing	Strong	Distinctive	Variable
Utility in crystal engineering	Unknown	Useful	Partly useful

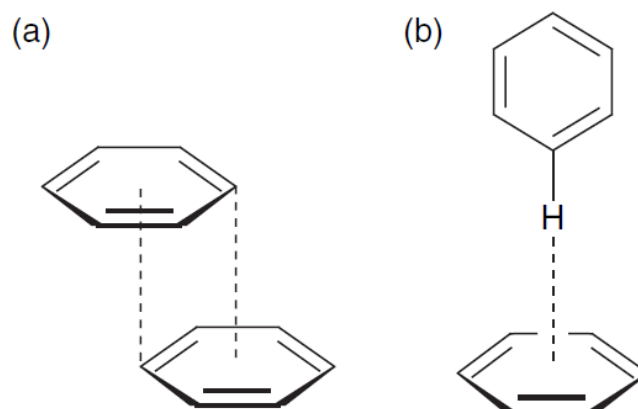
The weak hydrogen bond is differentiated from strong hydrogen bonds by the moderate to low electronegativity of the donor and/or acceptor atoms.⁵⁴ The structural influence of these interactions has been divided into three apparent roles – innocuous, supportive or intrusive. Intrusive interactions appear to affect the packing of molecules, supportive bonds correspond with the orientation requirements of other interactions in the structure and innocuous bonds have little or no impact on the structure.⁵⁴

The C–H...(O,N) type interactions are regarded as some of the most important of the weakly directional forces in a range of chemical and biological systems.²⁶ Typical C...O contact distances fall between 3.0–4.0 Å, with θ angles ranging from 100–180° with an increased frequency between 150–180°.²⁶

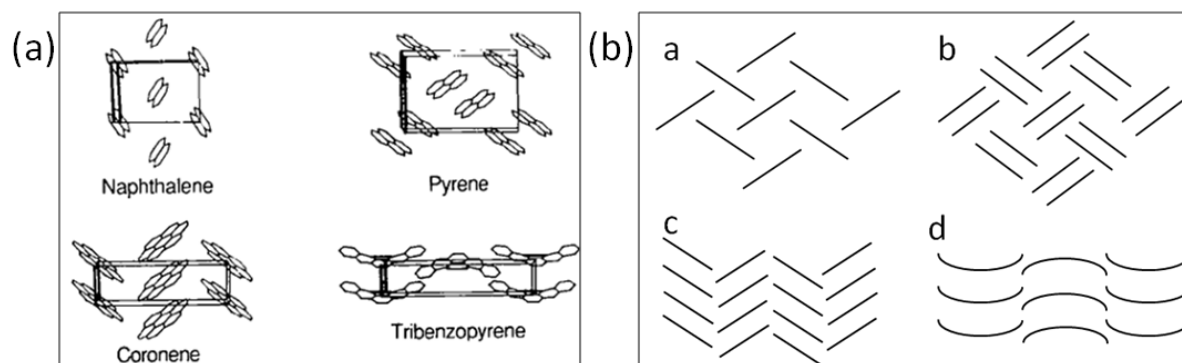
1.9.3 π-ACCEPTORS

The nature of π...π interactions is discussed in detail in *Chapter 3*. However a brief description of the terminology and concepts are outlined here. π-Interactions typically occur between π-delocalised electrons of aromatic moieties but can also involve delocalised electrons of double or triple bonds. π-Interactions result in two main interaction associations: π...π stacking, offset or eclipsed, and T-shaped edge-to-face interactions, which are in fact C–H...π interactions (Scheme 1.3). The arrangements of π...π interactions result in four

known packing motifs: herringbone, sandwich herringbone, gamma (γ) and beta (β) (Scheme 1.4).



Scheme 1.3 Geometries of aromatic $\pi\cdots\pi$ interactions: (a) offset face-to-face (b) edge-to-face. Figure reproduced from reference 5.



Scheme 1.4 The four basic aromatic crystal packing motifs as exemplified (a) by naphthalene (herringbone), coronene (γ), pyrene (sandwich) and tribenzopyrene (β). Reproduced from reference 55 and a diagrammatic representation (b) of the a) herringbone, b) sandwich herringbone, c) gamma (γ) and d) beta (β) packing motifs.

$\pi\cdots\pi$ Interactions and their consequent motifs are primarily observed in crystal structures of polyaromatic hydrocarbons (PAHs) where these are typically the only intermolecular interactions possible owing to a lack of strong hydrogen bond donors and/or acceptors. However, they are likely to occur in many crystal structures that involve strong hydrogen bonds (and/or other intermolecular interactions) as well, but are simply overshadowed by these stronger interactions and therefore overlooked in many crystal structure analyses.

1.9.4 VAN DER WAALS INTERACTIONS

Van der Waals interactions are dispersive type interactions and are therefore non-directional and of limited use in the design of supramolecular architectures. These interactions usually occur between molecules with separation distances larger than the sum of the van der Waals radii. Therefore, they are typically weak but collectively capable of contributing to the stability of supramolecular complexes. In the solid state molecules tend to pack efficiently, occupying all available space, while maximising energetically favourable van der Waals contacts.⁵⁶ These interactions are influential in the formation of inclusion compounds.⁵

1.9.5 LONE-PAIR... π INTERACTIONS

Lone-pair... π interactions have only recently been accepted as a type of supramolecular interaction and their occurrence is still a matter of debate.⁵⁷ This interaction was first identified by Egli and colleagues in a left-handed Z-DNA duplex,⁵⁸ and is most evident in bio-macromolecules but also occurs in small molecular host-guest systems. These interactions are reported to be energetically favourable,⁵⁸ with intermolecular contact distances less than 4 Å between the electron-pair donor atom and any atoms of the aromatic ring, whereas distances to the centroid of the ring do not exceed 4 Å.⁵⁸ More recently lone-pair... π interactions have also been demonstrated to be highly directional.⁵⁹

1.10 ASPECTS OF THIS STUDY

The preparation of metal-based supramolecular architectures using a self-assembly approach offers the advantage of simultaneous assembly of predetermined building blocks with relatively strong interactions that are also labile. This results in the generation of well-defined, discrete aggregates under thermodynamic equilibration since the coordinative bonds are kinetically labile, offering the possibility for self-correction of the assemblies.^{49,60}

The designed synthesis of self-assembled metallocycles has been reported in the works of Stang⁶¹ and Fujita.^{62,63} Their approach relies on the use of metal-ligand coordination of appropriate rigid and directional building units. In particular, they employ rigid linear units, with two active binding sites at the termini, and combine these with angular units, most often a metal centre, with predictable coordination geometry to create discrete metallocycle structures (Figure 1.2).^{60,61} The overall size and shape of the resulting metallocycles will depend on the type and stoichiometry of the selected building units. From these observations it is possible to establish a sort of “Molecular Library” from which the desired building blocks can be selected and combined to achieve the target architectures (Figure 1.3).

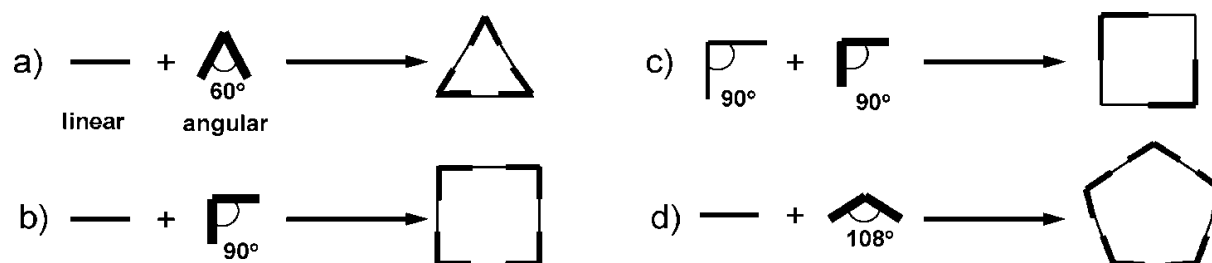


Figure 1.2 Schematic representation of the self-assembly of some simple metallocycles.⁶⁰








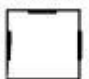


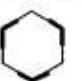

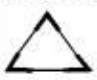
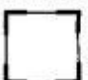

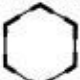
Ditopic Subunit \ Ditopic Subunit	A 60°	 90°	 109.5°	 120°	 180°
60°					
90°					
109.5°					
120°					
180°					

Figure 1.3 “Molecular Library” of cyclic molecular polygons created via the systematic combination of ditopic building blocks with predetermined angles.⁴⁹

In the Barbour research group, focus has been placed on the design of metallocycles using somewhat more flexible organic ligands with a variety of transition-metal salts. In particular, two imidazole coordinating groups are connected, through methylene linkages, to a central aromatic spacer group. The imidazole moieties are known to coordinate to metal centres reliably via the imino N-atoms. Introducing a degree of flexibility is somewhat risky in the endeavour to generate discrete supramolecular complexes because of the diverse conformations that the ligand may adopt in forming the coordination bond with the metal salt. However, it is believed that this flexibility may shed some light on the manner in which supramolecular architectures assemble.

Our main objective in the formation of these discrete units is to generate structures that are shape-incompatible and thus pack inefficiently in the solid state. To date only a small number of discrete metallocycles have been afforded by this method. However these structures have been shown to exhibit fascinating properties. Of most interest is the porosity exhibited by a few of these structures.^{64,65} The reaction of **A** (1,4-bis(2-methylimidazol-1-ylmethyl)benzene) with AgBF_4 in acetonitrile affords a metallocycle that includes the solvent of crystallisation within the apertures of the metallocycle (Figure 1.4).⁶⁴ The rectangular hosts stack to form one-dimensional channels that entrap acetonitrile guest molecules. These guest molecules are easily removed, by heating the crystals to 80 °C, without disrupting the packing arrangement of the host, thus yielding a porous lattice capable of absorbing various gases.

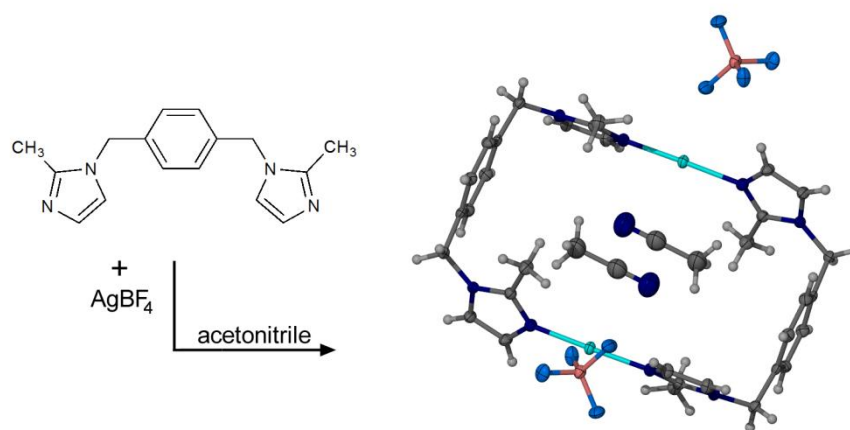


Figure 1.4 Formation of $[\text{Ag}_2\text{A}_2](\text{BF}_4)_2 \cdot 2\text{CH}_3\text{CN}$, where **A** = 1,4-bis(2-methylimidazol-1-ylmethyl)benzene. Figure reproduced from reference 64.

Modification to the aromatic spacer of the ligand (**A**) afforded a similar metallocycle using AgPF_6 in place of AgBF_4 (Figure 1.5). These metallocycles pack in an analogous manner, forming one-dimensional channels.⁶⁶ However, the arrangements of the channels in relation to one another are slightly different, possibly owing to the inclusion of a larger counter ion species. These small modifications to the structure produce slightly different gas sorption behaviour for the two different structures.

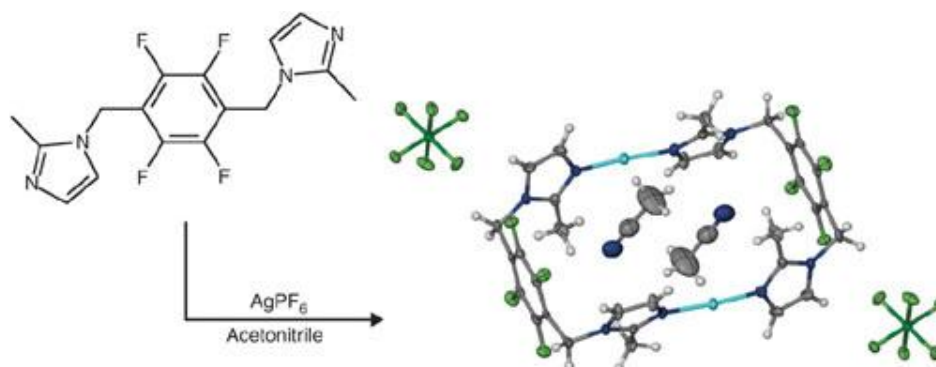


Figure 1.5 Formation of $[\text{Ag}_2\text{A}_2](\text{PF}_6)_2 \cdot 2\text{CH}_3\text{CN}$, the complex is shown in ball-and-stick representation. Figure reproduced from reference 66

A different metallocycle formed by the reaction of **B** (1,3-bis(imidazol-1-ylmethyl)-2,4,6-trimethylbenzene) with $\text{CuCl}_2 \cdot \text{H}_2\text{O}$ yielded an elongated rectangular metallocycle that occludes a hydrogen bonded adduct consisting of one water and one methanol molecule (Figure 1.6).⁶⁵ The metallocycles again stack one on top of another to form one-dimensional columns. The solvent included in the columns is easily removed by heating the crystals, under vacuum, to 60 °C. Single-crystal diffraction analysis confirms that this occurs as a single-crystal to single-crystal process. Unlike the previous structure the host lattice in this instance is not porous in the conventional sense. Instead the guest molecules are located in discrete pockets within the channels of the host (Figure 1.7). The fact that the guest molecules can be removed without significantly disrupting the host packing arrangement suggests that the

crystals remain permeable to small molecular entities despite their seemingly nonporous assembly. Indeed, these crystals have been demonstrated to be porous to a variety of gaseous guests.

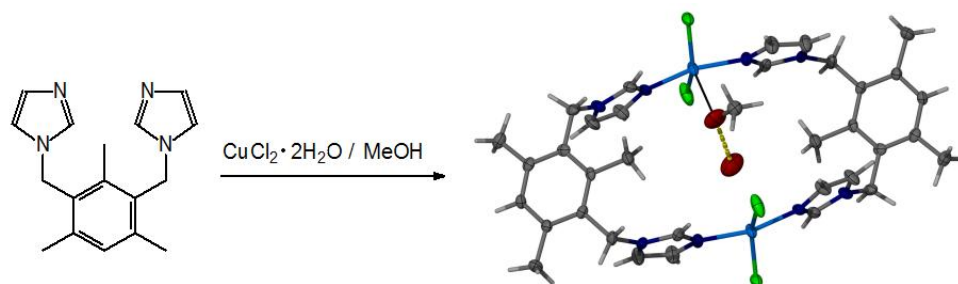


Figure 1.6 Formation of $[\text{Cu}_2\text{B}_2\text{Cl}_4] \cdot \text{CH}_3\text{OH} \cdot \text{H}_2\text{O}$. Figure reproduced from reference 65.

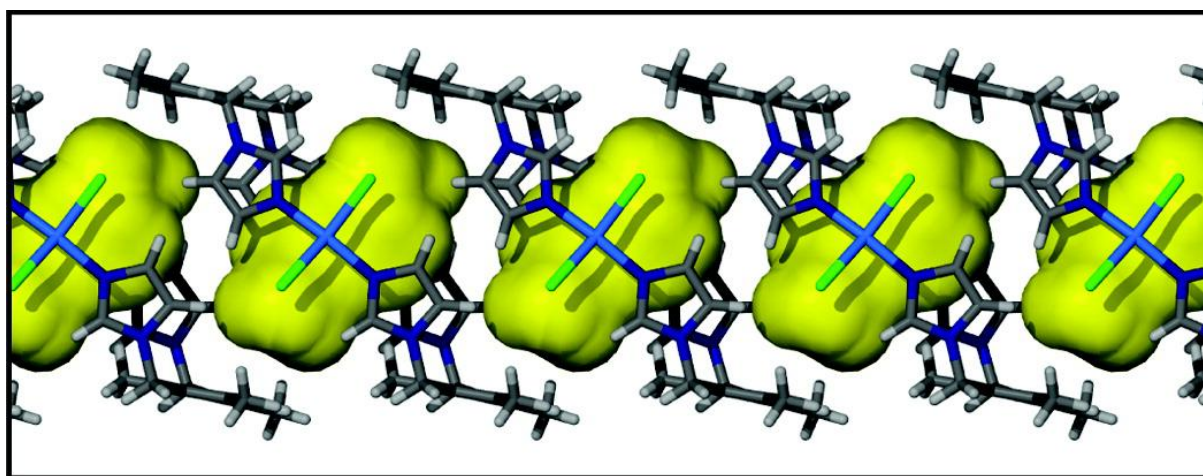


Figure 1.7 Columns of $[\text{Cu}_2\text{B}_2\text{Cl}_4]$ with guest-accessible pockets, shown as yellow Connolly surfaces ($r = 1.4 \text{ \AA}$, volume = ca. 108 \AA^3), in the guest-free structure. Figure reproduced from reference 65.

Another interesting phenomenon observed during the investigations of these zero-dimensional metalocycles is the single-crystal to single-crystal interconversion of four distinct molecular crystals.⁶⁷ Metallocycle complexes are constructed from an acetone solution containing the ligand **A** (1,4-bis[(2-methylimidazol-1-yl)methyl]benzene) and CuCl_2 . The host molecules (Figure 1.8) experience dramatic conformational, positional and topological changes upon uptake and release of solvent vapours. Remarkably, four different, reversible, conformations were obtained (Figure 1.9) and each is accompanied by a vapochromic response.

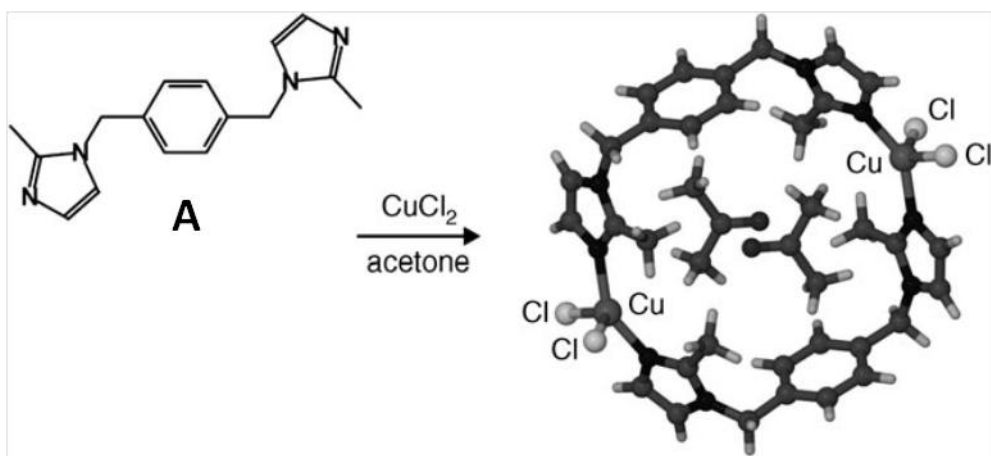


Figure 1.8 Formation of $[\text{Cu}_2\text{A}_2\text{Cl}_4]\cdot 2(\text{CH}_3)_2\text{CO}$. Figure reproduced from original communication.⁶⁷

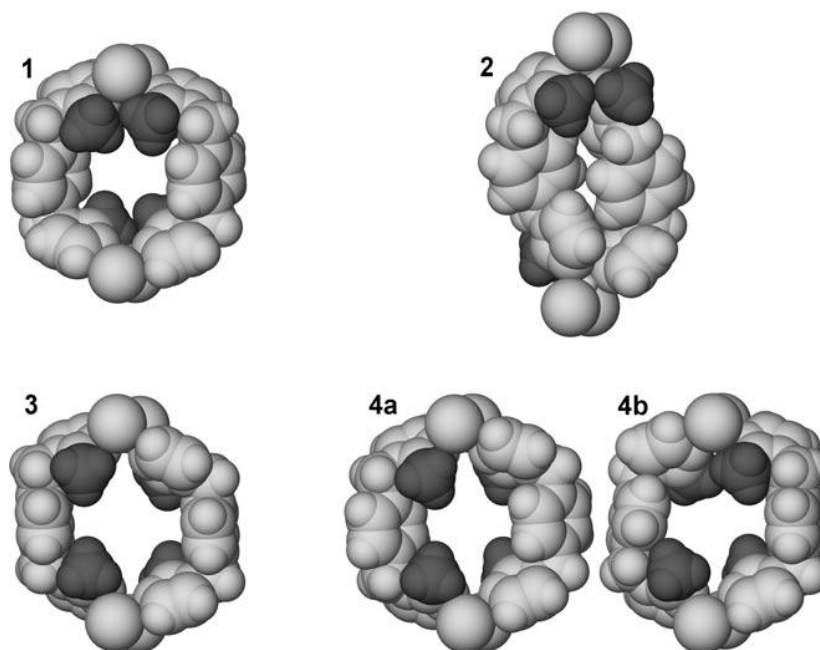


Figure 1.9 Space-filling projections of the metal complexes in phases 1 to 4. The methyl groups on the imidazole moieties are darkened to highlight the most significant conformational differences. Figure reproduced from original communication.⁶⁷

Other studies conducted by the group on metallocycles include the investigation of the template effect⁶⁸ on the formation of various metallocycle structures. From these investigations it is clear that metallocycles are highly intriguing target complexes. For this reason the design of novel metallocycles and the understanding of their self-assembly is of importance with the end goal being to design (and engineer) novel structures with unique properties and functions. Therefore, this study is focused on the synthesis and structural analysis of discrete metallocycles utilising novel imidazole-functionalised organic ligands.

The main aims of this study were to:

- synthesise novel imidazole-functionalised organic ligands;
- crystallise the ligands with a selection of transition-metal halide salts by self-assembly methods;
- analyse the resulting crystal structures;
- compare the structures obtained for any remarkable similarities or differences;
- assess the design aspects and make suggestions for the design of new metallocycle materials.

Experimental and analytical techniques used during the course of this study are outlined briefly in *Chapter 2*. *Chapter 3* details the survey and method development in the analysis of structural motifs resulting from $\pi\cdots\pi$ interactions in aromatic compounds. This entails a brief review of the theoretical classification of $\pi\cdots\pi$ interactions and previous investigations of the categorisation of aromatic hydrocarbons into one of the four classified $\pi\cdots\pi$ motifs. Subsequently, a robust, yet simple method developed for the classification of a number of compounds from the Cambridge Structural Database (CSD) is discussed. This method is then extended to the classification of some heteroaromatic compounds as well as cocrystals also obtained from the database.

A series of “isostructural” metallocyclic compounds obtained from a ditopic imidazole functionalised ligand is discussed in *Chapter 4*. These compounds were analysed by SCD and TGA and the calculated PXRD patterns are compared along with Crystal Packing Similarity calculations.

Chapter 5 presents the extraordinary concomitant formation of topological isomers of a copper-based metallocycle incorporating an imidazole-functionalised ligand containing a phenanthrenyl spacer. $\pi\cdots\pi$ Stacking interactions govern the formation of an infinite catenane structure, and the crystals are luminescent. Simple metallocycles of the same chemical composition are obtained concomitantly and are thought to be the kinetically favourable product of this reaction.

Design aspects in the formation of novel metallocycles are discussed in *Chapter 6*. The synthesis of four ditopic imidazole-functionalised ligands provides the opportunity to investigate the structural aspects in the self-assembly of discrete metallocycles.

A summary of the results obtained during this study can be found in the concluding chapter, as well as concluding remarks and suggestions for future investigations.

“The number, type, sophistication, and beauty of synthetic supramolecular entities are limited only by the boundless imagination of chemists and the practical considerations of the

currently available techniques for the separation, analysis and proper characterization of the resulting product. Moreover, just as in nature, function and use will follow and derive from form and greatly enhance and enrich such rapidly growing interdisciplinary fields as material science, bioengineering, and others.”⁶¹

1.11 REFERENCES

1. J.-M. Lehn, *Angew. Chem. Int. Ed.*, 1988, **27**, 89-112.
2. R. Pepinsky, *Phys. Rev.*, 1955, **100**, 971-971.
3. G. M. Schmidt, *J. Pure Appl. Chem*, 1971, **27**, 647-678.
4. J. W. Steed and J. L. Atwood, *Supramolecular Chemistry*, John Wiley & Sons, Ltd, 2000.
5. J. W. Steed, D. R. Turner and K. J. Wallace, *Core Concepts in Supramolecular Chemistry and Nanochemistry*, Wiley, 2007.
6. G. R. Desiraju, J. J. Vittal and A. Ramanan, *Crystal Engineering: A Textbook*, World Scientific, 2011.
7. G. R. Desiraju, *Angew. Chem., Int. Ed.*, 2007, **46**, 8342-8356.
8. L. Brammer, *Chem. Soc. Rev.*, 2004, **33**, 476-489.
9. C. B. Aakeröy and K. R. Seddon, *Chem. Soc. Rev.*, 1993, **22**, 397-407.
10. J.-M. Lehn, *Supramolecular Chemistry Concepts and Perspectives*, VCH, 1995.
11. J.-M. Lehn, *Chem. Soc. Rev.*, 2007, **36**, 151-160.
12. J. F. Stoddart, in *Self-Assembly in Supramolecular Systems*, eds. L. F. Lindoy and I. M. Atkinson, The Royal Society of Chemistry, 2000, pp. 1-6.
13. H. Davy, *Phil. Trans. R. Soc. Lond*, 1811, **101**, 155-162.
14. T. C. W. Mak and C.-K. Lam, in *Encyclopedia of Supramolecular Chemistry*, eds. J. L. Atwood and J. W. Steed, Marcel Dekker, Inc., New York; Basel, 2004, pp. 679-686.
15. T. C. W. Mak and B. R. F. Bracke, in *Comprehensive Supramolecular Chemistry*, eds. J. L. Atwood, J. E. D. Davies, D. D. MacNichol and F. Vögtle, Pergamon, 1996, pp. 23-60.
16. J. Szejtli, in *Comprehensive Supramolecular Chemistry* eds. J. L. Atwood, J. E. D. Davies, D. D. MacNichol and F. Vögtle, Pergamon, 1996, pp. 189-203.
17. K. J. Harrington, *Sep. Sci. Technol.*, 1982, **17**, 1443-1450.
18. S. G. Frank, *J. Pharm. Sci.*, 1975, **64**, 1585-1604.

19. M. D. Hollingsworth and K. D. M. Harris, in *Comprehensive Supramolecular Chemistry*, eds. J. L. Atwood, J. E. D. Davies, D. D. MacNichol and F. Vögtle, Pergamon, 1996, pp. 177-237.
20. R. M. Barrer, *J. Inclusion Phenom. Macrocyclic Chem.*, 1983, **1**, 105-123.
21. T. Bein, *Inclusion Chemistry of Organometallics on Zeolites*, Pergamon, 1996.
22. W. Morris, C. J. Doonan, H. Furukawa, R. Banerjee and O. M. Yaghi, *J. Am. Chem. Soc.*, 2008, **130**, 12626-12627.
23. R. Banerjee, A. Phan, B. Wang, C. Knobler, H. Furukawa, M. O'Keeffe and O. M. Yaghi, *Science*, 2008, **319**, 939-943.
24. M. H. Alkordi, Y. Liu, R. W. Larsen, J. F. Eubank and M. Eddaoudi, *J. Am. Chem. Soc.*, 2008, **130**, 12639-12641.
25. J. E. D. Davies, *J. Incl. Phenom.*, 1998, **32**, 499-504.
26. G. R. Desiraju, in *Comprehensive Supramolecular Chemistry*, eds. D. D. MacNichol, F. Toda and R. Bishop, Pergamon, Oxford, 1996, pp. 4-9.
27. L. R. Nassimbeni, *Acc. Chem. Res.*, 2003, **36**, 631-637.
28. E. Mitscherlich, *Ann. Chim. Phys.*, 1822, **19**, 350-419.
29. M. R. Caira, in *Encyclopedia of Supramolecular Chemistry*, eds. J. L. Atwood and J. W. Steed, Marcel Dekker, Inc., New York; Basel, 2004, pp. 767-775.
30. A. Kálmán, L. Parkanyi and G. Argay, *Acta. Crystallogr., Sect. B*, 1993, **49**, 1039-1049.
31. L. Fábián and A. Kálmán, *Acta. Crystallogr., Sect. B*, 1999, **55**, 1099-1108.
32. R. Weidenhagen, *Berichte der Deutschen Chemischen Gesellschaft (A and B Series)*, 1940, **73**, A157-A161.
33. S. Nishikiori, Y. Takahashi-Ebisudani and T. Iwamoto, *J. Inclusion Phenom. Macrocyclic Chem.*, 1990, **9**, 101-112.
34. J. Lipkowski, in *Comprehensive Supramolecular Chemistry*, eds. J. L. Atwood, J. E. D. Davies, D. D. MacNichol and F. Vögtle, Pergamon, 1996, pp. 691-714.
35. M. R. Caira, *Rev. Roum. Chim.*, 2001, **46**, 371-386.
36. R. S. Forgan, J.-P. Sauvage and J. F. Stoddart, *Chem. Rev.*, 2011, **111**, 5434-5464.
37. E. Wasserman, *J. Am. Chem. Soc.*, 1960, **82**, 4433-4434.
38. J.-F. Moulin, J. C. Kengne, R. Kshirsagar, M. Cavallini, F. Biscarini, S. Léon, F. Zerbetto, G. Bottari and D. A. Leigh, *J. Am. Chem. Soc.*, 2006, **128**, 526-532.
39. S. J. Cantrill, K. S. Chichak, A. J. Peters and J. F. Stoddart, *Acc. Chem. Res.*, 2004, **38**, 1-9.

40. J. F. Stoddart, in *Self-Assembly in Supramolecular Systems*, eds. L. F. Lindoy and I. M. Atkinson, The Royal Society of Chemistry, 2000, pp. 47-86.
41. J. F. Stoddart, in *Self-Assembly in Supramolecular Systems*, eds. L. F. Lindoy and I. M. Atkinson, The Royal Society of Chemistry, 2000, pp. 87-118.
42. J. P. Sauvage, *Acc. Chem. Res.*, 1990, **23**, 319-327.
43. C. O. Dietrich-Buchecker and J. P. Sauvage, *Chem. Rev.*, 1987, **87**, 795-810.
44. T. Hosokawa, S. Datta, A. R. Sheth, N. R. Brooks, V. G. Young and D. J. W. Grant, *Cryst. Growth Des.*, 2004, **4**, 1195-1201.
45. B. T. Ibragimov, *CrystEngComm*, 2007, **9**, 111-118.
46. G. R. Desiraju, *Nature*, 2001, **412**, 397-400.
47. A. Nangia, *J. Chem. Sci.*, 2010, **122**, 295-310.
48. F. A. Cotton, G. Wilkinson and P. L. Gaus, *Basic Inorganic Chemistry*, John Wiley & Sons, 1995.
49. S. Leininger, B. Olenyuk and P. J. Stang, *Chem. Rev.*, 2000, **100**, 853-908.
50. T. Steiner, *Angew. Chem., Int. Ed.*, 2002, **41**, 48-76.
51. T. Steiner and G. R. Desiraju, *Chem. Commun.*, 1998, 891-892.
52. D. Braga and F. Grepioni, in *Encyclopedia of Supramolecular Chemistry*, eds. J. L. Atwood and J. W. Steed, Marcel Dekker, Inc. , New York; Basel, 2004.
53. G. R. Desiraju, in *Encyclopedia of Supramolecular Chemistry*, eds. J. L. Atwood and J. W. Steed, Marcel Dekker, Inc. , New York; Basel, 2004, pp. 658-665.
54. G. R. Desiraju and T. Steiner, *The Weak Hydrogen Bond In Structural Chemistry and Biology*, Oxford University Press, 2006.
55. G. R. Desiraju and A. Gavezzotti, *Acta. Crystallogr., Sect. B*, 1989, **45**, 473-482.
56. D. V. Soldatov and I. S. Terekhova, *J. Struct. Chem.*, 2005, **46**, S1-S8.
57. A. Robertazzi, F. Krull, E.-W. Knapp and P. Gamez, *CrystEngComm*, 2011, **13**, 3293-3300.
58. T. J. Mooibroek, P. Gamez and J. Reedijk, *CrystEngComm*, 2008, **10**, 1501-1515.
59. T. J. Mooibroek and P. Gamez, *CrystEngComm*, 2012, **14**, 1027-1030.
60. S. J. Lee and W. Lin, *Acc. Chem. Res.*, 2008, **41**, 521-537.
61. P. J. Stang and B. Olenyuk, *Acc. Chem. Res.*, 1997, **30**, 502-518.
62. M. Fujita, F. Ibukuro, K. Yamaguchi and K. Ogura, *J. Am. Chem. Soc.*, 1995, **117**, 4175-4176.
63. M. Fujita and K. Ogura, *Coord. Chem. Rev.*, 1996, **148**, 249-264.
64. L. Dobrzańska, G. O. Lloyd, H. G. Raubenheimer and L. J. Barbour, *J. Am. Chem. Soc.*, 2005, **127**, 13134-13135.

65. L. Dobrzańska, G. O. Lloyd, H. G. Raubenheimer and L. J. Barbour, *J. Am. Chem. Soc.*, 2006, **128**, 698-699.
66. T. Jacobs, J.-A. Gertenbach, D. Das and L. J. Barbour, *Aust. J. Chem.*, 2010, **63**, 573-577.
67. L. Dobrzańska, G. O. Lloyd, C. Esterhuysen and L. J. Barbour, *Angew. Chem. Int. Ed.*, 2006, **45**, 5856-5859.
68. L. Dobrzańska, G. O. Lloyd and L. J. Barbour, *New J. Chem.*, 2007, **31**, 669-676.

CHAPTER 2

ANALYTICAL METHODS AND TECHNIQUES

This chapter describes the methods of analysis and experimental techniques that made this study possible.

2.1 SINGLE-CRYSTAL X-RAY DIFFRACTION (SCD)

Single-crystal X-ray diffraction is a non-destructive analytical technique that can be used to determine the atomic coordinates of atoms and molecules in three-dimensional space, including the connectivity of the atoms. This method is the most unambiguous in determining the structures of small molecules and in most instances the technique provides the user with accurate and precise measurements of molecular dimensions that are not possible by any other technique. The technique also provides information regarding the intermolecular interactions that occur in the solid state.

The general procedure was as follows. A suitable single crystal was first selected and covered with paratone oil before being mounted onto a MiTeGen mount, which was then placed onto the goniometer head of the single-crystal diffractometer for data collection. X-ray intensity data were collected on a Bruker SMART Apex II or Bruker Apex II DUO X-ray diffractometer. Molybdenum radiation ($\lambda = 0.71073 \text{ \AA}$) was used in most instances, although some experiments required the use of copper radiation ($\lambda = 1.54184 \text{ \AA}$). Data were captured with a CCD (Charge-Coupled Device) area-detector. All data collections were carried out at 100 K using an Oxford Cryosystems cryostat (700 Series Cryostream Plus) attached to the diffractometer. In most instances the crystals would deteriorate rapidly on removal from this nitrogen stream.

Data collection and reduction were carried out using the Bruker software package APEX2, using standard procedures. SMART¹ software was employed, within the APEX2 environment, to establish the best data collection strategy after a reliable unit cell had been determined. Standard ω - and ϕ -scans were used to obtain intensity data which were subsequently reduced and refined using SAINT² software. A multi-scan or numerical absorption correction was performed utilising SADABS,³ or TWINABS⁴ in the case of twinned crystals. All structures were solved by direct methods or a combination of Patterson and partial structure expansion using SHELXS-97.⁵ SHELXL-97 was employed within the X-Seed^{6,7} environment to anisotropically refine all non-hydrogen atoms by full matrix least-squares based on F^2 . Where appropriate, hydrogen atoms were placed using a riding model constraint based on idealized coordinates and geometrical constraints.⁸

2.2 POWDER X-RAY DIFFRACTION (PXRD)

Experimental patterns were collected using a PANalytical X'pert Pro diffractometer with Bragg-Brentano geometry employing Cu K α radiation ($\lambda = 1.5418 \text{ \AA}$) generated at 45 kV and 40 mA. The intensity data were captured with an X'Celerator Detector with 2θ scans performed in the range $5\text{--}50^\circ$ at a constant room temperature. All samples were prepared by gently crushing the crystals under mother liquor and loading them as quickly as possible onto a zero-background sample holder. Calculated PXRD patterns were also generated from the single-crystal data using the program Lazy Pulverix⁹ for comparison with the experimental data.

2.3 THERMOGRAVIMETRIC ANALYSIS (TGA)

Thermogravimetry (TG) is the measurement of changes in mass of a sample as a function of temperature, while the sample is subjected to a controlled temperature programme. The results of a TG analysis are represented as a plot of mass against temperature or time and the mass loss is represented as a step.¹⁰ In the examination of inclusion compounds, TG analysis can be helpful in quantifying the host-guest stoichiometry provided the mass loss can be accounted for by the loss of a volatile guest.¹¹

Thermogravimetric analysis was carried out using a TA Instruments Q500 system under a N₂ gas purge (flow rate 50.0 ml/min) using aluminium sample pans. A standard analysis procedure was used for all samples. Starting at ambient, the sample was heated to 600 °C at a ramp rate of 10 °C per minute with samples ranging from 1.5 to 4 mg. The results were analysed with the Universal Analysis 2000 program supplied with the instrument.

Sample preparation was kept to a minimum since most samples exhibited the release of volatile guests under ambient conditions. Therefore, single crystals were used for the analysis rather than a powdered sample. In most cases these crystals were removed from the mother liquor, blotted on filter paper and immediately transferred to the sample pan for analysis. If the transfer of sample was too slow it resulted in a slightly inaccurate analysis. If the sample was not appropriately dried the analysis showed an exaggerated weight loss; this occurs mostly when the mother liquor is a mixture of high-boiling solvents. The use of single crystals rather than powdered samples may alter the results of the analysis owing to the available surface area of the sample that is exposed. This, however, was the only viable method of analysis for these compounds.

2.4 COMPUTER PACKAGES

A number of computer packages were used in the detailed analysis and comparison of crystal structures, each program having its own advantages and disadvantages. These analytical tools allow the researcher to make more in-depth comparisons and observe structural features that may be missed if simply evaluated by “eye”.

2.4.1 MSRoll¹²⁻¹⁴

Solvent-accessible voids were visualised by calculating Connolly surfaces using the program MSRoll.¹²⁻¹⁴ The *accessible surface* is the trace of the probe sphere centre as it rolls over the molecule of interest. This was based on the ideas of Lee and Richards¹⁵ who suggested that the surface of a protein molecule can be identified by rolling a probe, the size of a water molecule over a molecule, typically the probe radius is between 1.4 and 1.7 Å. The molecular surface mapped by the exterior of the probe is referred to as the *contact surface*. Incorporating MSRoll into X-Seed^{6,7} it is possible to map either type of surface and obtain numerical data regarding the area and/or volume of these surfaces.

The cavities in the present study were mapped by first removing the solvent guest molecules from the atom list. An appropriate probe radius was then selected and the contact surface calculated using MSRoll. The output file .cav was imported into X-Seed and could be incorporated into the final structure visualisation using Pov-Ray. Images can be rendered with the guest molecules reinstated to show their location in these voids.

2.4.2 CAMBRIDGE STRUCTURAL DATABASE (CSD)

The Cambridge Structural Database¹⁶ (CSD) forms part of the Cambridge Crystallographic Data Centre's (CCDC) many utilities. As of January 2011 there were 541 748 entries in the database with approximately 43% of these structures being of organic compounds (Figure 2.1). The CSD itself is an excellent resource that allows the user to search published single-crystal and powder structural data.

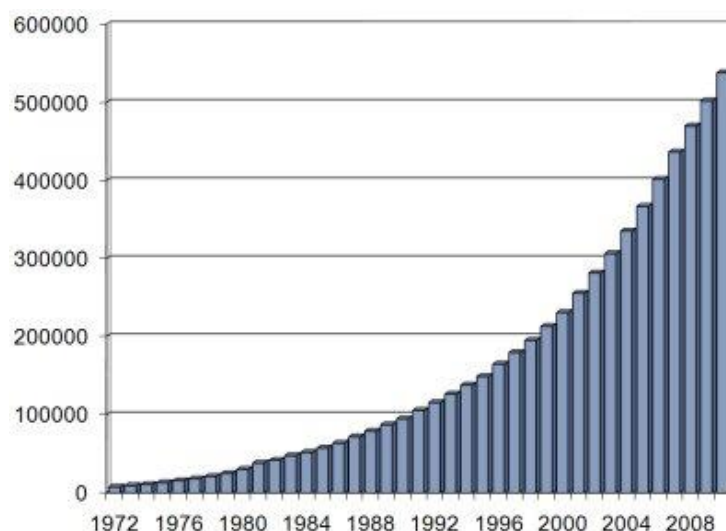


Figure 2.1: Growth of the Cambridge Structural Database since 1970. The graph is reproduced from the CCDC website: <http://www.ccdc.cam.ac.uk/products/csd/statistics/>

2.4.3 MERCURY^{17,18}

Mercury is a crystal structure visualisation and investigation tool within the CCDC suite. The program incorporates various tools; including overlaying of multiple structures, powder pattern and morphology calculations. These tools contribute to the existing visual and geometrical analysis of crystal structures in an attempt to understand the packing of molecular structures.¹⁷ In order to improve analysis of packing arrangements in numerous structures, a new functionality has been added to the Mercury suite called the *Materials Module*.

Mercury Materials Module – The module consists of three different functionalities: *Motif Searching*, *Crystal Packing Feature* and *Crystal Packing Similarity*. ‘*Motif searching*’ allows searches for particular functional groups that may be involved in specific interactions. More general packing-feature searches can be carried out with the ‘*Crystal Packing Feature*’ functionality where the user is able to select any feature in a crystal structure that they wish to search for. The final functionality in the module enables the comparison of crystal packing between structures that contain the same compound. In the *Crystal Packing Similarity* feature, two structures of the same crystal form can easily be identified. If the forms are different, the tool identifies to what extent the molecular packing is similar. This similarity calculation is based on the method used in the program COMPACK.¹⁹

2.4.4 CRYSTALEXPLORER²⁰

This computer program can be used to generate Hirshfeld²¹ surfaces of a selected molecule(s) within a well-defined crystal structure. Hirshfeld surfaces are used to visually identify intermolecular interactions between selected entities in a particular crystal structure. The

Hirshfeld surface has the distinct advantage in that it is defined by both the enclosed molecule(s) as well as its closest neighbours, allowing the identification of a number of intermolecular contacts.²²

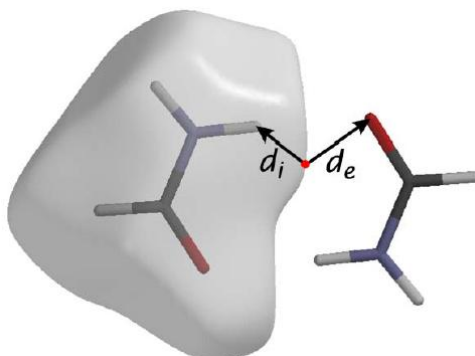


Figure 2.2 Definition of the d_i and d_e distances in establishing the Hirshfeld surface.¹⁵

The equation used to define a Hirshfeld surface is $w(r) = 0.5$ where $w(r)$ is the weight function described as

$$w(r) = \sum_{i \in \text{molecule}} \rho_i(r) / \sum_{i \in \text{crystal}} \rho_i(r);$$

where $\rho_i(r)$ is a spherical atomic electron distribution located at the i^{th} nucleus.

The surfaces generated for analysis in this study were all calculated using the d_{norm} function²³ such that the contact distance is normalised according to the formula

$$d_{norm} = \frac{d_i - r_i^{vdW}}{r_i^{vdW}} + \frac{d_e - r_e^{vdW}}{r_e^{vdW}},$$

where d_i is the distance from the surface to the nearest atom interior to the surface; d_e is the distance from the surface to the nearest atom exterior to the surface (Figure 2.2). The sum of the two distances would give an approximate contact distance.

A two-dimensional fingerprint plot²² can then be generated from the specified Hirshfeld surface by combining the d_i and d_e distances. The d_i , d_e pairs are binned in intervals of 0.01 Å and the colouring of each bin in the 2-D histogram is a function of the fraction of surface points in that bin. The sliding colour scale from blue (few points) through green to red (many points) indicates the concentration of points in each bin. Fingerprint plots can be used for the rapid visual comparison of two or more crystal structures by virtue of the fact that each

crystal structure affords a unique plot that is highly sensitive to the molecule's (species') immediate environment.²² A number of interaction types have distinctive shapes in the 2-D plot that can be used to quickly identify these interactions in the crystal structure (Figure 2.3).

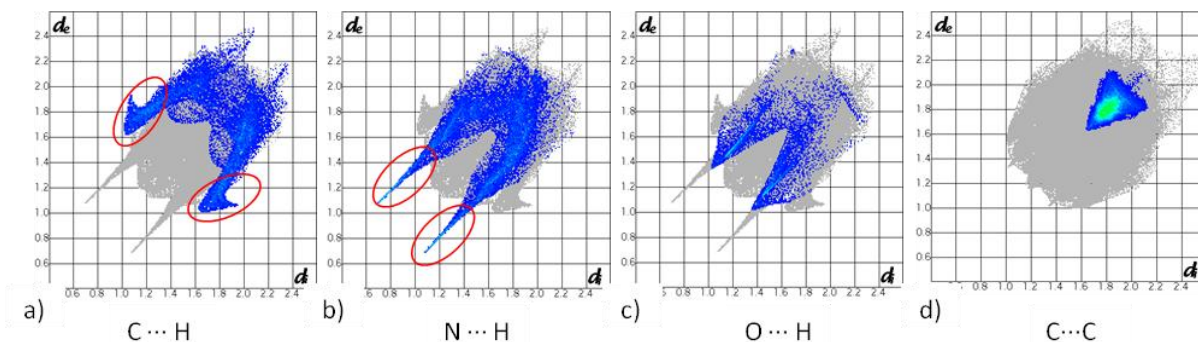


Figure 2.3 Selected characteristic patterns for symmetry-related interactions between molecules interior and exterior to the Hirshfeld surface. The blue areas highlight the specific interaction, while the grey areas represent the remainder of the intermolecular interactions. a) ‘Wings’ on either side of the plot represent C...H interactions, most often as C–H... π interactions, b) the outer tails are indicative of N...H interactions, c) O...H interactions are represented by inner tails, and d) the concentrated green area on the diagonal is indicative of C...C interactions, most often of the π ... π type.²⁴

2.4.5 PLATON – SQUEEZE

The electron density contributions of the solvent molecules included in the single-crystal structures were calculated using PLATON²⁵/SQUEEZE.²⁶ According to the SQUEEZE manual, “*the procedure takes care of the contribution of a (heavily) disordered solvent to the calculated structural factors by back-Fourier transformation of the continuous density found in a masked region of the difference map. The masked region is defined as the solvent accessible region left by the ordered part of the structure.*” For the structures reported in this study, the electron count calculated with SQUEEZE was used to confirm the occupancy of the guest molecules, particularly when the molecules are disordered. The calculation also yields the volume of the solvent accessible voids present in the structure, using a default probe radius of 1.2 Å. It is noted that high-quality structural data are required to obtain accurate results from these calculations.

In this study, SQUEEZE was used only as a tool for confirmation of the solvent included in the relevant structures and, not used to modify any ‘.hkl’ file to obtain the F_o^2 without solvent contribution. These results are also compared to results obtained from TG analysis.

2.5 SOLUTION NMR

Synthesised precursors and organic ligands were characterised by standard solution ^1H and ^{13}C NMR experiments. All experiments were performed at room temperature with either a 300 or 400 MHz Agilent Spectrometer using standard procedures.

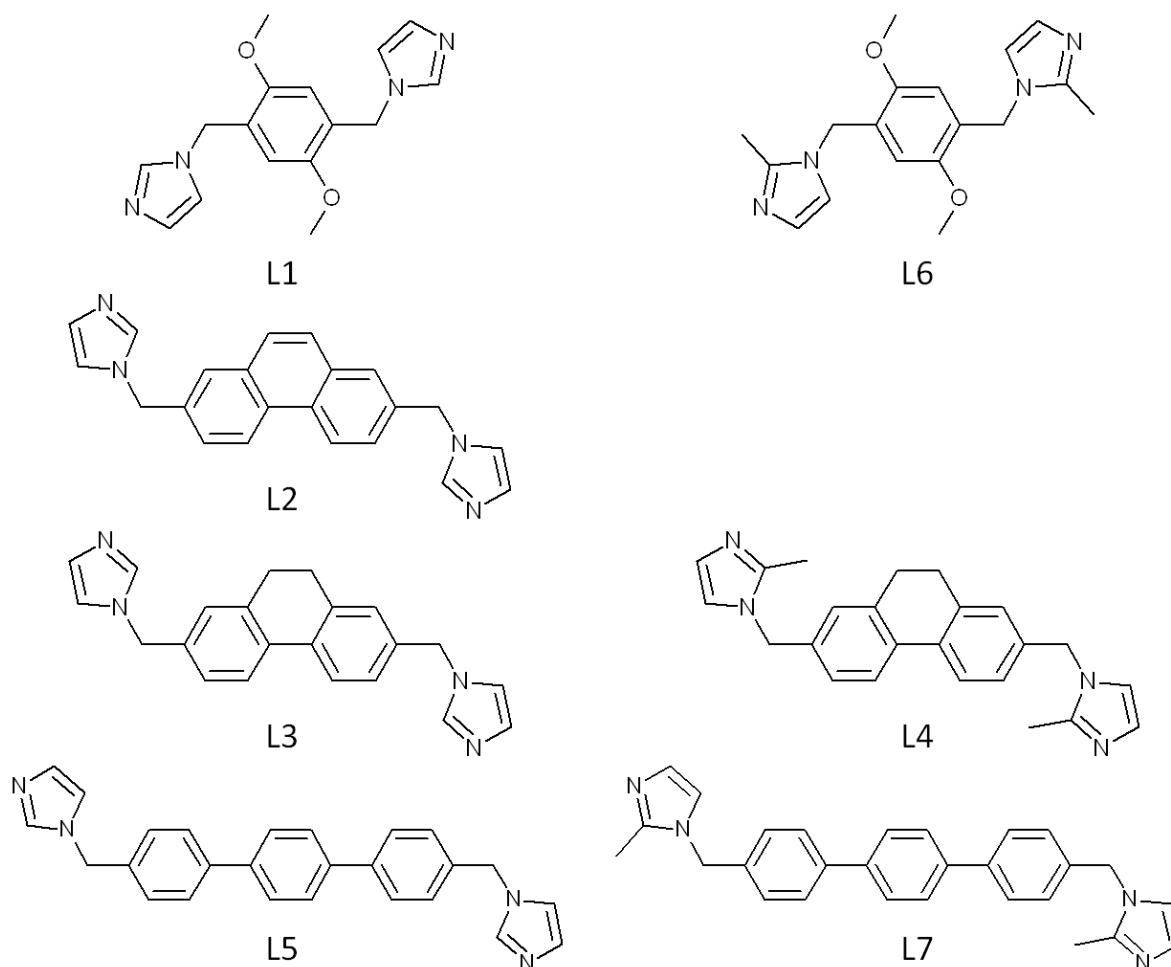
2.6 LIGAND DESIGN

The design of organic components is important for the purposes of this study. For comparisons to be made and for extrapolation of our findings to the design of new materials, it is important to maintain some consistency in the design of the ligand molecules. In the context on this study, we were interested in investigating the probability of a series of ligands forming discrete or zero-dimensional assemblies when coordinated to metal centres. With this in mind, we already know that the imidazole moiety is a suitable coordinating group, with imino nitrogen atoms that are readily able to form coordinative bonds with a variety of transition-metal salts. The main difficulty in the design may be the flexibility of the ligand molecule. It may be argued²⁷ that to guarantee the success of formation of discrete assemblies, one should consider ligands that already assume the desired conformation and simply require coordination to the metal centres in a suitable manner (i.e. preorganised conformation). However, this poses some difficulty in that the syntheses of these rigid ligands are challenging and therefore time-consuming as well as expensive. Another aspect is that, even with the use of rigid building blocks, preparation of the target complexes in crystalline form is still not guaranteed. Also to be considered is the information that we can obtain from the use of more flexible ligands that are able to arrange themselves freely in preferred conformations and orientations during the process of crystallisation. This is how we may come to understand some of the fundamental principles of crystallisation and the crystalline state.

Although the flexibility of the ligand can be advantageous in the formation of cyclic frameworks (metallocycles), it can also be a disadvantage in that the ligand can assume different conformations. The two obvious conformations are S-shaped and C-shaped, although there is also the possibility of assuming a conformation that is intermediate between the two. For the formation of metallocycles it is necessary for the ligand to coordinate to the metal centres in a C-shaped conformation. As yet there is no way of controlling the conformation assumed by the ligand before crystallisation, although it has been argued that

solvent (or other guest molecules) can be used to template the formation of these discrete cyclic complexes.²⁸

Seven imidazole-based ligands were synthesised during this investigation (Scheme 2.1). Three of these ligands (**L1**, **L5** and **L6**) have been synthesised previously, but no crystal structure data for any of the ligands have been reported. Synthesis details are provided at the end of the relevant chapters.



Scheme 2.1 Ligands synthesised as part of this study: **L1** – 1,1'-[(2,5-dimethoxybenzene-1,4-diyl)dimethanediyl]bis(1*H*-imidazole); **L2** – 1,1'-(phenanthrene-2,7-diyl)dimethanediylbis(1*H*-imidazole); **L3** – 1,1'-(9,10-dihydrophenanthrene-2,7-diyl)dimethanediylbis(1*H*-imidazole); **L4** – 1,1'-(9,10-dihydrophenanthrene-2,7-diyl)dimethanediylbis(2-methyl-1*H*-imidazole); **L5** – 1,1'-(terphenyl-2,7-diyl)dimethanediylbis(1*H*-imidazole); **L6** – 1,1'-[(2,5-dimethoxybenzene-1,4-diyl)dimethanediyl]bis(2-methyl-1*H*-imidazole); **L7** – 1,1'-(terphenyl-2,7-diyl)dimethanediylbis(2-methyl-1*H*-imidazole)

The ligands were selected in order to compare variations in length, rigidity and substituents on the aromatic spacer group. To further extend the study, the imidazole groups on several of these ligands were also exchanged for 2-methylimidazole groups (except in the case of **L2**, owing to time constraints). Each of these ligands was crystallised with a variety of metal halide salts in a 1:1 molar ratio, and under various conditions. Over 900 crystallisations were carried out during this study, many of which yielded powder

precipitates, and thirty crystal structures comprising discrete metallocycles were obtained. A series of 17 homeotypic metallocyclic structures was afforded with **L1** and these are discussed in *Chapter 4*. Two crystal structures obtained with **L2** are described in *Chapter 5* and structures obtained with **L3**, **L4** and **L5** are discussed in *Chapter 6*. Only one-dimensional polymeric chain structures were obtained with ligands **L6** and **L7**, and they will not be discussed further.

2.7 NOTE ON NOMENCLATURE

Because there is some ambiguity related to the classification of a series of crystal structures that are similar in some way or another, the following terms will be defined.

Isostructural refers to compounds that crystallise in the same space group with similar unit cell dimensions and nearly identical atomic coordinates. Substitutions of small moieties are allowed such as the replacement of an hydrogen atom with a CH₃ moiety. The term is used exclusively to describe organic compounds. According to the International Union of Crystallography (IUCr): “two crystals are said to be *isostructural* if they have the same structure, but not necessarily the same cell dimensions nor the same chemical composition, and with a ‘comparable’ variability in the atomic coordinates to that of the cell dimensions and chemical composition.”²⁹

*Homeostructural*³⁰ describes a more relaxed form of isostructurality, where replacement of larger moieties is allowed. For example, in the case of clathrates with similar host substructures but containing different guest molecules in common cavities. Again this term is specific to organic compounds.

Homeotypic can be used to describe structures of inorganic compounds in which large moieties such as guest molecules in a host-guest complex are replaced.

A series of inclusion compounds can be described as *isoskeletal* when the host packing motifs are essentially isostructural (identical in structure) even though variation in the guest is possible.

In this text: the term *homeotypic* will be used to describe inorganic host-guest inclusion compounds in which the metal centres of the host metallocycles are different and the guest molecules are also varied. *Isoskeletal* will be used to describe a series of host compounds in which the metallocycles have the same chemical composition but the included guest varies.

2.8 REFERENCES

1. SMART, Bruker AXS, Inc., Madison, WI, 2003
2. SAINT, Bruker AXS, Inc., Madison, WI, 2003
3. R. Blessing, *Acta Crystallogr., Sect. A*, 1995, **51**, 33-38.
4. G. M. Sheldrick, *TWINABS*, University of Göttingen, 2008.
5. G. M. Sheldrick, *Acta Crystallogr., Sect. A*, 2008, **64**, 112-122.
6. L. J. Barbour, *J. Supramol. Chem.*, 2001, **1**, 189-191.
7. J. L. Atwood and L. J. Barbour, *Cryst. Growth Des.*, 2003, **3**, 3-8.
8. G. M. Sheldrick, SHELX Manual, <http://shelx.uni-ac.gwdg.de/SHELX/shelx.pdf>.
9. K. Yvon, W. Jeitschko and E. Parthe, *J. Appl. Cryst.*, 1977, **10**, 73-74.
10. G. R. Heal, in *Principles of Thermal Analysis and Calorimetry*, The Royal Society of Chemistry, 2002, pp. 10-54.
11. M. A. White, in *Comprehensive Supramolecular Chemistry*, eds. J. E. D. Davies and J. A. Ripmeester, Pergamon, Oxford, 1996, pp. 179-197.
12. M. L. Connolly, *J. Mol. Graph*, 1993, **11**, 139-141.
13. M. Connolly, *J. Appl. Cryst.*, 1983, **16**, 548-558.
14. M. Connolly, *Science*, 1983, **221**, 709-713.
15. B. Lee and F. M. Richards, *J. Mol. Biol.*, 1971, **55**, 379-400.
16. F. Allen, *Acta Crystallogr., Sect. B*, 2002, **58**, 380-388.
17. C. F. Macrae, I. J. Bruno, J. A. Chisholm, P. R. Edgington, P. McCabe, E. Pidcock, L. Rodriguez-Monge, R. Taylor, J. van de Streek and P. A. Wood, *J. Appl. Cryst.*, 2008, **41**, 466-470.
18. C. F. Macrae, P. R. Edgington, P. McCabe, E. Pidcock, G. P. Shields, R. Taylor, M. Towler and J. van de Streek, *J. Appl. Cryst.*, 2006, **39**, 453-457.
19. J. A. Chisholm and S. Motherwell, *J. Appl. Cryst.*, 2005, **38**, 228-231.
20. S. K. Wolff, D. J. Grimwood, J. J. McKinnon, D. Jayatilaka and M. A. Spackman, *Crystal Explorer 2.1 (381)*, University of Western Australia, Perth, 2007.
21. F. L. Hirshfeld, *Theor. Chim. Acta*, 1977, **44**, 129-138.
22. M. A. Spackman and D. Jayatilaka, *CrystEngComm*, 2009, **11**, 19-32.
23. The CrystalExplorer Manual, http://hirshfeldsurface.net/wiki/index.php/Surface_Properties, Accessed 15 Dec 2008.
24. M. A. Spackman and J. J. McKinnon, *CrystEngComm*, 2002, 378-392.
25. A. L. Spek, *Acta Crystallogr., Sect. D*, 2009, **65**, 148-155.

26. P. Van Der Sluis and A. L. Spek, *Acta Crystallogr., Sect. A*, 1990, **46**, 194-201.
27. S. J. Lee and W. Lin, *Acc. Chem. Res.*, 2008, **41**, 521-537.
28. L. Dobrzańska, G. O. Lloyd, H. G. Raubenheimer and L. J. Barbour, *J. Am. Chem. Soc.*, 2005, **127**, 13134-13135.
29. Isostructural Crystals, http://reference.iucr.org/dictionary/Isostructural_crystals.
30. M. R. Caira, in *Encyclopedia of Supramolecular Chemistry*, eds. J. L. Atwood and J. W. Steed, Marcel Dekker, Inc., New York; Basel, 2004, pp. 767-775.

CHAPTER 3

A RUDIMENTARY METHOD FOR CLASSIFICATION OF $\pi\cdots\pi$ PACKING MOTIFS FOR AROMATIC MOLECULES

This chapter forms part of a peripheral study on the classification of packing motifs resulting from $\pi\cdots\pi$ interactions in simple aromatic molecules. An abbreviated version of this study was recently published as a communication¹ and will be included as a chapter in the forthcoming "Frontiers in Crystal Engineering Volume III: The Importance of π -Interactions in Crystal Engineering". Although the work presented here is not directly related to the work on metallocycles, the concepts are of importance to those researchers who endeavour to design crystal structures. The contributions from π -interactions are often overlooked, but they can have a distinct impact on the arrangements of molecules in the solid state as well as some crystal properties. The simple and relatively robust method developed as part of the current study is illustrated with relevant examples, followed by the extension of this method to more complex aromatic systems.

3.1 INTRODUCTION

Braga and Grepioni once stated: "(Crystal) Engineering implies function-oriented design of the superstructure, selection of the building blocks (on the basis of their chemical and physical stabilities and of their extramolecular bonding capacity), their assembly and characterisation, to end with evaluation of the properties of the resulting supramolecular aggregate."^{2,3} It is generally accepted that crystal engineering is based on the concepts of molecular recognition and self-organisation. Recognition events between complementary molecular fragments give rise to the organisation of molecules in the solid state.⁴ The recognition process relies on a number of factors, including hydrogen bonding between molecular functional groups, complementary geometry of molecules and other possible directing factors. Self-organisation is the basis upon which condensed matter is formed and the mechanisms are generally complex. Statistical analysis of structures retrieved from databases, combined with theoretical modelling, and implementation of these results into experimental work is a prerequisite for understanding intermolecular interactions.⁵ Much of the focus in crystal engineering has been directed towards the use of noncovalent interactions in the form of hydrogen bonds. With the establishment of a list of reliable supramolecular synthons^{6,7} it has become increasingly common to use these synthons since it is relatively easy to control desired outcomes. This would not have been possible without the extensive examination of organic (and inorganic) compounds obtained from the Cambridge Structural Database⁸ (CSD) as well as carefully planned experimental work. Along with the recognition of these supramolecular synthons, some researchers have gone further in an attempt to establish a hierarchy⁷ within known synthons. Although many of these synthons have proven

to be relatively predictable and reliable, most researchers tend to underestimate the effects of π -interactions in the construction of packing motifs. This is understandable since much of this work has involved cocrystal structures of relatively small molecules. So what do π -interactions have to do with all of this? For effective supramolecular design we need to understand all aspects of the interactions involved, and what effect these interactions may have on the properties of a material. Of course it can be argued that $\pi\cdots\pi$ interactions have little effect on the packing of molecules in a crystal and are simply the result of an arrangement enforced by stronger interactions. However, one should keep in mind that crystal structures are most often a compromise between many stabilising and destabilising interactions that cannot be separated. The existence of polymorphs shows that more than one crystalline form of a particular molecule or molecules may exist and that different interactions may be involved. Kinetic and thermodynamic reaction products may also exhibit dissimilar arrangements.

If the manner in which $\pi\cdots\pi$ interactions occur could be better understood, the implications would be significant since many processes involve these types of interactions. Many biological processes appear to be governed by molecular recognition of aromatic moieties, including DNA functionality and protein and enzyme activity. There is also much interest in optical properties that are often associated with aromatic compounds that most probably utilize $\pi\cdots\pi$ interactions. New insights could lead to more rational approaches to the economical design of new functional materials, which would be beneficial to a number of industries, particularly pharmaceutical and electronics manufacturers.

Despite much interest, the characterization of π -interactions is still complicated because they can be difficult to identify, mainly because they act over long ranges and there are multiple points of contact,⁹ making them relatively non-directional compared to other intermolecular interactions. π -Interactions are also difficult to identify in the solid state since there is very little overlap of the interacting atomic orbitals and the range of interaction is ill-defined. In fact overlap of the orbitals would probably lead to repulsion rather than attraction between atoms in most instances.¹⁰

3.2 THEORETICAL MODELS

A number of models have been used to describe $\pi\cdots\pi$ interactions, including the solvophobic model, the electron donor-acceptor model and the atomic charge model.¹¹ Hunter and Sanders¹¹ described an electrostatic model that suggests that the major energy components in

$\pi\cdots\pi$ interactions consist primarily of electrostatic and van der Waals components. In solution, the association and desolvation energies would play a role in the interaction between two molecules, but there would also be a large van der Waals contribution.¹¹ If we consider the equation for van der Waals interaction between two molecules that can be applied to crystals,

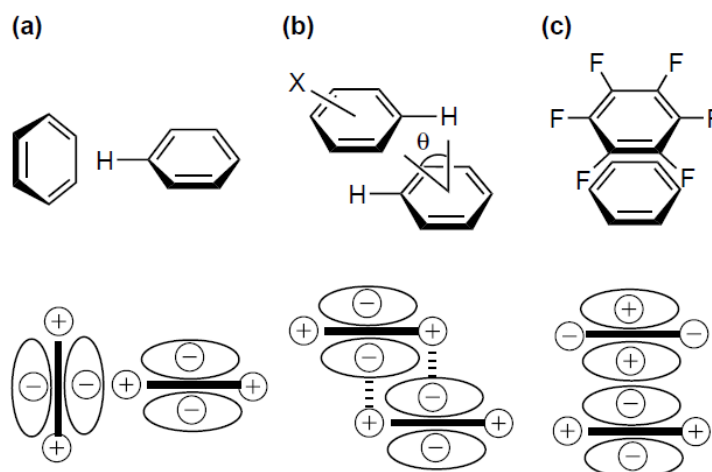
$$E_{\text{van der Waals}} = \sum_{ij} \left\{ A_{ij} \exp(-\alpha_{ij} r_{ij}) - \frac{C_{ij}}{r_{ij}^6} \right\}$$

then the interaction would be approximately proportional to the area of π -overlap.¹¹ However, if this is the primary force controlling the geometry of the interaction then molecules would maximise π -overlap, resulting in parallel stacking. Experimentally this is not observed; offset arrangements are favoured, along with edge-to-face interactions. Therefore, there must be a large electrostatic barrier to π -overlap.¹¹ Hunter and Sanders established three rules/guidelines¹¹ to explain the three types of $\pi\cdots\pi$ associations observed between neighbouring molecules. (1) $\pi\cdots\pi$ repulsion dominates in face-to-face geometry; (2) $\pi\cdots\sigma$ attraction dominates in edge-to-face geometry; (3) $\pi\cdots\sigma$ attraction dominates in an offset face-to-face arrangement. The insertion of heteroatoms into aromatic π -systems affects the polarisation of the molecule and thus the electrostatic interaction. Since like repels like, it is possible for molecules with slight polarisation to assemble in a manner that results in favourable face-to-face interactions. A further three rules have been introduced to include polarisation effects:¹¹ (4) charge-charge interactions dominate in interactions between highly charged atoms; (5) favourable interaction with a neutral or weakly polarised site requires the following π -polarisation: (a) a π -deficient atom in a face-to-face geometry (b) a π -deficient atom in the vertical T-group in the edge-to-face geometry and (c) a π -rich atom in the horizontal T-group in the edge-to-face geometry; (6) favourable interaction with a neutral or weakly polarised site requires the following σ -polarisation: (a) a positively charged atom in a face-to-face geometry, (b) a positively charged atom in the vertical T-group in the edge-to-face geometry and (c) a negatively charged atom in the horizontal T-group in the edge-to-face geometry. For a nontheoretical chemist it would be simpler to just consider that aromatic systems maintain π -delocalised electron density.¹² Stabilising dispersion interactions between aromatic molecules and their neighbours are enhanced by the fact that the π -electron density is polarisable. This polarisation can be further enhanced with the inclusion of more

polarisable (larger Z) atoms in π -delocalised bonding.¹² These stabilisations make the contributions from van der Waals interactions to the molecular stabilisation more favourable for π -delocalised aromatic molecules than analogues without such bonds.¹² An electrostatic component provides directionality to the interaction. Because there is minimal polarisation of C–H bonds in aromatic hydrocarbons there is a slightly negative charge over the π -core compared to the slightly positive edge of hydrogen atoms. This slight polarisation may or may not introduce a molecular dipole, depending on the molecular structure, but it will introduce higher multipoles.¹²

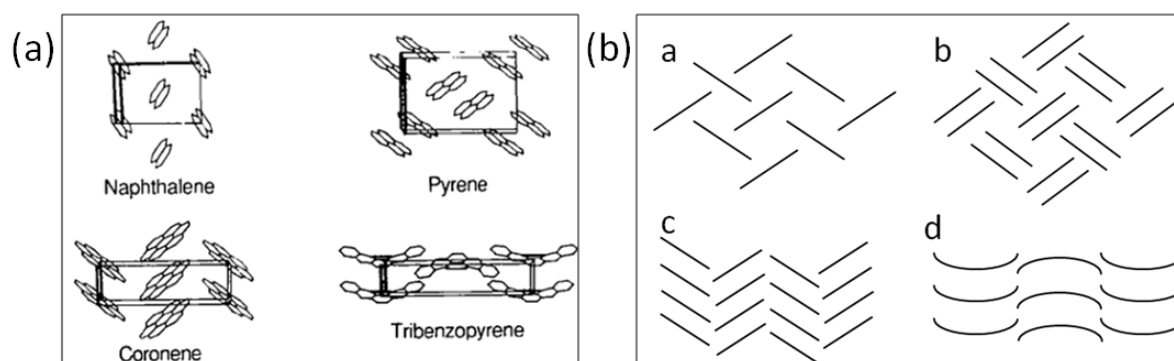
3.3 $\pi\cdots\pi$ INTERACTIONS

What exactly is considered a π -interaction? Currently it is considered to be any close contact between any π or delocalised electron system and a donor atom or another π -system. The donor could take the form of a strong donor atom (e.g. O, N), or a weaker donor such as C–H, an anion,¹³ or another π -system. These π -systems could be aromatic rings or alkene or alkyne moieties. The focus here is on interactions between aromatic moieties. In general, aromatic systems tend to be planar molecules (also alkene and alkyne moieties) with large surface-to-volume ratios. Because of their shape, there is a tendency for supramolecular space to surround the edges of these molecules.¹² The most reasonable packing arrangement for these molecules then, considering the concept of close packing,¹⁴ is for the molecules to stack on top of one another. According to experimental data this is actually the most uncommon packing arrangement in the solid state. Aromatic $\pi\cdots\pi$ interactions are known to associate with their nearest neighbours in one of three ways: face-to-face (also known as eclipsed face-to-face) stacking, offset face-to-face (or slipped or skewed) stacking and edge-to-face (also referred to as T-shaped or edge-on) (Scheme 3.1)



Scheme 3.1 Geometries of aromatic interactions. Reprinted from *Curr. Opin. Chem. Biol.*, 2002, 6, 736-741,¹⁵ © 2002, with permission from Elsevier.

The accepted plane separation for face-to-face and offset face-to-face interactions is currently 3.3–3.8 Å, while a centroid-to-centroid distance up to 5 Å is acceptable for edge-to-face interactions. Four distinct packing motifs arise from the associations between neighbouring molecules (Scheme 3.2). The rare occurrence of face-to-face stacking promotes the assembly of a graphitic-type layering, referred to as the β -motif. Edge-to-face interactions contribute to the formation of the well-known herringbone motif. Offset stacking, as well as edge-to-face interactions, are observed in the sandwich-herringbone motif, where molecules stack in pairs. The sandwich-herringbone is considered an intermediate between the herringbone motif and the γ -motif. In the γ -motif, molecules form infinite stacks along one direction and a form of herringbone motif along another direction.



Scheme 3.2 The four basic aromatic crystal packing motifs (a) as exemplified by naphthalene (herringbone), coronene (γ), pyrene (sandwich) and tribenzopyrene (β) and a diagrammatic representation of the a) herringbone, b) sandwich-herringbone, c) gamma (γ) and d) beta (β) packing motifs (b). Reproduced from reference 16 with permission from The Royal Society of Chemistry © 1989.

3.4 STRUCTURE PREDICTION AND COMPARISONS

Desiraju and Gavezzotti¹⁷ successfully predicted the packing arrangement of a number of polynuclear aromatic hydrocarbons (PAHs). PAHs are known to crystallise in one of four possible structural arrangements: herringbone, sandwich-herringbone, γ - or β -structures. From their investigation of 32 PAHs, Desiraju and Gavezzotti deduced that the length of the short axis of the unit cell is instrumental in determining the ultimate packing type assumed by the molecules. If one considers PAHs, there are three possible interaction types: C \cdots C, C \cdots H and H \cdots H. C \cdots C interactions are optimised between parallel molecules stacked at van der Waals separation, whereas C \cdots H interactions are more effective between inclined molecules.¹⁷ From this we infer that the β - and γ -structures are rich with C \cdots C interactions, and C \cdots H interactions are prevalent in the herringbone motif, while both C \cdots C and C \cdots H interactions are observed to a similar extent in the sandwich-herringbone packing mode.¹⁷ From these observations it appears that, within a PAH, there are certain areas of the molecular surface that contribute to the molecule's propensity to pack in a specific manner. Part of the surface is considered glide (or herringbone) promoting, while the other part would be stack (or layer) promoting, depending on the location within the molecule.¹⁶⁻¹⁸ It was rationalised that "it may be expected that whenever similar shapes are found in organic compounds, the effects on crystal structure should be the same, even if the compounds are not pure aromatic hydrocarbons"¹⁷ and concluded that this same method could be used for heteroatomic derivatives of the PAHs if the C atoms are replaced by heteroatoms such as N, O, S and P.

More than a decade later, Spackman and coworkers^{19,20} revisited the abovementioned study employing the program CrystalExplorer²¹ to substantiate the molecular free surface analyses. Fingerprint plots¹⁹ (2D representations of surface contacts) are useful in a visual comparison of similar molecules. Such plots are easily comparable in a series of PAHs,²⁰ if one considers their characteristic features.¹⁹ In comparing the series of PAHs, one observes the characteristic C–H $\cdots\pi$ wings located symmetrically on the sides of the plot and how these slowly withdraw as the PAHs progress to larger fused rings. As the C–H $\cdots\pi$ wings slowly withdraw, C \cdots C interactions appear in the characteristic region (± 1.8 Å, typical van der Waals radius). A metric multidimensional scaling (MMDS) plot was also used to make more quantitative comparisons.

To expand on the contributions of Desiraju and Gavezzotti,^{16,17} and building on the work carried out by Parkin et al.,²⁰ the packing motifs of N-aromatic and polyaromatic molecules

were extracted from the CSD to be examined with CrystalExplorer. It was thought that these molecules could contribute to the systematic examination of the effects on intermolecular interactions by the incorporation of heteroatoms into polyaromatic hydrocarbons. The inclusion of N atoms in these molecules would certainly alter the polarisation of the molecule, and therefore the molecular dipole, and then perhaps the packing motif as well. As yet, no theoretical studies have been performed to support this conjecture.

3.5 $\pi\cdots\pi$ INTERACTIONS IN HETEROAROMATIC MOLECULES

As an alternative to the somewhat complex analysis by Desiraju and Gavezzotti to predict the packing motifs of some heteroaromatic molecules, we used CrystalExplorer and fingerprint plots without extensive calculations (i.e. a more qualitative rather than quantitative approach). Firstly the 32 PAH structures from the previous studies were analysed and Hirshfeld Surfaces and fingerprint plots generated. The fingerprint plots were then deconstructed into the relative contributions of various interactions (%C \cdots H, %H \cdots H and %C \cdots C) and the ratio of %C \cdots H to %C \cdots C was calculated (see Table 3.1). These results were then analysed for any visible trends and compared to the actual packing motifs. The herringbone structures all have ratios greater than 4.5. Sandwich motifs fall in the range of 3.2–4.0; γ -motifs in the range 1.2–2.7 (the outlier at 7.9 is due to the presence of a nonaromatic molecule) and β -motifs are in the range 0.46–1.0 (with a few outliers) (Figure 3.1). Following this examination, the CSD was mined for N-derivatives of benzene, naphthalene and anthracene, which were analysed in a similar manner (Scheme 3.3).

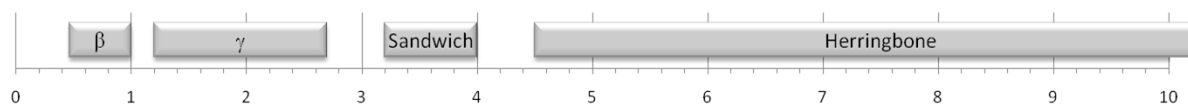


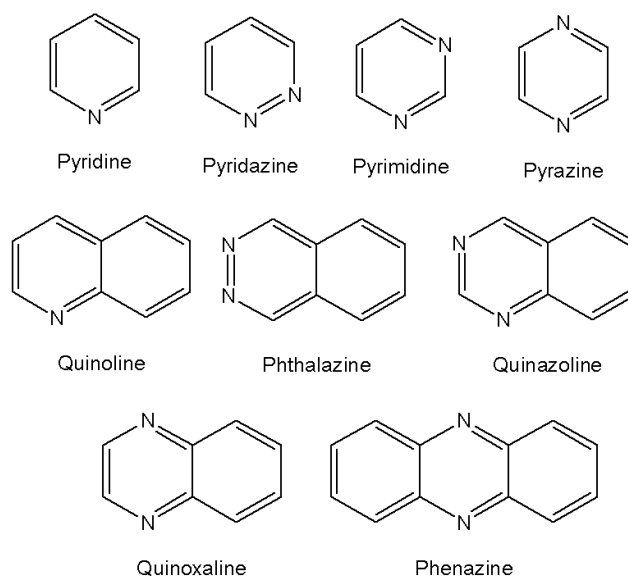
Figure 3.1 Bar chart showing the ratios of (%C \cdots H)/(%C \cdots C) interactions and the corresponding packing motifs of the PAHs.

It should be noted that the incorporation of nitrogen into the molecules allows for C–H \cdots N interactions that are still relatively weak, but stronger than the π -interactions being investigated. A heteroatom in the molecule means that there will be additional contacts possible between adjacent molecules in the form of N \cdots H, C \cdots N and N \cdots N interactions. These will, of course, skew relative contributions from the other types of interactions, although we expect that the (%C \cdots H)/(%C \cdots C) ratio will still provide us with important comparative data (Table 3.2).

Chapter 3: A Rudimentary Method for Classification of $\pi\cdots\pi$ Packing Motifs for Aromatic Molecules

Table 3.1 Summary of results obtained for PAHs used in previous studies arranged according to ratio %C \cdots H/% C \cdots C

COMPOUND	REFCODE	%C \cdots H	%C \cdots C	Ratio (%C-H/%C-C)	Motif Observed
Benzene (1)	BENZEN11	35.7	0	Infinite	Herringbone
Biphenyl (5)	BIPHEN04	48.1	0	Infinite	Herringbone
Quaterphenyl (12)	QUPHEN	56.7	0	Infinite	Herringbone
Dibenzanthracene (11)	DBNTHR02	59.2	0.1	592.00	Herringbone
Chrysene (8)	CRYSEN	58.0	0.4	145.00	Herringbone
Picene (10)	ZZZOYC01	60.1	0.5	120.20	Herringbone
Phenanthrene (4)	PHENAN08	51.0	0.5	102.00	Herringbone
Naphthalene (2)	NAPHTA10	45.1	0.6	75.17	Herringbone
Anthracene (3)	ANTCEN	49.1	1.8	27.28	Herringbone
18-Annulene (19)	ANULEN	37.9	4.8	7.90	γ
Triphenylene (6)	TRIPHE11	41.7	8.7	4.79	Herringbone
Benzo[<i>c</i>]phenanthrene (9)	BZPHAN	38.0	9.2	4.13	Herringbone
1,2-Benzopyrene (38)	CEQGEL	41.9	10.5	3.99	Sandwich
Benzperylene (15)	BNPERY	44.3	11.8	3.75	Sandwich
Perylene (14)	PERLEN01	42.3	11.8	3.58	Sandwich
Pyrene (13)	PYRENE02	36.6	10.8	3.39	Sandwich
Quaterrylene (17)	QUATER10	49.4	15.1	3.27	Sandwich
Diperinaphthyleneanthracene (32)	NAPANT01	40.4	13.8	2.93	β
Dibenzoperylene (20)	DBPERY	39.7	14.9	2.66	γ
Tetrabenzoperylene (29)	TBZPER	34.0	17.5	1.94	β
Kekulene (26)	KEKULN10	36.8	21.9	1.68	γ
Coronene (21)	CORONE	30.7	19.5	1.57	γ
Hexabenzocoronene (25)	HBZCOR01	36.2	24.8	1.46	γ
Benzopyrene (18)	BNPYRE10	25.0	19.3	1.30	γ
Ovalene (24)	OVALEN01	30.3	24.2	1.25	γ
Tribenzopyrene (27)	TBZPYR	21.2	22.1	0.96	β
Anthrabenzonaphthopentacene (31)	BOXGAW	15.0	31.4	0.48	β
Dibenzocoronene (42)	YOFCUR	16.2	34.9	0.46	β
Benzanthracene (7)	BEANTR	Structure incomplete (no H-atoms)			Herringbone
Dinaphthoanthracene (16)	DNAPAN	Structure incomplete (no H-atoms)			Sandwich
Benzobisanthrene (22)	BEANTH	3D Coordinates unavailable			γ
Dibenzocoronene (23)	DBZCOR	no H-atoms			γ
Violanthrene (28)	CORXAI10	no H-atoms			β
Diphenanthroperylene (30)	NAPPYR01	no H-atoms			β

Chapter 3: A Rudimentary Method for Classification of $\pi\cdots\pi$ Packing Motifs for Aromatic Molecules

Scheme 3.3 Structural diagrams of the nine N-aromatic compounds selected from the CSD for the purposes of this study.

Table 3.2 Summary of results obtained from fingerprint plot analysis arranged according to ratio (%C \cdots H/%C \cdots C).

COMPOUND	REFCODE	%C \cdots H	%C \cdots C	Ratio (%C \cdots H/%C \cdots C)	Motif Observed
N-Heterocycles					
Pyridine (Form II)	PYRDNA03	32.6	0.1	326.0	Herringbone
Quinoline	EDAVUA	39.3	0.4	98.3	Herringbone
Pyridine (Form I)	PYRDNA01	28.4	0.5	56.8	Herringbone
Phenazine (Form β)	PHENAZ11	29.1	7.5	3.9	Sandwich
Phenazine (Form α)	PHENAZ04	25.9	8.4	3.1	γ
Pyridazine	VOBJEB ²²	12.1	4.2	2.9	γ
Phthalazine	DAZNAP	23.8	8.5	2.8	Sandwich
Pyrimidine	PRMDIN01 ²³	9.3	5.7	1.6	γ
Quinazoline	QUINAZ	14.5	9.0	1.6	γ
Pyrazine	PYRAZI01 ²⁴	9.9	6.2	1.6	γ
Quinoxaline	HEYJOK01	10.3	11.3	0.9	γ - β
Cocrystals					
Hydroquinone + Pyrazine	QAMQUR	15.9	0.0	Infinite	Herringbone
Hydroquinone + Pyridine	ACESIL	24.7	2.0	12.4	Unknown
Hydroquinone + Pyridine	QAMRIG	20.1	10.4	1.9	γ
Hydroquinone + Quinoxaline	QEMKAV	19.2	11.1	1.7	γ
Hydroquinone + Phenazine	FOQHEY	18.3	15.8	1.2	γ

Pyridine has been reported in two polymorphic forms, both of which crystallise in orthorhombic space groups: Form I (PYRDNA01²⁵) in $Pna2_1$ and Form II (high pressure, PYRDNA03²⁶) in $P2_12_12_1$.

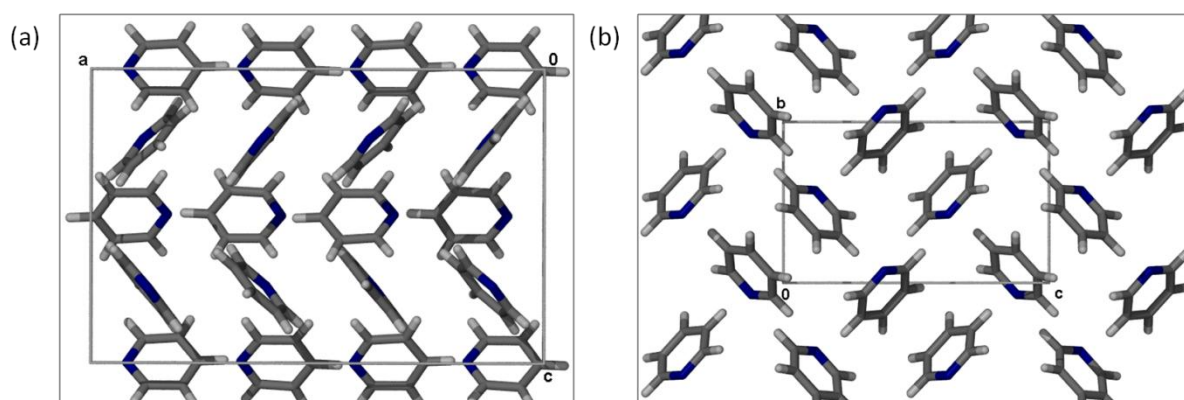


Figure 3.2 Herringbone motifs of the two forms of pyridine, (a) Form I (PYRDNA01), and (b) Form II (PYRDNA03).

It can reasonably be expected that the packing of pyridine would be similar to that of benzene and this is true to some extent. Both forms of pyridine assume the herringbone motif in the solid state (Figure 3.2). However, the angles at which the associated molecules interact are quite different, with the C–H of one pyridine molecule directed more towards the N-atom than the ring of its nearest neighbour.

The diazo-derivatives of benzene are slightly different; all three pack in a γ -motif (Figure 3.3). This is not completely unexpected since the polarisations of these three molecules are different from that of pyridine as well as each other. With a change in polarisation the molecules are able to orientate themselves in such a way that $\pi\cdots\pi$ stacking becomes more favourable, and herringbone interactions are still possible owing to the small size of the molecules.

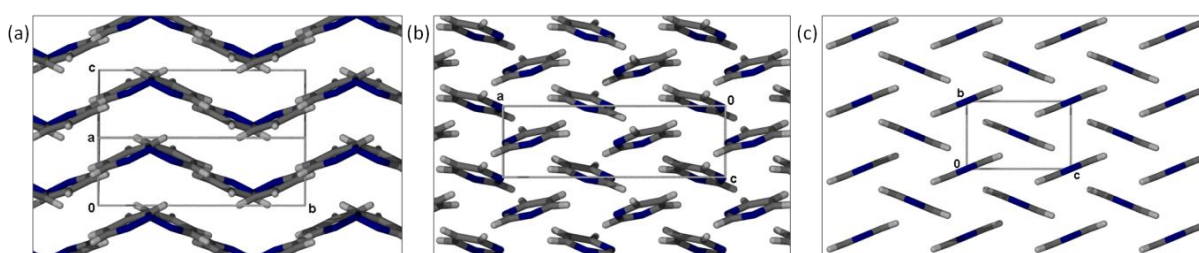


Figure 3.3 The γ -motifs found in the diazobenzene molecules (a) pyridazine VOBJEB²², (b) pyrimidine PRMDIN01²³ and (c) pyrazine PYRAZI01.²⁴

Quinoline (EDAVUA²⁷), with only one N atom, but a fused aromatic system, once again assumes a herringbone motif (Figure 3.4), while the diazanaphthalene derivatives progress from sandwich, to γ -motifs as the nitrogen atoms change positions around the ring. An interesting observation is that the molecules of phthalazine (DAZNAP²⁸) and quinazoline

(QUINAZ²⁹) are orientated at 180° to each other in forming the offset stacks in the sandwich and γ -motifs. However, quinoxaline (HEYJOK01³⁰) molecules are simply stacked in a slightly offset manner (Figure 3.5).

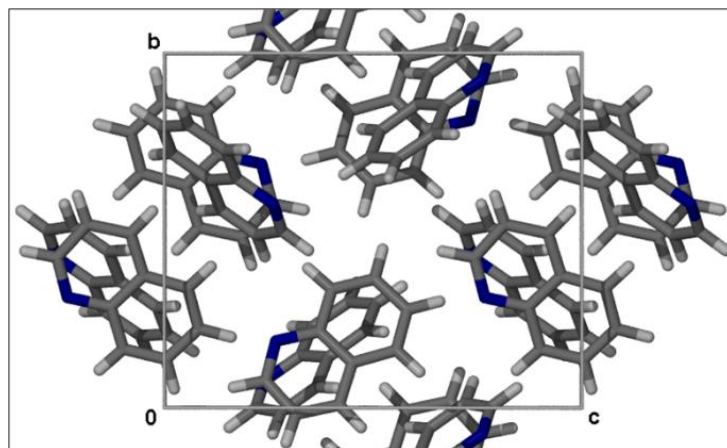


Figure 3.4 Herringbone motif of quinoline, EDAVUA.

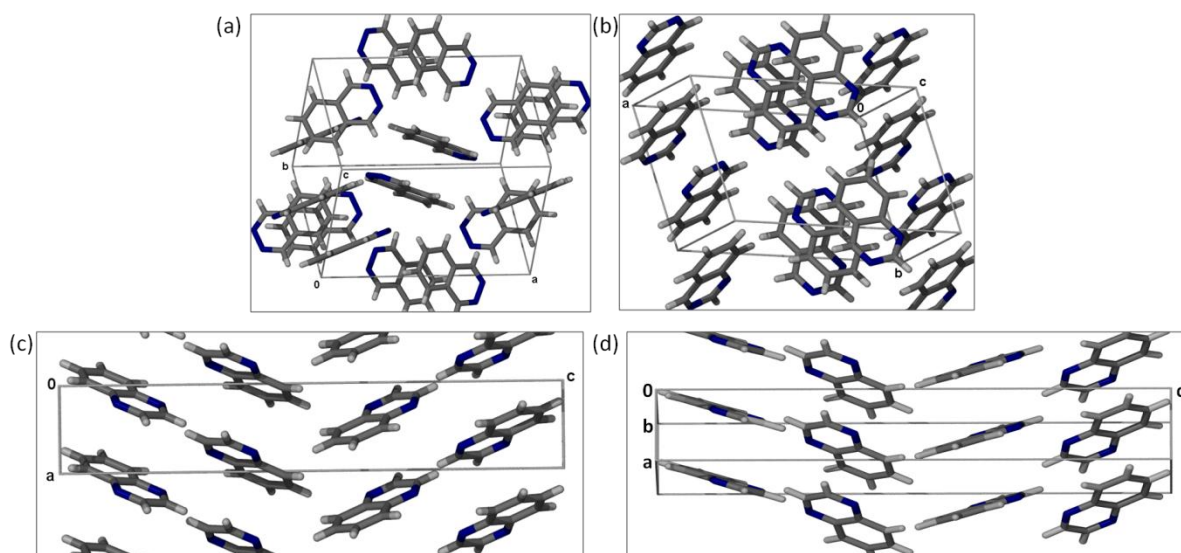


Figure 3.5 Sandwich-herringbone motif of phthalazine (DAZNAP, (a)), γ -motifs of quinazoline (QUINAZ, (b)) and quinoxaline (HEYJOK01, (c) and (d))

Phenazine crystallises in two forms: the α -form (PHENAZ04³¹) and the β -form (PHENAZ11³²). Both crystallise in $P2_1/n$, although with quite different unit cell parameters. The α -form packs in the γ -motif, while the β -form takes on the sandwich-herringbone motif (Figure 3.6). This is an important observation, since the same molecule assumes very different packing motifs. The polymorphism of phenazine may be a result of the solvents from which the crystals were grown or various other variables, such as temperature, stoichiometries and so on.

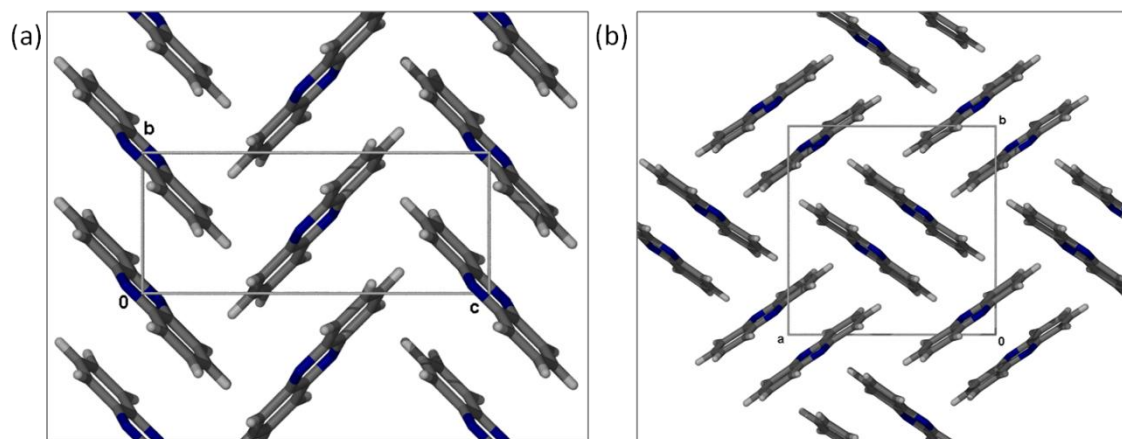


Figure 3.6 The α -form of phenazine (PHENAZ04, (a)) in the γ -motif and the β -form of phenazine (PHENAZ11, (b)) in the sandwich-herringbone motif.

From these structural analyses it can be said that the polarisation of the molecule seems to have an impact on the packing motif. Furthermore, the number of N atoms in the molecule appears to affect the motif as both the structures of pyridine and quinoline adopt the herringbone motif, while the diaza-derivatives adopt either the sandwich-herringbone or γ -motif. Whether this is due to the increased polarisation or the possibility of slightly stronger C–H \cdots N interactions is still to be determined.

3.6 $\pi\cdots\pi$ INTERACTIONS IN COCRYSTALS

To what extent are $\pi\cdots\pi$ interactions able to control molecular packing in the presence of strong hydrogen bond donors and/or acceptors? To address this question, cocrystal structures from the CSD have been compared. The combination of hydroquinone and pyridine has afforded two different forms. One form (ACESIL³³) consists of a 1:1 ratio that crystallises in $P\bar{1}$, while the other consists of a 1:2 ratio of hydroquinone to pyridine (QAMRIG³⁴) that crystallises in the monoclinic space group $P2_1/c$. In the first form the asymmetric unit (ASU) comprises two symmetry-independent half molecules of hydroquinone located on inversion centres, as well as an entire pyridine molecule. One of the hydroquinone molecules forms hydrogen bonds to two pyridine molecules, while the second hydroquinone molecule links these heterotrimers via O–H \cdots O interactions to the first hydroquinone molecule (Figure 3.7). In this structure it appears that the hydrogen bonds play a dominant role in the molecular arrangement, but there is still a discernable herringbone motif. Indeed, this herringbone motif is substantiated by the fingerprint plot analysis. In the other form (QAMRIG) the components form a heterotrimer between hydroquinone and pyridine, and these pyridine molecules stack in an \cdots ABAB \cdots pattern along the c axis (Figure 3.8). This arrangement is consistent with the γ -motif and is also supported by fingerprint analysis.

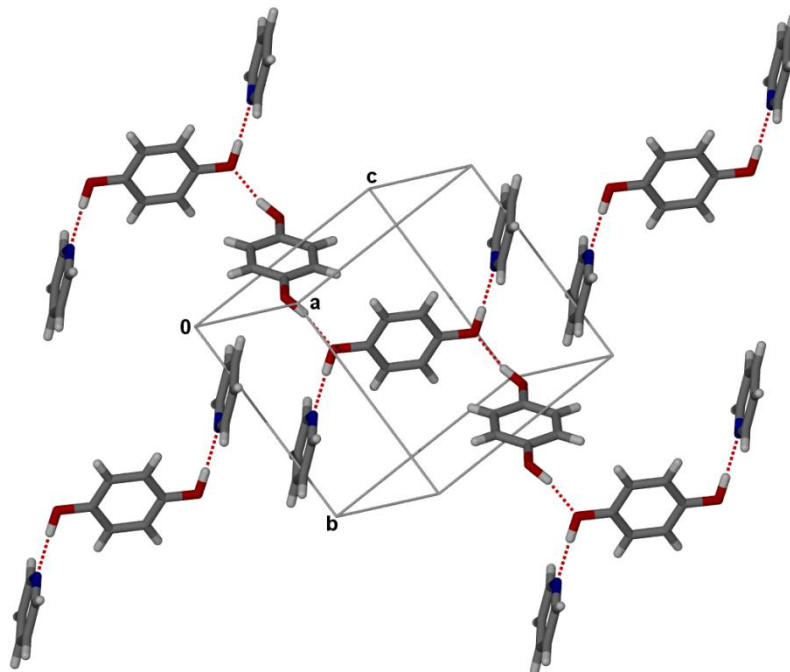


Figure 3.7 Partial packing arrangement of ACESIL showing the hydroquinone-linked heterotrimers.

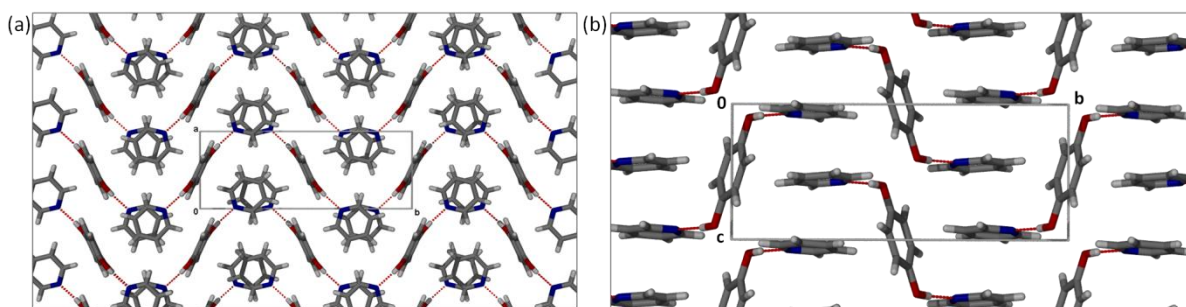


Figure 3.8 Packing arrangement of QAMRIG demonstrating the stacking of pyridine molecules when viewed down (a) [001] and (b) [100].

The cocrystal of hydroquinone with pyrazine (QAMQUR³⁴) crystallises in the monoclinic space group $P2_1/c$ with each molecule located on an inversion centre (i.e. half of each is present in the ASU). It is easy to see that hydrogen bonds form between the O–H moiety of the hydroquinone molecule and the N atoms of the pyrazine molecules to form one-dimensional polymeric chains (Figure 3.9). In this structure $\pi\cdots\pi$ interactions do not seem to play a substantial role in the arrangement of the molecules, and the fingerprint plot analysis is consistent with a herringbone motif for the pyrazine molecules.

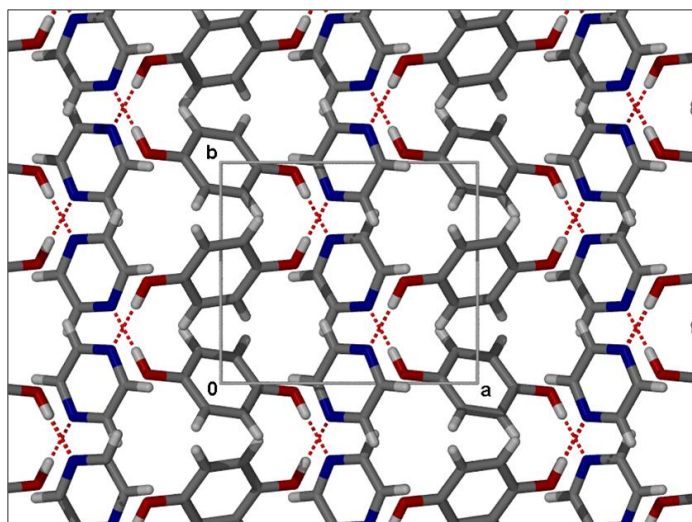


Figure 3.9 Packing arrangement of QAMQUR viewed along [001]

We now consider the structure of the cocrystal of hydroquinone and quinoxaline (QEMKAV³⁵). It crystallises in the triclinic space group $P\bar{1}$, with half a molecule of hydroquinone, located on an inversion centre, and an entire molecule of quinoxaline in the ASU. Although there are two possible acceptor sites for O–H \cdots N hydrogen bonds, only one such interaction is present, resulting in a heterotrimer. These adducts are then linked via $\pi\cdots\pi$ stacking of the quinoxaline molecules that are orientated antiparallel relative to one another (Figure 3.10). The quinoxaline molecules stack in an \cdots ABAB \cdots fashion with plane separations of 3.39 Å and 3.49 Å.

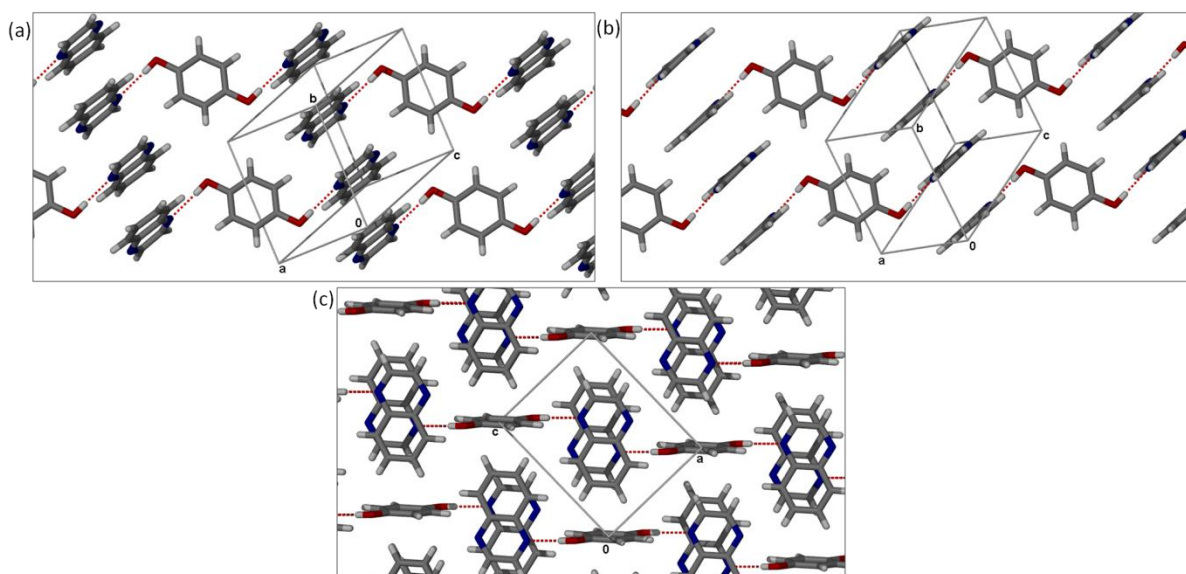


Figure 3.10 The packing arrangement of QEMKAV, demonstrating the γ -motif of the phenazine molecules

To extend this comparison one step further, we examined the cocrystal of hydroquinone and phenazine (FOQHEY³⁶) (Figure 3.11). This structure also assumes the triclinic space group $P\bar{1}$ with half a molecule of hydroquinone and an entire molecule of phenazine in the

ASU. As in the previous structure, hydroquinone hydrogen bonds to phenazine in a 1:2 ratio, forming similar heterotrimers. The phenazine molecules then stack down the *a* axis in an \cdots ABAB \cdots fashion with plane separation of 3.50 Å and 3.47 Å.

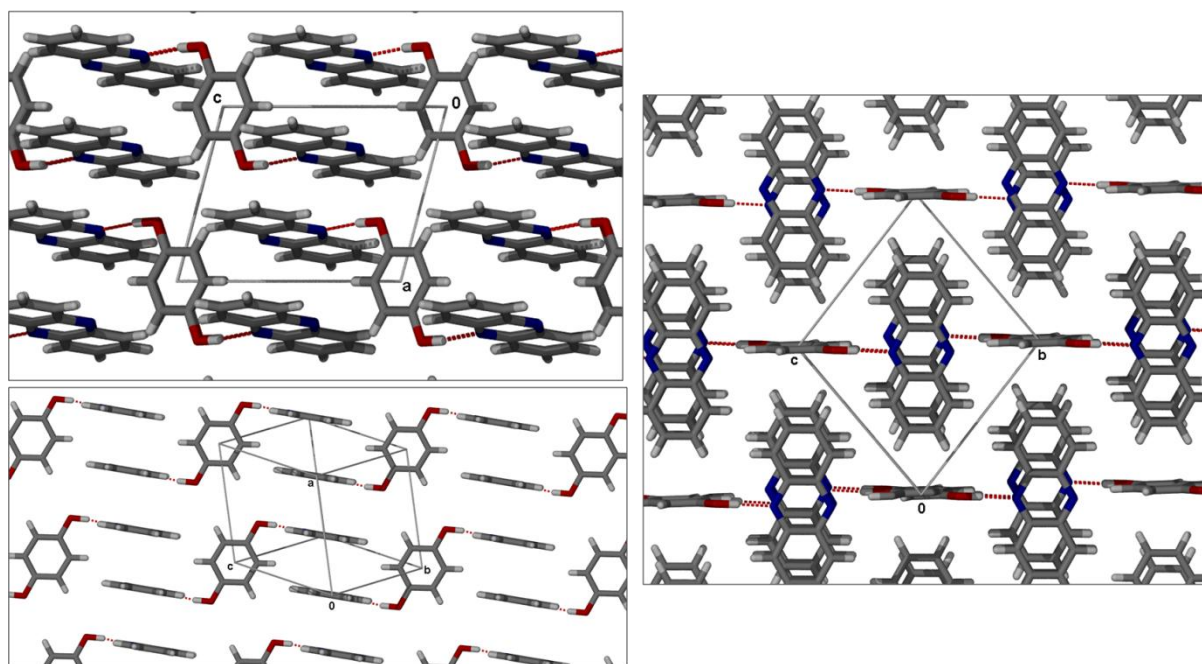


Figure 3.11 Stacking of phenazine molecules in the cocrystal FQOHEY

It might be expected that the stronger hydrogen bonds would be more influential in directing molecules into specific packing motifs. However, in these examples the extension of one aromatic molecule appears to affect the entire arrangement of molecules as a result of increased $\pi\cdots\pi$ interactions. It could be argued that the cocrystals obtained are but one form of many possible and thus no conclusions can be made. However the same could be said for the single-component crystal structures and the fact that these structures are found in the literature may have some bearing on the matter.

Sarma *et al.*³⁷ also highlighted the impact of $\pi\cdots\pi$ interactions in other cocrystals containing phloroglucinol and phenazine. They demonstrated that four different forms can be obtained from the same components; three forms (Figure 3.12) were obtained concomitantly while a fourth was obtained from a different starting stoichiometry. They observed that there was a gradual increase in significance of $\pi\cdots\pi$ stacking with an increasing ratio of phenazine (1:1.5, 1:1.75, 1:2) in the resultant cocrystals. They also identified a corresponding reduction in interplanar separation. The increase in $\pi\cdots\pi$ interactions also brought about a decrease in hydrogen bonding.

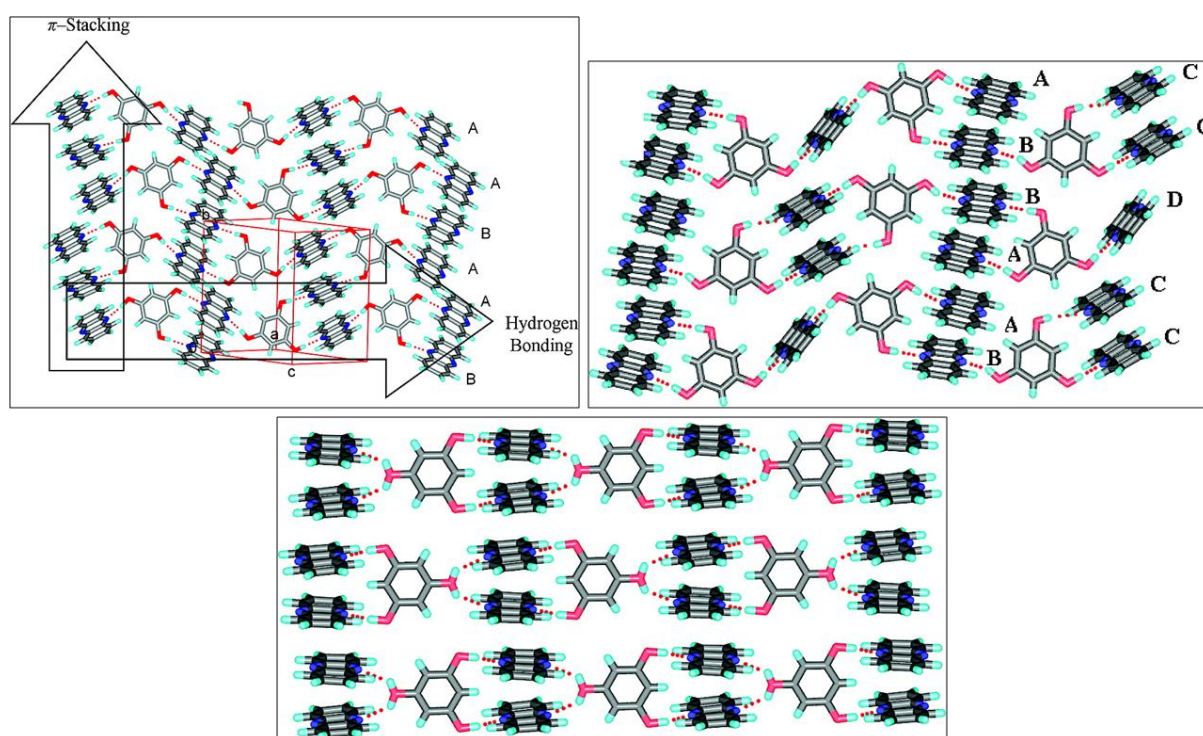


Figure 3.12 Packing motifs of cocrystals 1-3 as reported in reference 37. Reprinted with permission from © 2008 American Chemical Society.

With only limited data available for cocrystals of this type, it is difficult to make any generalisations about the impact of $\pi\cdots\pi$ interactions on the packing motifs of these molecules. However, for this series of hydroquinone cocrystals there appears to be a trend towards more pronounced $\pi\cdots\pi$ interaction with increasing surface area of the aromatic molecules. This suggests that there may be a cumulative effect of aromatic interactions that are influential enough to disrupt stronger hydrogen bonds in crystal structures that involve aromatic molecules.³³ Because strong hydrogen bonds in cocrystals are often dominant, the effects of π -interactions may be overlooked. However, using fingerprint plot deconstruction it is possible to distinguish certain motifs without a great deal of effort.

3.7 SUMMARY

From a theoretical perspective it has been established that π -interactions comprise primarily van der Waals interactions with a contribution from electrostatic forces. Because of these energy contributions, there are three possible associations between neighbouring molecules, namely face-to-face, offset face-to-face, or edge-to-face. These associations, in turn, lead to four possible packing motifs: herringbone, sandwich-herringbone, γ - and β -motifs. These associations and motifs have been examined in a number of carbon-based PAHs to establish the necessary criteria that give rise to one of the four motifs in the solid state. With a view to

applying these criteria to slightly polarised polyaromatic molecules, a more simplified method was employed. In this case N-containing small aromatic molecules were selected from the CSD. The polarisation of these molecules may be slightly different from one another depending on the number and positions of the N atoms in the aromatic system. An adjustment in polarisation is believed to contribute to more favourable face-to-face interactions and this is observed in the structures of pyridine as compared to the diazobenzenes (pyridazine, pyrimidine and pyrazine), and is also comparable to the fused-ring systems of quinoline and the diazonaphthalenes (phthalazine, quinazoline and quinoxaline).

In cocrystals the presence of stronger hydrogen bonds may overshadow π -interactions and the analysis used here becomes more significant in determining structural motifs. In the cocrystals presented here it appears that $\pi\cdots\pi$ interactions between the N-aromatic rings play a more significant role as the number of fused rings increases.

It has been demonstrated that fingerprint plots generated in CrystalExplorer can be used to rapidly and semi-quantitatively compare structures to identify packing motifs by means of a simple ratio calculation. Although only a limited number of structures are presented here, the potential of a simple database search and in-depth examination of more obscure trends or structural motifs is vast.

3.8 REFERENCES

1. L. Loots and L. J. Barbour, *CrystEngComm*, 2012, **14**, 300-304.
2. D. Braga, L. Maini, M. Polito, E. Tagliavini and F. Grepioni, *Coord. Chem. Rev.*, 2003, **246**, 53-71.
3. D. Braga and F. Grepioni, in *Encyclopedia of Supramolecular Chemistry*, eds. J. L. Atwood and J. W. Steed, Marcel Dekker, Inc., New York; Basel, 2004, pp. 357-363.
4. C. B. Aakeröy and K. R. Seddon, *Chem. Soc. Rev.*, 1993, **22**, 397-407.
5. C. B. Aakeröy, *Acta Crystallogr., Sect. B.*, 1997, **53**, 569-586.
6. G. R. Desiraju, *Angew. Chem., Int. Ed., Eng*, 1995, **34**, 2311-2327.
7. T. R. Shattock, K. K. Arora, P. Vishweshwar and M. J. Zaworotko, *Cryst. Growth Des.*, 2008, **8**, 4533-4545.
8. F. Allen, *Acta Crystallogr., Sect. B.*, 2002, **58**, 380-388.
9. C. A. Hunter, K. R. Lawson, J. Perkins and C. J. Urch, *J. Chem. Soc., Perkin Trans.*, 2001, 651-669.
10. A. K. Tewari and R. Dubey, *Bioorg. Med. Chem.*, 2008, **16**, 126-143.
11. C. A. Hunter and J. K. M. Sanders, *J Am Chem Soc*, 1990, **112**, 5525-5534.

12. I. Dance, in *Encyclopedia of Supramolecular Chemistry*, eds. J. L. Atwood and J. W. Steed, Marcel Dekker, Inc. , New York; Basel, 2004, pp. 1076-1092.
13. T. J. Mooibroek, P. Gamez and J. Reedijk, *CrystEngComm*, 2008, **10**, 1501-1515.
14. D. V. Soldatov and I. S. Terekhova, *J. Struct. Chem.*, 2005, **46**, S1-S8.
15. M. L. Waters, *Curr. Opin. Chem. Biol.*, 2002, **6**, 736-741.
16. G. R. Desiraju and A. Gavezzotti, *Acta Crystallogr., Sect. B*, 1989, **45**, 473-482.
17. G. R. Desiraju and A. Gavezzotti, *J. Chem. Soc., Chem. Commun.*, 1989, 621-623.
18. G. R. Desiraju, *Prog. Solid St. Chem.*, 1987, **17**, 295-353.
19. M. A. Spackman and J. J. McKinnon, *CrystEngComm*, 2002, 378-392.
20. A. Parkin, G. Barr, W. Dong, C. J. Gilmore, D. Jayatilaka, J. J. McKinnon, M. A. Spackman and C. C. Wilson, *CrystEngComm*, 2007, **9**, 648-652.
21. S. K. Wolff, D. J. Grimwood, J. J. McKinnon, D. Jayatilaka and M. A. Spackman, *CrystalExplorer 2.1 (381)*, University of Western Australia, Perth, 2007.
22. A. J. Blake and D. W. H. Rankin, *Acta Crystallogr., Sect. C*, 1991, **47**, 1933-1936.
23. S. Furberg, J. Groggaard and B. Smedsrud, *Acta Chem. Scand. B*, 1979, **33**, 715-724.
24. G. d. With, S. Harkem and D. Feil, *Acta Crystallogr., Sect. B*, 1976, **32**, 3178-3185.
25. D. Mootz and H. G. Wussow, *J. Chem. Phys.*, 1981, **75**, 1517-1522.
26. S. Crawford, M. T. Kirchner, D. Bläser, R. Boese, W. I. F. David, A. Dawson, A. Gehrke, R. M. Ibberson, W. G. Marshall, S. Parsons and O. Yamamuro, *Angew. Chem., Int. Ed.*, 2009, **48**, 755-757.
27. J. E. Davies and A. D. Bond, *Acta Crystallogr., Sect. E*, 2001, **57**, o947-o949.
28. C. Huiszoon, W. B. Van Der Waal, A. B. Van Egmond and S. Harkema, *Acta Crystallogr., Sect. B*, 1972, **28**, 3415-3419.
29. C. Huiszoon, *Acta Crystallogr., Sect. B* 1976, **32**, 998-1003.
30. S. Ranganathan, S. Mahapatra, T. S. Thakur and G. R. Desiraju, *Acta Crystallogr., Sect. E*, 2010, **66**, o2789.
31. K. Woźniak, B. Kariuki and W. Jones, *Acta Crystallogr., Sect. C*, 1991, **47**, 1113-1114.
32. W. Jankowski and M. Gdaniec, *Acta Crystallogr., Sect. C*, 2002, **58**, o181-o182.
33. I. D. H. Oswald, W. D. S. Motherwell and S. Parsons, *Acta Crystallogr., Sect. E*, 2004, **60**, O1967-O1969.
34. I. D. H. Oswald, W. D. S. Motherwell and S. Parsons, *Acta Crystallogr., Sect. B*, 2005, **61**, 46-57.
35. A. Kadzewski and M. Gdaniec, *Acta Crystallogr., Sect. E*, 2006, **62**, o3498-o3500.

Chapter 3: A Rudimentary Method for Classification of $\pi\cdots\pi$ Packing Motifs for Aromatic Molecules

36. V. R. Thalladi, T. Smolka, R. Boese and R. Sustmann, *CrystEngComm*, 2000, **2**, 96-101.
37. B. Sarma, L. S. Reddy and A. Nangia, *Cryst. Growth Des.*, 2008, **8**, 4546-4552.

CHAPTER 4

ISOSTRUCTURALITY IN METALLOCYCLES

4.1 INTRODUCTION

The concept of isostructurality in crystals usually refers to the identical or near identical packing arrangements of chemically distinct compounds. This can be seen as reciprocal to the concept of polymorphism where a single compound can crystallise in two or more distinct packing arrangements.¹ The term “isostructural” can then be used to describe the same three-dimensional arrangement of geometrically similar structural units in two different crystals.¹ In the area of inclusion chemistry, “isostructural” typically describes the inclusion of different guests in the voids of a common host framework.¹ The simplest classification designates “isostructural” crystals as having similar unit cell parameters, the same space group and near identical atomic coordinates for common atoms.¹ This suggests that the entire packing arrangement could, in theory, be superimposed on that of its isostructural relative.¹ While the term is useful in the description of organic compounds, it is not as appropriate for the description of metal-organic hosts, since the hosts may be isostructural but the guests can differ. For metal-organic hosts, the preferred term to describe crystals that contain a common host framework with interchangeable guests is “isoskeletal”. We can classify this even further to describe host frameworks that differ in their composition, such as exchanging of a metal cation, but maintain similar packing arrays – these crystal structures can be referred to as “homeotypic”.

Inclusion compounds that exhibit isostructurality offer the opportunity to investigate structure-property relationships, since the host compound is effectively constant.¹ This may lead to further understanding and interpretation of the mechanisms of processes such as thermal decomposition and guest exchange.¹ The thermal analysis of such compounds can be used to establish whether guest loss occurs via similar pathways and whether or not the thermodynamic and kinetic parameters are similar.¹ Most of these analyses have been accomplished with organic host compounds, although these techniques can also be extended to metal-organic complexes. Isostructural crystal structures are most easily recognized from corresponding powder X-ray diffraction patterns. Of course isostructurality can also be inferred from similar unit cell parameters, but this should not be used as the only means of identifying potentially isostructural crystals. Because a structure’s lattice parameters govern the peak positions in the diffraction pattern, and the atomic coordinates of two isostructural compounds generally differ by only a small percentage, their PXRD patterns should coincide. Differences in peak intensities can be attributed to differences in the structures, particularly the included guests and their respective orientations.¹ In many instances, it is the inherent

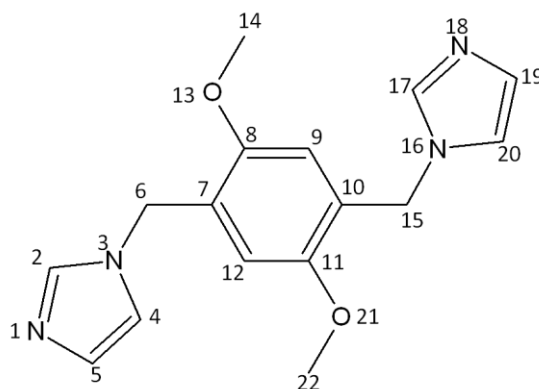
stability of the host-framework that mediates the formation of the isostructural series. However, there may be other instances where the host is unstable and can only form as a guest-included structure, leading to an isostructural series.¹

Kálmán has been at the forefront of the investigations of isostructural crystals, developing methods to quantify the extent of the packing similarities in these structures. Isostructural crystals can be compared by calculating the *Unit Cell Similarity Index* as well as the *Isostructurality Index* or the *Volumetric Isostructurality Index*. Details of these descriptors can be found in the discussion section of this chapter as well as in the seminal papers by Kálmán *et al.*^{2,3} The Materials Suite in the program Mercury⁴ provides a simple tool to quantify the similarity in molecular packing between crystal structures. *Crystal Packing Similarity* can be calculated for crystal structures containing the same compound. The program also allows one to perform a least-squares overlay of pairs of crystal structures. This feature can be somewhat biased since the user selects the pairs of atoms in the structures that should be superimposed and the calculated root-mean-square (RMS) value is thus not always an accurate representation.

The current study describes the structural analysis of a homeotypic series of metalloccycles. The same ditopic, exobidentate, imidazole-based ligand was employed in the preparation of these complexes with a variety of transition metal halide salts using an assortment of organic solvents. In total, 20 crystal structures (of which 18 are novel) were obtained. All structures form metalloccyclic structures that entrap solvents of crystallisation. Also, quite remarkably, all metalloccycle crystal structures were only obtained from the crystallisations prepared with metal bromide salts even though crystallisation experiments were set up with a variety of metal halides salts. The crystal structures of all the compounds in the homeotypic series were determined (see Table 4.1), as well as their thermal decomposition profiles, which were obtained by TG analysis. Comparison of the calculated PXRD patterns provides further evidence of the isostructural nature of the compounds. However, because these structures form part of a homeotypic series, only the structures in the cobalt bromide series of metalloccycles, which includes different guests (solvatomorphs), will be discussed. Each of these will be described in terms of its unique structural properties and any differences in arrangements will be highlighted. A second series of isoskeletal metalloccycle structures formed using copper bromide, which do not share the same packing arrangement as the first series, will be discussed in section 4.10 of this chapter.

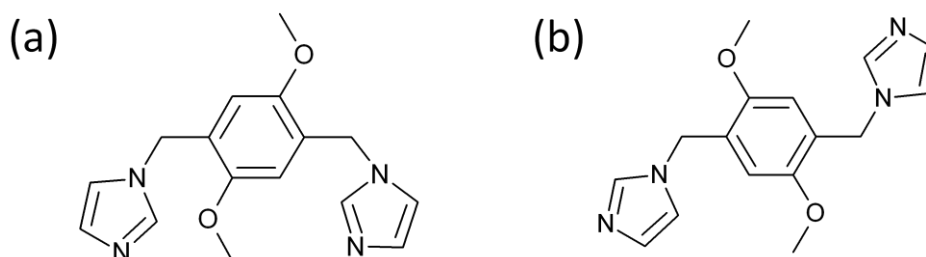
4.2 THE HOST ASSEMBLY

In the structure descriptions that follow, the assembly of the host remains virtually unchanged while the guest inside the cavity of the metallocycle varies. A general description of the host assembly is provided and applies approximately to all the structures in the series. Of course, there may be slight variations in this assembly depending on the guest and also the metal salt employed, and these variations will be highlighted in the relevant sections.



Scheme 4.1 Ligand **L1** - 1,1'-[(2,5-dimethoxybenzene-1,4-diyl)dimethanediyl]bis(1*H*-imidazole)

The metallocyclic compounds were all prepared using the same method (see Experimental section 4.16), which involved dissolving the ligand (**L1**, Scheme 4.1) in the selected organic solvent, adding a layer of pure acetonitrile followed by a layer of the chosen metal salt (bromide anion), also in acetonitrile, and then capping the vial. Crystals typically formed within two to three days under ambient conditions and all have the general formula $[M_2Br_4L_2] \cdot 2MeCN \cdot nG$, where M is cobalt, nickel or zinc and G is usually the solvent in which the ligand had been dissolved. An interesting aspect, common to all structures in the homeotypic series, is the inclusion of MeCN guest molecules in interstitial spaces located between metallocyclic complexes. Each metal cation is coordinated to two ligand molecules and two bromide counter ions in a tetrahedral coordination geometry. The ligand **L1** assumes a C-shaped conformation (Scheme 4.2) and coordinates ditopically through the imino nitrogen atoms of the imidazole moieties to the two metal centres.



Scheme 4.2 Ligand **L1** has various possible conformations with the most recognised being either (a) a C-shaped conformation or (b) an S-shaped conformation when forming coordination complexes.

The two ligands in the metallocycle are related to each other by inversion symmetry such that the imidazole moieties of one ligand are both up and those of the other are both down. The simplified shape of the metallocycle is that of a hexagon in an open chair conformation (Figure 4.1).

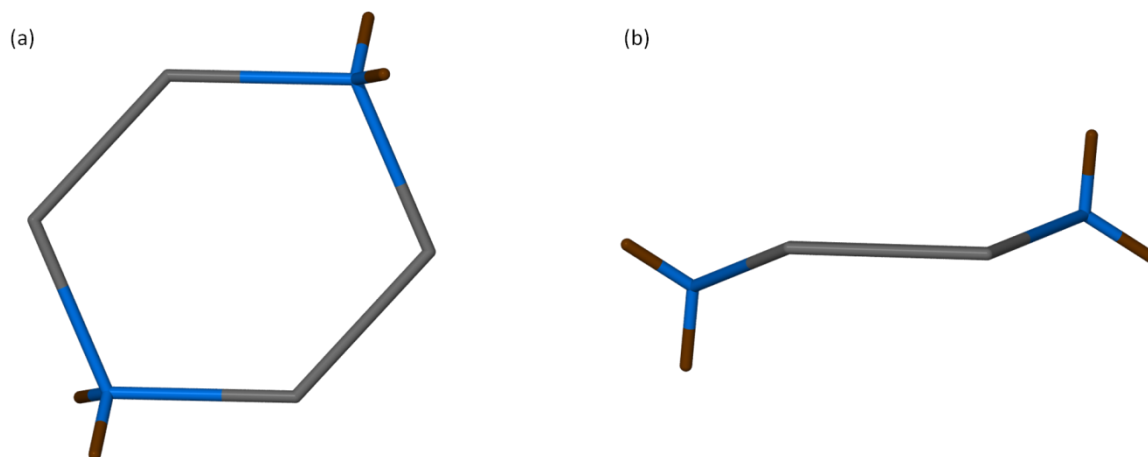


Figure 4.1 The simplified shape of the metallocycles in the homeotypic series when reduced to a skeletal structure by connecting selected nodes of the cycle. (a) Viewed from above the metallocycle assumes a hexagonal shape, whereas viewed from the side (b) (looking at the phenyl moieties) the chair conformation is revealed.

Owing to the symmetry of the metallocycle, the *p*-methoxyphenyl moieties of the ligands are positioned parallel to each another. The *p*-methoxyphenyl moieties tilt towards the plane of the metallocycle so that it appears to be folded in on itself and the methoxy groups of these moieties are thought to contribute to the observed packing inefficiency of the metallocycles. The angle at which these groups (assigned as Plane 2, Figure 4.2 (a) and (d)) are tilted relative to the plane of the metallocycle, assigned as Plane 1 (Figure 4.2), is likely to vary according to the nature of the included guest molecules. This tilt angle can also be evaluated relative to Plane 3 – the plane passing through the metal centres and the bromide counterions. Other geometric parameters that may be defined for comparison are the deviation of the imidazole rings (Planes 4 and 6) in relation to the plane specified by the atoms labelled 1 to 4 (Figure 4.2 (d)), assigned Planes 5 and 7 or, in other words, the tilting of the imidazole moieties into or out of the metallocycle cavity.

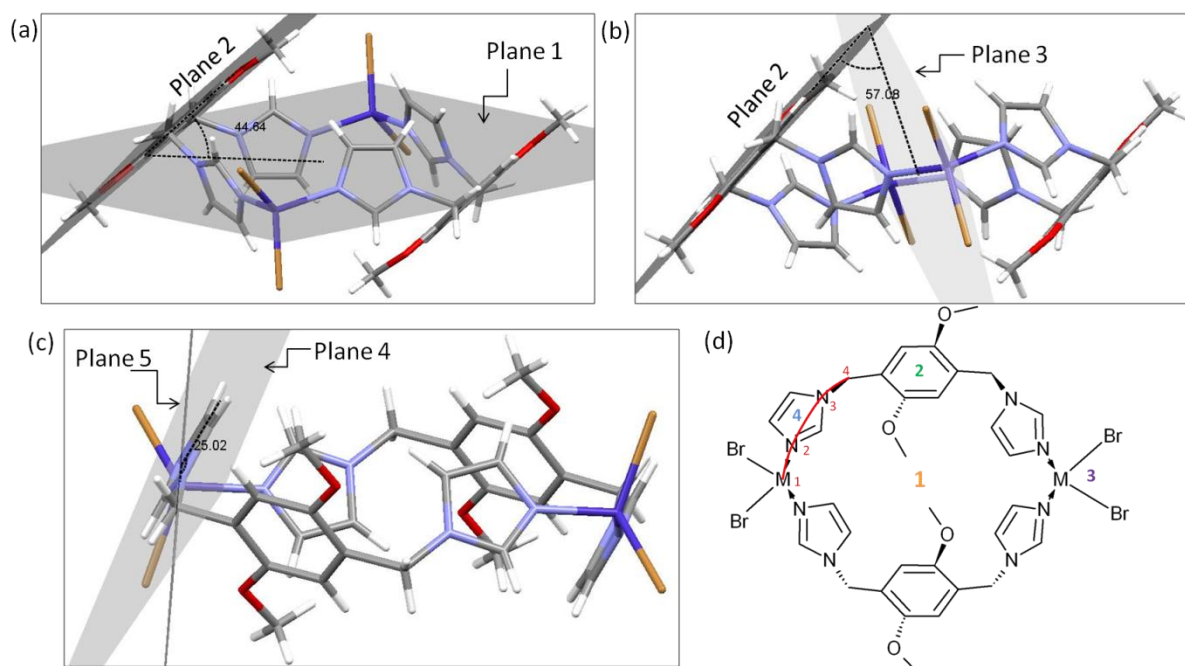


Figure 4.2 Assignment of the planes in the metalloclusters (MC series) used to determine tilt angles (a) between *p*-methoxyphenyl moiety (Plane 2) and horizontal plane (Plane 1); (b) between *p*-methoxyphenyl moiety and vertical plane (Plane 3) and (c) of the imidazole group (Plane 4) from its axis position (Plane 5). (d) Indicates the four different planes, labelled 1-4, and Plane 5 is depicted by the line and atoms labelled in red.

The metalloclusters are stabilised by weak $\pi \cdots \pi$ stacking interactions between phenyl rings of adjacent metalloclusters with interplanar spacing ranging from 3.66 to 3.88 Å (Figure 4.3). These phenyl moieties associate in a slightly offset manner and arrange the metalloclusters into weakly connected one-dimensional chains.

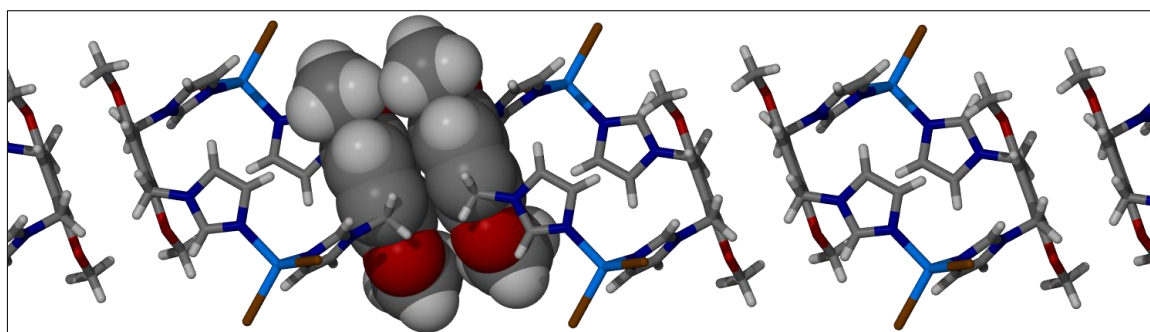


Figure 4.3 Offset $\pi \cdots \pi$ interactions between methoxyphenyl moieties of adjacent metalloclusters in the homeotypic series.

These chains arrange in an offset manner to form layers (Figure 4.4). Weak C–H \cdots Br intermolecular interactions, extending from the bromide ion of one metallocluster to a C-atom in a neighbouring imidazole group maintain the layers. These layers, in turn, are stacked on top of one another in an offset \cdots ABAB \cdots fashion such that the methoxy groups of one layer are directed towards the apertures of the metalloclusters in the neighbouring layers (Figure 4.5). C–H \cdots Br interactions are again observed, this time between the methoxymethyl groups

of the metalloacycles in one layer and the bromide ions of the metalloacycles in the layer above (or below).

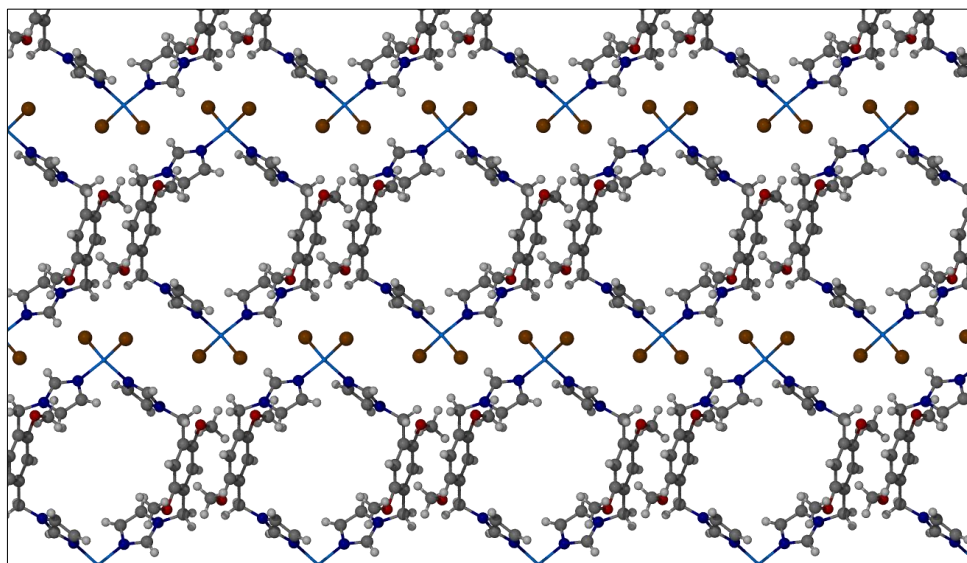


Figure 4.4 Representation of a single layer of metalloacycles in the homeotypic series connected via offset $\pi\cdots\pi$ interactions between the methoxyphenyl moieties.

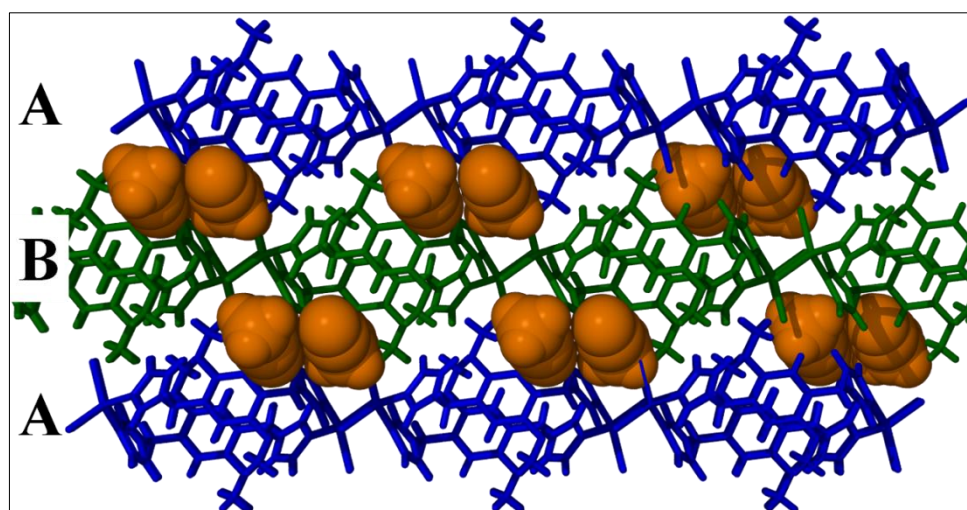


Figure 4.5 Metalloacycles in the homeotypic series pack in an $\cdots ABAB \cdots$ arrangement with two MeCN molecules interrupting the layers. Acetonitrile molecules are in space-fill representation (in orange) and the metalloacycles are shown as capped-sticks. Different layers of metalloacycles are shown in green and blue.

Owing to the awkward molecular shape of the metalloacycles, they are unable to pack efficiently on their own, thus creating small interstitial spaces. These spaces are formed between six metalloacycles: four in the equatorial plane, and two in axial positions, as shown in Figure 4.6. Two molecules of MeCN, aligned in an offset head-to-tail dimer, fill these spaces (Figure 4.5 and 4.6). These molecules are offset such that there are weak $\pi\cdots\pi$ interactions between their respective nitrile functionalities. The separation distance between these MeCN molecules varies slightly in the structures presented in this series. The interstitial MeCN molecules are also weakly associated to the methylene carbon atoms (C6 and C15) of

the metalloacycles by C–H...N interactions. Although guest molecules are conventionally not considered part of the host framework, the series of crystal structures presented here all feature two MeCN molecules in the interstitial spaces. Therefore, these guests are considered part of the isoskeletal assembly in the series. It is presumed that removal of these molecules would require rearrangement of the metalloacycles in the crystal.

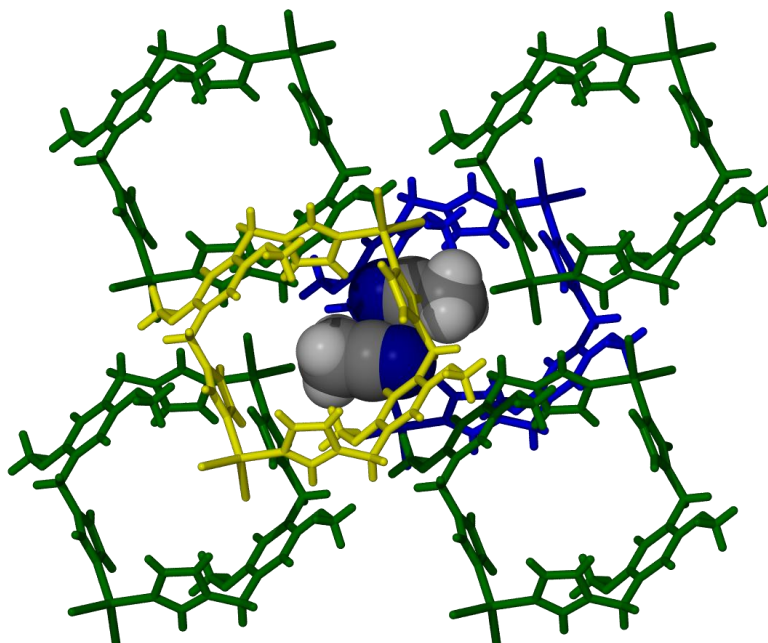


Figure 4.6 In all structures of the homeotypic series, the two interstitial acetonitrile molecules are surrounded by four metalloacycles in the equatorial plane (shown in green) and two in axial positions (yellow above and blue below). The metalloacycles are depicted as capped sticks while the acetonitrile molecules are in van der Waals representation, clearly showing the close proximity of the nitrile groups to each other.

Apart from the interstitial MeCN guests, other guest molecules are occluded in the cavities of the metalloacycles themselves. The voids within the cycles can be described as small pockets and these pockets are filled by various guests throughout this series of isoskeletal crystals (Figure 4.7). The guests included in these cavities are dependent on the solvent system from which the crystal is obtained. The host structure appears to remain relatively unchanged, irrespective of this secondary guest. The guest-filled pockets are connected to each other via the interstitial space – filled by the MeCN molecules – to form continuous one-dimensional channels (Figure 4.8). So in essence the MeCN molecules in the interstitial spaces assist in occluding the other guest in the cavity of the metalloacycle. The channels propagate through the centre of one metalloacycle and between four metalloacycles alternating in this manner. As depicted in Figure 4.8, the channel is not linear but rather undulates along its length.

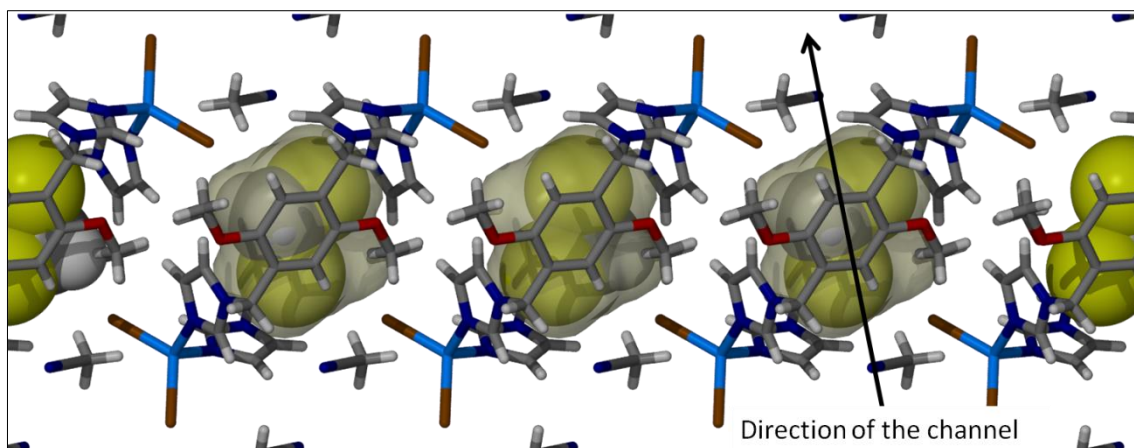


Figure 4.7 Perspective view of the solvent-filled pockets within the metalloclusters in the homeotypic series. The pocket is represented by the semi-transparent surface which, in this instance, is filled with DCM molecules that are disordered over two possible positions. The guests inside the pockets are shown in van der Waals representation in order to demonstrate the space occupied by these molecules. Interstitial MeCN molecules and the metallocluster hosts are depicted as capped-sticks.

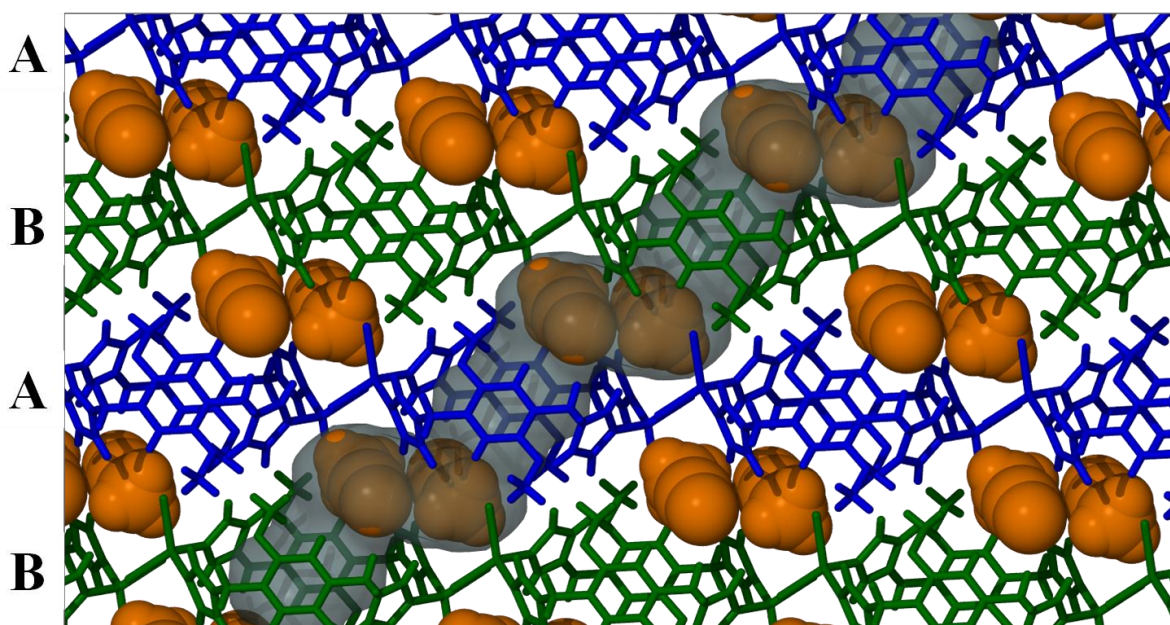


Figure 4.8 The host assembly common to the homeotypic series. A single channel (semi-transparent grey surface) has been mapped using a probe radius of 1.5 Å. The cavity-included guest molecules of the metalloclusters are omitted in this figure, which therefore represents only the host assembly common to all structures in the series. The interstitial MeCN molecules are shown in orange in space-filling representation.

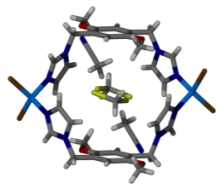
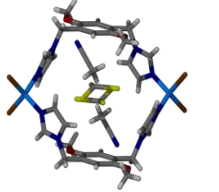
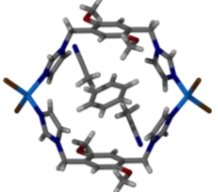
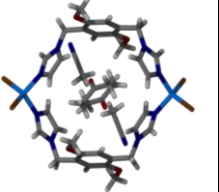
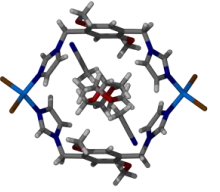
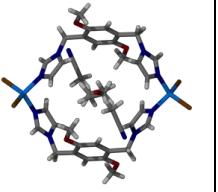
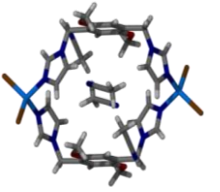
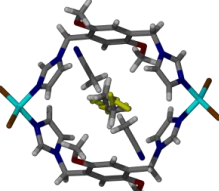
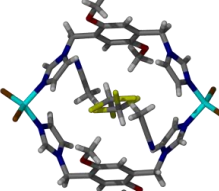
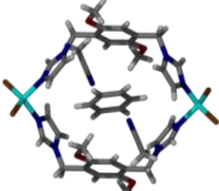
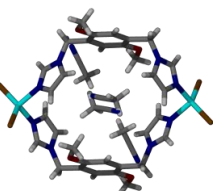
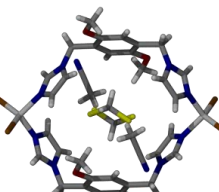
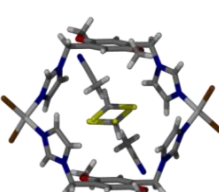
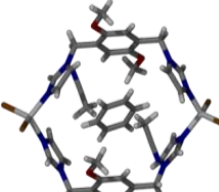
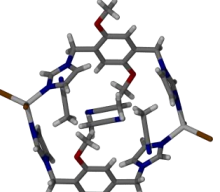
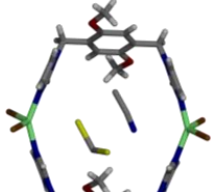
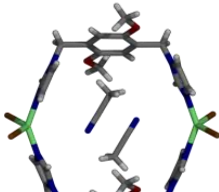
The alternation of guest molecules along the channel may give an indication of how the complexes form in solution and subsequently crystallise (i.e. the metallocluster is templated by the cavity-included guest, followed by the packing of the metalloclusters, with any open spaces filled by the MeCN dimers).

The one-dimensional channels are mapped by Connolly surfaces using a probe radius of 1.2 Å. Although this radius is not optimal for determining the solvent-accessible void volume, it allows comparison with results obtained from SQUEEZE.⁵ By using the same probe radius in each case it is also possible to compare approximate channel volumes across

the series of isoskeletal structures (Table 4.2). In all cases in the homeotypic series, this volume approximates the space occupied by the guest included in the metallochrom cavity as well as by two interstitial MeCN molecules.

Selected inter- and intramolecular interactions, bond and tilt angles as well as calculated void volumes for all the structures in the series are tabulated at the end of the chapter. Because the crystal structures obtained in this series are homeotypic, only the structures containing cobalt bromide (isoskeletal series) will be discussed in detail. Any variations in the structures of the metallochroms containing other metal salts will be discussed as necessary. A second set of analogous metallochroms was obtained with copper bromide and is discussed independently at the end of the chapter.

Table 4.1 Crystal structures of the metallocycles obtained in this study using ligand **L1** and MBr_2 where M is Co, Ni, Zn or Cu. Blank entries represent crystal structures that have not yet been obtained.

	DCM	$CHCl_3$	Benzene	Acetone	Dioxane	EtOH	MeCN
Cobalt (MC1)							
Nickel (MC12)							
Zinc (MC13)							
Copper (MC11)							

4.3 DICHLOROMETHANE SOLVATE

$\text{MC1}_{\text{DCM}} - [\text{Co}_2\text{Br}_4\text{L1}_2] \cdot 2\text{MeCN} \cdot \text{DCM}$

The combination of ligand **L1** and CoBr_2 in a solvent mixture of dichloromethane (DCM) and acetonitrile (MeCN) resulted in the formation of the discrete (zero-dimensional) metalloacycle. The complex crystallises in the triclinic space group $P\bar{1}$ with the asymmetric unit (ASU) consisting of half a metalloacycle and a single molecule each of MeCN and DCM (Figure 4.9).

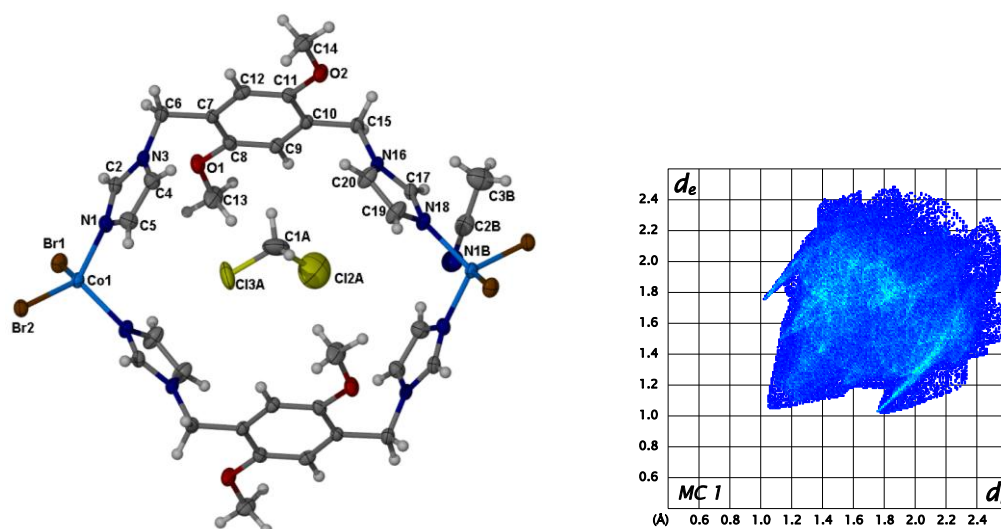


Figure 4.9 Thermal ellipsoid plot (50%) of the discrete 0-D metalloacycle in MC1_{DCM} . Only the ASU is labelled. The alternate DCM position has been omitted for clarity. The representative fingerprint plot of the metalloacycle is shown on the right.

Owing to their approximately spherical shape, the complexes tend to pack inefficiently in the solid state. Host-host interactions exist in the form of offset $\pi \cdots \pi$ stacking between phenyl rings of adjacent metalloacycles separated by a distance of 3.698 Å. Apart from these weak interactions between the host complexes, there are few other notable interactions that influence the packing arrangement of the complexes.

The disordered DCM guest is located about a centre of inversion within the cavity of the metalloacycle such that the molecule has two possible positions, each with equal probability. The preferred position of the guest in the pockets is most likely random since there are no apparent connections between the guests in independent pockets. Only very weak intermolecular interactions exist between the DCM and the host framework. The DCM molecules are orientated in the pockets such that the chloride atoms are directed, at an angle, towards the centroids of the imidazole rings of the metalloacycle in lone-pair $\cdots \pi$ interactions (3.355 Å and 3.519 Å). The only other noteworthy interactions are C–H $\cdots \pi$ contacts between the DCM carbon atom and the proximal phenyl rings (at a distance of 3.912 Å). However,

this separation is at the upper limit suggested for this type of interaction. Because there are no remarkable host-guest interactions it is assumed that the DCM guest is included owing to a size/shape fit.

Despite a distinct lack of host-guest interactions, guest-guest interactions appear to be more prevalent. These interactions occur in the form of weak intermolecular interactions of the C–H...Cl type between the MeCN and DCM molecules (3.719(1) Å). It appears that these lone-pair... π interactions are partially responsible for the orientation of the DCM molecules within the cavities, thereby minimising their interaction with the oxygen atoms of the host methoxy groups. The fingerprint plot (Figure 4.9) for the metallocycle alone confirms the lack of strong interactions between the host and the guests included in the structure, with no distinct features being apparent.

The solvent-accessible void volume, calculated using SQUEEZE, is 291 Å³ per unit cell, which corresponds to the space occupied by the disordered DCM molecule and two MeCN molecules, one above and one below the metallocycle (Figure 4.10).

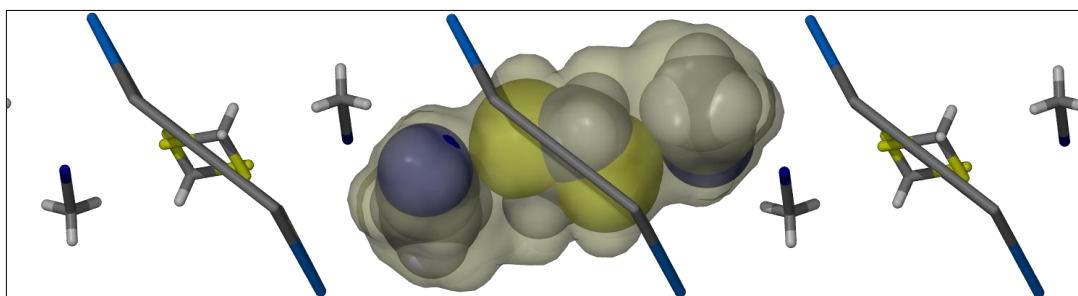


Figure 4.10 A simplified representation of the metallocycles of $\text{MCl}_{1\text{DCM}}$. The semi-transparent surface represents the solvent accessible space for each metallocycle. The guest molecules that are housed within this space are shown in van der Waals representation.

The lack of strong intermolecular interactions between host and guest molecules allows the guest molecules to be removed under mild conditions and, indeed, desolvation commences shortly after the crystals are removed from the mother liquor. Thermogravimetric analysis confirms that volatile guest molecules are removed from ambient temperature until approximately 50 °C, after which the complex is stable, approaching onset of decomposition at approximately 300 °C. A total weight loss of 14.4% corresponds well with the calculated value (13.9%) for one DCM and two MeCN molecules per metallocycle as observed in the crystal structure. The small discrepancy between the calculated and experimental values can be ascribed to solvent on the surface of the sample and not that included within the crystal structure.

Attempts were made to grow the same crystals from different solvent systems so as to exclude the MeCN molecules and facilitate the formation of one-dimensional channels;

however these efforts yielded only precipitate product or crystal structures containing polymeric chains. Solvent exchange experiments were also carried out with a few single crystals; however these yielded only polycrystalline material, which could not be analysed further. As mentioned previously, upon removal from the mother liquor the crystals rapidly lose solvent, during which time the deep blue crystals become opaque. While the crystals appear to retain their integrity, it is apparent from X-ray analysis that the elimination of solvent results in major structural rearrangement – i.e. the crystals no longer yield a diffraction pattern. This is also evidenced in the PXRD analysis since the sample produces only a very weak diffractogram.

Attempts to re-solvate the crystals were undertaken by immersing them in a variety of common solvents. A colour change was observed with the addition of a few drops of water to the deep blue crystals, firstly to a greenish-blue and eventually to a light pink colour. Regrettably, these crystals became severely fractured during the process and could not be subjected to further analysis. Recognising any structural changes or exchange of guest molecules by PXRD is also problematic owing to the poor quality of the diffractograms and this analytical technique was therefore also insufficient.

4.4 CHLOROFORM SOLVATES

Though the structures of MC1_{DCM} and $\text{MC1}_{\text{CHCl}_3}$ are isoskeletal, they can also be referred to as solvates of one another, or solvatomorphs, since the host assembly is identical in composition. The only difference is the guest included in the cavities of the metallocycles. The same applies for the nickel- and zinc-based structures where the DCM guests are replaced by CHCl_3 .

$\text{MC1}_{\text{CHCl}_3} - [\text{Co}_2\text{Br}_4\text{L}_2] \cdot 2\text{MeCN} \cdot \text{CHCl}_3$

A metallocycle structurally similar to that in MC1_{DCM} was successfully grown from a solvent mixture of chloroform (CHCl_3) and MeCN. The crystal system is the same as that in MC1_{DCM} : triclinic $P\bar{1}$, with similar unit cell parameters (see Table 4.8). The ASU is practically identical to that of MC1_{DCM} apart from the chloroform guest included within the confines of the metallocycles (Figure 4.11). The intramolecular Co...Co distance (11.554(2) Å) is approximately the same as that in MC1_{DCM} (11.544(2) Å), although the N–Co–N angle increases slightly from 108.79(12)° in the DCM solvate to 110.20(12)° in the CHCl_3 solvate. This increase is most probably due to the inclusion of CHCl_3 , which has a larger molecular volume compared to DCM and so the metallocycle adapts to accommodate the larger

molecule. As in the DCM solvate, the chloroform molecule is located about an inversion centre and therefore has two possible positions of equal (i.e. 50%) occupancy.

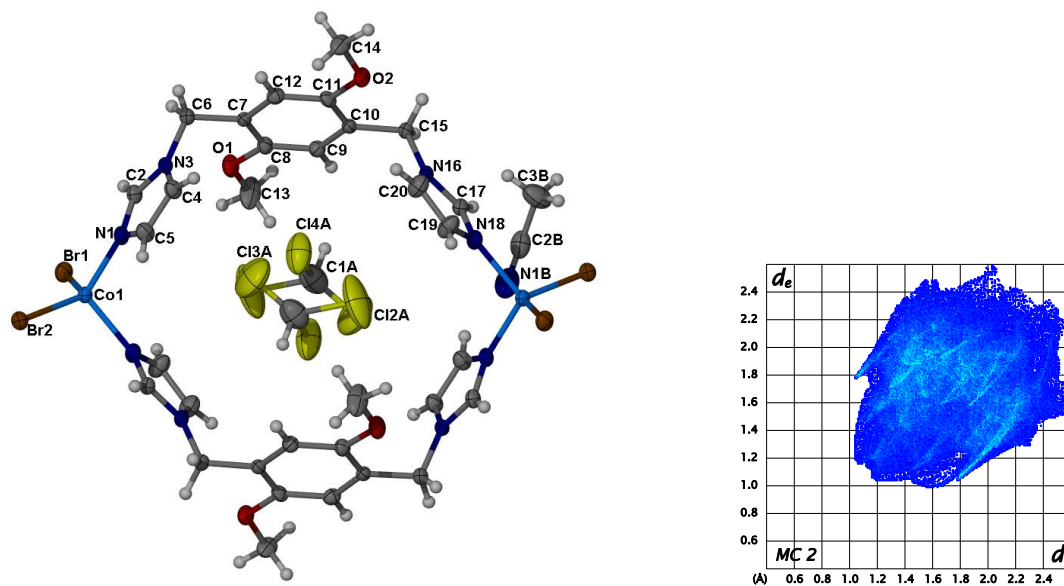


Figure 4.11 Anisotropic displacement (50%) ellipsoid plot of $MC1_{CHCl_3}$ (left). Only the atoms of the ASU have been labelled. The fingerprint plot of the metallosupramolecular assembly is shown on the right.

As in the DCM solvate, the phenyl moieties of the metallosupramolecular assemblies are associated in an offset $\pi \cdots \pi$ stack. Although the moieties are ideally positioned, the separation distance (3.864 Å) is at the upper limit of the accepted range for $\pi \cdots \pi$ interactions and is also slightly further than that observed in the DCM solvate.

Apart from these very weak $\pi \cdots \pi$ interactions and those already mentioned in the description of the host assembly, there appear to be no other noteworthy intermolecular interactions between the host molecules. Weak lone-pair $\cdots \pi$ interactions exist between two of the chlorine atoms of the $CHCl_3$ guest and the delocalised π -system of the imidazole rings (3.412 and 3.430 Å) of the host. The remaining chlorine atom of the $CHCl_3$ molecule is directed towards the aperture of the metallosupramolecular assembly and takes part in weak C–H \cdots Cl interactions (3.643(6) Å) with the MeCN molecules that occupy the adjoining interstitial space. This same chlorine atom is also sufficiently close to a neighbouring metallosupramolecular assembly to form a halogen bond to the nearest bromide ion (3.448(3) Å). The fingerprint plot (Figure 4.11) of the metallosupramolecular assembly indeed reveals that only weak interactions are present between the metallosupramolecular assembly and the included guests. The most prevalent interaction is an H \cdots Br interaction, while most of the other features of the plot are heavily overshadowed by van der Waals contacts, indicating that the arrangement is mainly due to close-packing effects.

These particular crystals are moderately more stable under ambient conditions than the DCM analogue. The increased stability may be linked to the elevated boiling point of $CHCl_3$

as compared to that of DCM. However the physical properties of the guest do not necessarily dictate those of the inclusion compound. Thermogravimetric analysis reveals that the DCM and CHCl_3 solvates have comparable thermal decomposition profiles. Volatile guests in the CHCl_3 solvate are released immediately at 25 °C and are completely removed by 50 °C. After initial solvent loss, the thermogram plateaus until the onset of decomposition at approximately 316 °C. The percentage weight loss (16.4%) corresponds to the value calculated (16.3%) for release of one CHCl_3 and two MeCN molecules per metallocluster. Unfortunately, although the complex appears to be stable after solvent loss, the removal of the MeCN presumably induces a rearrangement of the metalloclusters to fill the previously occupied space. The nature of this rearranged state could not be elucidated by SCD or PXRD analysis owing to a significant decrease in crystallinity. This is also true for the DCM solvate.

4.5 BENZENE SOLVATES

$\text{MC1}_{\text{Benz}} - [\text{Co}_2\text{Br}_4\text{L1}_2] \cdot 2\text{MeCN} \cdot \text{C}_6\text{H}_6$

The isoskeletal series was expanded with the reaction of ligand **L1** with cobalt bromide in benzene and MeCN. The crystals obtained from this mixture were similar to those described above, crystallizing in the triclinic space group $P\bar{1}$ with related unit cell parameters. The ASU includes a single ligand molecule coordinated to a cobalt cation, which is in turn coordinated to two bromide counter ions. Inversion symmetry generates the other half to form the metallocluster. Also making up the ASU are half a benzene molecule situated in the interior of the metallocluster and an entire MeCN molecule located exterior to the metallocluster (Figure 4.12). The benzene guest is situated on a special position such that half of the molecule is generated by inversion symmetry. The anisotropic displacement ellipsoids of the benzene molecule suggest that it may experience some dynamic in-plane rotation within the cavity. It was confirmed that this motion is not due to disorder of the molecule over two positions; were this the case, one would expect the ellipsoids to be unidirectional.

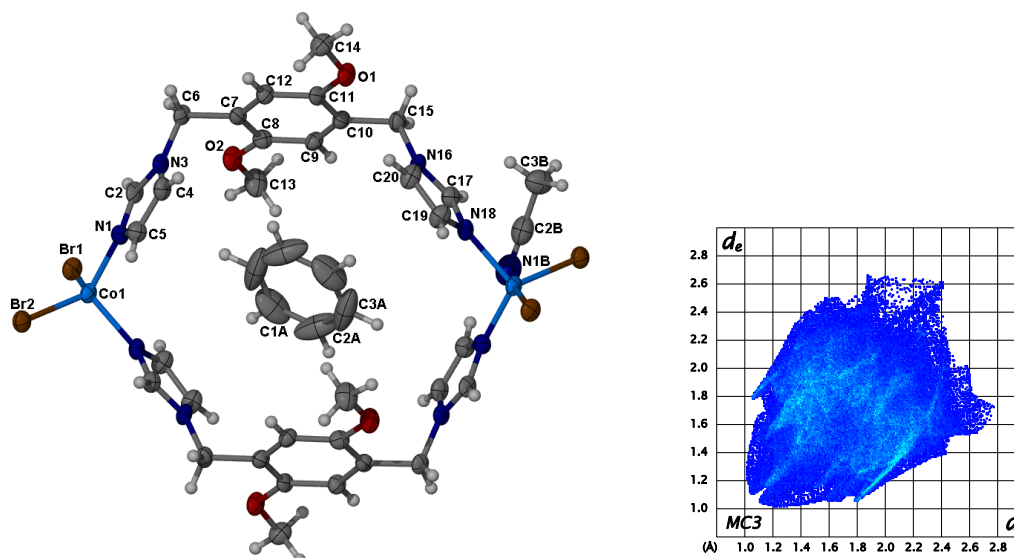


Figure 4.12 Anisotropic displacement ellipsoid representation of $MC1_{Benz}$ at 50% probability. Only the ASU has been labelled. The fingerprint plot for the metallocycle is on the right.

If the structure is viewed in its entirety the benzene molecules are all angled in the same direction throughout the channels, suggesting that there is a slight preference in orientation. The benzene molecule is orientated almost parallel to the phenyl moieties of the metallocycle. On closer inspection, it seems that alignment in the opposite direction would result in unfavourable host-guest interactions or, indeed, repulsion between the host and guest. It is therefore rather surprising that benzene is included in the metallocycle at all. The benzene molecule is tilted at an angle of 26.1° relative to the *p*-methoxyphenyl moieties; this angle is considerably larger than these same tilt angles observed in the isoskeletal nickel- and zinc-based structures, which are 13.8° and 19.7° , respectively.

Analogous to the DCM and $CHCl_3$ structures, the metalloCycles are involved in offset $\pi \cdots \pi$ interactions between the phenyl moieties in the ligand spacers of adjacent metalloCycles at a separation distance of 3.839 \AA . This distance is comparable to that observed in the $CHCl_3$ solvate but slightly longer than in the DCM solvate.

With the inclusion of an aromatic guest molecule in the confines of the metallocycle, one would expect that $\pi \cdots \pi$ interactions would exist between the host and the guest. The fact that the aromatic moieties are dissimilar would allow for favourable $\pi \cdots \pi$ stacking. However, it is noted that the benzene molecule is canted inside the metallocycle and $\pi \cdots \pi$ stacking interactions are thus not observed. However, the centroid separation distance between the host and benzene guest is at the upper limit for $C-H \cdots \pi$ interactions (4.633 \AA). Somewhat shorter $C-H \cdots \pi$ interactions (3.640 \AA), in an edge-to-face orientation (Figure 4.13), are observed between the benzene molecule and the two imidazole moieties located across from

each other. It is assumed that this orientation is a compromise such that the molecules occupy the most favourable position within the cavity of the metalloccycles. Therefore, in this instance the benzene slots into the space between the parallel aligned host phenyl rings and tilts slightly so that there are also favourable interactions with the imidazole moieties of the host. In fact Figure 4.13 suggests that the metalloccycle actually deforms slightly to accommodate the benzene guest.

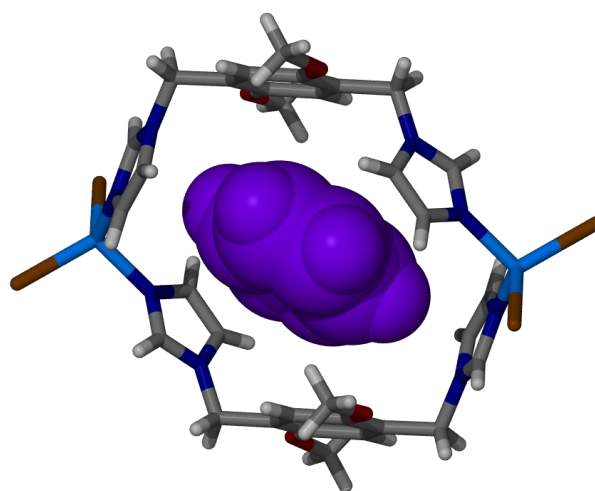


Figure 4.13 Space-filling representation of the benzene molecule included in the metalloccycle cavity of **MC1_{Benz}**. This figure clearly indicates the C–H \cdots π (edge-to-face) interactions of the benzene guest with two of the imidazole moieties of the metalloccycle.

There appear to be no substantial intermolecular interactions between the benzene guest and the nearest MeCN molecules. C–H \cdots π interactions between the benzene and nearby MeCN molecules are at the limit of the accepted distance (4.586 Å). The fingerprint plot (Figure 4.12, right) confirms the lack of significant intermolecular interactions, the major contribution to this plot being from weak van der Waals interactions.

The thermogravimetric analysis of **MC1_{Benz}** was expected to yield a different thermal profile to that of the DCM and CHCl₃ solvates based on the volatility of the pure organic solvents. However, as in the previous compounds liberation of the guest starts immediately at ambient and proceeds until 50 °C. The thermogram flattens out after this first event and is followed by a decomposition event at *ca* 300 °C. The first thermal event accounts for a 14.1% weight loss, which corresponds well with the percentage weight calculated for one benzene and two MeCN molecules per metalloccycle (13.4%). The small discrepancy between the calculated and experimental values can be ascribed to surface solvent on the crystals.

4.6 $\text{MC1}_{\text{Diox}} - [\text{Co}_2\text{Br}_4\text{L}_2] \cdot 2\text{MeCN} \cdot \text{C}_4\text{H}_8\text{O}_2$

Crystals grown from a mixture of 1,4-dioxane (dioxane) and MeCN are isoskeletal to those already discussed. The ASU is also analogous, comprising a cobalt cation coordinated to one ligand **L1** and two bromide counter ions, as shown in Figure 4.14. In addition, a single molecule of MeCN is located exterior to the metallocycle and two symmetry-independent half molecules of dioxane are located within its cavity.

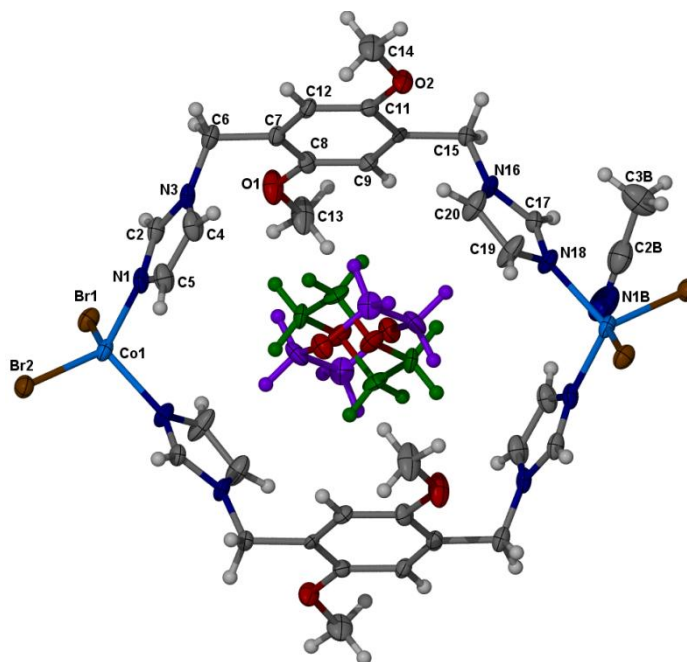


Figure 4.14 Anisotropic displacement ellipsoid plot of MC1_{Diox} shown with 50% ellipsoids. The ASU of the metallocycle has been labelled while the disordered dioxane molecules are not. The higher occupancy component (55%) is shown in green and the minor component (45%) in purple, with only half of each of these molecules being present in the ASU.

The dioxane molecules in the cavity assume a chair conformation with the oxygen atoms directed towards the apertures of the metallocycle. The dioxane molecules are orientated somewhat parallel to the phenyl moieties of the metallocycle, much like that observed for the benzene-included structure. In this instance the dioxane molecule is disordered over two positions with different site occupancies. The major component has an occupancy of approximately 55% and is shown in green, while the other possible orientation is occupied 45% of the time and is represented in purple (Figure 4.15). If one imagines a rotation axis bisecting these two positions, the two sites are rotated by 57.2° relative to each other about this axis (Figure 4.16). The orientation of the guests within the cavities is such that the dioxane molecules are at an angle of approximately 37.2° or 24.3° relative to the phenyl moieties in the high- and low-occupancy positions, respectively. Least-squares planes of the guests are defined by the four carbon atoms of each molecule.

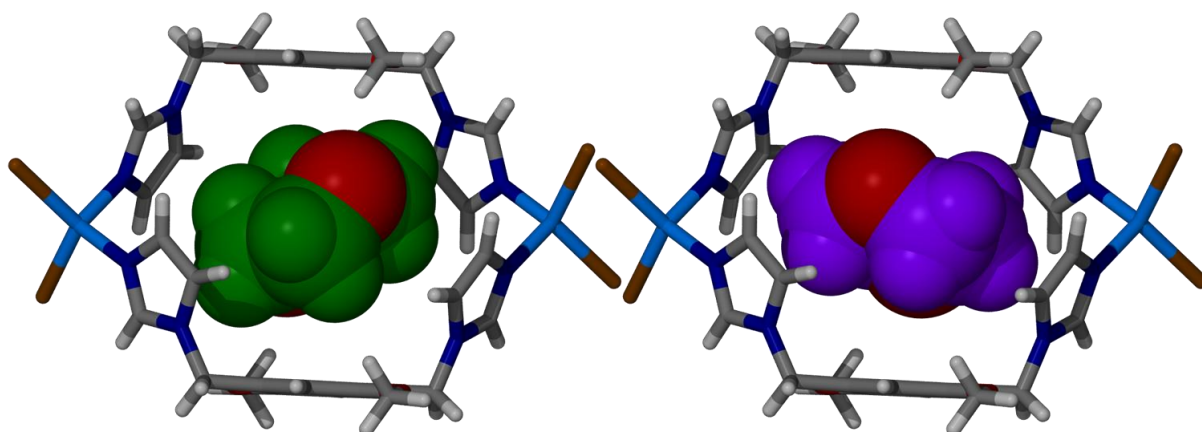


Figure 4.15 The two possible sites occupied by the dioxane molecules in $\text{MCl}_{1\text{Diox}}$. The green space-fill representation on the left depicts the position of 55% site occupancy while that on the right (purple) represents the site of 45% occupancy. Oxygen atoms are shown in red.

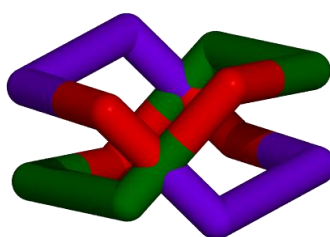


Figure 4.16 Disordered dioxane molecules in $\text{MCl}_{1\text{Diox}}$ viewed along the imaginary rotation axis which bisects the two molecules. The position of highest occupancy is depicted in green, while the lower occupancy position is in purple. Hydrogen atoms have been omitted for clarity. Positions are rotated approximately 60° to each other.

Once again the intermolecular interactions are primarily of the weaker variety. When in the lower occupancy position, the dioxane is involved in $\text{C-H}\cdots\pi$ interactions with the imidazole moieties nearest to the methylene carbon atoms of the dioxane (3.287 \AA). In this position, the oxygen atoms of the dioxane are also involved in $\text{C-H}\cdots\text{O}$ interactions ($3.212(7) \text{ \AA}$) with the MeCN guests above and below the metalloclusters (Figure 4.17, right). In contrast, when the dioxane is situated in the slightly more favoured position, a different set of intermolecular interactions appear to govern its stabilisation in the cavity. In this instance, there are a number of $\text{C-H}\cdots\pi$ interactions between the guest and the host. These interactions exist between the sp^3 carbon atoms of the dioxane and the phenyl moieties of the host (3.749 \AA), as well as with the imidazole moieties (3.528 \AA). Slightly stronger $\text{C-H}\cdots\text{O}$ interactions are also present between the oxygen atoms of the dioxane and the methoxymethyl groups ($3.379(8) \text{ \AA}$) on either side of the metallocluster (Figure 4.17, left). Although the intermolecular interactions are still of a weak nature, there are a greater number of these interactions and they may act collaboratively in stabilising the guest.

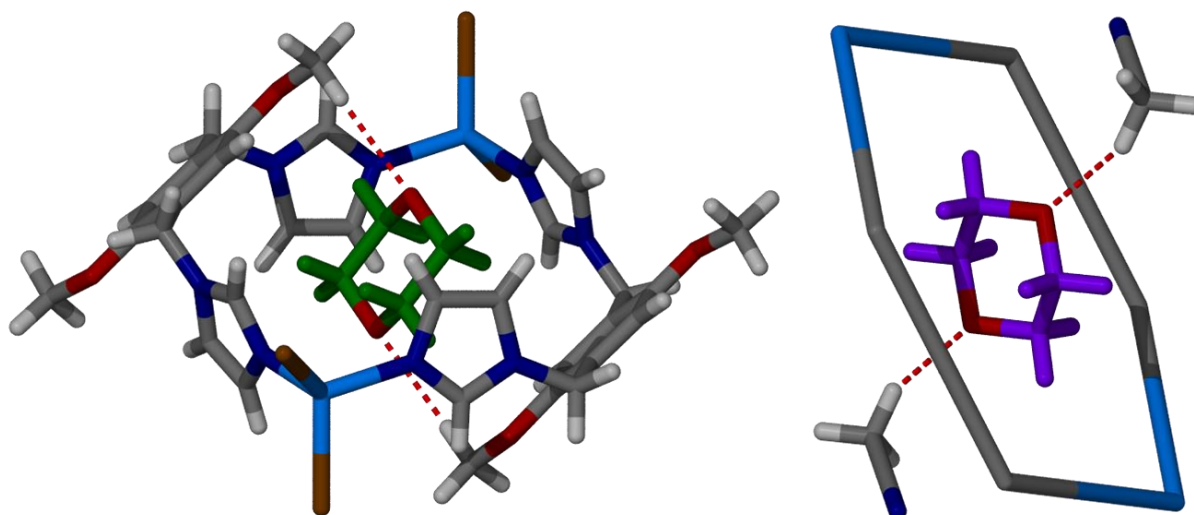


Figure 4.17 Weak C–H...O interactions that occur in MCl_{Diox} are shown as fragmented red lines. These exist between the dioxane guest in the higher-occupancy position (green) and the host metallocluster (shown on the left) while the dioxane guest in the lower-occupancy position (purple molecule shown on the right) is involved in C–H...O interactions with the MeCN guests in the interstitial spaces.

This small rotation of the dioxane molecule has significant implications for the intermolecular interactions. The higher occupancy site allows for C–H...O interactions with the host metallocluster, whereas the site of lower occupancy interacts with the other guest. It is interesting then that the site occupancy factors are not even more partial to the position with more stabilising interactions, which is presumably the position experiencing C–H...O interactions with the host.

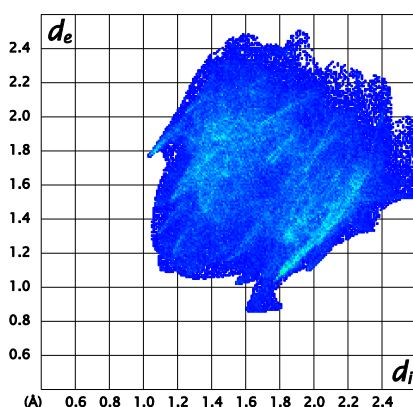


Figure 4.18 Fingerprint plot of the metallocluster in MCl_{Diox} . The characteristic wing on the right hand side on the plot is due to C–H... π interactions of the lower-occupancy dioxane with the imidazole moieties.

It was expected that the inclusion of an oxygen atom in the guest molecule would facilitate stronger hydrogen bonds between the host metallocluster and the guest. Of course conventional hydrogen-bond donors are not present in the metallocluster for such interactions to occur. However, the C–H...O interactions do appear somewhat more stabilising than the C–H... π type interactions. The fingerprint plot (Figure 4.18) correlates with the weak

intermolecular interactions discussed. The wing on the right is characteristic of the C–H $\cdots\pi$ interaction between the lower-occupancy dioxane guest and the imidazole moieties of the host metalloacycle.

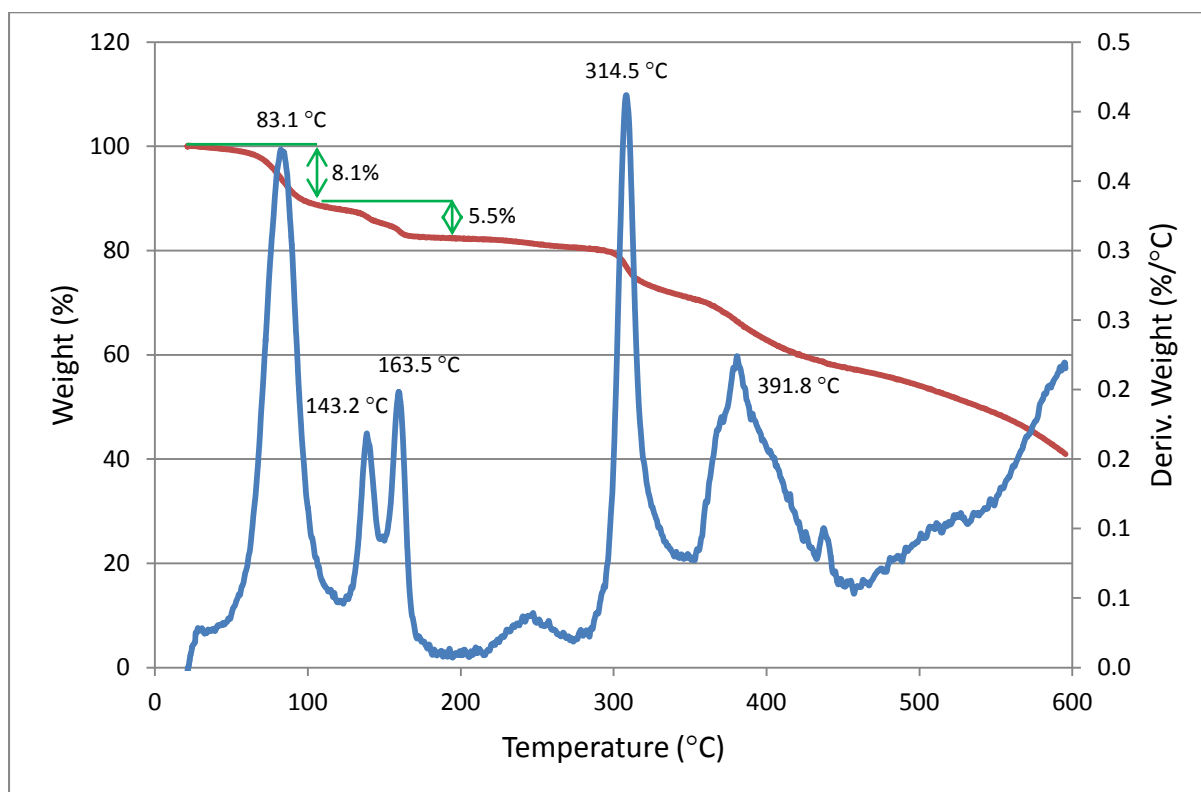


Figure 4.19: TG analysis of MCl_{Diox} . The red trace shows the percentage weight loss as a function of temperature ($^{\circ}C$) and the blue trace represents the first derivative of the same weight loss.

Although these interactions are still considered weak, they may explain the different thermal properties of this compound compared to others in the series. The thermogravimetric analysis of this compound is vastly different from the other compounds in this series (Figure 4.19). The first thermal event takes place at approximately $65^{\circ}C$, after which the thermogram stabilises momentarily before the second thermal event occurs in the range 130 – $139^{\circ}C$. This second event is immediately followed by another at approximately $150^{\circ}C$. The first thermal event accounts for the most substantial weight loss, with the second and third events representing a multistep weight loss with no apparent stable intermediates. After $160^{\circ}C$ the compound is thermally stable until $240^{\circ}C$, at which temperature a small event, resembling a glass transition, occurs. This is followed by decomposition of the complex, which commences at approximately $310^{\circ}C$. Unfortunately, because these events overlap one another, it is not possible to characterise the compound at any of the intermediate stages. The total mass loss before decomposition is 13.4% , which is close to the expected 14.1% calculated for one dioxane and two MeCN molecules. The first thermal event corresponds

approximately to a weight loss of 8.3%; it is assumed that this event coincides with the release of the two MeCN molecules ($\text{MeCN}_{\text{bp}} = 81.6\text{ }^{\circ}\text{C}$), although we expect only 6.8% weight loss. Because the three thermal events coincide to some extent, it is difficult to interpret the data. In future studies it may be possible to elucidate the exact nature of these thermal events using a DSC-hotstage, and TGA-MS. Although we cannot unambiguously correlate the thermal events to structural events in the crystals, it is nevertheless an interesting result. This is the only thermogram in the series of isoskeletal structures that shows guest retention above $60\text{ }^{\circ}\text{C}$ and more than one thermal event before decomposition. Because the dioxane guest is disordered over two positions it is difficult to establish what causes the guests to be retained at higher temperatures compared to the other solvates. When comparing this result to the thermal data of the other structures in this series, we speculate that the release of the guest molecules occurs through a cooperative mechanism, i.e. as one guest is removed, the other guests are also “pulled” out of the structure. This seems plausible if there is a rearrangement of the host metalloacycles as one guest is removed to facilitate the removal of the cavity-included guest. Of course, it is speculative to explain the mechanism of guest removal/release without further investigation. It should be noted that 1,4-dioxane is the only included guest in this series that has a boiling point above that of MeCN.

In further efforts to make sense of the thermal data, the residual electron density count in the solvent-accessible void was calculated using SQUEEZE, which reports 105 residual electrons residing in this channel per unit cell. This corresponds sufficiently well with the 92 electrons expected for one molecule of dioxane and two MeCN molecules. Therefore, the TG analysis is consistent with the SQUEEZE data.

4.7 $\text{MC1}_{\text{Acetone}} - [\text{Co}_2\text{Br}_4\text{L1}_2] \cdot 2\text{MeCN} \cdot \text{Me}_2\text{CO}$

The combination of **L1** and cobalt bromide in a solvent mixture of acetone and MeCN yields another isoskeletal crystal structure in the series of cobalt bromide metalloacycles. The structure crystallises in the space group $P\bar{1}$, with the ASU comprising one ligand molecule coordinated to a cobalt cation which in turn is coordinated to two bromide counter ions. A single molecule of MeCN and one molecule of acetone are also included in the ASU (Figure 4.20). As in the previous structures, the MeCN molecule is located in the interstitial space and aligned in a head-to-tail dimer with a symmetry-related partner. The acetone molecule is included in the cavity of the metalloacycle and is located near a site of inversion symmetry such that a second molecule is generated across this symmetry site. These two sites cannot be occupied simultaneously but, owing to symmetry, there is an equal distribution over these

positions. It is presumed that the acetone is distributed randomly in either of these positions along the length of the channel.

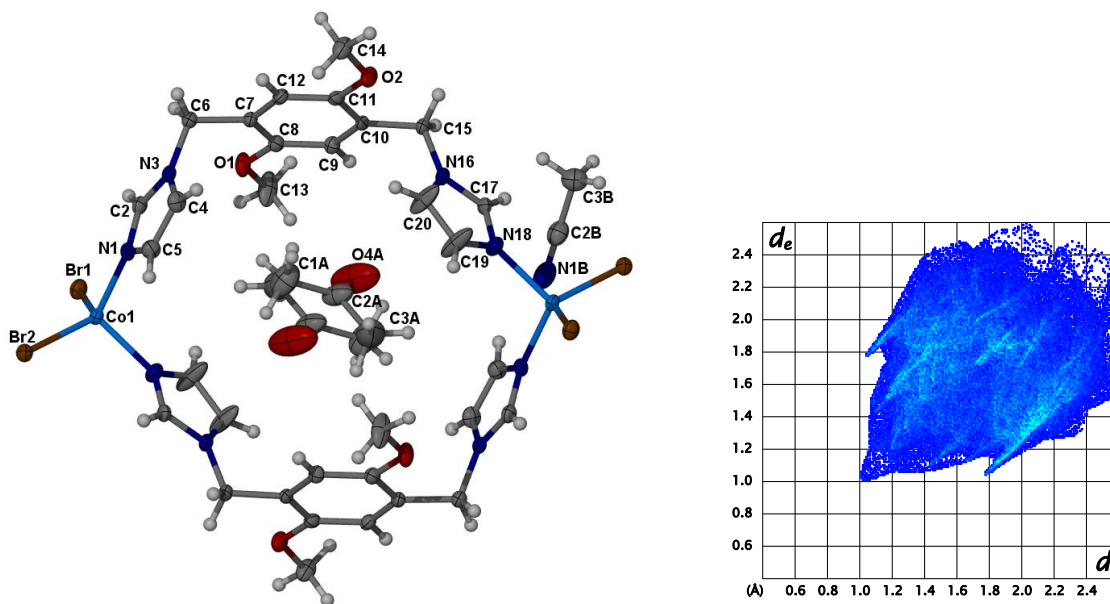


Figure 4.20 Structure of $MCl_{Acetone}$ represented as anisotropic displacement ellipsoids at 50% probability (left). Only the atoms of the ASU are labelled. On the right is the fingerprint plot generated for the metallosolvate of $MCl_{Acetone}$

Analogous to the dioxane solvate, the oxygen atoms of the acetone molecules are directed towards the apertures of the metallosolvates. These carbonyl oxygen atoms take part in weak C–H...O interactions (3.182(8) Å) with the nearby methyl groups of the MeCN guests within the channel (Figure 4.21). The acetone molecules are also weakly associated with the host metallosolvate by means of C–H... π interactions with the imidazole moieties (3.643 and 3.744 Å). In contrast to the dioxane solvate, the oxygen atoms of the guest are positioned furthest from the methoxy groups of the metallosolvate; these oxygen atoms are instead positioned for weak C–H...O interactions with the carbon atoms (C9 and C12, Figure 4.20) located in the α -position relative to the methoxy groups (3.361(8) Å). In this instance these host-guest interactions are weaker than the guest-guest interactions of the same type.

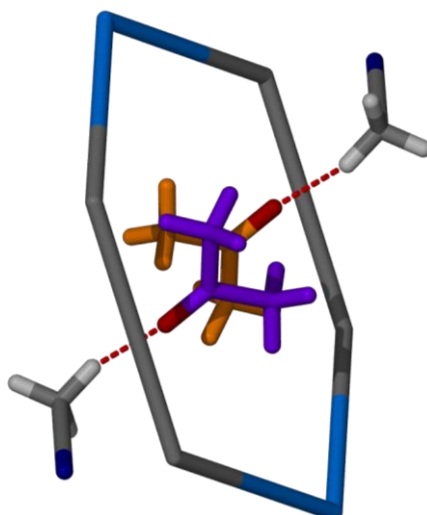


Figure 4.21 A simplified representation of the metallocycle of $\text{MC1}_{\text{Acetone}}$ including the acetone molecule (in two possible positions) showing the weak C–H...O hydrogen bond to the MeCN molecules.

Very weak offset $\pi\cdots\pi$ interactions exist between the phenyl moieties of the metallocycles, with a separation of 3.840 Å. As with all the previously described structures, the MeCN molecules are associated by weak $\pi\cdots\pi$ interactions between their respective nitrile groups. Slightly shorter $\pi\cdots\pi$ interactions are present between the nearest-neighbour MeCN guest molecules (3.302 Å).

Thermogravimetric analysis of the compound is remarkably similar to the other compounds in the series (apart from the dioxane solvate). The first thermal event commences at room temperature before an intermediate phase is reached at approximately 50 °C. The thermogram stabilises until the onset of decomposition at approximately 313 °C. The mass loss associated with the first thermal event accounts for a 10.8% weight loss, which is slightly less than expected for one acetone and two MeCN molecules per metallocycle (11.9%). The discrepancy in the experimental and calculated values can be ascribed to the loss of volatile guests at room temperature.

4.8 $\text{MC1}_{\text{EtOH}} - [\text{Co}_2\text{Br}_4\text{L}_1\text{L}_2] \cdot 2\text{MeCN} \cdot \text{EtOH}$

Another isoskeletal crystal structure in the series of cobalt bromide complexes was grown from an ethanol (EtOH) – MeCN mixture. The ASU consists of a complete ligand molecule coordinated to a cobalt cation, which is further coordinated to two bromide counter ions (Figure 4.22). Two guest molecules, one each of MeCN and EtOH are also part of the ASU. The EtOH molecule is positioned about an inversion centre such that it may occupy one of two positions with equal distribution. These two positions, however, cannot be occupied simultaneously in the same cavity. Because the positions have equal occupancies it is

assumed that occupation of the symmetry-related sites is randomly distributed in the crystal. The anisotropic displacement ellipsoid plot of the ethanol molecules does, however, suggest that there is some movement of the molecules within the cavity.

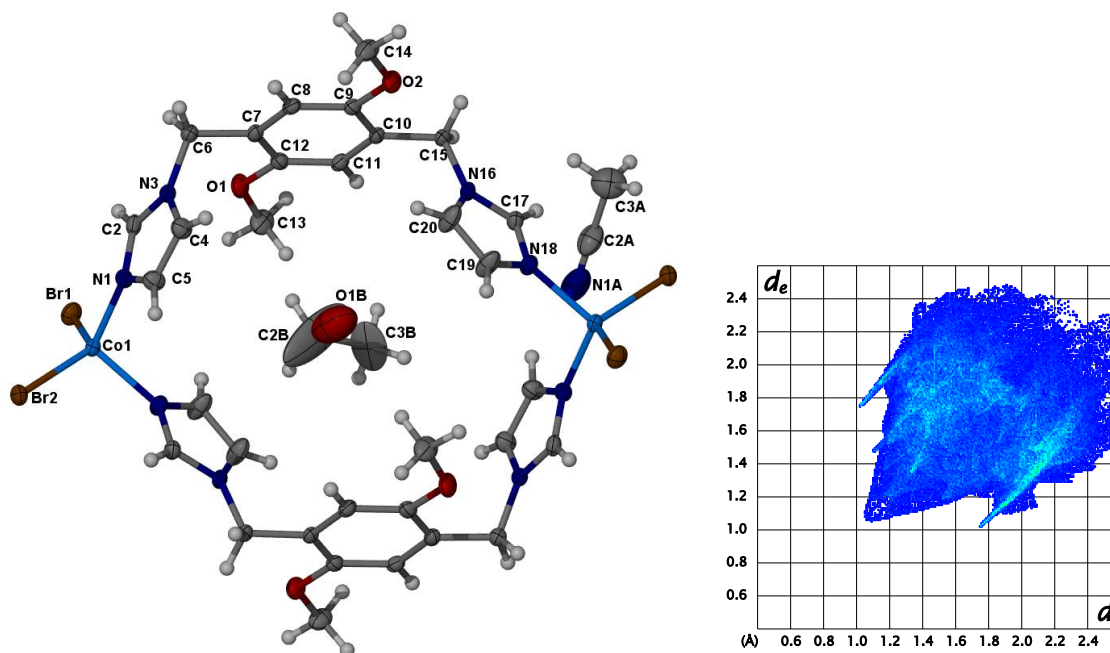


Figure 4.22 Anisotropic displacement (50%) ellipsoid plot of the structure of MCl_{EtOH} where only the ASU is labelled. Only one of the possible sites for the ethanol molecule is shown here for clarity since there is significant overlap of the two possible sites. The fingerprint plot generated for the metallocluster is depicted on the right.

There are very few noteworthy intermolecular interactions, other than those inherent to the host assembly, as described at the beginning of this chapter. The EtOH molecule is positioned much like the acetone is in $\text{MCl}_{\text{Acetone}}$, with the hydroxyl group directed out of the metallosupramolecular assembly. The hydrogen atom of the hydroxyl group could not be located in the electron density map and is therefore excluded from the model. Weak C–H \cdots O interactions (3.598(8) Å) are present between the hydroxyl oxygen of the EtOH guest and the methoxymethyl group of the metallosupramolecular assembly. Another weak interaction exists between the methylene carbon of the EtOH and the nearest imidazole moiety in a C–H \cdots π type contact (3.835 Å). The only other interactions that can be identified are C–H \cdots O contacts between the methyl group of the MeCN and the oxygen atom of the EtOH guest (3.202(9) Å) as shown in Figure 4.23. The fingerprint plot (Figure 4.22, right) generated for this structure confirms the existence of mainly van der Waals type interactions even when a hydrogen bond donor (EtOH) is present. The short tails that are visible on either side of the plot are indicative of the interactions with the bromide counter ions in the host assembly.

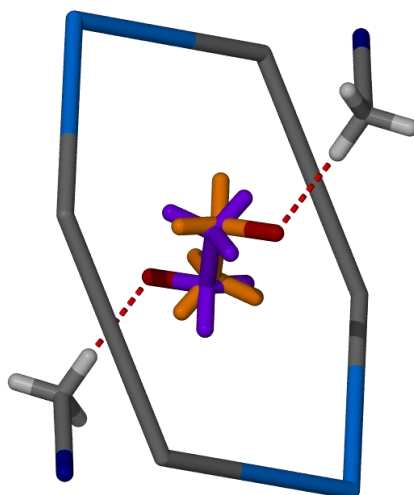


Figure 4.23 Weak C–H...O interactions between the ethanol and MeCN guest molecules in MC1_{EtOH} . The metallocycle is shown as a simplified molecular graph and the weak intermolecular interactions are shown as fragmented red lines.

The thermal profile for this compound is somewhat similar to that of the rest of the isoskeletal series. There is immediate release of the guests at ambient temperature until approximately 50 °C. This weight loss is 16.1% of the total molecular weight, which is somewhat higher than expected from the single-crystal analysis. A single EtOH molecule and two MeCN molecules per metallocycle should yield a 10.9% weight loss. The excess weight loss can be attributed to insufficient drying of the sample before analysis.

4.9 $\text{MC1}_{\text{MeCN}} - [\text{Co}_2\text{Br}_4\text{L}_1\text{L}_2] \cdot 3\text{MeCN}$

Recognising that these metallocycles can be synthesised from a number of different solvents (in the presence of MeCN), it was considered that there may be the potential to tune the packing arrangement of the metallocycles by exploring even bulkier solvents. The conjecture was that solvent (guest) molecules with a larger molecular volume could potentially expand the metallocycles sufficiently to disrupt the packing arrangement and allow the formation of continuous one-dimensional channels that are not interrupted by MeCN molecules. From the analysis of the solvates already obtained it was determined that small variations to these guests would be the most suitable option for a comparative study. Even if this result was not obtained it would be interesting to investigate the effects of these larger molecular volumes on the metallocycles.

Crystals were subsequently grown from toluene, *p*-xylene and ethyl acetate (EtOAc) in the presence of MeCN. Toluene and *p*-xylene were selected because of their similarity to benzene, as well as their ready availability. EtOAc is also readily available and has a molecular structure somewhat reminiscent of acetone. It was anticipated that the increased size of the guest molecules may be an influential factor for the methoxy functional groups of

the ligands to “open up”, allowing the formation of continuous channels or a different arrangement of the metalloclusters. This would most likely disrupt the symmetry of the metalloclusters, and it was expected that if these guest molecules are too large for the cavities they would be excluded from the metalloclusters (i.e. occupy spaces between the metalloclusters) or not permit the formation of the metalloclusters at all, resulting rather in the formation of polymeric chains.

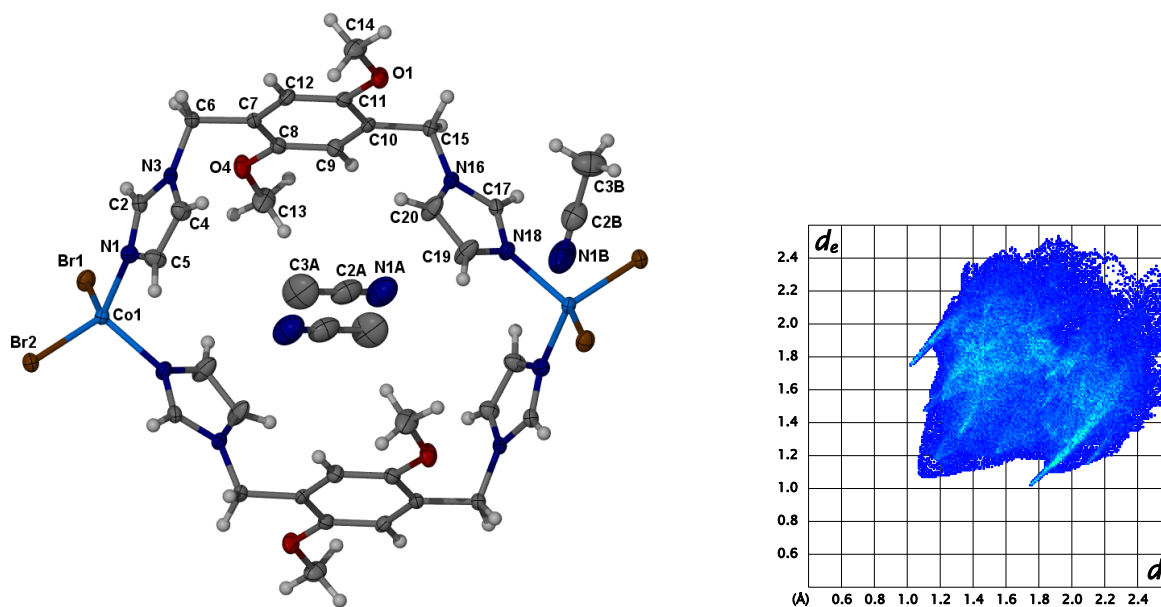


Figure 4.24 Anisotropic displacement ellipsoid plot (50% probability) of the structure of MCl_1MeCN . Only the atoms of the ASU are labelled and hydrogen atoms of the cavity included MeCN have been omitted for clarity. This structure is representative of the structures crystallised from toluene, *p*-xylene and EtOAc. The fingerprint plot for the metallocluster is shown on the right.

Surprisingly, the crystal structures obtained from these solvent mixtures are all identical. The metalloclusters are arranged in an isoskeletal manner to the structures already discussed. The ASU consists of a single ditopic ligand molecule coordinated to a cobalt cation, in a distorted tetrahedral geometry, which is further coordinated to two bromide counter ions (Figure 4.24). In this instance, two molecules of MeCN are incorporated in the ASU, one positioned in the interstitial space, as in all the other structures, and the other molecule is contained within the metallocluster. The MeCN guest in the metallocluster is disordered about an inversion centre and therefore has two potential occupancy sites with equal distributions. These two positions lie very close to the inversion centre and therefore cannot be occupied concurrently.

The orientation of the MeCN molecule inside the cavity is such that the nitrile moiety is directed towards the aperture of the metallocluster (Figure 4.25). Because the two possible positions of the MeCN molecule cannot be occupied simultaneously, it is assumed that the orientations are random within the crystal. The MeCN molecule in one cavity is not expected

to affect the orientation of the molecule in the next cavity along the channel; although it is not certain if the same is true for the molecules occupying cavities in the neighbouring channels. The centres of the channels are separated by a distance of 11.982 Å, which is probably too distant for any communication between the guests. Of course, this cannot be confirmed by crystallographic methods alone.

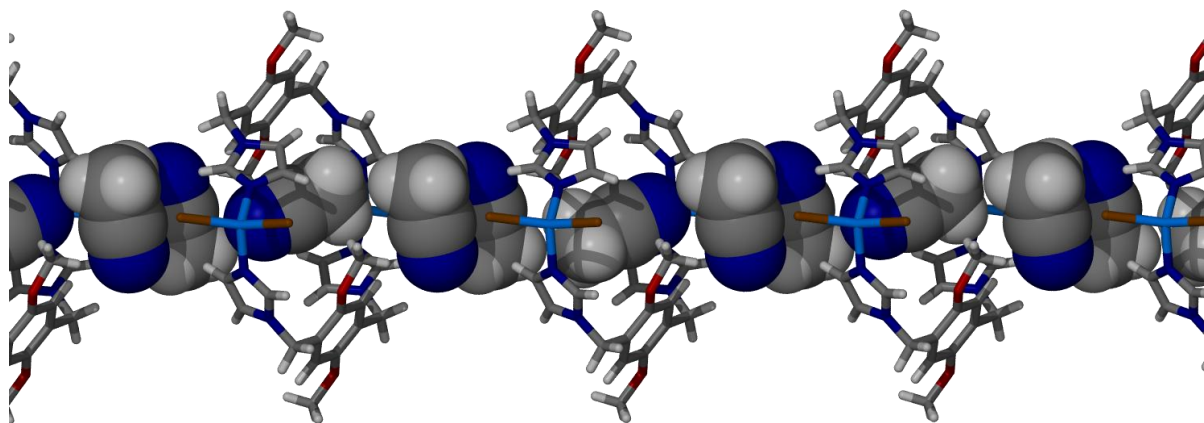


Figure 4.25 Packing diagram showing a single column of MCI_{MeCN} . The cavity of the metallocycle can accommodate only one MeCN molecule aligned perpendicularly to the molecules in the interstitial spaces and the preferred orientation of this molecule appears to be random throughout the channel.

Weak C–H...N interactions are present between the independent MeCN guest molecules (3.452(9) Å) (i.e. between a MeCN in the cavity and one exterior to the metallocycle – see Figure 4.26). Weak C–H... π can be identified between the methoxymethyl group of the metallocycle and the nitrile moiety of the cavity-included MeCN. The inclusion of only one MeCN molecule in the cavity of the cycle has implications for the conformation of the overall metallocycle. The most significant conformational change can be observed in the out-of-plane (Plane 4 from Plane 5, Figure 4.2) tilt angle of one imidazole moiety (25.0°). This is by far the greatest adjustment of the metallocycle in accommodating the guest, especially when compared to the tilt angle of this same moiety in the benzene solvate (10.60° out of the plane). This is clearly illustrated in the structure overlay of MCI_{Benz} and MCI_{MeCN} in Figure 4.27.

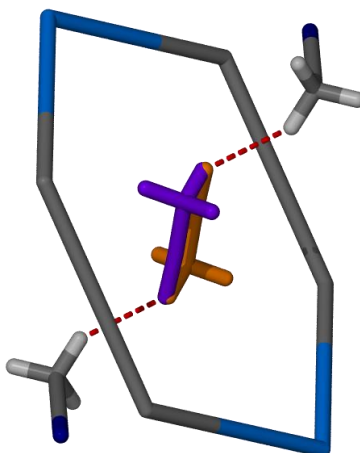


Figure 4.26 Weak C–H...N interactions between the two unique MeCN molecules of MC1_{MeCN} . The two possible positions of the cavity-included MeCN molecules are shown in purple and orange. The metalloccycle has been reduced to a simple molecular graph so that the guests are easily visible.

The inclusion of MeCN has a marked effect on the shape (molecular conformation) of the metalloccycle when compared to the larger guest-included structures. The intramolecular Co...Co separation distance (11.421(1) Å) is analogous to that observed in the acetone solvate (11.420(1) Å), as is the N–Co–N angle (107.89(9)°). The phenylene rings of adjacent metalloccycles are involved in offset π ... π stacks (3.663 Å) that have a similar separation to that observed in the DCM solvate. Interestingly, the π ... π stack that forms between the interstitial MeCN guest molecules experiences the greatest separation in this structure (3.380 Å).

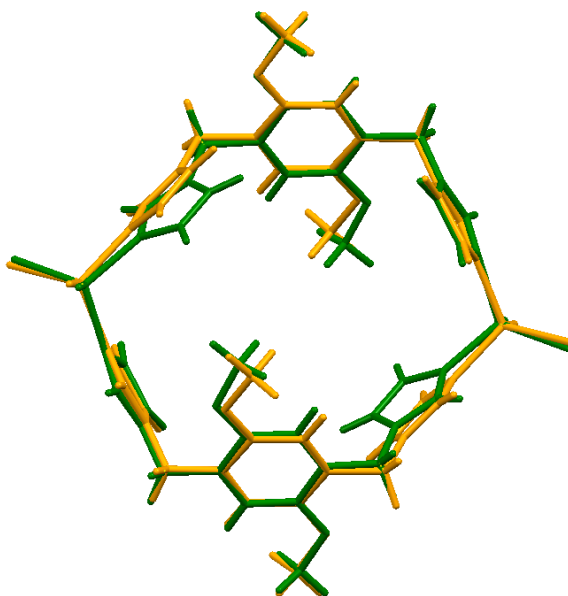


Figure 4.27 Structure overlay of the MeCN-included structure MC1_{MeCN} (green) with that of the benzene solvate MC1_{Benz} (orange)

This outcome is of interest for a number of reasons; firstly it demonstrates that toluene, *p*-xylene and EtOAc in all probability cannot be included within the metalloccycle because their

molecular volume is too large for the cavity, or that there are other interactions between the host and these particular guests that are unfavourable, thus preventing their inclusion. Secondly, it should not be ruled out that the metalloCycle selectively includes MeCN over toluene, *p*-xylene and EtOAc for reasons other than size and shape of the guests (but it is not believed to be the case). From these results, one might assume that it is possible to obtain the same structure by crystallisation from a single solvent system of MeCN; however this method results in immediate precipitation of a polycrystalline product. Owing to poor PXRD patterns, the guest included in the metalloCycle cavities cannot be determined, and TG analysis would be meaningless without other analysis. It also raises the question of why MeCN is not selectively included in the cavities of all the other structures in this series. The metalloCycle is presumably selective towards the solvents included in the cavities over that of the MeCN in all the other structures. If this is the case, what drives the selectivity? Other metalloCycles in this series (DCM and EtOH) show similar metalloCycle conformations to that observed for the MeCN structure. Another question that arises then is: What drives the metalloCycle to take up two different guests rather than only one? This would require in-depth investigation, including computational studies to understand this phenomenon.

4.10 COPPER-BASED METALLOCYCLES

A simple representation of these metalloCycles shows that they too are approximately hexagonal. However, unlike the structures discussed above, these hexagons are more planar and not in the chair (or boat) conformation. It is therefore presumed that the copper-based metalloCycle is more rigid than the other transition metal metalloCycles

4.10.1 $\text{MC11}_{\text{DCM}} - [\text{Cu}_2\text{Br}_4\text{L}_1\text{L}_2] \cdot \text{MeCN} \cdot \text{DCM}$

Analogous metalloCycles can be obtained by crystallisation of **L1** with CuBr_2 . MC11_{DCM} crystallises in the space group $P\bar{1}$ with an ASU analogous to those in the **MC1** series – one entire ligand molecule coordinated to a copper cation that is further coordinated to two bromide counter ions (Figure 4.28). Also in the ASU are two solvent molecules, namely one MeCN and one DCM molecule.

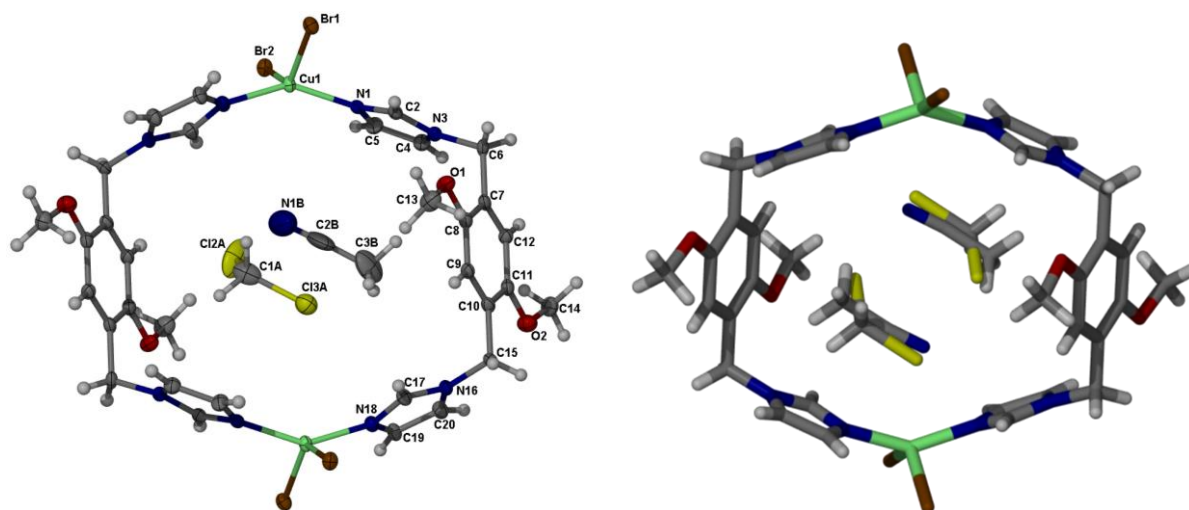


Figure 4.28 Anisotropic displacement ellipsoid representation of **MC11_{DCM}**. The atoms of the ASU are labelled, with only one of each of the guests shown for clarity. The capped-stick representation on the right shows the averaged structure with the two different guests in both possible sites.

What make these structures intriguing are the coordination geometry of the copper centre and the consequent shape of the metalloclycles. The geometry around the copper centre is still tetrahedral but the M...M distance (9.797 Å, with an N–Cu–N angle of 145.4(1)°) is significantly shorter than that in the other transition metal complexes. The more rigid shape of the copper metalloclycles presumably enables them to pack in a more regular manner with the exclusion of void spaces between the complexes. While the connectivity of the metalloclycles is the same as those already described, the difference in the geometry of the metal centre appears to alter the overall shape of the metallocycle. The shape of the metallocycle in turn influences the packing arrangement of these entities. Because the metalloclycles are more rectangular, they tend to pack more efficiently such that there are no large interstitial spaces that require space-filling solvent molecules. The two solvents of crystallisation are accommodated within the metalloclycles. Both the DCM and MeCN molecules occupy the same sites, but with differing distributions. The MeCN molecule occupies the site with 66% probability while the DCM molecule is present for the remainder i.e. 34% of the time. These different guests each have two possible sites that they can occupy with equal probability. It is, however, impossible to establish when each of the guests is present in the cavity and it is therefore assumed that they are randomly distributed throughout the crystal. It is possible for each metallocycle to house two guest molecules per cycle, and it may even be possible to accommodate two different guests per cavity. If the pocket were to contain two DCM molecules, the molecules would form a halogen bonded dimer with Cl...Cl distances of 3.51(1) Å. If two MeCN molecules occupy the pocket the interactions between the guests would be slightly weaker, with the two molecules aligned in a head-to-tail dimer

with C–H...N interactions (3.86(2) Å). If one of each of the guest molecules is present in the pocket, there is the possibility for Cl...N interactions (2.83(2) Å). A SQUEEZE electron count suggests that there is one DCM and one MeCN molecule per void (i.e. per metallocycle).

The exclusion of solvent from between the metallocycles results in the formation of discrete solvent-filled pockets (Figure 4.29) rather than continuous one-dimensional channels as observed in the previous series of structures (**MC1**). When viewed along [100] the structure appears to contain one-dimensional solvent-filled channels. However, when viewed from another perspective it is clear that the metallocycles pack in an offset manner such that the cavities of the metallocycles are blocked by methoxymethyl groups of adjacent metallocycles (Figure 4.29). Although these pockets are discrete, it is nevertheless possible to remove guest molecules from these cavities while leaving the host framework intact in a single-crystal to single-crystal transformation (see Section 4.10.3 for further discussion). This is in stark contrast to the metallocycles derived from the other transition metal salts in this series. This is quite remarkable since a structural rearrangement is presumably necessary for desolvation.

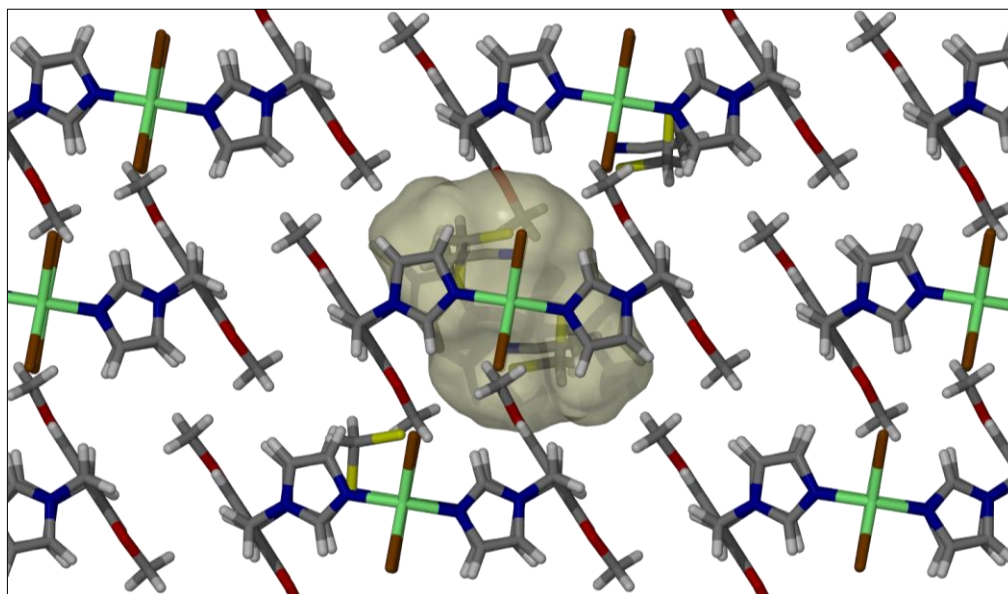


Figure 4.29 Packing arrangement of **MC11_{DCM}**. The semi-transparent surface depicts a solvent accessible void in the cavity of a single metallocycle.

The only host-guest interaction of significance is the C–H... π contact between the cavity-included DCM carbon atom and an imidazole moiety of the metallocycle (3.773 Å). Other host-guest interactions occur between the DCM carbon atom and the methoxy oxygen atom of a neighbouring metallocycle (3.14(2) Å), and a similar interaction between the methoxy oxygen atom and the carbon atom of an included MeCN (3.503(9) Å).

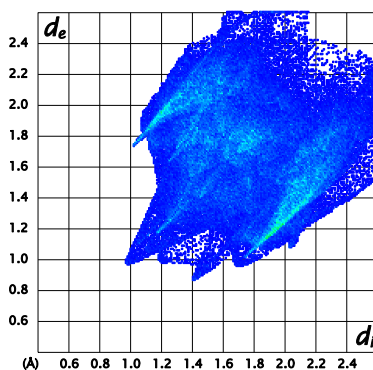


Figure 4.30 Fingerprint plot of the metallocluster of MC11_{DCM}

The fingerprint plot (Figure 4.30) confirms that there are no remarkable interactions involving the host metallocluster. The tail on the right is due to the C–H...O interactions of the methoxy oxygen atom of the metallocluster with the carbon atom of the DCM molecule in the metallocluster above or below.

The $\pi\cdots\pi$ interactions between the phenyl moieties no longer govern the packing arrangement of the metalloclusters (as in the previous series); instead there are a number of $\pi\cdots\pi$ stacking interactions between imidazole moieties of neighbouring metalloclusters (3.446 Å). These same interactions are present for all four of the imidazole moieties of the metallocluster and are assumed to provide greater stabilisation of the metallocluster positions (Figure 4.31). The interacting imidazole rings are orientated parallel to each other in order to facilitate favourable interactions. Other interactions of interest in the assembly of the host framework are C–H...Br interactions of the imidazole moieties with the bromide counter ions of neighbouring metalloclusters (3.728(4) and 3.779(4) Å). The other bromide counter ion is involved in C–H...Br interactions with the methylene bridging carbon atom of an adjacent metallocluster (3.778(4) Å). Although these interactions are rather weak, it is thought that they may make a small contribution to the overall stabilisation of the host assembly.

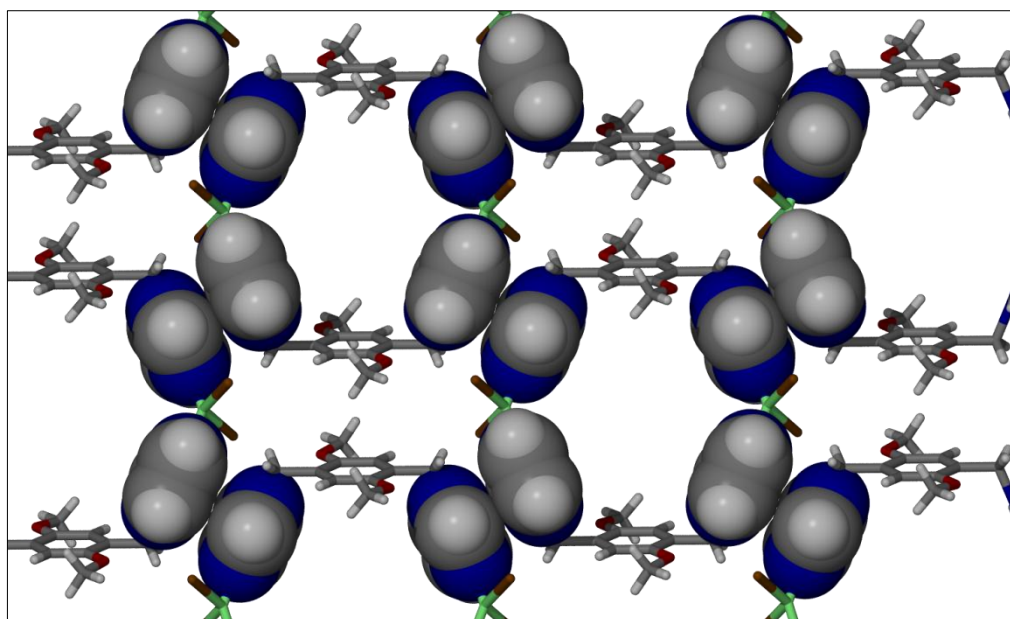


Figure 4.31 Representation of the $\pi\cdots\pi$ interactions between the imidazole moieties of neighbouring metalloacycles in MC11_{DCM} . Imidazole moieties are shown in van der Waals representation to highlight the close proximity of the rings. Interacting rings are aligned in an up-down manner to stabilise the interactions.

Although there are no $\pi\cdots\pi$ interactions between the phenyl moieties they interact by means of $\text{C-H}\cdots\pi$ interactions (3.698 Å) between the methoxymethyl group of one ring and the phenyl moiety of the neighbouring metalloacycle (Figure 4.32).

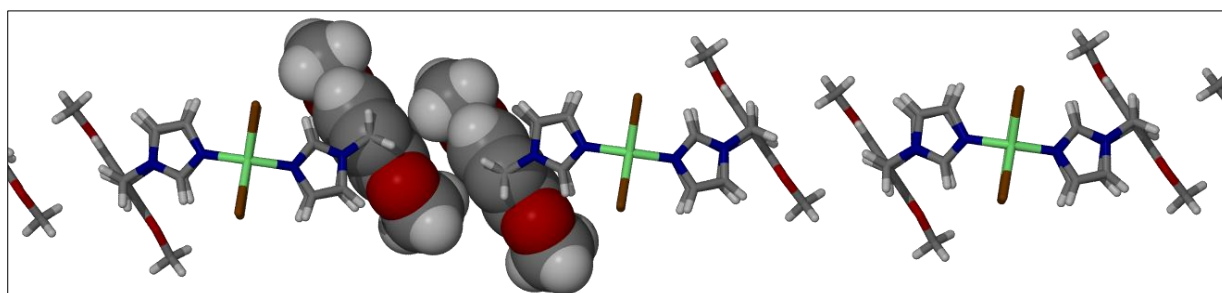


Figure 4.32 $\text{C-H}\cdots\pi$ interactions between the p-methoxyphenyl groups of neighbouring metalloacycles of MC11_{DCM}

The thermogravimetric analysis of this structure (Figure 4.33) is vastly different to that of the homeotypic series of metalloacycles that incorporate other transition metal cations. Indeed, the thermal profile is more similar to that of the dioxane solvate i.e. MC1_{Diox} . The sample begins to lose volatile guests at the outset of the analysis and continues to lose weight in a multi-stage thermal event. The first step occurs in the temperature range 25-75 °C, the second in the range of 75-135 °C and the third between 135-200 °C. The thermogram does not appear to stabilise at any point during the analysis and decomposition occurs near 200 °C. The percentage weight loss before decomposition amounts to approximately 10.3%. This weight loss correlates well with the calculated loss of one MeCN and one DCM molecule per metalloacycle (10.8%). In conjunction with the description of the single-crystal structure, it

appears that each metallocycle accommodates one of each of the guests within its cavity. This result is remarkable since it is possible to remove the guest molecules from the cavities in a single-crystal to single-crystal transformation even though the TG trace suggests that there is no stable phase before decomposition. Of course, DSC analysis may provide a suitable explanation but problems with phase purity and sample size prevented such analysis.

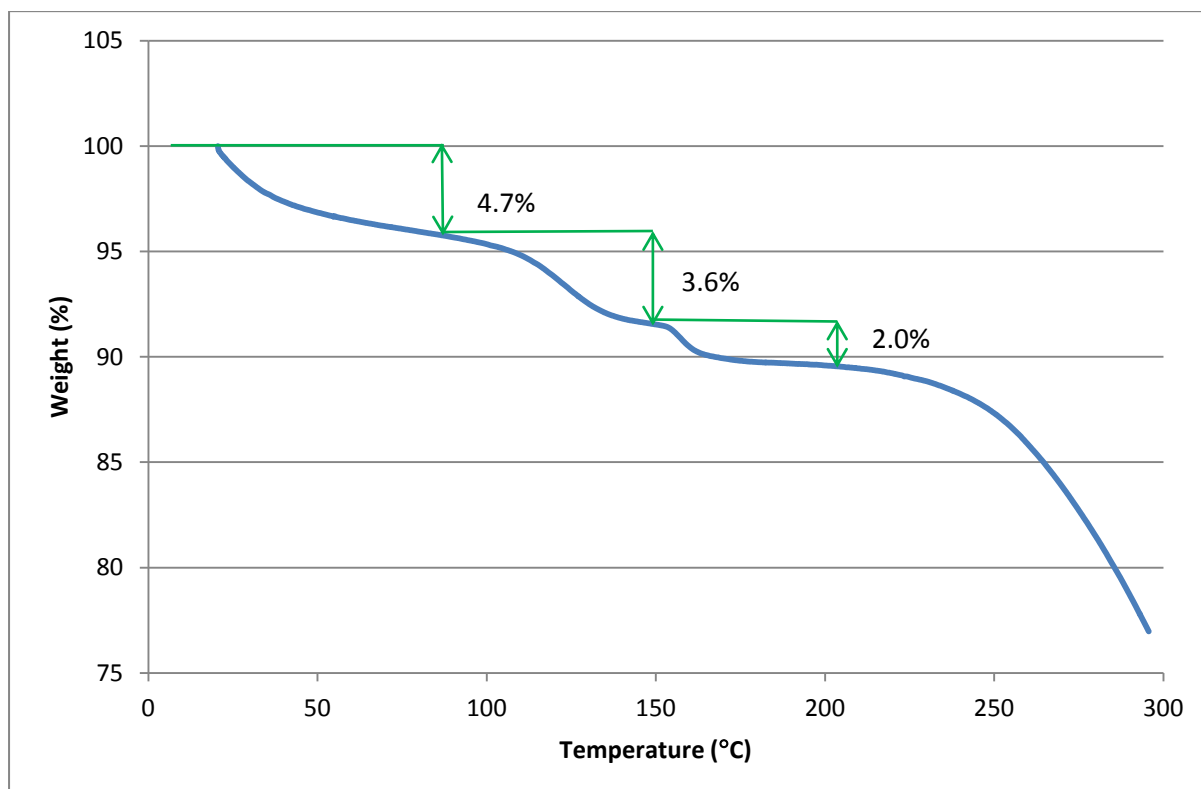


Figure 4.33 TG analysis of MC11_{DCM}

4.10.2 MC11_{CHCl₃} – [Cu₂Br₄L₁]₂·MeCN CHCl₃

Crystallisation of CuBr₂ and **L1** from a CHCl₃/MeCN solvent mixture yielded a solvatomorph of MC11_{DCM} (the space group is also $P\bar{1}$ and the unit cell parameters are similar). The ASU (Figure 4.34) is analogous to that of the previous structure, containing a copper cation coordinated to an entire ligand molecule and two bromide counter ions arranged in a distorted tetrahedral geometry. One molecule of MeCN is situated within the metallocycle. From the electron density maps, it is inferred that a molecule of CHCl₃ is also present in the metallocycle, but it is of very low occupancy (approximately 10%) and cannot be modelled adequately. The ORTEP plot, shown in Figure 4.34, depicts the guest MeCN atoms as large round ellipsoids, indicating that the molecule is either experiencing some anisotropic displacement within the cavity or that there is actually another molecule present in the cavity. Because the CHCl₃ molecules have very low site occupancies it seems

irrelevant to discuss the intermolecular interactions with these guests since they clearly have little influence on the overall structure. It is more appropriate to analyse the effects of the MeCN molecule on the formation and stability of the metalloCycles.

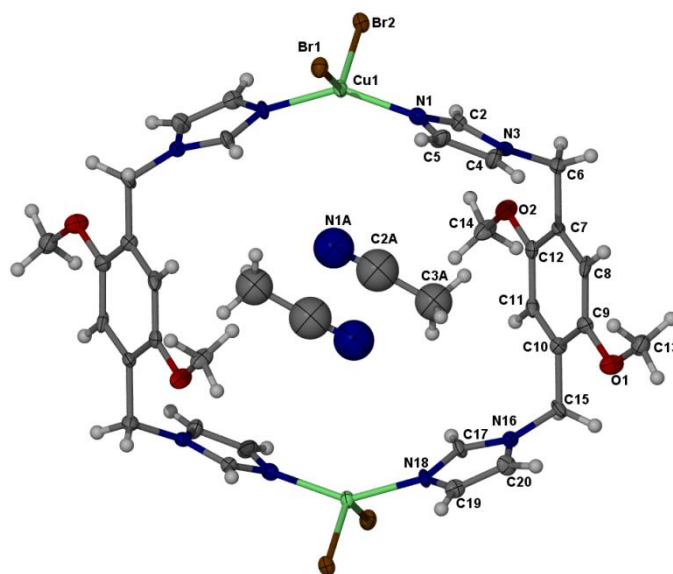


Figure 4.34 Anisotropic displacement (50%) ellipsoid plot of **MC11**_{CHCl₃}. The ASU is labelled; however the chloroform molecules could not be adequately modelled and are therefore not included here.

As in the DCM-occluded structure, the host-host contacts primarily consist of $\pi\cdots\pi$ stacking interactions of the imidazole moieties in adjacent metalloCycles (Figure 4.35). The imidazole moieties align in an anti-parallel arrangement with a separation distance of 3.486 Å. This distance is comparable to that observed between the metalloCycles of **MC11**_{DCM}. The phenyl moieties of the metalloCycle associate by means of C–H $\cdots\pi$ interactions between the methoxymethyl group of the one cycle and the phenyl group of its nearest neighbour (3.733 Å). Few host-guest interactions exist in the structure although these are difficult to evaluate since the CHCl₃ molecules could not be modelled adequately. The MeCN guest on the other hand experiences a number of weak intermolecular interactions with its surrounding host. C–H $\cdots\pi$ interactions exist between the methyl group of the guest and the nearby imidazole moiety (3.855 Å) as well as the nearest phenyl moiety (3.588 Å) of the host. A fingerprint plot for this structure was not included owing to the inadequate modelling of the CHCl₃ guest molecules, which would produce an inaccurate result.

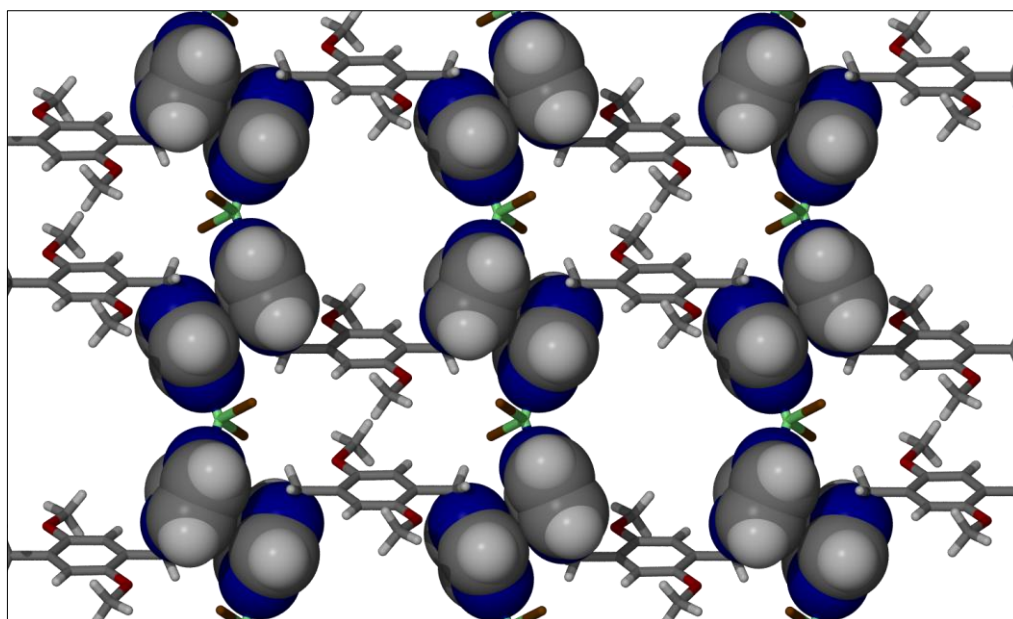


Figure 4.35 Packing arrangement of one layer of metalloclusters in $\text{MC11}_{\text{CHCl}_3}$ demonstrating the $\pi\cdots\pi$ stacking interactions between anti-parallel imidazole moieties of adjacent metalloclusters.

4.10.3 $\text{MC11}_{\text{vac}} - [\text{Cu}_2\text{Br}_4\text{L}_2]$

TG analysis of MC11_{DCM} established that solvent loss occurs around 110 °C. MC11_{vac} was obtained by placing crystals of the solvated structure (in this instance CHCl_3) in a vacuum oven for approximately 5 hours at 100 °C. A suitable crystal was then selected for data collection. The crystals undergo a colour change from red to green upon desolvation; the red crystals are fully solvated, whereas the green crystals are amorphous and do not diffract X-rays. A few orange crystals were also present and one of them was selected for SCD analysis (Figure 4.36). No residual electron density peaks were located within the cavities previously occupied by the MeCN and chlorinated guests, implying that desolvation occurs as a single-crystal to single-crystal transformation for these particular crystals.

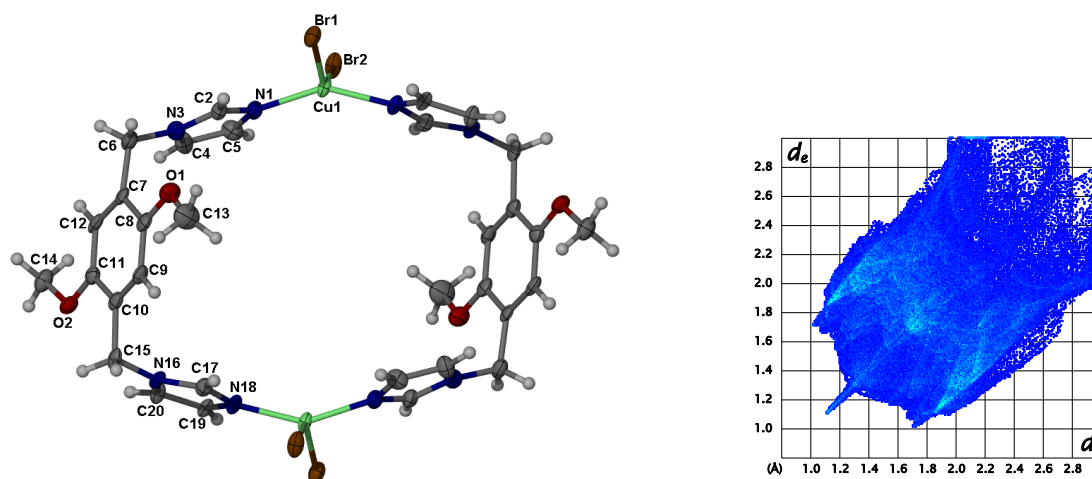


Figure 4.36 Anisotropic displacement ellipsoid representation of the fully evacuated **MC11_{vac}**. The fingerprint plot rendered for this structure is depicted on the right.

The metallosupramolecular structure appears to be relatively robust, maintaining its overall shape even after the guests have been removed, although the metallosupramolecular undergoes some conformational changes to its geometry. Firstly the intramolecular Cu...Cu distance becomes somewhat shorter than in the solvated structures ($\Delta \approx 0.8 \text{ \AA}$) and the geometry around the copper centre is also altered – bond angles becomes more obtuse ($147.7(3)^\circ$ and $131.93(6)^\circ$ compared with $144.9(3)^\circ$ and $128.58(7)^\circ$ in the solvated structure); i.e. there is a cooperative change. The methoxyphenyl moieties are observed to be in a more upright rather than tilted position in relation to the plane of the metallosupramolecular (51.8° compared to 47.3° in the solvated metallosupramolecular). Compared to the solvated structures, the imidazole moieties remain approximately perpendicular relative to the plane of the metallosupramolecular resulting in a more rectangular metallosupramolecular than in the solvated structures. These changes are clearly demonstrated in the structure overlay of **MC11_{CHCl₃}** and **MC11_{vac}** in Figure 4.37. In terms of the packing arrangement of the guest-free structure, there appear to be very subtle changes in the intermolecular interactions. The arrangement of the imidazole moieties in relation to each other is slightly different, with the $\pi \cdots \pi$ stacks becoming more offset (3.656 and 3.536 Å, Figure 4.38). Adjacent metallosupramoleculars are connected via weak C–H... π interactions between the methoxymethyl group of one metallosupramolecular and the phenyl moiety of the next (3.504 Å). So the phenyl groups tend towards each other while the imidazole moieties become further apart. With the removal of the guest molecules, the layers of metallosupramoleculars move closer to one another so that the methoxy groups of adjacent layers protrude into the cavities of the metallosupramoleculars above and below, as depicted in Figure 4.39. This movement of the layers gives rise to C–H...O interactions (3.57(1) Å) between the two methoxymethyl groups of metallosupramoleculars in independent layers. The fingerprint plot (Figure 4.36) shows that there are

few distinct intermolecular interactions in the structure of **MC11**_{vac}. There is a large contribution from van der Waals contacts between the peripheral hydrogen atoms of the metalloporphyrins.

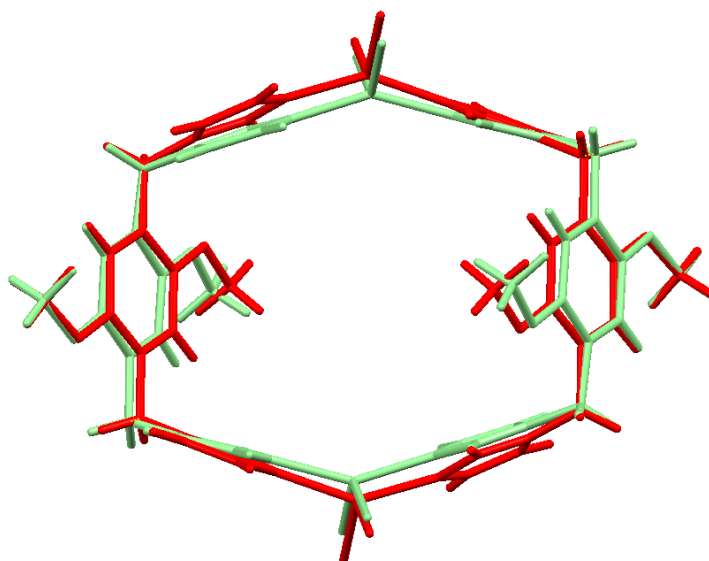


Figure 4.37 Structural overlay of the metalloporphyrins of **MC11**_{CHCl₃} (represented in red capped-sticks) and the empty structure **MC11**_{vac} (shown in green). The overlay shows the minor conformational changes in the metalloporphyrin upon guest removal, and specifically the change in the positions of the copper centres in the respective metalloporphyrins.

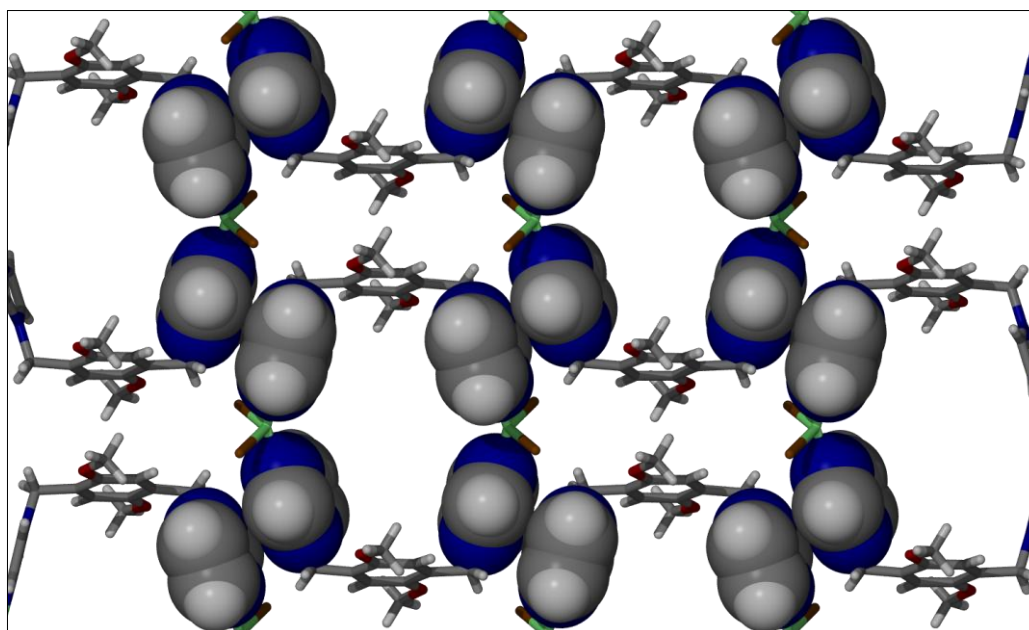


Figure 4.38 Packing arrangement of one layer of metalloporphyrins in **MC11**_{vac} indicating the more distant and offset imidazole moieties involved in $\pi \cdots \pi$ interactions.

With the movement of the metalloporphyrins upon desolvation, there is a reduction in size of the solvent-accessible voids. In fact, the methoxymethyl groups penetrating into the metalloporphyrins in adjacent layers, results in the deformation of the discrete pocket (Figure 4.39). The calculated void volume for the empty metalloporphyrin is 140 \AA^3 (using a 1.2 \AA probe).

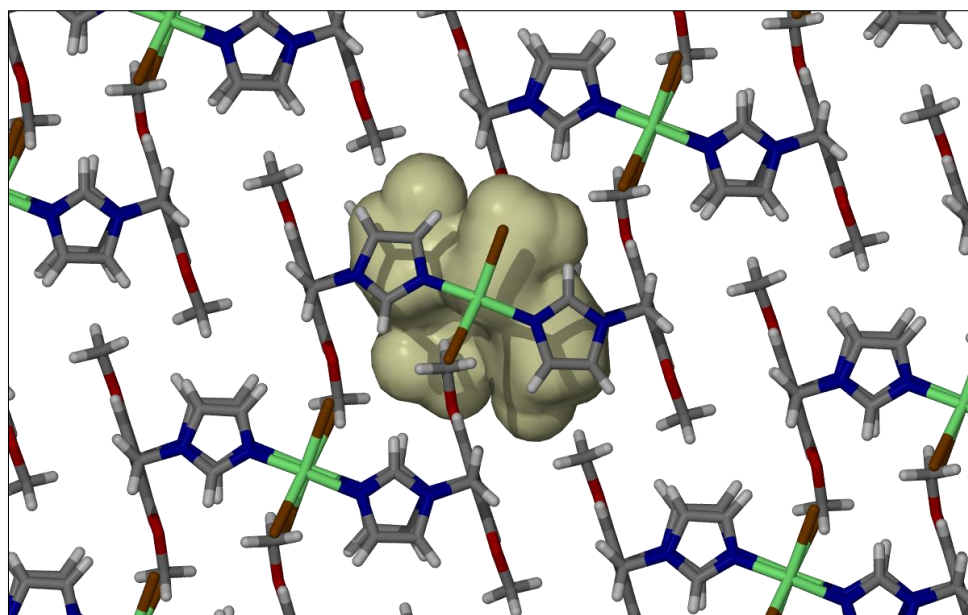


Figure 4.39 Packing arrangement of the metalloclusters of $MC11_{vac}$ showing the slight changes in the arrangement, resulting in deformed pockets that are mapped within the central metallocluster (depicted as light yellow surfaces)

4.11 FURTHER ANALYSIS AND DISCUSSION

Solvent-accessible voids in each of the structures can be calculated using SQUEEZE (Table 4.2), but MSRoll⁵ can also be used (Figure 4.40). However, because the solvent-accessible voids are one-dimensional channels, the space to be mapped can be erroneously defined by the user and also do not necessarily provide the accessible-volume per unit cell. SQUEEZE is also a widely accepted method used to define the solvent-accessible voids compared to MSRoll, which is used more frequently in protein structure analysis. Each method has its own advantages and disadvantages but for consistency, and simplicity, SQUEEZE was selected for calculating the volumes of solvent-accessible voids.

Table 4.2 Solvent-accessible volumes (\AA^3) calculated per unit cell for each of the metalloclusters described in this chapter. Results obtained from SQUEEZE using a 1.2 \AA probe radius

	DCM	$CHCl_3$	Benzene	Acetone	Dioxane	EtOH	MeCN	Vacuum
Cobalt	291	311	317	295	302	290	286	
Nickel	293	306	308				280	
Zinc	290	303	308				279	
Copper	202	203						140

From the results shown in Table 4.2 it is clear that the channels in the benzene solvates are the largest, and those including MeCN the smallest, as might be expected. The structures obtained with different metal cations are also comparable in each group of solvates (where comparison is possible), except in the instance of the benzene solvates where the void volume

is substantially larger in the cobalt complex. The copper metalloCycles, of course, are not comparable to the other metalloCycles as they have a completely different structural arrangement, with the formation of discrete pockets rather than continuous one-dimensional channels. What is remarkable about these discrete pockets is that the void per metalloCycle is not much smaller compared to the channels in the isoskeletal series. These pockets in the copper-based metalloCycles remain constant regardless of the solvent system from which the crystals were grown, confirming the robust nature of the metalloCycle. The volume of the void decreases dramatically with the removal of the guests (evacuated structure) from these crystals owing to rearrangement of the metalloCycles.

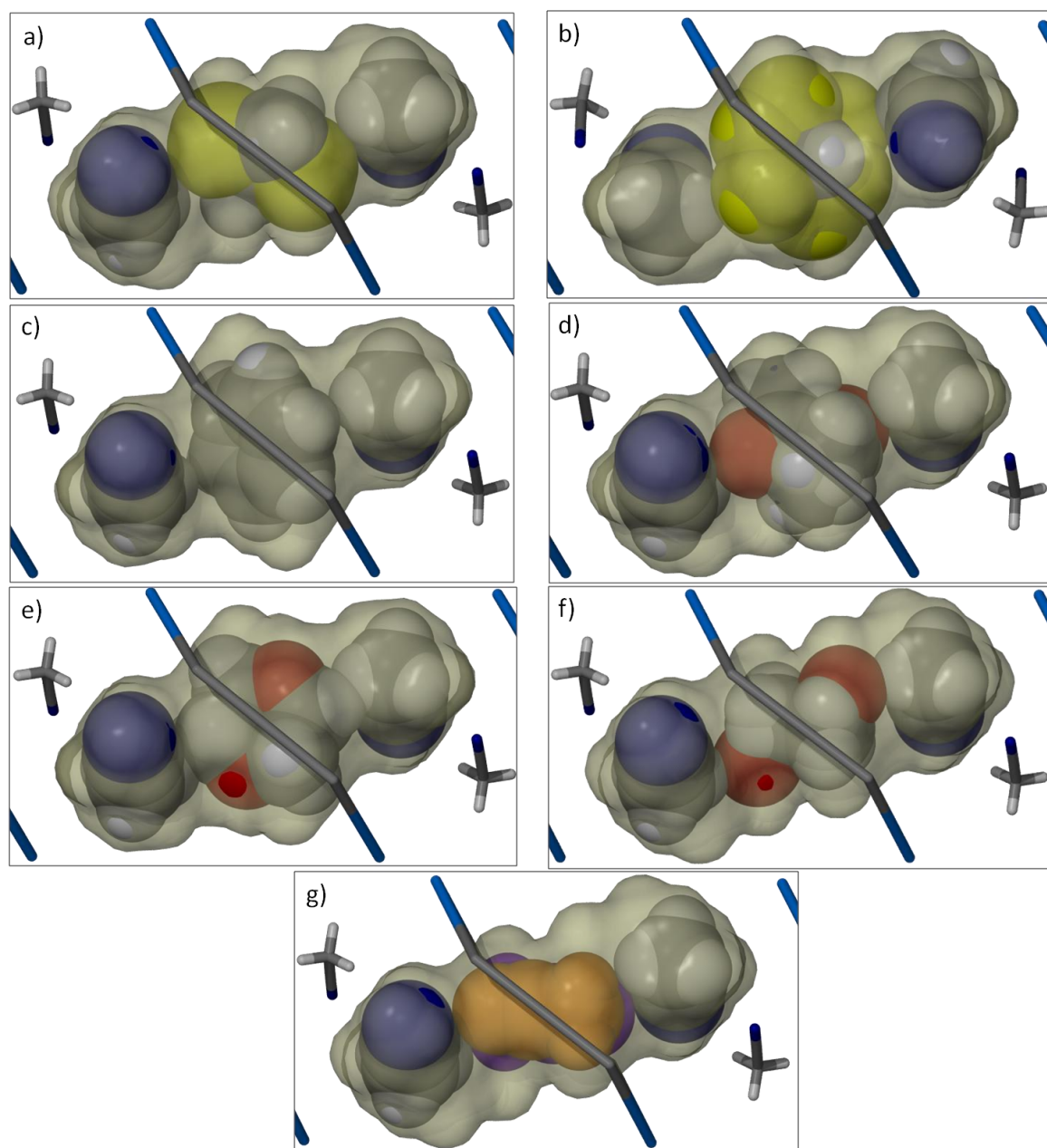


Figure 4.40 Comparison of the solvent-accessible surfaces mapped with a probe radius of 1.2 Å in each of the cobalt-based metalloCycles (MC1) a) DCM b) CHCl_3 c) benzene d) acetone e) dioxane f) EtOH and g) MeCN.

4.12 THERMOGRAVIMETRIC ANALYSIS

TG analysis of all the structures in the homeotypic series yielded similar results; solvent loss occurs at relatively low temperatures and, in most cases, begins at ambient temperature. This suggests that there are no significant interactions between the host and its various guests. From the weight loss percentages it is possible to calculate stoichiometric host:guest ratios in the samples. In most cases these percentages correlate to the host:guest ratios observed in the single-crystal structures obtained. However, there are some discrepancies for some of the samples, and these differences can be ascribed to sample preparation and subsequent sample loading. Either the samples were not sufficiently dried or had already started to lose their guest molecules before analysis. On the other hand, an increased weight loss percentage is most probably due to solvent situated on the surface of the crystals.

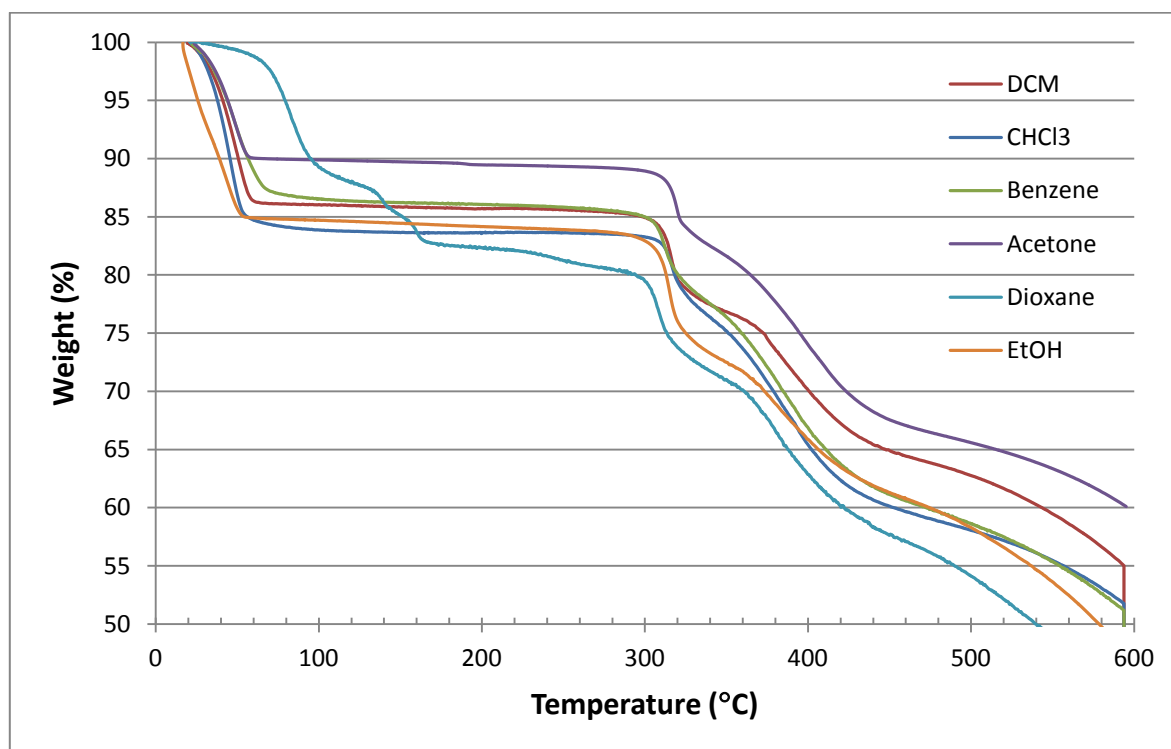


Figure 4.41 TG analysis of the cobalt-based metalloccycles. All have similar profiles, apart from the dioxane-included metalloccycle (MCl_{Diox}).

In general, the samples containing the same metal salt, e.g. the cobalt-based metalloccycle solvates, all possess similar thermal profiles, with the exception of the dioxane solvate as shown in Figure 4.41. The thermal profile of the metalloccycles comprising zinc and nickel salts are slightly different to the cobalt metalloccycles as well as to each other. All samples lose volatile guests under ambient conditions and remain stable until decomposition of the host. The primary difference between the thermal profiles is the shape of the decomposition curve. The metalloccycles incorporating cobalt cations all undergo a two-step decomposition,

commencing just after 300 °C (Figure 4.41), with the first step leading immediately to the second. The dioxane-included structure exhibits a slightly different thermogram that can probably be ascribed to the weak host-guest interactions present in the structure, which are likely to stabilise the guest within the metallocycle cavities.

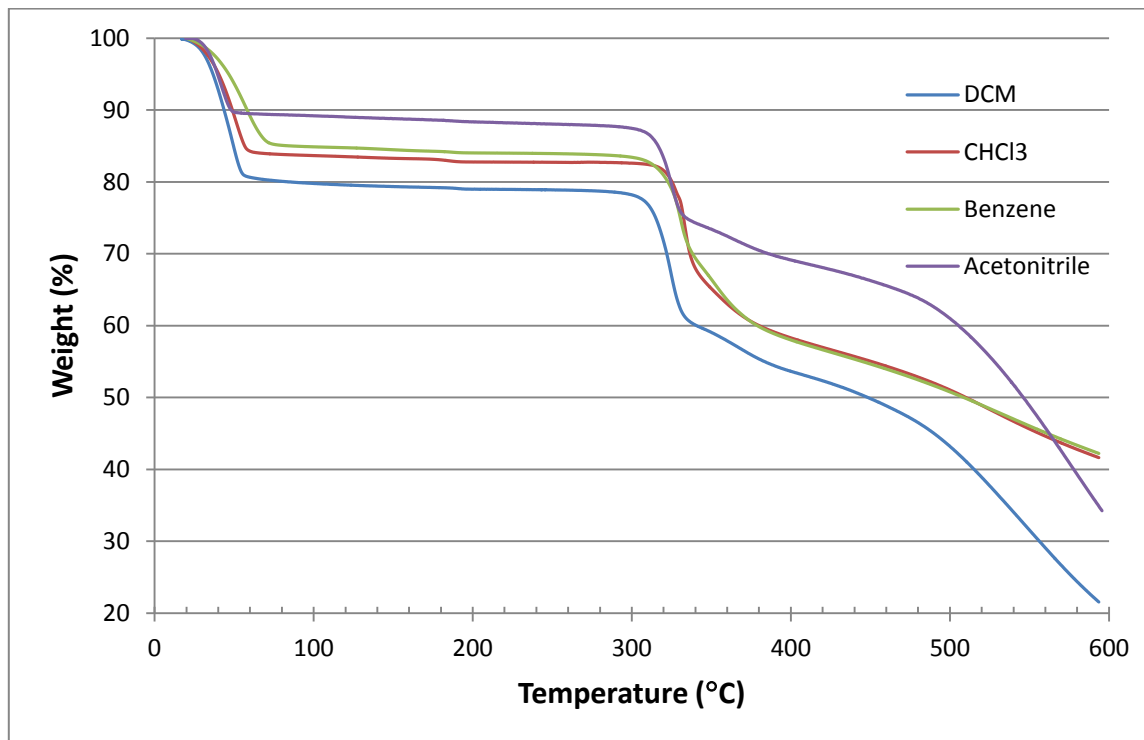


Figure 4.42 TG analysis of the nickel-based metallocycles.

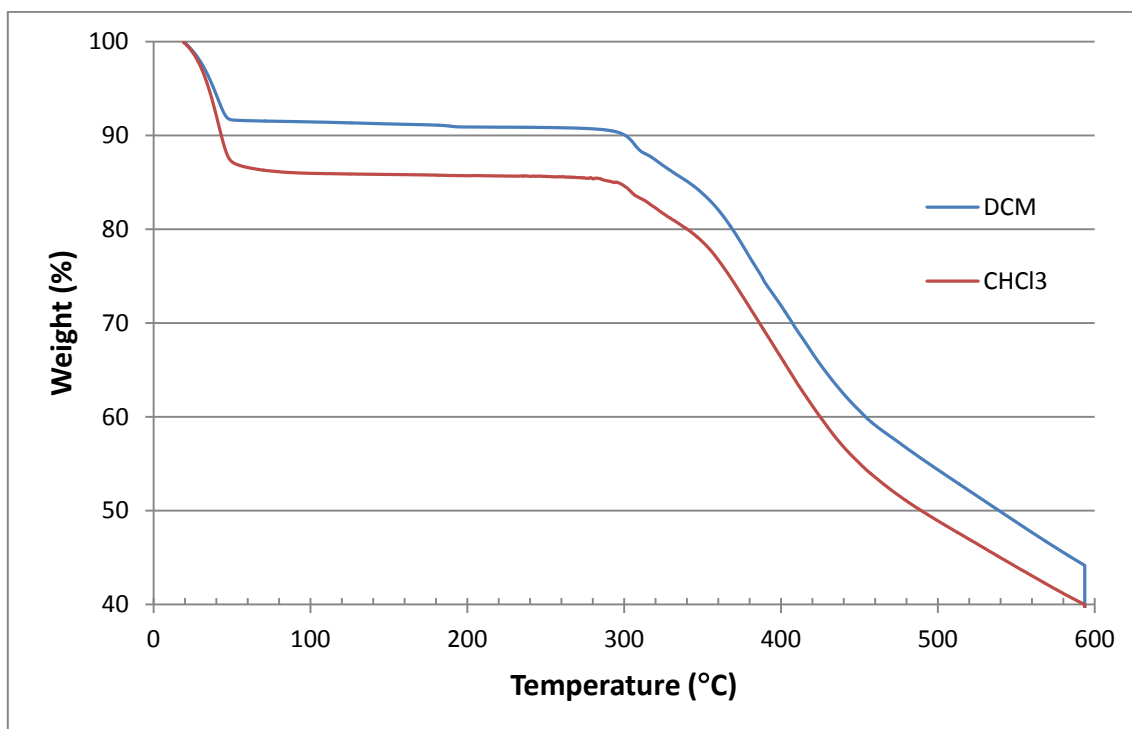


Figure 4.43 TG analysis of the zinc-based metallocycles, not including the benzene-included metallocycle.

The nickel complexes start decomposing at approximately the same temperature. However, it appears that these complexes follow a slightly different type of decomposition since there is a large initial step, followed by a more gradual decomposition (Figure 4.42) and the decomposition of the zinc complexes occurs in the same range but starts with a very small initial step before rapid decomposition (Figure 4.43).

The copper complexes follow a slightly different profile to the isoskeletal series (Co-, Ni- and Zn-based metallocycles), with a much lower decomposition temperature at approximately 250 °C (Figure 4.44). The copper complexes have an initial solvent loss, after which the complexes attain a stable solvent-free phase as confirmed by SCD. Because the single-crystal structure of the solvent-free phase was obtained with heat and vacuum it is presumed that this structure corresponds to a position on the thermogram after 150 °C. However, the step in the TGA curve may also suggest that there is another phase after the guest-free phase that has not been elucidated by SCD.

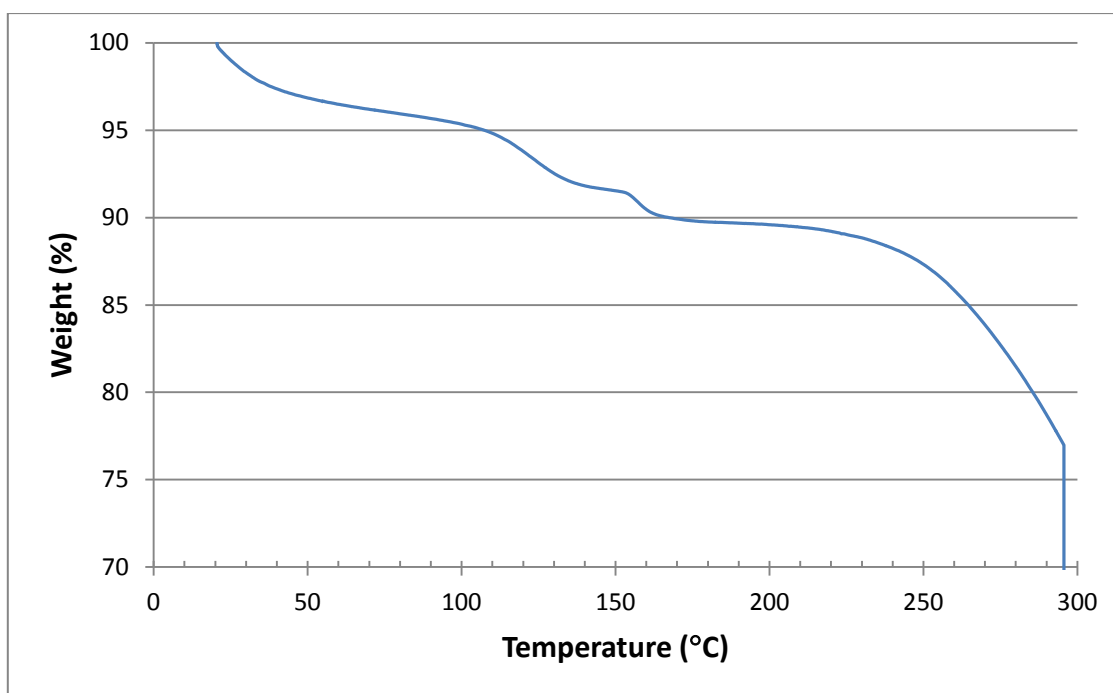


Figure 4.44 TG analysis of MC11_{DCM} – DCM included

The fact that the guests are easily removed from the series of isoskeletal structures suggests that there are more prominent interactions between the guests in the one-dimensional channels of these metallocycles than between the hosts and the guests. That is, the guest-guest interactions are more significant in these structures than the host-guest or host-host interactions, as already highlighted in the structure descriptions. One may then speculate that the solvent molecules included in the cavities act as templates for the formation of the metallocycles and then simply become trapped in these cavities during crystallisation.

Unfortunately, the structure of the guest-free structure for these metalloacycles could not be determined since the crystals undergo severe cracking upon desolvation, presumably owing to dramatic rearrangement of the metalloacycles in the crystal structure.

4.13 POWDER X-RAY DIFFRACTION ANALYSIS

Powder X-ray diffraction proved challenging for the analysis of these homeotypic compounds. Although the metalloacycles themselves may be robust, the internal arrangement of the crystals is probably not. According to the TG analysis, solvent loss occurs readily, and this includes the release of the MeCN molecules in the interstitial spaces. These MeCN molecules most probably stabilise the crystals so that, once they are removed, the crystal structure collapses. Since there is a loss in crystallinity, the resolution of the PXRD pattern becomes very low and peak positions and intensities are difficult to determine accurately. To overcome this problem, a number of options were explored to increase the stability of the crystals long enough for collection of a reasonable diffractogram. Various sample treatments were evaluated, including the use of viscous oils or films to prevent solvent loss during the data collection. These treatments were evaluated based on their ability to yield good diffractograms without making a large contribution to the background. The most viable option was determined to be commercially available cling-film (polyethene), which was used to cover the sample during data collection, preventing the loss of solvent from the crystals. Although, the cling-film makes a small contribution to the background, this can easily be corrected for during data processing. While this method yielded improved diffractograms, the quality of the diffractograms was still inadequate and conclusions cannot be drawn from the analysis. Owing to weak experimental powder diffraction data, patterns calculated from the single-crystal data are used for comparison of the solvated structures. Even though the patterns are not of high quality for any structural analysis, it is possible to establish that the single-crystal structures are representative of the bulk material in each sample vial.

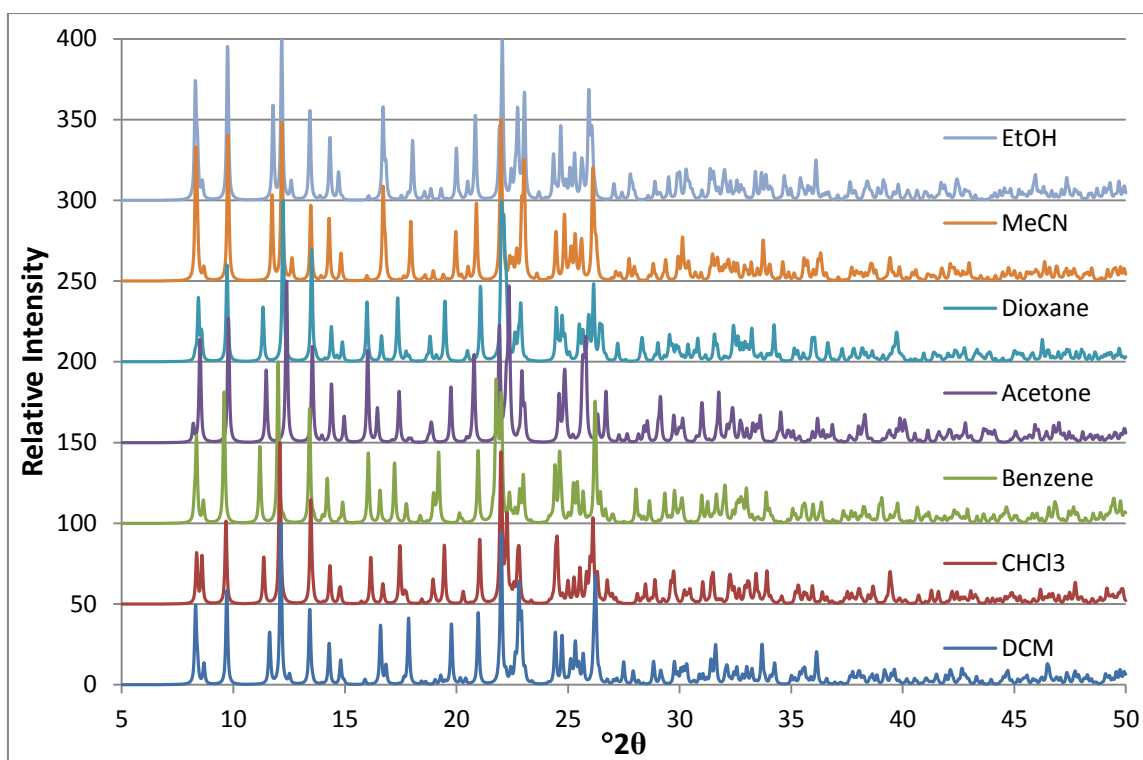


Figure 4.45 Calculated PXRD patterns of the cobalt-based metalloclusters (MC1), illustrating the high degree of similarity between the structures.

From the calculated powder patterns of the cobalt-based metalloclusters (Figure 4.45) it seems that only very minor differences occur with the inclusion of different guest molecules. The different guests included in the structures should only influence the peak intensities of the powder patterns although in this instance there are also differences in the peak shapes as well as their positions, starting at approximately $2\theta = 18^\circ$. The pattern for the MeCN-included structure is most dissimilar to the others and this is somewhat expected since the size and shape of the metallocluster changes considerably in comparison to the other structures. The patterns for the DCM, EtOH and MeCN included structures show a high degree of similarity; this also correlates with the single-crystal structure analyses and will be referred to later in the section on isostructural calculations.

The calculated patterns of the homeotypic DCM structures prepared with different transition metal salts are shown in Figure 4.46 and it is clear that the structures of the cobalt- and zinc-based metalloclusters are isoskeletal. The pattern for the nickel-based metallocluster is subtly different and it is presumed that these differences arise because the model for this metallocluster includes a second position for the DCM guest.

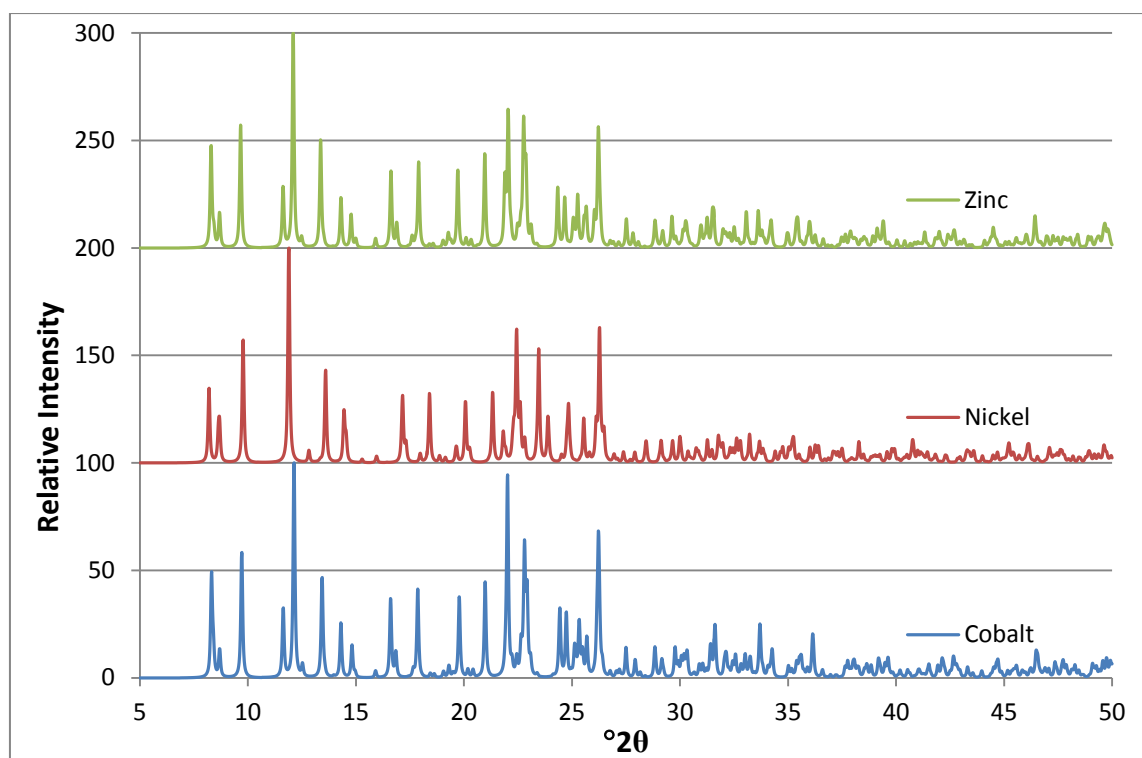


Figure 4.46 Comparison of the calculated PXRD patterns of the DCM solvates of the homeotypic series.

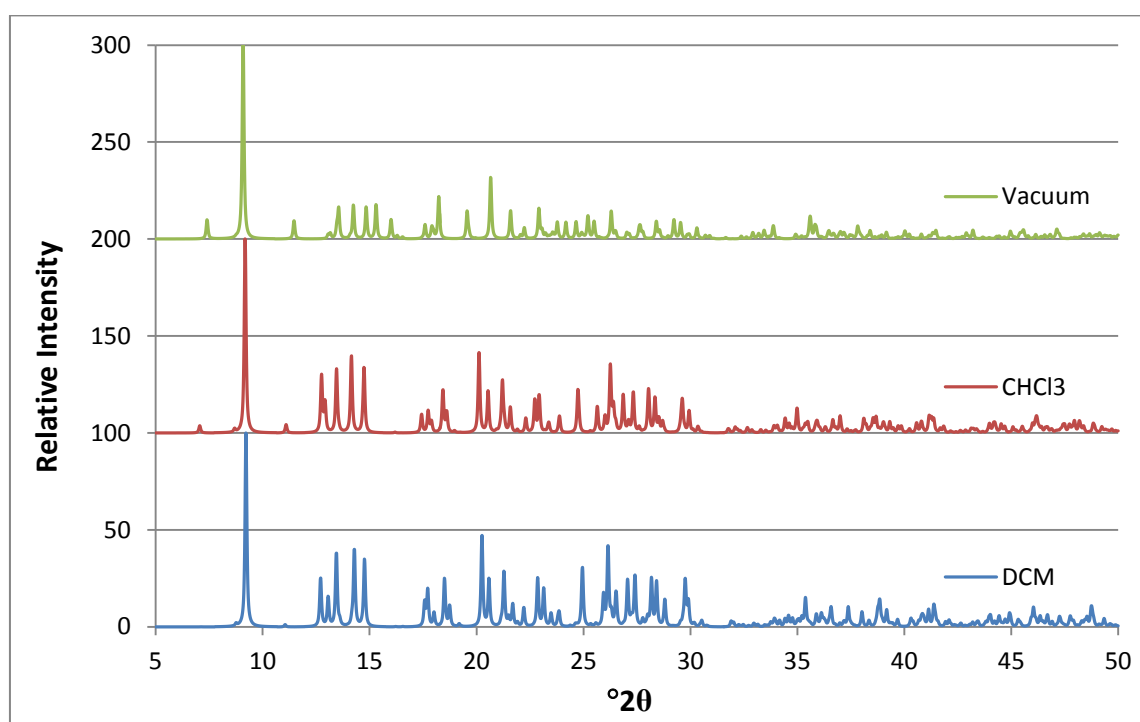


Figure 4.47 Comparison of the calculated PXRD patterns of the copper-based metalloclusters (MC11_{DCM} , $\text{MC11}_{\text{CHCl}_3}$, and MC11_{Vac})

The calculated PXRD patterns for the copper-based metalloclusters (Figure 4.47) show similarities in the positions of the peaks, which indicate striking similarities in the atomic coordinates of the structures. The main discrepancies lie in the peak shapes and intensities, which give an indication that the guests in the structures are somewhat different. The vacuum

structure is most dissimilar to the others, which is to be expected since the metalloccycles undergo a shift in their arrangement. Even so, it is still evident that there is a high degree of similarity between the three structures.

4.14 ISOSTRUCTURALITY CALCULATIONS

Prerequisites for isostructural packing motifs are that the crystals have similar unit cell parameters, crystallise in the same space group and have near identical atomic coordinates for the common atoms.¹ In isostructural organic compounds it is possible to determine the degree of isostructurality and the structures can then be compared in terms of (a) the unit-cell similarity (Π) and (b) the isostructurality index (I_i).² The unit-cell similarity index is defined as:

$$\Pi = [(a + b + c)/(a' + b' + c')] - 1 \approx 0,$$

where a , b , c and a' , b' , c' are the orthogonalised unit cell parameters of the related crystals. Similar unit cells will have $\Pi \approx 0$. This index relies heavily on the orthogonalisation scheme applied and therefore one can only compare results orthogonalised using the same method. This can be more problematic when comparing structures in triclinic crystal systems since all three angles of the unit cell require orthogonalisation.

The isostructurality index supplies a method to compare the internal arrangement of molecules within the unit cell. In other words, common atoms of the two structures occupy approximately the same atomic coordinates and this relationship is expressed as:

$$I_i(n) = \left| \left[\frac{\sum(\Delta R_i)^2}{n} \right]^{1/2} - 1 \right| \times 100,$$

where ΔR_i values are the differences between the orthogonalised coordinates of n identical heavy atoms in the related structures. For comparative purposes the molecules have to be transformed to the same asymmetric unit and origin choice. Once again, this descriptor is not without limitations, discussion of which can be found in the original paper by Fábíán and Kálmán.³ These issues prompted the development of a more comprehensive isostructurality descriptor. Instead of comparing the atomic coordinates, which can vary, it was thought that the volumes occupied by the atoms in the unit cell should be closely related. The volumetric measure of isostructurality is defined as the “the percentage ratio of the overlapping volume of molecules in the analysed structures to the average of the corresponding molecular volumes.”³ With this description it is possible to compare host molecules when the guests are exchanged. Thus the volumetric isostructurality index (I_v) is expressed as

$$I_v = \frac{2V_{\cap}}{V_1 + V_2} \times 100\%,$$

where V_1 and V_2 are the volumes of the compared fragments and V_{\cap} is the intersection of these volumes. Identical structures will result in I_v values equal to 100%, while no volume overlap will result in $I_v = 0\%$. The analytical calculation of V_{\cap} is nontrivial, requiring extremely complicated formulae and therefore no simple calculation of I_v can be performed.³

A simpler and more accessible method for the comparison of similar crystal structures and their packing motifs is found in the Mercury Materials Module, which forms part of the Cambridge Crystallographic Data Centre's (CCDC) suite of programs. There are a number of ways in which to compare the structures. Comparison of the host molecules can be made by structure or molecule overlays, which gives a root mean square value for the similarity of the structures. Or one can compare a series of compounds based on a set of desired parameters. For the structures reported in this study, the decision was taken to make use of the Crystal Packing Similarity in an attempt to quantify the similarities between the structures. During this analysis, it was found that it is not possible to quantify the similarities of the metallocycles comprising different metal cations. It is not clear why this is, since the structures are remarkably similar. Even so, it is possible to quantify the similarities between the solvatomorphs in this series of compounds and the results can be found in Table 4.3. Note that, for comparative purposes, the compounds have been labelled according to the guest. The Crystal Packing Similarity also provides quantitative comparison of the PXRD patterns calculated from the single-crystal data, providing further confirmation of structural similarity.

Table 4.3 Crystal Packing Similarities of the cobalt-based metallocycle structures (**MC1**) in order of decreasing RMS values. Both guests are ignored in the calculation

Reference	Comparison	Molecules in common	RMS	PXRD similarity
EtOH	Dioxane	15 out of 15	0.517	0.9910
MeCN	Dioxane	15 out of 15	0.517	0.9923
EtOH	Benzene	15 out of 15	0.443	0.9919
Benzene	MeCN	15 out of 15	0.442	0.9928
Acetone	MeCN	15 out of 15	0.427	0.9922
EtOH	Acetone	15 out of 15	0.427	0.9902
DCM	Acetone	15 out of 15	0.411	0.9920
CHCl ₃	MeCN	15 out of 15	0.365	0.9941
Benzene	Acetone	15 out of 15	0.364	0.9930
EtOH	CHCl ₃	15 out of 15	0.354	0.9935
DCM	Dioxane	15 out of 15	0.353	0.9944
DCM	Benzene	15 out of 15	0.341	0.9940
CHCl ₃	Acetone	15 out of 15	0.299	0.9939
DCM	CHCl ₃	15 out of 15	0.271	0.9965
Acetone	Dioxane	15 out of 15	0.255	0.9959
Benzene	Dioxane	15 out of 15	0.195	0.9951
DCM	EtOH	15 out of 15	0.137	0.9977
Benzene	CHCl ₃	15 out of 15	0.137	0.9966
CHCl ₃	Dioxane	15 out of 15	0.130	0.9981
DCM	MeCN	15 out of 15	0.129	0.9984
EtOH	MeCN	15 out of 15	0.083	0.9989

The data obtained from these studies are easy to interpret: the Root Mean Square (RMS) value indicates the extent to which the structures agree – a low value represents a high similarity between the structures. The more the PXRD patterns coincide with each other, the closer the similarity value tends to 1 (see section on PXRD analysis above). The “Molecules in common” column shown in the tables represents the size of the molecular cluster used to compare the packing similarity of the structures. The analysis of the results obtained in this study shows that, in general, as the RMS values decrease – more similarity between host frameworks – the PXRD similarity tends towards 1, which is to be expected. It is interesting to note that the most similar structures are those of the MeCN- and EtOH-, followed by the DCM- and MeCN-included structures in the series of cobalt-based metallocycles. This was also noted in the comparison of the calculated PXRD patterns in the previous section. The structures obtained from nickel bromide (**MC12**) (Table 4.4) and zinc bromide (**MC13**) (Table 4.5) show a similar trend in similarity in their respective series. However, the structures do not compare as well as they do for the cobalt-based metallocycles. The copper-based metallocycle solvates (DCM and CHCl₃) are highly similar in their packing

arrangements, which is to be expected (Table 4.6). Owing to the rearrangement of the layers in the guest-free structure, this structure is not as similar to the others in its overall packing arrangement. As already mentioned, the MeCN molecules in the interstitial spaces can be considered to form part of the host assembly and this was confirmed during the packing similarity analysis.

The results obtained from the crystal packing similarity calculations compare well with the observations already made in the crystal structure descriptions. The overlay function was also employed as a visual aid in comparing the metalloccycles of each of the crystal structures. Overlaying only the host metalloccycles of these crystal structures presents the opportunity to observe the conformational differences between the metalloccycles, specifically the tilting of the imidazole moieties in response to the different guests.

Table 4.4 Crystal Packing Similarities of the nickel-based metalloccycle structures (MC12) in order of decreasing RMS values

Reference	Comparison	Molecules in common	RMS	PXRD Similarity
MeCN	Benzene	15 out of 15	0.366	0.9920
MeCN	CHCl ₃	11 out of 15	0.358	0.9913
DCM	CHCl ₃	11 out of 15	0.326	0.9921
DCM	Benzene	15 out of 15	0.312	0.9929
Benzene	CHCl ₃	15 out of 15	0.191	0.9967
MeCN	DCM	15 out of 15	0.127	0.9980

Table 4.5 Crystal Packing Similarities of the zinc-based metalloccycle structures (MC13) in order of decreasing RMS values

Reference	Comparison	Molecules in common	RMS	PXRD Similarity
MeCN	Benzene	15 out of 15	0.372	0.9947
MeCN	CHCl ₃	15 out of 15	0.347	0.9947
DCM	CHCl ₃	15 out of 15	0.265	0.9964
DCM	Benzene	15 out of 15	0.259	0.9959
MeCN	DCM	15 out of 15	0.161	0.9973
Benzene	CHCl ₃	15 out of 15	0.134	0.9973

Table 4.6 Crystal Packing Similarities of the copper-based metalloccycle structures (MC11) in order of decreasing RMS values

Reference	Comparison	Molecules in common	RMS	PXRD Similarity
CHCl ₃	Vacuum	7 out of 15	0.716	0.9660
DCM	Vacuum	7 out of 15	0.677	0.9638
DCM	CHCl ₃	11 out of 15	0.092	0.9969

4.15 GENERAL DISCUSSION

During this study, a total of 15 homeotypic metallocyclic structures were obtained that can be subdivided into three series of isoskeletal structures (solvatomorphs). These crystal structures have been described according to the organisation of the host assembly and each novel solvate in the cobalt bromide isoskeletal series (**MC1**) has been described and analysed for unique structural features. There are no noteworthy host-guest interactions (apart from in the dioxane solvate) but rather the structures are dominated by guest-guest interactions. It appears that the size and shape of the guest is a mediating factor for the inclusion of a particular guest in the host metallocycle. These structures form unconventional one-dimensional channels that include alternating guest molecules. These structures all have similar thermal profiles and their calculated PXRD patterns coincide with a high degree of similarity. The structures obtained from the nickel and zinc bromide salts exhibit similar structural features to the cobalt bromide solvates.

During analysis of the various metallocycles obtained, it was realised that most included solvents have boiling points lower than that of MeCN (apart from EtOH and dioxane). So, in attempts to increase the stability of the metallocycles to the loss of these guests, crystallisations were set up with organic solvents that have boiling points above that of MeCN ($T_{bp} = 81-82\text{ }^{\circ}\text{C}$). Crystals were successfully grown from solvent mixtures, namely cyclohexane/MeCN, CCl_4/MeCN as well as THF/MeCN. Crystals grown from these solvent systems were of poor quality and crystal structure determination could not be achieved by SCD. However, unit cell determination was possible for the THF/MeCN crystals and these parameters suggest that the complex that forms is an isoskeletal metallocycle assembly. It is impossible to determine whether or not THF molecules are included in the structure from these data alone since variations in the unit cell parameters are very small. TG analysis may indicate the identity of these guests, but this too can be difficult to interpret unambiguously owing to the use of a mixed solvent system, especially if the thermogram follows the same profile as the majority of structures in the series.

From the crystal structure analysis of the nine solvates it is evident that subtle changes in the conformation of the metallocycles are brought about in response to the inclusion of different guest molecules. The physical properties of the host molecule most likely dictate which guest molecules may be included in the cavity. This is based on the compatibility of the guest with the host molecule, which could be based on charge, polarity as well as the size and/or shape of the cavity. In this series of isoskeletal compounds it appears that the size and

shape of the guests are more pertinent than other physical or chemical properties. It was also observed that the host is moderately flexible, enabling various guest molecules to be accommodated in the cavities. If the host metallocycle can no longer conform to the size and shape of a guest it will then exclude that particular guest from the crystal structure. To compensate, the metallocycle incorporates MeCN (which is present in the solvent mixture) in the cavity as well as in the interstitial spaces.

Competition experiments were not conducted as part of this study. However it is suggested that this be carried out in future to determine the preference of the metallocycle for different guests, and to determine if there is any selectivity towards any of these guests in the presence of others. Since solvent exchange experiments were not successful, this task would be a challenging one. In addition these crystals were grown from a mixed solvent system and one of these solvents forms part of the structure scaffold, but can also be taken up into the interior of the metallocycle. It also appears that MeCN is generally a poor choice for inclusion in the cavities, unless the other guests are too large, as was observed for the crystals grown from toluene, *p*-xylene and EtOAc. With reference to Table 4.7 it is interesting to note the similarity between the selected geometrical parameters of certain guest-included structures, particularly the structures with DCM, EtOH and MeCN. All three structures have similar conformations of the host assembly. Why then does the metallocycle choose to include the EtOH or DCM in the cavities over the MeCN? Why not simply include MeCN? There do not appear to be any host-guest interactions that might be considered strong enough to induce selectivity of one guest over the other. So it is remarkable that the resulting crystals include different guests that alternate along the one-dimensional channels.

From these observations it may be concluded that the guest molecule surrounded by the metallocycle acts as a template for the formation of the host. The formation of the metallocycle and the inclusion of the particular guest are then assumed to occur at the time of crystallisation. It seems unlikely that the metallocycle would selectively include these molecules once the complexes are already formed. If the guests *were* included after formation, one would expect to find an incommensurate-type structure where some metallocycles contain one guest while another includes a different guest. Instead, we find that there are alternating solvents in a one-dimensional channel-type structure.

A second series, somewhat related to the other three but not considered homeotypic owing to a different packing arrangement, was obtained with copper bromide and ligand **L1** (**MC11**). The metallocycles in these structures are able to pack more efficiently than the other metallocycles owing to their more regular shape and they include two different guests within

the cavity of each host. These structures present different thermal profiles to the other series and it is possible to obtain a guest-free form in a single-crystal to single-crystal transformation.

This study demonstrates that metalloccycles are most probably formed at the time of crystallisation with the help of a template molecule. It is shown that the nature of the template is not as important as its size and shape in relation to the size of the ligand components. It is believed that a number of other metalloccycles can be obtained by employing different but appropriately shaped guests and possibly other transition metal salts. It has been shown that under the right conditions the formation of metalloccycles, with the organic ligand highlighted here, is highly favourable.

Table 4.7 Selected geometric parameters and intermolecular interactions of the cobalt-based metalloccycle structures (MC1).

	DCM	CHCl ₃	Benzene	Acetone	Dioxane	EtOH	MeCN
M...M / Å	11.544(2)	11.554(2)	11.584(2)	11.420(1)	11.562(1)	11.466(1)	11.421(1)
N-M-N / °	108.8(1)	110.2 (1)	111.2(2)	107.9(1)	109.5(1)	107.58(9)	107.89(9)
Br-M-Br / °	120.66(2)	119.40(2)	119.41(4)	118.48(2)	119.40(2)	120.48(2)	120.89(2)
π...π (phenyl) / Å	3.698	3.864	3.839	3.84	3.863	3.685	3.663
π...π (C≡N) / Å	3.365	3.363	3.367	3.302	3.297	3.361	3.38
H...G (π...π) / Å			4.633		4.633		
Plane 1-2 / °	43.95	48.05	48.04	50.62	48.84	44.42	43.05
Plane 2-3 / °	56.99	52.43	50.94	51.32	52.1	57.69	58.68
Plane 1-3 / °	79.07	79.53	81.02	78.1	79.06	79.91	78.3
Planes 4 and 5 (N1-N3) / °	21.12	13.66	10.6	16.6	11.76	24.03	24.97
*Planes 6 and 7 (N16-N18) / °	3.92	3.86	5.97	5.22	1.79	3.23	4.33

*Planes 6 and 7 are defined in the same way as Planes 4 and 5 but are used to describe the imidazole moieties labelled N16-N18

4.16 EXPERIMENTAL

All crystals were prepared in a similar manner, while varying only the metal salt and the organic solvent used for ligand dissolution. The ligand and metal salt were always mixed in a 1:1 molar ratio although the concentrations of the respective solutions were not monitored as strictly.

Crystallisation of the cobalt-based metalloccycles (MC1):

A solution of CoBr_2 in acetonitrile (0.024 mmol) was slowly layered on top of a solution of **L1** (0.024 mmol) in the relevant solvent (DCM, CHCl_3 , benzene, acetone, dioxane, EtOAc, toluene or xylene) to afford deep blue plate-shaped crystals that were suitable for SCD studies.

Crystallisations of the nickel-based metalloccycles (MC12):

$\text{NiBr}_2 \cdot \text{H}_2\text{O}$ (0.024 mmol) was dissolved in acetonitrile and slowly layered onto a solution of **L1** (0.024 mmol) (DCM, CHCl_3 , benzene or toluene), yielding purple/blue coloured plate-shaped crystals that could be analysed by SCD.

Crystallisations of the zinc-based metalloccycles (MC13):

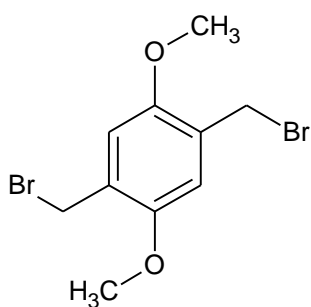
Onto a solution of **L1** (0.024 mmol), in the relevant organic solvent (DCM, CHCl_3 , benzene or toluene), was added ZnBr_2 (0.024 mmol) in acetonitrile to afford colourless plate-shaped crystals.

Crystallisations of the copper-based metalloccycles (MC11):

A solution of CuBr_2 in acetonitrile (0.024 mmol) was slowly layered onto a solution of **L1** (0.024 mmol) in DCM (**MC11_{DCM}**) or CHCl_3 (**MC11_{CHCl3}**) to afford red plate-shaped crystals. **MC11_{vac}** was prepared by placing crystals of **MC11_{CHCl3}** in a vacuum oven at 100 °C for approximately 5 hrs.

LIGAND SYNTHESIS

Ligand **L1** was synthesized via a two-step process, involving the preparation of the methylene bromide precursor followed by an $\text{S}_{\text{N}}2$ reaction to yield the ditopic imidazole ligand.

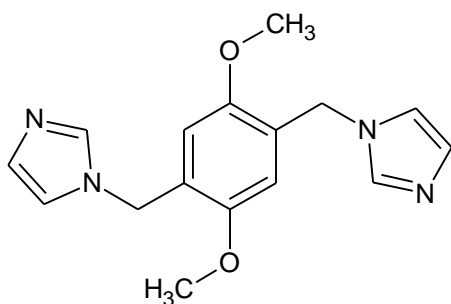
PRECURSOR (P1) 1,4-bis(bromomethyl)-2,5-dimethoxybenzene

Synthesis of the precursor **P1** was adapted from literature procedures.^{6,7} Acetic acid (25 ml) was added to a flask containing 1,4-dimethoxybenzene (36 mmol, 5.00 g) and paraformaldehyde (2.37 g) while stirring. Hydrogen bromide (33% in acetic acid) was added drop-wise, dissolving the white suspension. This mixture was stirred at 50 °C for 55 hours, and left to cool to room temperature.

The resultant white precipitate was filtered and washed numerous times with water (until the pH of the filtrate was 5), followed by methanol and then left to dry in air. The white powder was recrystallised from boiling chloroform, affording thin colourless needle-shaped crystals. A suitable crystal was selected and the X-ray structure determined. Structural data can be found in the appendices and will not be discussed here.

Yield: 65-68%; ¹H NMR (400 MHz, *CDCl*₃) δ ppm 3.88 (s, 6 H) 4.54 (s, 4 H) 6.88 (s, 2 H); ¹³C NMR (400 MHz, *CDCl*₃) δ ppm 28.56, 56.24, 113.82, 127.40, 151.25.

Crystal data C₁₀H₁₂Br₂O₂, *M* = 324.02, 0.34 × 0.14 × 0.05 mm³, triclinic, space group *P* $\bar{1}$ (No. 2), *a* = 4.382(2), *b* = 8.068(4), *c* = 8.154(4) Å, α = 90.167(5), β = 91.615(5), γ = 104.510(5)°, *V* = 279.0(2) Å³, *Z* = 1, *D*_c = 1.929 g/cm³, *F*₀₀₀ = 158, Bruker APEX CCD area - detector, MoK α radiation, λ = 0.71073 Å, *T* = 100(2)K, 2 θ _{max} = 55.7°, 3094 reflections collected, 1226 unique (*R*_{int} = 0.0280). Final *Goof* = 1.073, *RI* = 0.0213, *wR2* = 0.0548, *R* indices based on 1173 reflections with *I* > 2 σ (*I*) (refinement on *F*²), 65 parameters, 0 restraints. *Lp* and absorption corrections applied, μ = 7.237 mm⁻¹.

LIGAND (L1) 1,1'-[(2,5-dimethoxybenzene-1,4-diyl)dimethanediyl]bis(1*H*-imidazole)

This ligand **L1** has previously been synthesised by Rajakumar et al.⁸⁻¹⁰ however, the synthetic route used was adapted from another synthesis. A flask was charged with imidazole (17 mmol, 1.15 g) and sodium hydroxide (17 mmol, 0.68 g) in DMSO (8 ml) and stirred for 1 hour at 60 °C. The precursor was added to

the now dark orange solution. This mixture was stirred for a further 5 days (monitoring the reaction with TLC) until all starting materials were consumed. The reaction mixture was

allowed to cool to room temperature, leaving a sticky orange solid suspended in solution. The reaction was quenched by addition of water (200 ml) to yield a white precipitate that was filtered and washed once more with water (50 ml). The product was purified by dissolution in chloroform (200 ml) and washing with water (5 x 100 ml). The organic layer was extracted and the solvent removed under reduced pressure to yield a light yellow powder.

Yield: 53-65%; ^1H NMR (400 MHz, CDCl_3) δ ppm 3.72 (s, 6 H) 5.08 (s, 4 H) 6.50 (s, 2 H) 6.92 (s, 2 H) 7.06 (s, 2 H) 7.56 (s, 2 H), ^{13}C NMR (400 MHz, CDCl_3) δ ppm 45.71, 55.90, 111.53, 119.29, 125.46, 129.36, 137.53, 150.87.

Table 4.8 Selected crystallographic data for the cobalt-based metalloclusters (MC1)

	MC1 _{DCM}	MC1 _{CHCl3}	MC1 _{Benz}	MC1 _{Diox}	MC1 _{Acetone}	MC1 _{EtOH}	MC1 _{MeCN}
Molecular, Empirical formula	C ₁₆ H ₁₈ N ₄ O ₂ CoBr ₂ ·CH ₂ Cl ₂ ·MeCN	C ₁₆ H ₁₈ N ₄ O ₂ CoBr ₂ ·CHCl ₃ ·MeCN	C ₁₆ H ₁₈ N ₄ O ₂ CoBr ₂ ·C ₆ H ₆ ·MeCN	C ₁₆ H ₁₈ N ₄ O ₂ CoBr ₂ ·C ₄ H ₈ O ₂ ·MeCN	C ₁₆ H ₁₈ N ₄ O ₂ CoBr ₂ ·C ₃ H ₆ O·MeCN	C ₁₆ H ₁₈ N ₄ O ₂ CoBr ₂ ·C ₂ H ₅ O·MeCN	C ₁₆ H ₁₈ N ₄ O ₂ CoBr ₂ ·2MeCN
M_r / g.mol⁻¹	596.78	617.83	595.68	602.19	587.18	580.82	577.50
Crystal System	Triclinic	Triclinic	Triclinic	Triclinic	Triclinic	Triclinic	Triclinic
Space Group	<i>P</i> $\bar{1}$	<i>P</i> $\bar{1}$	<i>P</i> $\bar{1}$	<i>P</i> $\bar{1}$	<i>P</i> $\bar{1}$	<i>P</i> $\bar{1}$	<i>P</i> $\bar{1}$
a/Å	9.256(2)	9.343(2)	9.420(2)	9.31(1)	9.21(1)	9.1922(3)	9.1862(5)
b/Å	11.967(3)	11.964(3)	11.860(2)	11.890(2)	11.822(1)	12.0115(4)	11.9555(6)
c/Å	11.983(3)	12.213(3)	12.216(3)	12.323(2)	12.451(1)	12.0393(4)	11.9821(7)
α/°	116.791(2)	117.358(2)	116.558(2)	62.215(1)	61.810(1)	117.391(2)	116.818(3)
β/°	98.823(2)	100.442(3)	101.176(2)	78.808(2)	79.870(1)	91.471(2)	98.088(2)
γ/°	91.204(2)	90.670(3)	90.634(2)	89.773(2)	89.668(1)	97.685(2)	91.516(2)
Z	2	2	2	2	2	2	2
V/Å³	1164.7(5)	1185.3(5)	1190.2(4)	1178.0(2)	1171.7(2)	1163.90(7)	1156.7(1)
T /K	100	100	100	100	100	100	100
D_{calc} /g cm⁻³	1.702	1.731	1.662	1.698	1.664	1.657	1.658
N-total	12612	12698	13962	12023	14097	9797	13252
N-independent	4966	5052	5392	4928	4668	5197	5842
N-observed	3981	3998	3726	3545	3773	4307	4748
R₁ [I>2σ(I)]	0.0372	0.0341	0.0753	0.0376	0.0304	0.0299	0.0325
wR₂	0.0907	0.0790	0.1982	0.0721	0.0624	0.0658	0.0701
GOF	1.038	1.037	1.003	1.004	1.008	1.024	1.024

Table 4.9 Selected crystallographic data for the nickel-based metalloacycles (MC12)

	MC12 _{DCM}	MC12 _{CHCl3}	MC12 _{Benz}	MC12 _{MeCN}
Molecular, Empirical formula	C ₁₆ H ₁₈ N ₄ O ₂ NiBr ₂ ·CH ₂ Cl ₂ ·MeCN	C ₁₆ H ₁₈ N ₄ O ₂ NiBr ₂ ·CHCl ₃ ·MeCN	C ₁₆ H ₁₈ N ₄ O ₂ NiBr ₂ ·C ₆ H ₆ ·MeCN	C ₁₆ H ₁₈ N ₄ O ₂ NiBr ₂ ·2MeCN
M_r/ g.mol⁻¹	597.39	617.58	593.93	578.42
Crystal Symmetry	Triclinic	Triclinic	Triclinic	Triclinic
Space Group	<i>P</i> $\bar{1}$	<i>P</i> $\bar{1}$	<i>P</i> $\bar{1}$	<i>P</i> $\bar{1}$
a/Å	9.1926(8)	9.303(4)	9.394(1)	9.131(2)
b/Å	11.670(1)	12.036(5)	11.836(1)	11.724(2)
c/Å	12.222(1)	12.097(5)	12.103(1)	12.130(2)
α/°	117.137(1)	117.858(4)	116.980(1)	117.117(2)
β/°	93.665(1)	92.234(5)	92.969(1)	93.067(2)
γ/°	96.942(1)	99.699(5)	99.044(1)	96.903(2)
Z	2	2	2	2
V/Å³	1147.7(2)	1169.6(8)	1172.7(2)	1138.8(3)
T /K	100	100	100	100
D_{calc} /g cm⁻³	1.729	1.754	1.682	1.687
N-total	13484	14081	14231	19730
N-independent	5462	5531	5602	4303
N-observed	4330	3942	4708	3747
R₁ [I>2σ(I)]	0.0315	0.0413	0.0287	0.0262
wR₂	0.0623	0.0802	0.0697	0.0593
GOF	1.061	1.019	1.019	1.029

Table 4.10 Selected crystallographic data for the zinc-based metalloacycles (MC13)

	MC13 _{DCM}	MC13 _{CHCl3}	MC13 _{Benz}	MC13 _{MeCN}
Molecular, Empirical formula	C ₁₆ H ₁₈ N ₄ O ₂ ZnBr ₂ ·CH ₂ Cl ₂ ·MeCN	C ₁₆ H ₁₈ N ₄ O ₂ ZnBr ₂ ·CHCl ₃ ·MeCN	C ₁₆ H ₁₈ N ₄ O ₂ ZnBr ₂ ·C ₆ H ₆ ·MeCN	C ₁₆ H ₁₈ N ₄ O ₂ NiBr ₂ ·2MeCN
M_r/ g.mol⁻¹	607.48	624.27	603.64	584.30
Crystal Symmetry	Triclinic	Triclinic	Triclinic	Triclinic
Space Group	<i>P</i> $\bar{1}$	<i>P</i> $\bar{1}$	<i>P</i> $\bar{1}$	<i>P</i> $\bar{1}$
a/Å	9.302(7)	9.338(3)	9.437(1)	9.203(1)
b/Å	11.953(9)	11.951(3)	11.932(1)	11.905(1)
c/Å	12.001(9)	12.147(3)	12.056(2)	12.006(1)
α/°	116.850(9)	117.387(3)	116.542(1)	116.876(2)
β/°	91.158(9)	100.526(3)	100.570(2)	98.535(2)
γ/°	98.697(9)	90.331(4)	90.827(2)	90.730(2)
Z	2	2	2	2
V/Å³	1171(2)	1177.1(6)	1186.7(2)	1155.5(2)
T /K	100	100	100	100
D_{calc} /g cm⁻³	1.723	1.761	1.689	1.679
N-total	12428	13706	11736	10610
N-independent	5072	5353	4208	5858
N-observed	2737	3280	3389	5019
R₁ [I>2σ(I)]	0.1030	0.0490	0.0303	0.0317
wR₂	0.2674	0.0970	0.0604	0.0829
GOF	0.988	0.989	1.007	1.048

Table 4.11 Selected crystallographic data for the copper-based metalloclusters (MC11)

	MC11 _{DCM}	MC11 _{CHCl3}	MC11 _{Vac}
Molecular,	C ₁₆ H ₁₈ N ₄ O ₂ CuBr ₂	C ₁₆ H ₁₈ N ₄ O ₂ CuBr ₂	C ₁₆ H ₁₈ N ₄ O ₂ CuBr ₂
Empirical formula	·CH ₂ Cl ₂ ·MeCN	·CHCl ₃ ·MeCN	(CuKα Radiation)
M_r/ g.mol⁻¹	577.56	565.42	521.70
Crystal Symmetry	Triclinic	Triclinic	Triclinic
Space Group	P $\bar{1}$	P $\bar{1}$	P $\bar{1}$
a/Å	8.042(1)	8.005(8)	7.8621(5)
b/Å	10.756(2)	10.82(1)	11.0507(6)
c/Å	13.189(2)	13.281(13)	13.0417(9)
α/°	109.659(2)	109.31(1)	66.720(5)
β/°	92.558(2)	92.23(1)	81.138(6)
γ/°	94.269(2)	94.31(1)	79.990(5)
Z	2	2	2
V/Å³	1068.3(3)	1080(2)	1020.4(1)
T /K	100	100	100
D_{calc} /g cm⁻³	1.795	1.739	1.698
N-total	12072	10671	7526
N-independent	4599	4941	2866
N-observed	3588	3129	2203
R₁ [I>2σ(I)]	0.0351	0.0622	0.0497
wR₂	0.0730	0.1724	0.1201
GOF	1.030	1.067	1.051

4.17 REFERENCES

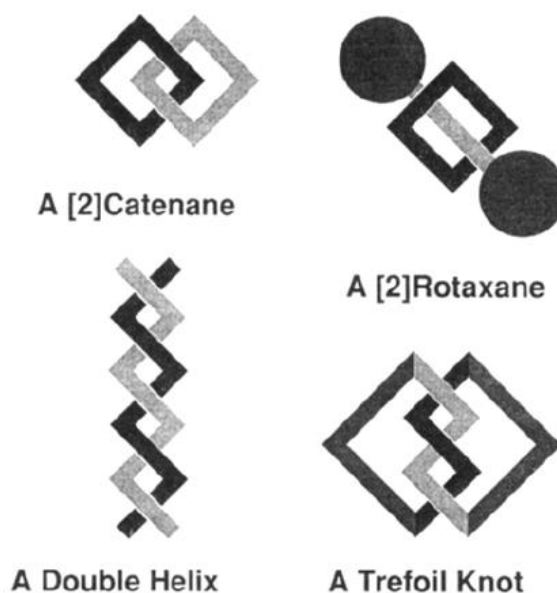
1. M. R. Caira, in *Encyclopedia of Supramolecular Chemistry*, eds. J. L. Atwood and J. W. Steed, Marcel Dekker, Inc., New York; Basel, 2004, pp. 767-775.
2. A. Kálmán, L. Parkanyi and G. Argay, *Acta Crystallogr., Sect. B*, 1993, **49**, 1039-1049.
3. L. Fábián and A. Kálmán, *Acta Crystallogr., Sect. B*, 1999, **55**, 1099-1108.
4. C. F. Macrae, I. J. Bruno, J. A. Chisholm, P. R. Edgington, P. McCabe, E. Pidcock, L. Rodriguez-Monge, R. Taylor, J. van de Streek and P. A. Wood, *J. Appl. Crystallogr.*, 2008, **41**, 466-470.
5. P. Van Der Sluis and A. L. Spek, *Acta Crystallogr., Sect. A*, 1990, **46**, 194-201.
6. I. Brehm, S. Hinneschiedt and H. Meier, *Eur. J. Org. Chem.*, 2002, **2002**, 3162-3170.
7. G. Ambrosi, M. Formica, V. Fusi, L. Giorgi, E. Macedi, M. Micheloni and R. Pontellini, *Inorg. Chim. Acta*, 2009, **362**, 2667-2677.
8. P. Rajakumar, A. Senthilmurugan and K. Srinivasan, *J. Chem. Res.*, 2006, **6**, 359-361.
9. R.-H. Cui and Y.-Q. Lan, *Acta Crystallogr., Sect. E*, 2007, **63**, o4515.
10. S.-L. Li, Y.-Q. Lan, J.-F. Ma, Y.-M. Fu, J. Yang, G.-J. Ping, J. Liu and Z.-M. Su, *Cryst. Growth Des.*, 2008, **8**, 1610-1616.

CHAPTER 5

CHEMICAL TOPOLOGY OF CONCOMITANT METALLOCYCLES

5.1 INTRODUCTION

The concept of chemical topology first appeared in 1961 in a seminal paper by Wasserman and Frisch.¹ Since then complex topologies have captured the imaginations of numerous scientists around the world, not only for their aesthetic beauty, but also owing to the interesting properties² and applications^{3,4} of these materials, particularly in the field of nanoscale machinery.^{2,5,6} Mechanically entangled structures are well known in nature⁷ – the first catenated structure of DNA was discovered in 1967⁸ and trefoil knots in double⁹- and single-stranded¹⁰ DNA were discovered soon after. In the study of chemical topology, complex entanglements can be divided into a number of classes including the relatively simple catenanes and rotaxanes as well as the more complex pretzelanes, trefoil knots, Borromean links and higher-order architectures (Scheme 5.1).^{7,11} The reader is referred to the recent publication by Stoddart *et al.*⁷ for a comprehensive review of molecular knots, links and entanglements and further reviews can be found by Amabilino³ and Siegal.¹² Although there are a number of topologically fascinating architectures, the focus of this chapter is on catenanes.

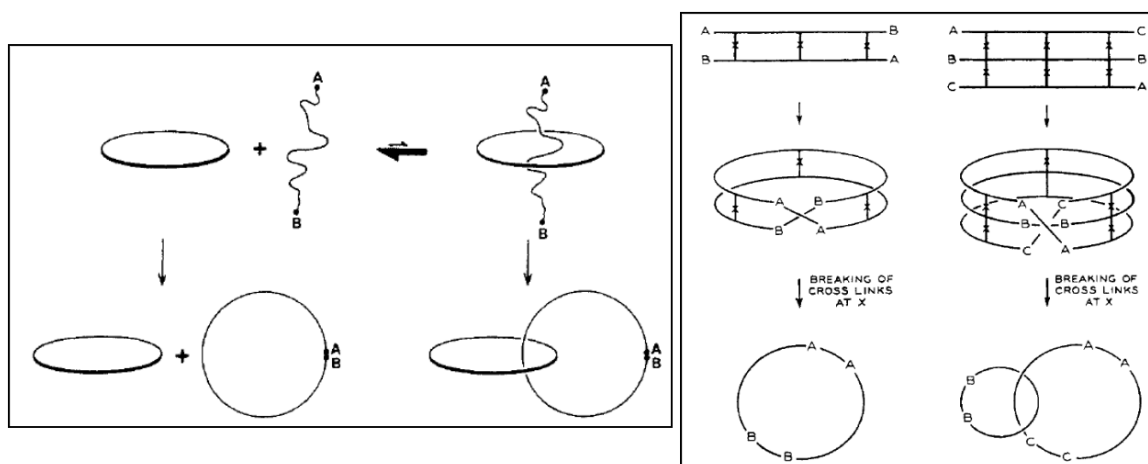


Scheme 5.1 Diagrammatic examples of some interesting topologies or entanglements. Image taken from reference 3

The word catenane stems from the Latin *catena*, meaning chain³ or a connected series of things. In terms of chemical topology the “series of things” refers to cyclic species that are mechanically interlinked with one another.⁴ Because the individual components are mechanically linked they cannot be disentangled without cleaving a chemical bond.^{3,4}

The synthesis of catenanes usually follows one of five techniques: Statistical threading,¹ the Möbius strip approach (Scheme 5.2), directed synthesis – around a central

core, templated synthesis or self-assembly of a number of components. Statistical threading^{1,13,14} involves the synthesis of a cyclic component and relying on the statistical probability of a linear molecule being threaded through the ring and subsequently cyclised to form the catenane (Scheme 5.2, left). This synthesis normally requires high dilutions for cyclisation to occur. However the threading process is more favourable at high concentrations.¹³ For these reasons, this approach often affords extremely low yields of the desired catenane.¹³



Scheme 5.2 Cartoon representation of the synthetic approaches used in formation of catenanes: Statistical Threading¹⁴ (left) and Möbius Strip¹ (right). Figure reproduced from reference 14.

Directed synthesis¹⁴⁻¹⁶ is accomplished by constructing two rings about a central core. The core is selected such that it can be removed to leave the components mechanically linked as a $[n]$ catenane (typically $[2]$ catenanes). The Möbius strip^{1,13,14,17} approach is viewed as a compromise between the statistical and directed synthesis routes. This approach relies on the ends of ladder-shaped molecules being able to twist prior to cyclisation (Scheme 5.2) and then breaking of cross-links to form the product. The number of twists in the ladder before cyclisation determines whether the catenane or separate macrocycles are formed.^{7,14} All these techniques require either multiple-step syntheses and/or harsh conditions (elevated temperatures and/or pressures) to achieve the catenated systems, and still only low yields are obtained. Improved syntheses of the interconnected systems have been facilitated by a variety of templating techniques,¹⁸ including, but not limited to, metal-ion templation,¹⁹⁻²³ hydrogen-bonding²³⁻²⁶ and donor-acceptor interactions,²⁷⁻³⁰ and anion coordination.^{31,32} Self-assembly of the components is often used as a last resort to the formation of these complicated architectures owing to a lack of control and the low yields associated with these processes. Fujita *et al.*^{17,20,33-36} has demonstrated the use of the coordinate bond in the synthesis of self-assembled Pt- and

Pd-based catenanes and has even demonstrated the reversible switching of the so-called molecular lock.³⁶

Self-assembly processes are unpredictable and success of this method often relies on preorganisation and appropriate conformations of the components to mediate the formation of the catenated structure. Moreover, relatively strong interactions are considered necessary to direct the self-assembly process. Consequently, $\pi\cdots\pi$ interactions are selected largely as recognition targets in directing the self-assembly of the catenated systems.^{22,30,37}

Only a few structures have been reported in recent years that describe catenanes containing stacking of π -delocalised rings as part of their structure. In these structures, two, four^{27,29,34,38} or six³⁹ aromatic rings are stacked within the catenane and these intermolecular interactions are typically brought about by other stronger intermolecular interactions dominating the structures. Batten *et al.*⁴⁰ recently reported the structure of a [2]catenane that boasts an unprecedented eight-membered aromatic stack. This stack forms by the interactions between dissimilar pyridyl and phenyl groups alternating along the length of the catenane array.

The naming of catenanes can become quite involved, depending on the overall topology of the structure. Therefore, systematic guidelines for the nomenclature of mechanically interlocked assemblies have been outlined by Vögtle *et al.*⁴¹ In the naming of catenanes, the number in square brackets – [n]catenane – indicates the number of components (cycles) that are mechanically linked. Thus, a [2]catenane, also known as a Hopf link, involves two links as depicted in Scheme 5.1. The term “prime links” can be used to describe the disconnected components. Catenanes with up to seven links⁴² have been synthesised successfully but the majority of reported catenanes are composed of two or three mechanically linked fragments. Branched catenanes are also known with the most illustrious being that of Olympiadane⁴³ which resembles the five rings in the Olympic emblem. Polycatenanes remain elusive by means of these synthetic strategies, with only two reports of (inorganic) infinite [n]catenanes appearing in the literature.^{24,44}

5.2 TOPOLOGY

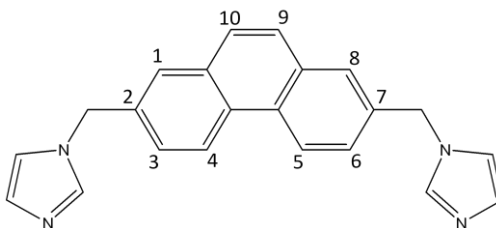
In the theory of topology, a molecule can be described in its simplest form by reducing the structure to a series of connected nodes, also known as a molecular graph.⁴ Using this terminology, a macrocycle (or metalloacycle) can be reduced to a simple circle represented in a planar graph. Transformations of an object (graph) are only permitted if they can be

carried out (and reversed) by a continuous transition.⁴ Therefore, interlocking two macrocycles will result in the nonplanar molecular graph of a catenane.⁴ If the circle of the planar graph is identical to that of the constituent circles of the catenane, these structures are known as topological isomers.⁴⁵ In chemical terms, topological isomers (Scheme 5.3) can be described as two entities composed of the same atoms and chemical bond connectivities, but which cannot be interconverted by a continuous transformation i.e. without breaking a bond.^{7,46} Topological isomers often possess vastly different chemical properties and functions as a result of their alternative structural arrangements.⁴⁵



Scheme 5.3 A schematic representation of topological isomers. Image reproduced from reference 3.

Discussed here are the preliminary results of the concomitant self-assembly of an infinite $[n]$ catenane (**1**) and the disconnected metallochromes (**2**) of the same building blocks. Combining **L2** (Scheme 5.4) with $\text{CuCl}_2 \cdot \text{H}_2\text{O}$ in a mixture of dichloromethane (DCM) and methanol (MeOH) yields crystals of differing morphologies, green needles (**1**) as well as blue oval-shaped plates (**2**) in the same crystallisation vial. Single-crystal X-ray diffraction studies reveal that the host molecules in **1** and **2** are topological isomers. The two structures exhibit similar chemical composition – two ditopic ligand molecules (**L2**) coordinated to two CuCl_2 centres to form neutral metallochromes with the general formula $[\text{Cu}_2\text{Cl}_4\text{L}_2] \cdot x\text{CH}_2\text{Cl}_2 \cdot y\text{MeOH}$ where $x = 1$ and $y = 0$ in **1**, and are undetermined for **2**.



Scheme 5.4 Schematic representation of the organic ligand **L2** – 1,1'-(phenanthrene-2,7-diyl)dimethanediyl)bis(1*H*-imidazole). The phenanthrene moiety is numbered according to the IUPAC system as in the parent compound, phenanthrene.

5.3 RESULTS

5.3.1 An infinite $[n]$ catenane (1)

Crystals of **1**, $[\text{Cu}_2\text{Cl}_4\text{L}_2] \cdot \text{CH}_2\text{Cl}_2$, form in the space group *Iba*2 with half a metallocycle and a single molecule of dichloromethane (DCM) in the asymmetric unit (ASU) (Figure 5.1). Two independent halves of the ligand **L2** are present in the ASU with the other half of each being generated by a 2-fold rotation axis located perpendicular to the plane of the phenanthrene moiety. This symmetry element imposes disorder of the carbon atoms in the 9 and 10 positions (Scheme 5.4) of the phenanthrene ring, such that this aromatic group resembles a pyrene moiety. These are of course average positions for the carbon atoms and therefore it is assumed that the carbon atoms alternate positions in order to facilitate favourable intermolecular interactions. Thus, the molecules may opt for either one of the two positions along the chain, at random or possibly in an organised manner. Intermolecular interactions may influence the orientation of these moieties somewhat to align them in the most favourable positions but, because the differences are subtle, the preferred positions cannot be determined by X-ray crystallography alone.

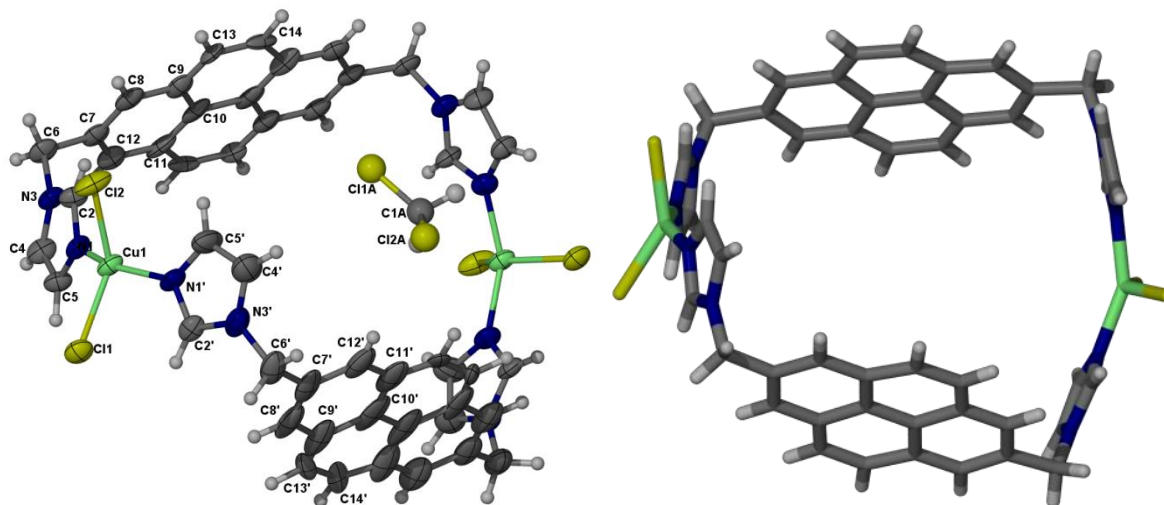


Figure 5.1 Structure of one of the links in the infinite $[n]$ catenane, **1**. In the thermal ellipsoid plot (50% probability) on the left, the atoms of the ASU are labelled. The included guest DCM is shown in ball-and-stick representation as the thermal ellipsoids are large owing to the thermal motion of the molecule. The capped-stick representation of the metallocycle, on the right, gives a better view of the prime link metallocycle.

The metallocycles that are formed interlock in order to form an infinite $[n]$ catenane topology. Individual metallocycles of the catenane chain are related by the glide planes located perpendicular to $[010]$. The most significant feature of this catenane is the infinite stack of phenanthrene moieties. Offset face-to-face π -interactions are present between the centroids of these groups and propagate along $[001]$. Although this is not the first

example of an infinite catenane structure, it is, to the best of our knowledge, the first example of a catenane containing an infinite $\pi\cdots\pi$ stack that also governs the formation of the catenane. Other examples make use of either hydrogen bonding²⁴ or Ag \cdots Ag interactions⁴⁴ for the formation of $[n]$ catenanes. The occurrence of these $\pi\cdots\pi$ stacks gives an indication that these relatively weak intermolecular interactions experience some form of cooperativity in order to achieve sufficient stability in the formation of the catenane. For this to occur, it is essential that the $\pi\cdots\pi$ interactions are favourable along the entire array. Therefore, the phenanthrene moieties rotate about their plane such that the stack is offset in an $\cdots ABCD\cdots$ fashion along the catenane chain (Figure 5.2).

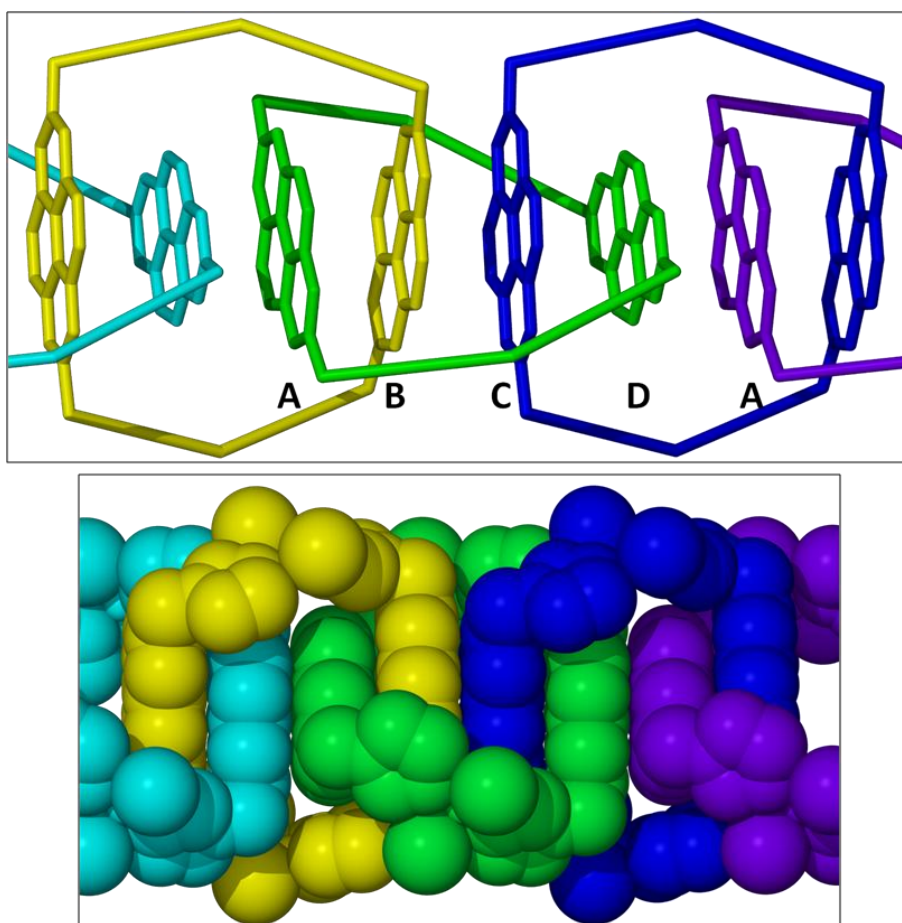


Figure 5.2 Simplified model of **1** showing the $\pi\cdots\pi$ stacking of the phenanthrene moieties in the catenane chain depicting the $\cdots ABCD\cdots$ stack (top). The molecular structure has been simplified in order to better observe the arrangement of the aromatic groups. The space-filling representation of the catenane (bottom) indicates the close proximity of the aromatic rings promoting favourable $\pi\cdots\pi$ stacking along the entire array.

This rotation of the phenanthrene moieties is believed to contribute to the stabilisation of these weak interactions. The relative angle of rotation of these moieties can be determined by defining arbitrary planes through the phenanthrene moieties. Therefore, if a plane is generated through the centre of the phenanthrene rings, (C2 to C7, Scheme 5.4) perpendicular to the plane of the ring system (Figure 5.3), the rotation angles of these

moieties can be determined. Moieties **A** and **B** (Figure 5.2) experience a rotation of approximately 70° relative to each other, **B** and **C** 40° and **C** and **D** are rotated by 70° , and so on. The phenanthrene moieties in the individual metalloCycles (i.e. **A** and **D**) are rotated 40° relative to each other. Each metalloCycle includes two phenanthrene moieties from adjacent metalloCycles.

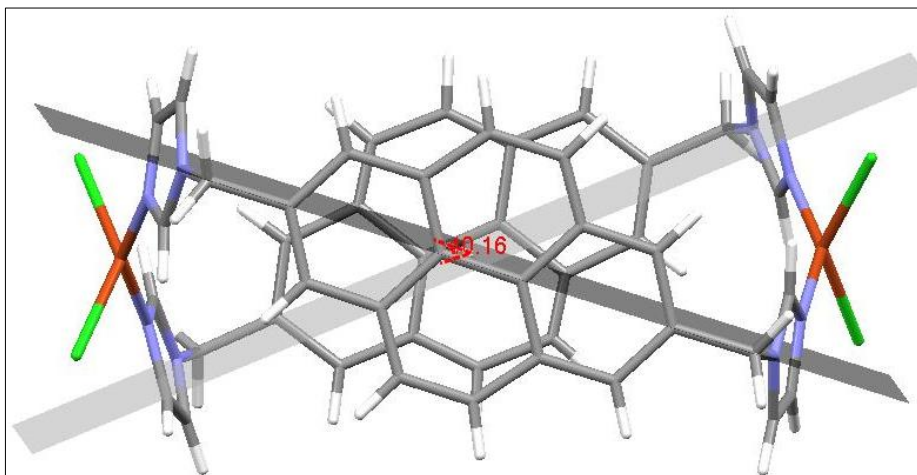


Figure 5.3 Perspective view of one metalloCycle of **1**, depicting the planes cutting through the phenanthrene moieties used to determine the rotation of these groups in relation to one another. Depicted here are the planes through the moieties of an individual metalloCycle that are rotated by 40° relative to one another.

It is thought that the size and shape of the metalloCycle plays an important role in the establishment of the catenated architecture. In this particular case, the diameter of the metalloCycle, measured phenanthrene-to-phenanthrene, is 10.178 \AA . This distance appears optimal for the formation of the $\pi\cdots\pi$ stack, provided the interactions are stabilising. We observe centroid separation distances between 3.38 \AA [(**A**)-(**B**); (**C**)-(**D**)] and 3.40 \AA [(**B**)-(**C**); (**D**)-(**A**)], which are well within the accepted range ($3.3\text{--}3.8 \text{ \AA}$) for π -stacks. As mentioned earlier, there is disorder about the positions of the carbon atoms 9 and 10 as well as 9' and 10' (Scheme 5.4) of the ligand moieties. It is assumed that the phenanthrene moieties are orientated 180° with respect to one another along the catenane array. The symmetry of the crystal means that we only see the average of these positions along all the arrays in the structure, which then accounts for the disorder that we observe.

To further accommodate these orientations of the phenanthrene moieties, the metalloCycles adapt their shape such that the copper cation centres assume a heavily distorted square-planar geometry with bond angles of $152.5(2)^\circ$ (N-Cu-N) and $140.65(8)^\circ$ (Cl-Cu-Cl) with intramolecular Cu \cdots Cu distances of 12.318 \AA . C-H \cdots Cl contacts (C4 \cdots Cl $3.367(7) \text{ \AA}$ and C5 \cdots Cl $3.449(6) \text{ \AA}$) between adjacent catenane chains, as well as weak offset $\pi\cdots\pi$ interactions between the distinct imidazole groups, help to

stabilise the chains in the overall packing arrangement.

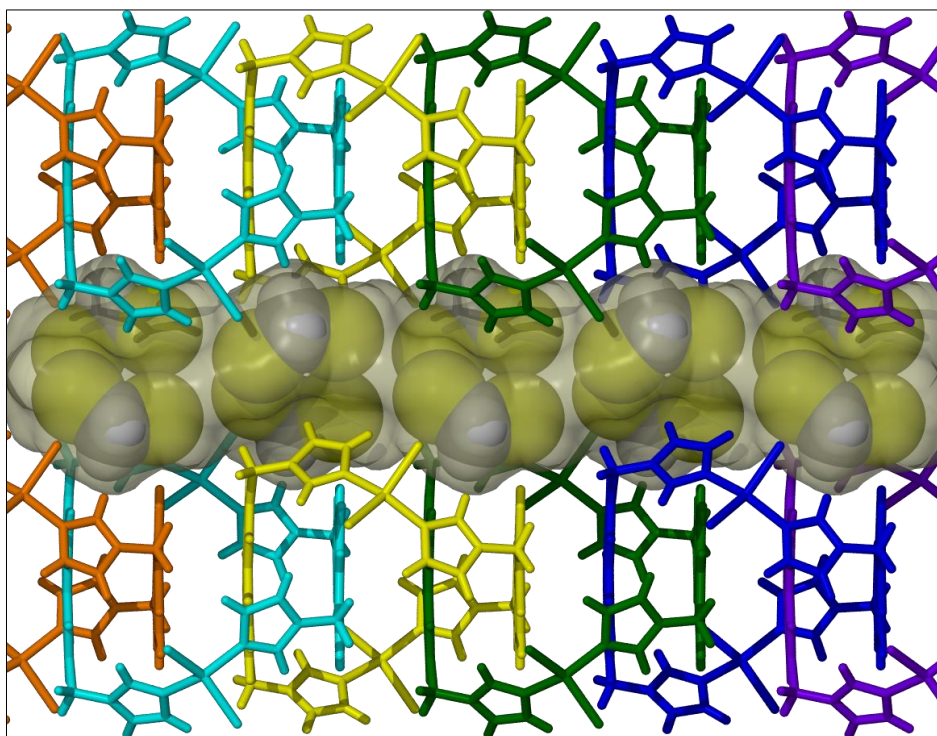


Figure 5.4 Channel formed by four surrounding catenane chains in **1**. Catenanes are shown in capped stick representation with their component metalloccycles coloured individually. The dichloromethane guests are represented in a space-filling model. The semi-transparent surface represents the solvent accessible void calculated with MSRoll using a probe radius of 1.4 Å.

Also of interest in this structure is the inclusion of dichloromethane in the channel-like space between the catenane chains (Figure 5.4). Four catenanes surround each of these channels. The DCM molecules included in these channels appear to associate in pairs, with short Cl...Cl halogen interactions (3.34(2) Å) between symmetry-related (2-fold screw axis) chlorine atoms (Cl2A), whereas the other two chlorine atoms are located further apart at a distance of 4.06(2) Å. These pairs of DCM molecules are related to the next pair in the channel by the glide plane perpendicular to [010] and, when viewed from above, the DCM molecules appear to form a spiral down the length of the channel (Figure 5.5). The DCM pairs connect the four surrounding catenane chains by means of weak C–H...Cl interactions (3.66(2) Å) between the methylene carbon atom of the DCM guest and chloride counter ions of the metalloccycles. The chloride counter ion that is not involved in these interactions participates in C–H...Cl interactions with the nearest imidazole moieties of neighbouring metalloccycles in adjacent chains.

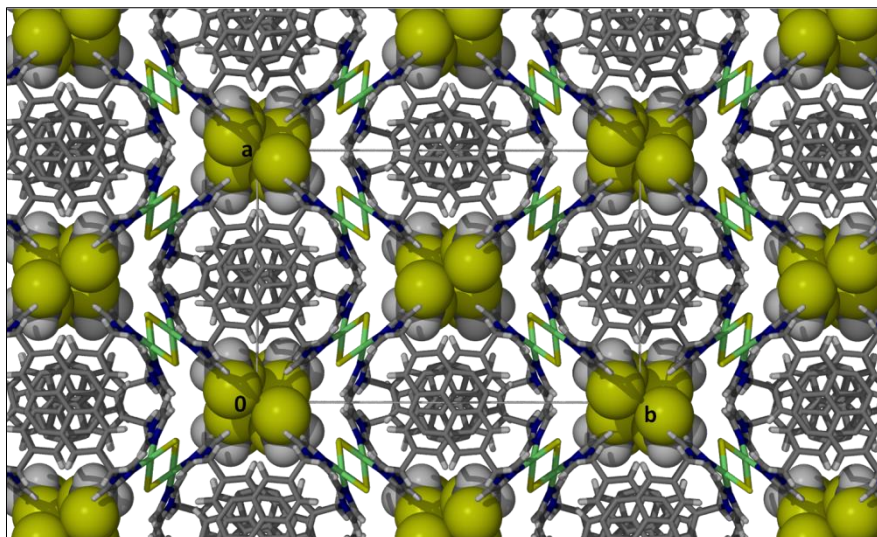


Figure 5.5 Packing arrangement of the catenane chains in **1** depicted as capped-stacks viewed down the crystallographic *b* axis. Dichloromethane guests included in the channels are shown in van der Waals representation, indicating how they associate in spiralling pairs along the channels.

Although the DCM guest is situated in a channel, it can only be removed by heating the crystals to approximately 210 °C (determined by hotstage microscopy) and, as the crystals lose solvent they become opaque ($T_{\text{dec}} = 234$ °C). Owing to the small amount of sample obtained from the crystallisations, it was not possible to verify these observations by TG analysis. Therefore, we cannot determine whether the compound is stable at any point subsequent to solvent removal. It is suspected that the retention of the (typically volatile) guest to such elevated temperatures is due to a combination of the weak host-guest interactions as well as the guest-guest interactions experienced by these molecules. The spiralled shape of the channel is also thought to play a role in the retention of the guests, making the passage of the molecules through the channel more difficult.

In light of the fact that the crystal structure of **1** contains an infinite stack of aromatic moieties it is proposed that the crystals may have interesting optical properties owing to the amplified $\pi \cdots \pi$ electron system. A quick test of a few of these crystals was carried out by observing their response to exposure to a standard laboratory UV lamp. At wavelengths of 254 and 365 nm the crystals emit blue-purple light i.e. the crystals are luminescent. As part of an ongoing study, the wavelength of maximum light emission (luminescence) is to be determined. Once established it may be possible to characterise the luminescence in terms of the primary components contributing to this property – i.e. ligand-localised, ligand-to-metal charge transfer (LMCT) or metal-to-ligand charge transfer (MLCT).⁴⁷ To this end, samples have been submitted to the Laser Research Institute (LRI) in the Physics Department at the University of Stellenbosch for further

analysis.

It is believed that the DCM guest included in the structure may influence the optical properties of the compound, and therefore attempts to crystallise the same catenane structure from different solvents, as well as solvent exchange experiments are currently under way. The copper cation centre in the metalloCycles may also influence the optical properties observed and therefore other transition metal salts should also be assessed for their ability to form catenated structures with ligand **L2**.

5.3.2. The Prime Link – Disconnected MetalloCycles (2)

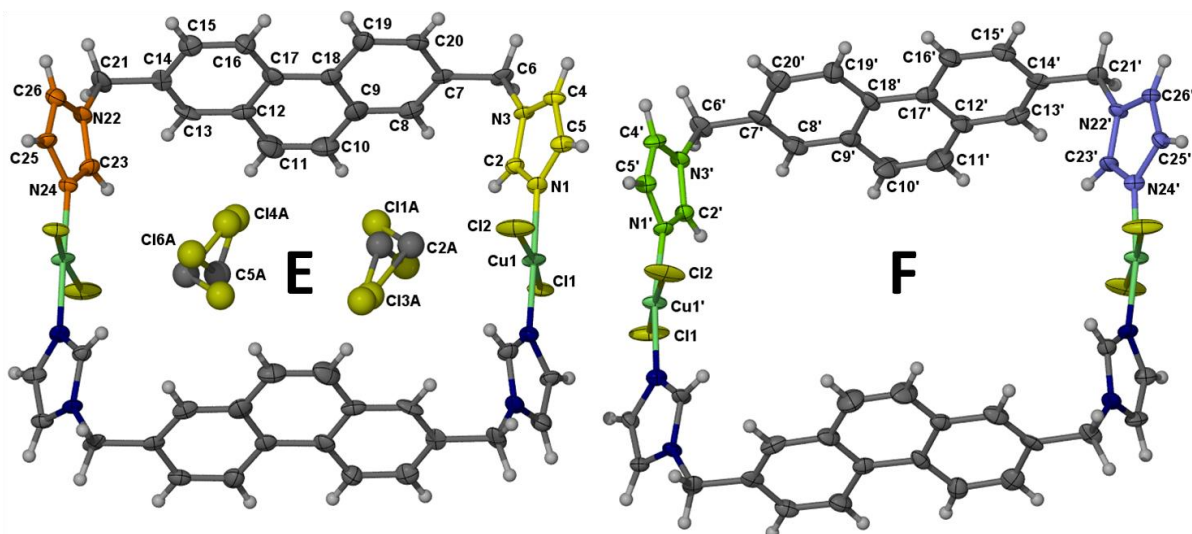


Figure 5.6 MetalloCycles **E** and **F** of **2** depicted as 50% probability thermal ellipsoids. Only the atoms of the ASU are labelled. Guest molecules in metalloCycle **E** are shown in ball and stick representation whereas the guests included in **F** cannot be adequately modelled. The unique imidazole groups have been coloured – orange, yellow, green and blue – for ease of discussion in the following sections.

Crystals of **2**, $[\text{Cu}_2\text{Cl}_4\text{L}_2\text{L}_2] \cdot x\text{CH}_2\text{Cl}_2 \cdot y\text{MeOH}$, form in the space group $P2_1/c$ with an ASU comprised of two half metalloCycles that are symmetry unrelated (**E** and **F**, Figure 5.6). Both are centred on inversion centres such that the remaining halves of the complexes are generated by symmetry. As in the structure of **1**, each metalloCycle consists of two ditopic ligand molecules, in a C-shaped conformation, coordinated by N-donors to two copper cation centres. The charges of the complexes are balanced by the coordination of two chloride counter ions to each of the copper centres. Two molecules of dichloromethane and at least one other unknown guest molecule are also present in the ASU. In comparison to the structure of **1**, the copper centres in **2** assume a more regular square-planar geometry with N–Cu–N bond angles of $177.8(3)^\circ$ (MC **E**) and $172.2(3)^\circ$ (MC **F**) and Cl–Cu–Cl angles of $172.1(1)^\circ$ (MC **E**) and $177.1(1)^\circ$ (MC **F**).

Because there are two half metalloCycles in the ASU the structure was checked for

missed symmetry and it was found that there is no missing symmetry in the structure. So what prompts the components to form two symmetry independent metalloCycles of similar structure? Since the residual electron density within the one metalloCycle (**F**) could not be modelled, it is suspected that the nature of the guest is either different to that in metalloCycle **E** or that the guest is in a different orientation within the cavity. Because **2** was crystallised from a mixed solvent system it is not trivial to determine the composition of the guest. During structure refinement the residual electron density was modelled as a DCM molecule as well as a molecule of methanol, though neither of these refined satisfactorily. Results obtained from the structure analysis utilising SQUEEZE are uninformative in identifying this guest. SQUEEZE suggests that between 91 and 93 electrons are accommodated in the cavities of the metalloCycles. Two molecules of DCM would account for 84 electrons, which is sufficiently close to that proposed. However, a combination of DCM and three molecules of MeOH per cavity would provide 96 electrons per cavity. Therefore, the SQUEEZE results do not facilitate unambiguous characterisation of the guest molecules. It seems plausible that the included guest is in fact another DCM molecule. However, the potential inclusion of methanol cannot be ruled out. It is unusual that this guest cannot be easily refined, given that it is confined to a small cavity. Numerous datasets were collected in an attempt to elucidate the guest, with no improvement in the structure refinement. The packing arrangement is such that the guest molecules are confined to small pockets within the metalloCycles. Each metalloCycle is assumed to contain two guest molecules within its pocket (Figure 5.7). Further investigation is necessary and with the aid of hotstage microscopy coupled to a mass spectrometer, or NMR experiments it may be possible to determine the stoichiometric ratio of the included guests.

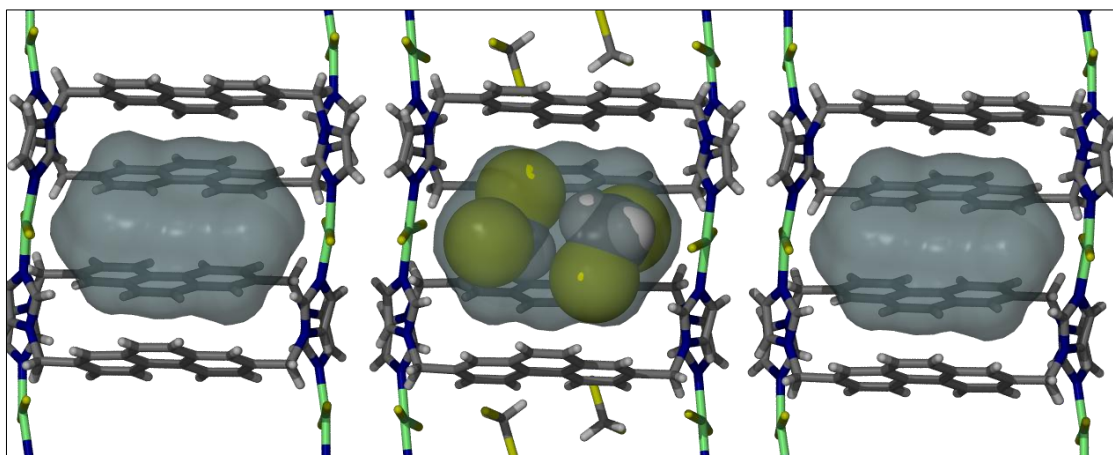


Figure 5.7 Stacking arrangement of the metalloCycles in **2**, alternating **F** and **E**. The transparent Connolly surfaces depict the size and shape of the solvent-accessible voids. Dichloromethane molecules included in the voids of MC **E** are also shown.

When examining the Connolly surfaces mapped for the different metallocycles it is evident that the contours of the surfaces are slightly dissimilar. This is due to the divergent conformations of the imidazole groups in the independent metallocycles. The extent to which the imidazole orientations differ can be quantified relative to a horizontal least-squares plane defined by the four methylene bridging carbon atoms of the metallocycles; the tilt angles of the imidazole groups have been measured with reference to these planes (Figure 5.8).

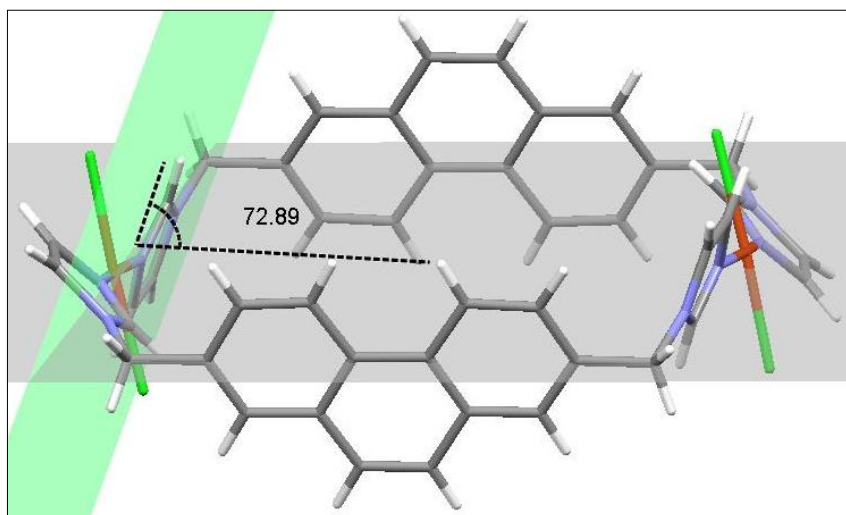


Figure 5.8 Example of tilt angle determination in **2**.

Tilt angles for the imidazole moieties in metallocycle **E** are 58.23° (orange, Figure 5.6) and 60.33° (yellow) compared to those in metallocycle **F**, which are 46.45° (green) and 72.89° (blue). An explanation for the large deviation of the imidazole moiety (blue) of metallocycle **F** cannot be put forward conclusively; however, the inclusion of different guests in the confines of the metallocycle may provide a reasonable explanation. The dramatic tilt of the imidazole ring (blue) in **F** may also be a reason for difficulty in modelling the guest molecule(s) owing to excessive movement of the guest in this pocket.

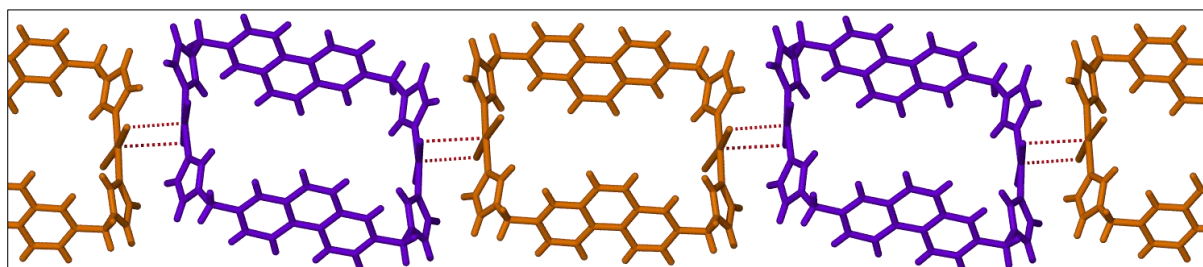


Figure 5.9 Weakly associated chains of metallocycles in **2**. The close Cu...Cl contacts are shown as red fragmented lines. The alternating pattern of metallocycles is indicated by different colouring of the cycles. Metallocycle **E** is shown in orange, whereas metallocycle **F** is depicted in purple.

Short Cu...Cl contacts ($2.911(3)$ Å and $3.318(4)$ Å) between adjacent complexes aid in organising the alternating (**E** and **F**) metallocycles into associated chains along [100]

(Figure 5.9). Neighbouring chains are associated along [010] by weak offset $\pi\cdots\pi$ interactions between phenanthrene moieties, thus arranging the metalloporphyrins into layers (Figure 5.10 (a)). These layers are then organised in offset stacks (brickwork pattern) such that the openings of the metalloporphyrins are blocked by two nearby complexes. In fact there appear to be weak edge-to-face C–H $\cdots\pi$ interactions between phenanthrene moieties of neighbouring layers (Figure 5.11). These edge-to-face interactions organise the metalloporphyrins such that the arrangement of the aromatic moieties resembles a sandwich herringbone motif (Figure 5.10(b)).

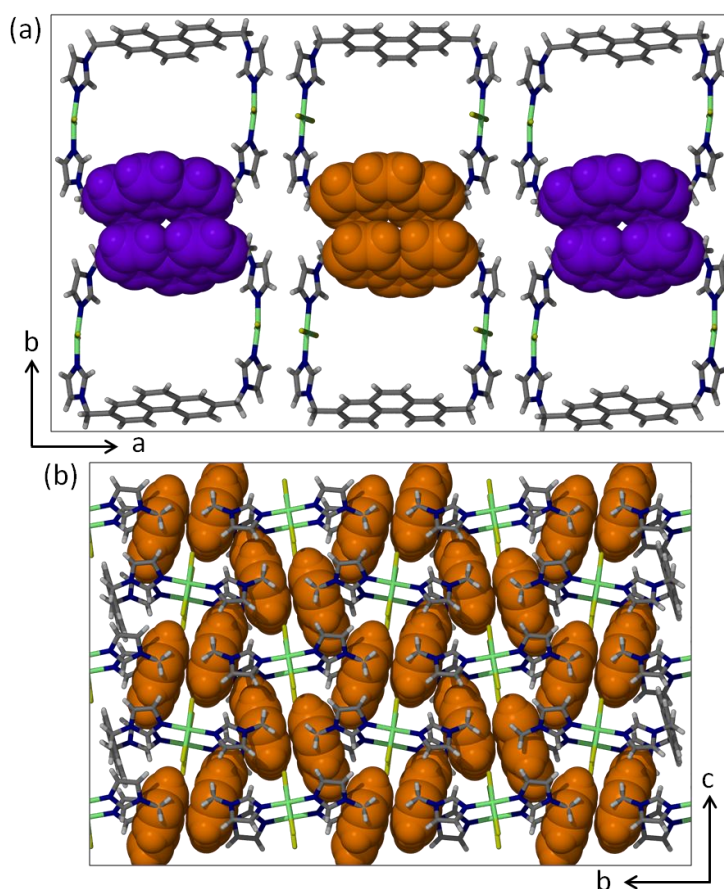


Figure 5.10 Offset $\pi\cdots\pi$ interactions between adjacent chains of metalloporphyrins in **2** are depicted in (a). Phenanthrene moieties are depicted in van der Waals representation with moieties of MC E coloured orange while those of MC F are shown in purple. (b) Packing arrangement of MC E viewed along [100] displaying the sandwich-herringbone motif of the phenanthrene moieties.

Due to the arrangement of the metalloporphyrins, solvent molecules become trapped within the confines of the metalloporphyrins. Metalloporphyrin E contains two molecules of DCM disordered over two possible positions. One position is 70% occupied, while the other position is only 30% occupied. There are no apparent intermolecular interactions between the host and the guest, or between the two guest molecules held within the metalloporphyrins. It is impossible to determine if this is the case for metalloporphyrin F since the guests cannot be modelled satisfactorily. However, the volume of the void suggests that it is large

enough to accommodate two guests in the cavity without significant guest-guest interactions. Nevertheless, it is postulated that the independent metalloccycles are hosts to different guests or differing stoichiometric ratios of these guest molecules.

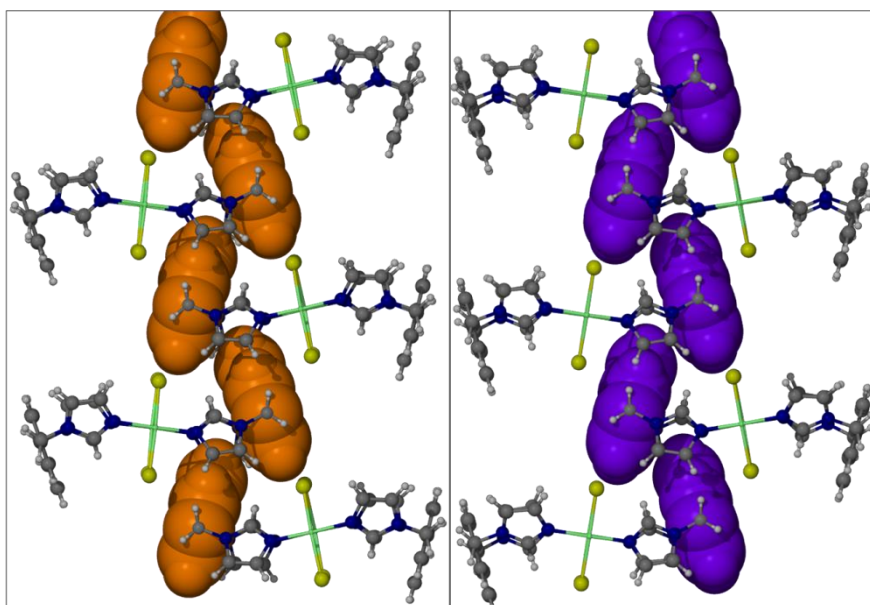


Figure 5.11 C–H... π interactions of the phenanthrene moieties in metalloccycles in **2**. Interacting rings in MC **E** are shown on the left in orange, and those in MC **F** are in purple on the right. Neighbouring metalloccycles have been omitted for clarity.

The thermal profile obtained by TG analysis indicates loss of solvent at approximately 60 °C, accounting for about 6% of the weight of the sample. If we assume that there are two independent metalloccycle hosts and two DCM molecules per host, then the calculated weight loss is 8.2%, assuming that all the solvent is removed at 60 °C. However, if we assume that each host accommodates a different guest, i.e. two DCM and two methanol molecules per two metalloccycles, we would expect a 6% weight loss. This percentage weight loss corresponds to the results obtained from the TG analysis, but does not correlate as well with the structural data and SQUEEZE calculations. The compound eventually undergoes a convoluted decomposition, commencing with a small step at 240 °C and then more rapid thermal decomposition at 326 °C.

5.4 DISCUSSION AND CONCLUDING REMARKS

The chemical topology of molecules in the solid state has become an area of great interest over the past few decades. Much of this has been spurred by the possibility of creating a number of topological architectures with potential applications in nanoscale machinery. With the knowledge gained from analysing these topologies, the ability to control the synthesis of interlocked molecules is becoming a reality. The introduction of labile coordination bonds and use of molecular recognition processes between suitable building

blocks has led to an increased number of self-assembled catenane structures being observed. However, the self-assembly of more than two components into complex structures such as catenanes is often still discovered by chance.

The major products of crystallisation, in this experiment, are the disconnected metallocycles or prime links. However, when the conditions of crystallisation are slightly modified (30 °C), the majority of crystals are those of **1**. Therefore, it is speculated that the structure of **1** may be thermodynamically more stable than that of **2**.

The thermal data for the two isomers implies that the structures have differing properties and this corresponds to the suggestion of thermodynamic *vs.* kinetic crystallisation products. Also noteworthy is that the solvent included in the small pockets of **2** is more easily removed than the solvent included in channels found in **1**. This is counterintuitive, since it would appear easier to remove guests from an “open” channel rather than from closed off pockets. This could imply a number of things: (1) that the edge-to-face π -interactions experienced by the metallocycles in **2** are not strong enough to prevent slippage of the layers to release the guest from the pockets; (2) there is a lack of host-guest interactions to maintain the guests within the pockets; (3) the host-guest and guest-guest interactions observed in the structure of **1** are stable enough to prevent the release of the guest even at elevated temperatures and thus the guest is only released just prior to decomposition; or (4) the spiral shape of the channel in **1** is such that the path out of the crystal is not linear, requiring more energy for the DCM to be removed.

Apart from the obvious differences between the two structures, there are a number of subtle conformational differences in the metallocycles of each of the crystal structures. These differences bestow dissimilar properties on each of the materials. Assigning specific properties to individual structural features is nontrivial since structural arrangements are often the result of compromise between stabilising and destabilising interactions. Therefore, although it is assumed that the luminescence exhibited by the [*n*]catenane is due to the $\pi\cdots\pi$ interactions of the ligand phenanthrene moieties, the geometry of the copper ion may be a contributing factor. The origin of the luminescence cannot be determined by simply comparing the catenane structure to the structure of the disconnected metallocycles since the conformations of the metallocycles are so vastly different. The inclusion of solvent in the structural arrangement may affect the properties of the resulting compound, but may also be responsible for templating the crystal structure. In the case of **2**, the guest molecules can be removed with gentle heating,

resulting in a loss of crystallinity, which probably occurs due to a structural rearrangement. The catenane structure, on the other hand, retains its guest molecules above 200 °C. As previously mentioned topological isomers are assumed to possess different physical properties and this is observed for the two crystal structures reported here. In terms of their thermal profiles, crystals of **1** are stable up to *ca* 210 °C before the solvent is driven out of the channels and decomposition of the crystals occurs shortly afterwards (235 °C). On the other hand, heating to approximately 60 °C releases the guests from within the pockets of **2** and decomposition commences near 230 °C. So, although the thermal profiles are somewhat different with regard to loss of the guests; the onset of decomposition in the two compounds seems to coincide.

The formation of two different structural topologies from similar crystallisation conditions cannot be explained but is analogous to the formation of concomitant polymorphs and may be rationalised in terms of thermodynamic and kinetic products of crystallisation. From our observations, it is assumed that **2** forms first as the kinetic product and that **1** is only able to form once an equilibrium has been reached (thermodynamic product) or additional energy is added to the system to induce formation of the thermodynamic product. It may also be the result of a change in concentration as one product crystallises out of solution, providing optimal conditions from which the other product may form.

If indeed the $\pi\cdots\pi$ interactions direct the self-assembly of the catenane, it may be possible to produce analogous catenanes incorporating different metal centres or guest molecules. Varying the metal cation may yield interesting properties for the resulting crystals, thus providing an opportunity to tune the properties, and hence the functions of the crystals for a wide range of applications.

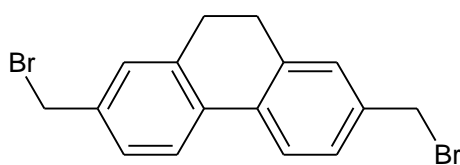
The first example of a [*n*]catenane governed by an infinite $\pi\cdots\pi$ array is described herein, as well as the crystal structure of its topological isomer, which was obtained concomitantly.

5.5 EXPERIMENTAL

CRYSTALLISATION OF (1) AND (2)

A methanolic solution of $\text{CuCl}_2 \cdot \text{H}_2\text{O}$ (4 mg, 0.024 mmol) was allowed to diffuse slowly into a dichloromethane solution of **L2** (8 mg, 0.024 mmol) in a capped vial at ambient temperature. Green needles of **1** as well as blue plates of **2** were obtained after approximately 1 week. The majority of crystals, in repeated crystallisations, were those of **2**. If the temperature of crystallisation is held constant at 30 °C, the equilibrium of crystallisation appears to shift and the major product is **1**, with fewer crystals of **2** present.

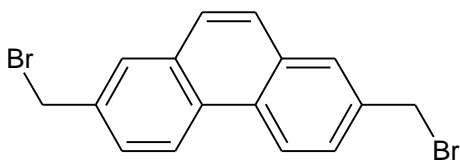
PRECURSOR (P2) 2,7-bis(bromomethyl)-9,10-dihydrophenanthrene⁴⁸



The synthesis of **P2** followed the same procedure as that in the literature.⁴⁸ 9,10-dihydrophenanthrene (29 mmol, 5.27 g), paraformaldehyde (128 mmol, 3.86 g), hydrogen bromide (48%), phosphoric acid (85%) and hydrogen bromide (33% in HOAc) were placed in a round-bottom flask and heated to 80 °C under an inert atmosphere. The mixture was stirred for approximately 24 hours after which the temperature was increased to 120 °C for a further 12 hours (monitoring with TLC). Once the solution had cooled, the solid was filtered, washed with acetone and recrystallised from benzene to yield fine white needle-shaped crystals.

Yield: 40-45%, ¹H NMR (400 MHz, CHCl_3 -d) δ ppm 2.88 (s, 4 H) 4.53 (s, 4 H) 7.28 (d, $J=1.75$ Hz, 2 H) 7.34 (dd, $J=7.99, 1.95$ Hz, 1 H) 7.71 (d, $J=7.99$ Hz, 2 H); ¹³C NMR (400 MHz, CHCl_3 -d) δ ppm 28.74, 33.56, 124.22, 127.74, 128.86, 134.17, 137.03, 137.91.

INTERMEDIATE (P2.1) 2,7-bis(bromomethyl)phenanthrene⁴⁹



The dehydrogenation of **P2** was accomplished by modification of a known synthetic procedure.^{48,49} 2,7-Bis(bromomethyl)-9,10-dihydrophenanthrene was added to a mixture of dichloro dicyano quinone (DDQ) (15 mmol, 3.42 g) and dry benzene, freshly distilled (22 ml). The orange mixture was heated under reflux for 3 days (reaction progress monitored by TLC). The dark solid that formed was dissolved in benzene (200 ml) and filtered through a pad of neutral alumina leaving a clear solution. The solvent was removed under reduced pressure affording a semi-crystalline

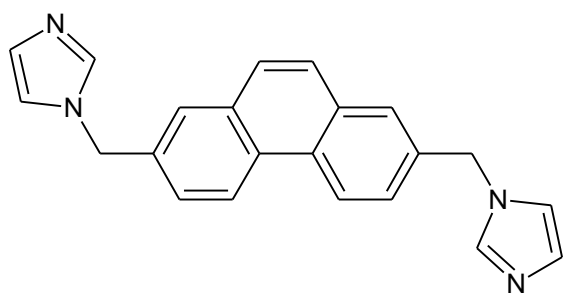
white solid. Recrystallisation from a chloroform/hexane mixture resulted in crystals suitable for structure determination. The single-crystal structure of the precursor has not been reported in the literature. The NMR analysis compares well with that reported in the literature.

Yield: 25%; ^1H NMR (300 MHz, CDCl_3) δ ppm 4.72 (s, 4 H) 7.70 (ddd, $J=8.47, 1.72, 1.54$ Hz, 4 H) 7.73 (s, 2 H) 7.90 (d, $J=1.91$ Hz, 2 H) 8.64 (d, $J=8.51$ Hz, 2 H) ^{13}C NMR (300 MHz, $\text{CHCl}_3\text{-}d$) δ ppm 33.44, 46.17, 123.49, 123.58, 127.04, 127.29, 127.58, 128.33, 128.70, 129.82, 132.21, 136.20.

Crystal data for **P2.1**: $\text{C}_{16}\text{H}_{12}\text{Br}_2$, $M = 364.08$, Colourless Plate, $0.24 \times 0.22 \times 0.08$ mm³, monoclinic, space group $P2_1/c$ (No. 14), $a = 14.073(3)$, $b = 8.4828(15)$, $c = 11.281(2)$ Å, $\beta = 101.917(2)^\circ$, $V = 1317.7(4)$ Å³, $Z = 4$, $D_c = 1.835$ g/cm³, $F_{000} = 712$, Bruker APEX CCD area-detector, MoK α radiation, $\lambda = 0.71073$ Å, $T = 100(2)$ K, $2\theta_{\text{max}} = 52.6^\circ$, 7323 reflections collected, 2666 unique ($R_{\text{int}} = 0.0383$). Final $\text{Goof} = 1.027$, $RI = 0.0348$, $wR2 = 0.0865$, R indices based on 2104 reflections with $I > 2\sigma(I)$ (refinement on F^2), 163 parameters, 0 restraints. Lp and absorption corrections applied, $\mu = 6.129$ mm⁻¹.

LIGAND (L2) 1,1'-(phenanthrene-2,7-diyl)dimethanediyl)bis(1H-imidazole)

The synthesis of **L2** was adapted from literature procedures.^{50,51} Imidazole (6.4 mmol, 0.44 g), sodium hydroxide (6.4 mmol, 0.26 g) and DMSO were stirred at 60 °C. After 1 hr. 2,7-



bis(bromomethyl)phenanthrene (**P2.1**) (2.9 mmol, 1.06 g) was added. The reaction mixture was monitored (by TLC) over 7 days until all reaction precursors were consumed. The reaction mixture was quenched with water (200 ml) and the light yellow

precipitate filtered, dissolved in chloroform and washed again with water. The organic layer was extracted and solvent removed under reduced pressure to afford a light yellow powder. Single crystals were grown by the dropwise addition of a chloroform solution in *n*-hexane. The crystal data was subsequently collected and the structure solved and refined as a non-merohedral twin.

Yield: 71%; ^1H NMR (300 MHz, $\text{DMSO-}d_6$) δ ppm 5.41 (s, 4 H) 6.95 (s, 2 H) 7.26 (t, $J=1.17$ Hz, 2 H) 7.56 (dd, $J=8.51, 1.76$ Hz, 2 H) 7.80 (s, 2 H) 7.83 (d, $J=1.76$ Hz, 2 H) 7.85 (s, 2 H)

8.78 (d, $J=8.66$ Hz, 2 H) ^{13}C NMR (300 MHz, $\text{DMSO}-d_6$) δ ppm 49.37, 119.66, 123.60, 126.31, 126.93, 127.11, 128.81, 128.92, 131.55, 136.38, 137.54.

Crystal data for **L2**: $\text{C}_{24}\text{H}_{18}\text{N}_4$, $M = 362.42$, Colourless shard, $0.082 \times 0.295 \times 0.345$ mm³, monoclinic, space group $P2_1/n$ (No. 14), $a = 6.3522(14)$, $b = 5.5996(13)$, $c = 23.548(5)$ Å, $\beta = 94.630(3)^\circ$, $V = 834.9(3)$ Å³, $Z = 2$, $D_c = 1.442$ g/cm³, $F_{000} = 380$, Bruker APEX CCD area -detector, MoK α radiation, $\lambda = 0.71073$ Å, $T = 100(2)\text{K}$, $2\theta_{\text{max}} = 50.3^\circ$, 2800 reflections collected, 1496 unique ($R_{\text{int}} = 0.0674$). Final $\text{Goof} = 1.080$, $RI = 0.0940$, $wR2 = 0.2780$, R indices based on 1062 reflections with $I > 2\sigma(I)$ (refinement on F^2), 127 parameters, |0 restraints. Lp and absorption corrections applied, $\mu = 0.088$ mm⁻¹.

Table 5.1 Selected crystal data for crystals **1** and **2** as well as ligand **L2** and ligand intermediate **P2.1**.

	1	2	L2	P2.1
Molecular, Empirical formula	$\text{C}_{22}\text{H}_{18}\text{N}_4\text{CuCl}_2 \cdot \text{CH}_2\text{Cl}_2$	$\text{C}_{22}\text{H}_{18}\text{N}_4\text{CuCl}_2 \cdot \text{CH}_2\text{Cl}_2$	$\text{C}_{22}\text{H}_{18}\text{N}_4$	$\text{C}_{16}\text{H}_{12}\text{Br}_2$
M_r / g.mol⁻¹	533.58	555.54	358.39	364.08
Crystal Symmetry	Orthorhombic	Monoclinic	Monoclinic	Monoclinic
Space Group	<i>Iba2</i>	<i>P2_1/c</i>	<i>P2_1/n</i>	<i>P2_1/c</i>
a/Å	15.2832(9)	30.411(9)	6.352 (1)	14.073(3)
b/Å	23.159(2)	14.622(4)	5.600(1)	8.483(2)
c/Å	13.5599(8)	10.548(3)	23.548(5)	11.281(2)
α/°	90	90	90	90
β/°	90	97.834(4)	94.630(3)	101.917(2)
γ/°	90	90	90	90
Z	8	8	2	4
V/Å³	4799.4(5)	4647(2)	834.9(3)	1317.7(4)
T/K	100	100	100	100
D_{calc} /g cm⁻³	1.459	1.595	1.426	1.835
N-total	14191	23907	2799	7323
N-independent	3651	8235	1495	2666
N-observed	2860	5528	1061	2104
R_1 [$I > 2\sigma(I)$]	0.0485	0.0993	0.0913	0.0347
wR₂	0.1221	0.2422	0.2656	0.0859
GOF	1.053	1.111	1.091	1.025

5.6 REFERENCES

1. H. L. Frisch and E. Wasserman, *J. Am. Chem. Soc.*, 1961, **83**, 3789-3795.
2. S. Durot, F. Reviriego and J.-P. Sauvage, *Dalton Trans.*, 2010, **39**, 10557-10570.
3. D. B. Amabilino and J. F. Stoddart, *Chem. Rev.*, 1995, **95**, 2725-2828.
4. A. Rang and C. A. Schalley, in *Encyclopedia of Supramolecular Chemistry*, eds. J. L. Atwood and J. W. Steed, Marcel Dekker, Inc., New York; Basel, 2004, pp. 206-213.

5. J. O. Jeppesen, J. Perkins, J. Becher and J. F. Stoddart, *Angew. Chem. Int. Ed.*, 2001, **40**, 1216-1221.
6. J.-P. Sauvage, *Chem. Commun.*, 2005, 1507-1510.
7. R. S. Forgan, J.-P. Sauvage and J. F. Stoddart, *Chem. Rev.*, 2011, **111**, 5434-5464.
8. D. A. Clayton and J. Vinograd, *Nature*, 1967, **216**, 652-657.
9. L. F. Liu, C.-C. Liu and B. M. Alberts, *Cell*, 1980, **19**, 697-707.
10. L. F. Liu, R. E. Depew and J. C. Wang, *J. Mol. Biol.*, 1976, **106**, 439-452.
11. S. J. Cantrill, K. S. Chichak, A. J. Peters and J. F. Stoddart, *Acc. Chem. Res.*, 2004, **38**, 1-9.
12. J. S. Siegel, *Science*, 2004, **304**, 1256-1258.
13. G.-J. M. Gruter, O. S. Akkerman and F. Bickelhaupt, *Tetrahedron*, 1996, **52**, 2565-2572.
14. C. O. Dietrich-Buchecker and J. P. Sauvage, *Chem. Rev.*, 1987, **87**, 795-810.
15. G. Schill and A. Lüttringhaus, *Angew. Chem., Int. Ed.*, 1964, **3**, 546-547.
16. D. B. Amabilino, P. R. Ashton, L. Pérez-García and J. F. Stoddart, *Angew. Chem., Int. Ed.*, 1995, **34**, 2378-2380.
17. M. Fujita, F. Ibukuro, H. Seki, O. Kamo, M. Imanari and K. Ogura, *J. Am. Chem. Soc.*, 1996, **118**, 899-900.
18. D.-H. Qu and H. Tian, *Chem. Sci.*, 2011, **2**, 1011-1015.
19. C. O. Dietrich-Buchecker, J. P. Sauvage and J. P. Kintzinger, *Tetrahedron Lett.*, 1983, **24**, 5095-5098.
20. M. Fujita, F. Ibukuro, H. Hagihara and K. Ogura, *Nature*, 1994, **367**, 720-723.
21. D. A. Leigh, P. J. Lusby, S. J. Teat, A. J. Wilson and J. K. Y. Wong, *Angew. Chem. Int. Ed.*, 2001, **40**, 1538-1543.
22. S. Y. Brauchli, E. C. Constable, K. Harris, D. Häussinger, C. E. Housecroft, P. J. Rösel and J. A. Zampese, *Dalton Trans.*, 2010, **39**, 10739-10748.
23. C. Dietrich-Buchecker, B. X. Colasson and J.-P. Sauvage, in *Top. Curr. Chem.*, eds. C. A. Schalley, F. Vögtle and K. H. Dötz, Springer Berlin / Heidelberg, 2005, pp. 211-225.
24. Z. Yin, Y. Zhang, J. He and J.-P. Cheng, *Chem. Commun.*, 2007, 2599-2601.
25. C. A. Hunter, *J. Am. Chem. Soc.*, 1992, **114**, 5303-5311.
26. E. N. Guidry, S. J. Cantrill, J. F. Stoddart and R. H. Grubbs, *Org. Lett.*, 2005, **7**, 2129-2132.

27. S. A. Vignon, J. Wong, H.-R. Tseng and J. F. Stoddart, *Org. Lett.*, 2004, **6**, 1095-1098.
28. P. R. Ashton, T. T. Goodnow, A. E. Kaifer, M. V. Reddington, A. M. Z. Slawin, N. Spencer, J. F. Stoddart, C. Vicent and D. J. Williams, *Angew. Chem., Int. Ed.*, 1989, **28**, 1396-1399.
29. D. G. Hamilton, J. K. M. Sanders, J. E. Davies, W. Clegg and S. J. Teat, *Chem. Commun.*, 1997, 897-898.
30. G. Koshkakaryan, K. Parimal, J. He, X. Zhang, Z. Abliz, A. H. Flood and Y. Liu, *Chem. Eur. J.*, 2008, **14**, 10211-10218.
31. M. R. Sambrook, P. D. Beer, J. A. Wisner, R. L. Paul and A. R. Cowley, *J. Am. Chem. Soc.*, 2004, **126**, 15364-15365.
32. B. Huang, S. M. Santos, V. Felix and P. D. Beer, *Chem. Commun.*, 2008, 4610-4612.
33. M. Fujita, *Acc. Chem. Res.*, 1998, **32**, 53-61.
34. M. Fujita and K. Ogura, *Coord. Chem. Rev.*, 1996, **148**, 249-264.
35. K.-i. Yamashita, M. Kawano and M. Fujita, *J. Am. Chem. Soc.*, 2007, **129**, 1850-1851.
36. M. Fujita, F. Ibukuro, K. Yamaguchi and K. Ogura, *J. Am. Chem. Soc.*, 1995, **117**, 4175-4176.
37. V. Blanco, M. D. Garcia, C. Peinador and J. M. Quintela, *Chem. Sci.*, 2011, 2407-2416.
38. Y. Liu, A. Bruneau, J. He and Z. Abliz, *Org. Lett.*, 2008, **10**, 765-768.
39. V. Blanco, M. Chas, D. Abella, C. Peinador and J. M. Quintela, *J. Am. Chem. Soc.*, 2007, **129**, 13978-13986.
40. J. Lu, D. R. Turner, L. P. Harding, L. T. Byrne, M. V. Baker and S. R. Batten, *J. Am. Chem. Soc.*, 2009, **131**, 10372-10373.
41. O. Safarowsky, B. Windisch, A. Mohry and F. Vögtle, *J. Prakt. Chem.*, 2000, **342**, 437-444.
42. D. B. Amabilino, P. R. Ashton, S. E. Boyd, J. Y. Lee, S. Menzer, J. F. Stoddart and D. J. Williams, *Angew. Chem., Int. Ed.*, 1997, **36**, 2070-2072.
43. D. B. Amabilino, P. R. Ashton, A. S. Reder, N. Spencer and J. F. Stoddart, *Angew. Chem., Int. Ed.*, 1994, **33**, 1286-1290.
44. C.-M. Jin, H. Lu, L.-Y. Wu and J. Huang, *Chem. Commun.*, 2006, 5039-5041.
45. J. W. Steed and J. L. Atwood, *Supramolecular Chemistry*, John Wiley & Sons, Ltd, 2000.

46. D. B. Amabilino, in *Encyclopedia of Supramolecular Chemistry*, eds. J. L. Atwood and J. W. Steed, Marcel Dekker, Inc., 2004, pp. 229-235.
47. M. D. Allendorf, C. A. Bauer, R. K. Bhakta and R. J. T. Houk, *Chem. Soc. Rev.*, 2009, **38**, 1330-1352.
48. A. Helms, D. Heiler and G. McLendon, *J. Am. Chem. Soc.*, 1992, **114**, 6227-6238.
49. A. I. Khalaf, A. R. Pitt, M. Scobie, C. J. Suckling, J. Urwin, R. D. Waigh, R. V. Fishleigh, S. C. Young and W. A. Wylie, *Tetrahedron*, 2000, **56**, 5225-5239.
50. S.-L. Li, Y.-Q. Lan, J.-F. Ma, Y.-M. Fu, J. Yang, G.-J. Ping, J. Liu and Z.-M. Su, *Cryst. Growth Des.*, 2008, **8**, 1610-1616.
51. R.-H. Cui and Y.-Q. Lan, *Acta. Cryst.*, 2007, **63**, o4515.

CHAPTER 6

STRUCTURAL ANALYSIS OF IMIDAZOLE-FUNCTIONALISED METALLOCYCLES

6.1 INTRODUCTION

A number of organic ligands were designed and synthesised for the formation of zero-dimensional (discrete) metallocycles. The principle behind the investigation presented in this chapter is the endeavour to build on our comprehension of the formation of and interactions with which these metallocycles can be constructed. This study aims to highlight some of the structural aspects involved and to ascertain if it is possible to synthesise these metallocycles reliably, and subsequently provide suggestions on the future design of these complexes.

From a crystal engineering perspective it was decided to assess the influence of four related imidazole-functionalised organic linkers on the formation of metallocycles. For ease of discussion, the chapter is divided into sections according to the ligand used. The first two ligands contain a 9,10-dihydrophenanthrene-spacer, which is somewhat similar to a biphenyl moiety. The addition of a nonaromatic methylene bridge (9,10 carbon atoms) restricts the ligand's rotational movements, resulting in a semi-rigid linker. Both the imidazole- (**L3**, Figure 6.1) and 2-methylimidazole-functionalised (**L4**) ligands were employed in complexation experiments. The last ligand that will be discussed incorporates a *p*-terphenyl-spacer, which resembles the biphenyl moiety more closely but is longer than both biphenyl and the spacers of the other ligands.

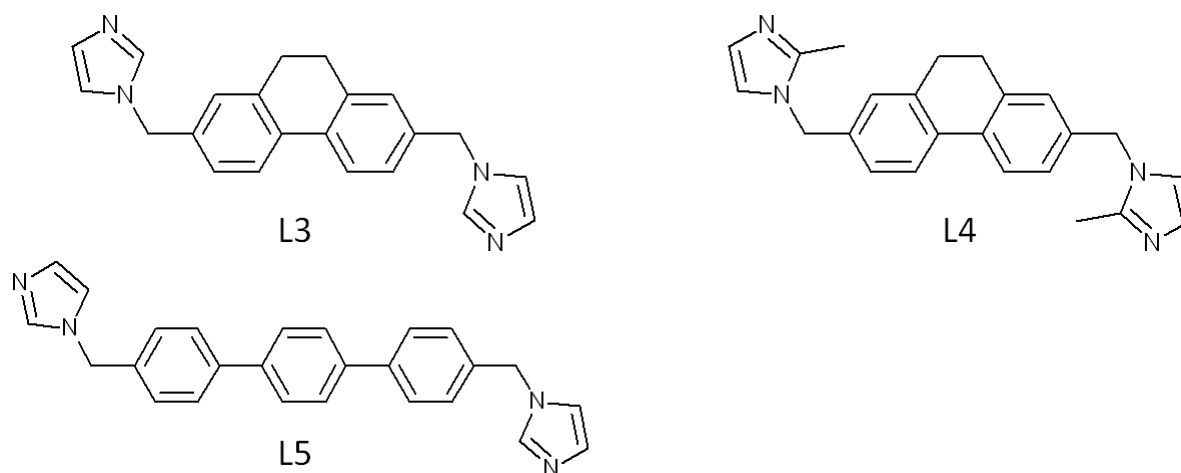


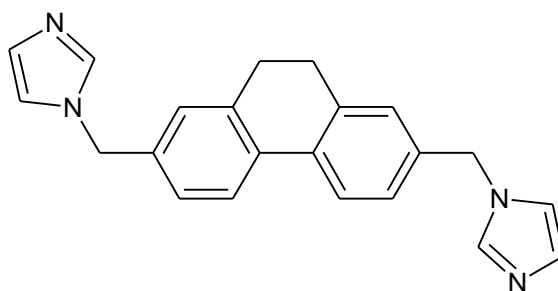
Figure 6.1 Imidazole- (**L3** and **L5**) and 2-methylimidazole-functionalised (**L4**) ligands employed in the crystallisations of metallocycles in this investigation.

Because this is an exploratory investigation of these metallocycles, the focus of the study is on the crystal structure analysis rather than the properties of the resulting compounds. Twelve metallocyclic structures were analysed and they will be discussed in the following sections. Comparisons between the metallocycle structures will be highlighted where appropriate and crystallographic data for the structures can be found in the tables at the conclusion of the chapter.

6.2 RESULTS

6.2.1 STRUCTURES WITH A 9,10-DIHYDROPHENANTHRENE SPACER

The first set of results outlines the crystal structures obtained from crystallisations using an organic linker characterised by the 9,10-dihydrophenanthrene moiety, which acts as an aromatic spacer (Scheme 6.1). As already mentioned above, the 9,10-dihydrophenanthrene spacer is interesting because its rotational freedom is more restricted when compared to the biphenyl and terphenyl moieties, but less restricted than the phenanthrene spacer (discussed in Chapter 5). With the slightly restricted rotation of the spacer unit, it was anticipated that the resulting structures will be somewhat rigid in their conformations and possibly robust to changes in their environments – e.g. guest removal. Seven metalloccycles containing this aromatic spacer were obtained and each is discussed in terms of its structural characteristics and intermolecular interactions.



Scheme 6.1 Ligand **L3**, 1,1'-(9,10-dihydrophenanthrene-2,7-diyl)dimethanediylbis(1*H*-imidazole)

6.2.1.1 $\text{MC21}_{\text{Benz}} - [\text{Co}_2\text{Br}_4\text{L3}_2] \cdot \text{C}_6\text{H}_6$

The combination of **L3** (Scheme 6.1) with cobalt bromide resulted in the formation of a discrete metalloccycle as depicted in Figure 6.2. $\text{MC21}_{\text{Benz}}$ crystallises in the monoclinic space group $C2/m$. The ASU consists of a quarter of a metalloccycle, i.e. half a cobalt cation coordinated to half a ligand molecule and a bromide counter ion; a single benzene molecule is also part of the ASU. The cobalt cation assumes a distorted tetrahedral geometry and the ligand molecules are aligned parallel to each other. The **L3** ligand molecules assume a C-shaped conformation, coordinating to two metal centres to form discrete cyclic entities. The ligands are tilted at an angle of 29.1° relative to the plane of the metalloccycles (Figure 6.3).

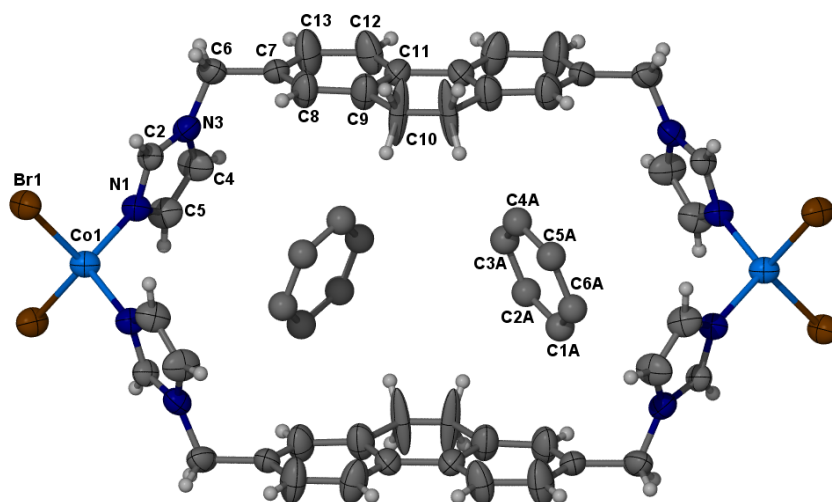


Figure 6.2 50% Probability thermal ellipsoids plot of $\text{MC21}_{\text{Benz}}$. Only atoms of the ASU are labelled. The included benzene molecules are shown in ball and stick representation, with hydrogen atoms omitted for clarity

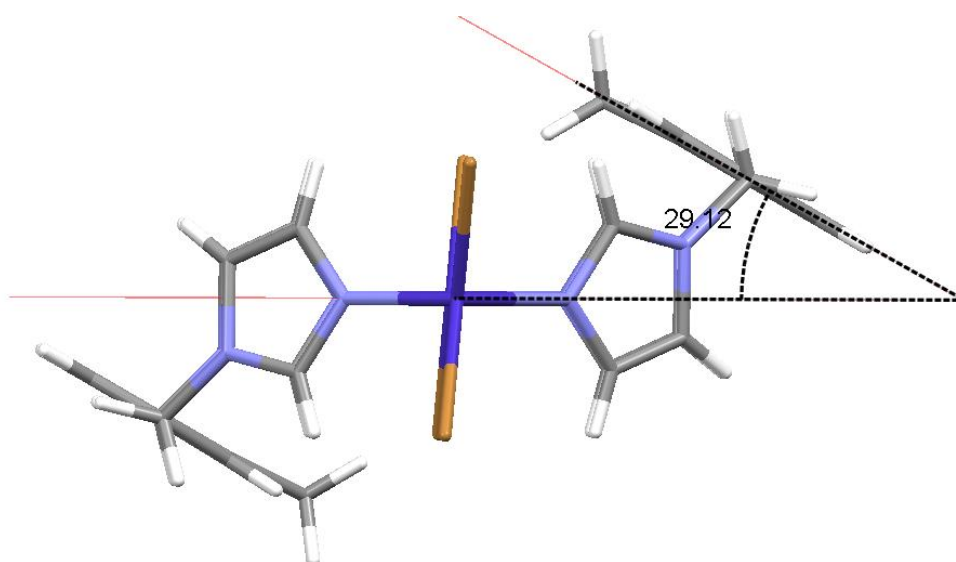


Figure 6.3 Tilt angle of dihydrophenanthrene moiety relative to the horizontal plane of the metalloccycle of $\text{MC21}_{\text{Benz}}$.

Host-host $\pi \cdots \pi$ stacking interactions (3.756 Å) occur between imidazole moieties of the adjacent metalloccycles to yield layers of metalloccycles parallel to (100) (Figure 6.4). These layers pack one on top of another to form a series of one-dimensional channels that propagate along [001]. These one-dimensional channels are filled with benzene molecules which, although easily located in the electron density maps, cannot be modelled sufficiently well. They were consequently constrained using an AFIX 66 command in SHELXL. The benzene molecules were modelled with a site occupancy of 0.5 and thus alternate their orientation throughout the channel. Initially it was thought that because the benzene molecules reside in a relatively large channel they are in motion (either as they move out of the channels or they are simply moving about) and therefore cannot be modelled in an average position. It appears, however, that the symmetry of the structure may be grounds for the poorly refining

guest molecules (Figure 6.5). It is apparent from Figure 6.5 that the guest molecules are located between two metalloporphyrins in adjacent layers that form the channels.

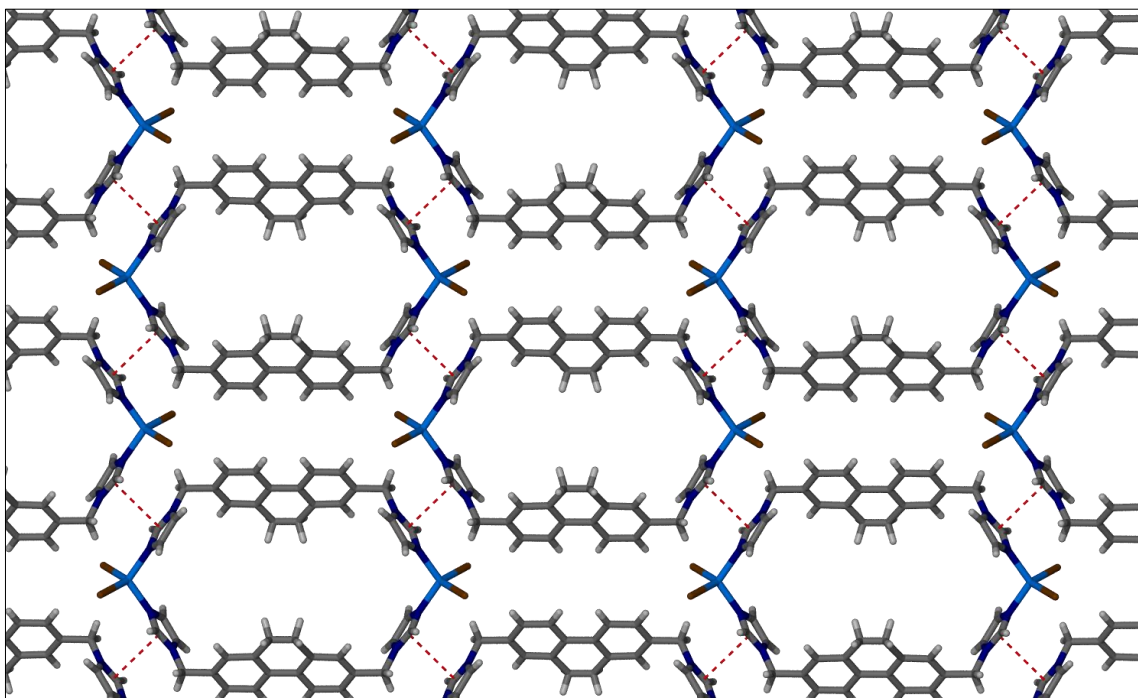


Figure 6.4 Packing arrangement of MC21_{Benz} showing one layer of the metalloporphyrins. Layers are maintained by weak $\pi \cdots \pi$ interactions between anti-parallel aligned imidazole moieties of adjacent metalloporphyrins. The benzene guest molecules have been omitted for clarity.

The displacement ellipsoids of the carbon atoms of the dimethylene bridge (C10 in Figure 6.2) are elongated in comparison to the other atoms, indicating either disorder over two positions or some thermal motion. Though these atoms are symmetry related to each other, it is thought that the movement of the bridge is asymmetrical (wave-like) rather than hinge-like. This may account for the large anisotropic displacement of this atom as it represents an average position throughout the system. This bridge probably flexes in response to movement of the benzene guests in the channel.

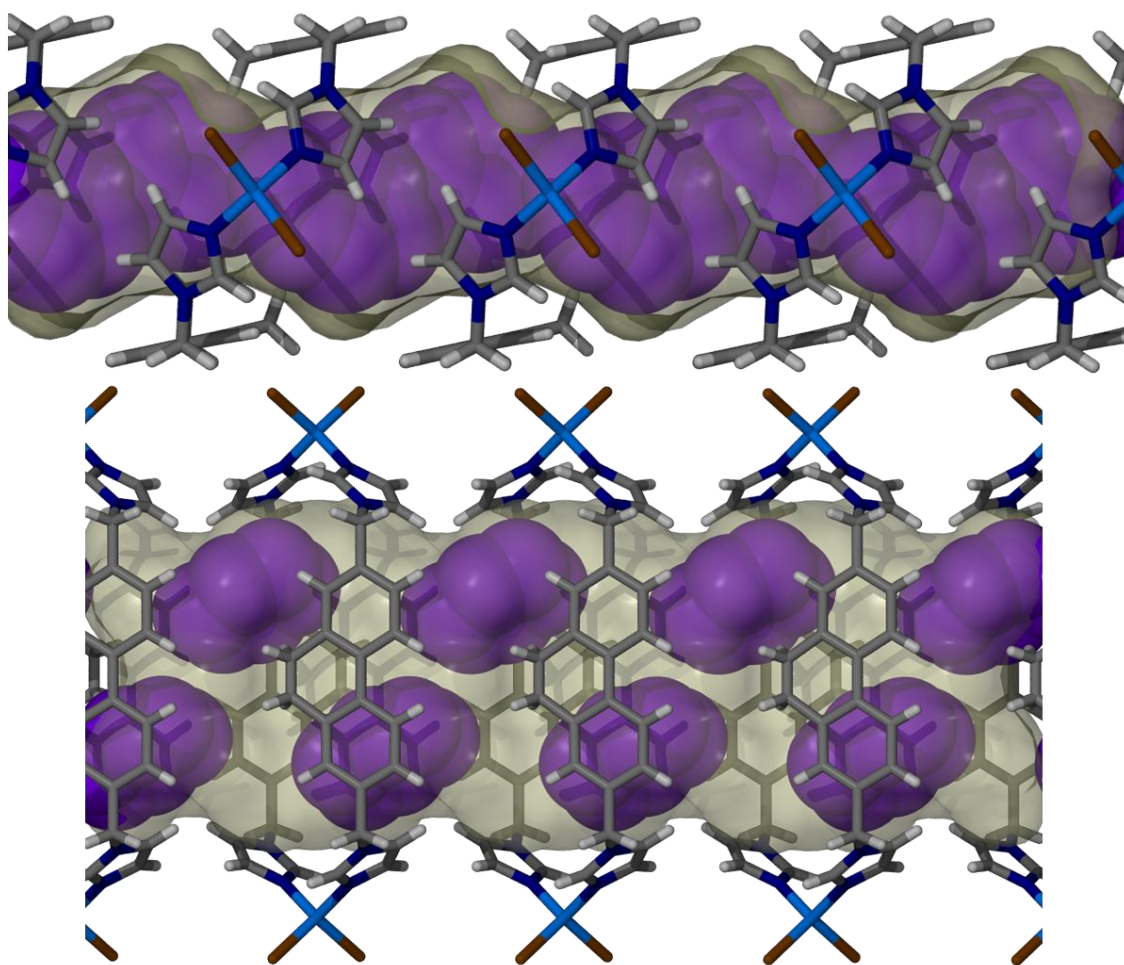


Figure 6.5 A one-dimensional channel in $\text{MC21}_{\text{Benz}}$ viewed along [010] (top) and perpendicular to (100) (bottom). Only one of the two possible orientations of the benzene guest is shown for clarity.

The benzene guests do not participate in any strong interactions with the host. However, weak $\text{C-H}\cdots\pi$ contacts do occur between the dimethylene bridging carbon atoms (C10) of the host and the π -electrons of the benzene guest. The same type of interaction also occurs between the benzene guest and the imidazole moiety of an adjacent host metalloccycle. These are believed to be van der Waals or electrostatic interactions as the entities, in both instances, are too distant for typical $\text{C-H}\cdots\pi$ interactions. The fingerprint plot (Figure 6.6) generated from the Hirshfeld surface for the metalloccycle substantiates the lack of significant intermolecular interactions in the structure.

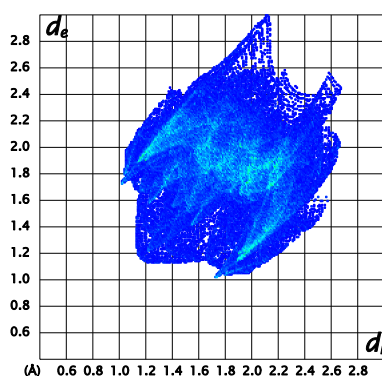


Figure 6.6 Fingerprint plot of the metalloclycle of MC21_{Benz}

It was postulated that, because the guest molecules are located within open channels, and because there are no obvious interactions retaining the guests within these channels, the benzene molecules can be removed without difficulty. However, if a few single crystals are placed under vacuum at 60 °C for 3 hours, the benzene molecules can still be located within the channels after SCD analysis.

The thermal analysis of these crystals appears to contradict this finding, revealing that the sample begins to lose volatile guests immediately at ambient temperature. When this analysis is carried out on a sample of single crystals it appears that the desolvation process occurs relatively slowly, with complete solvent loss reached just before 200 °C. When the same analysis is performed on a powdered sample, guest removal occurs at a much higher rate and appears to be complete at approximately 50 °C. Indeed, it is a well-known phenomenon that the rates of desorption are related to the particle size distribution of the sample.

6.2.1.2 MC22 – [Cd₂I₄L₃]₂·2C₆H₆·2MeCN

The combination of L3 and CdI₂ crystallised from a solvent mixture of benzene and MeCN yields the structure of MC22 (Figure 6.7), which crystallises in the space group *C2/m* with an ASU consisting of half a metalloclycle, two MeCN molecules and two quarter benzene molecules. The metalloclycle and the two benzene molecules are situated on a mirror plane such that the ASU contains two cadmium cations and four iodide counter ions, all of which are half occupied. The MeCN molecules are each disordered over two positions of equal occupancy.

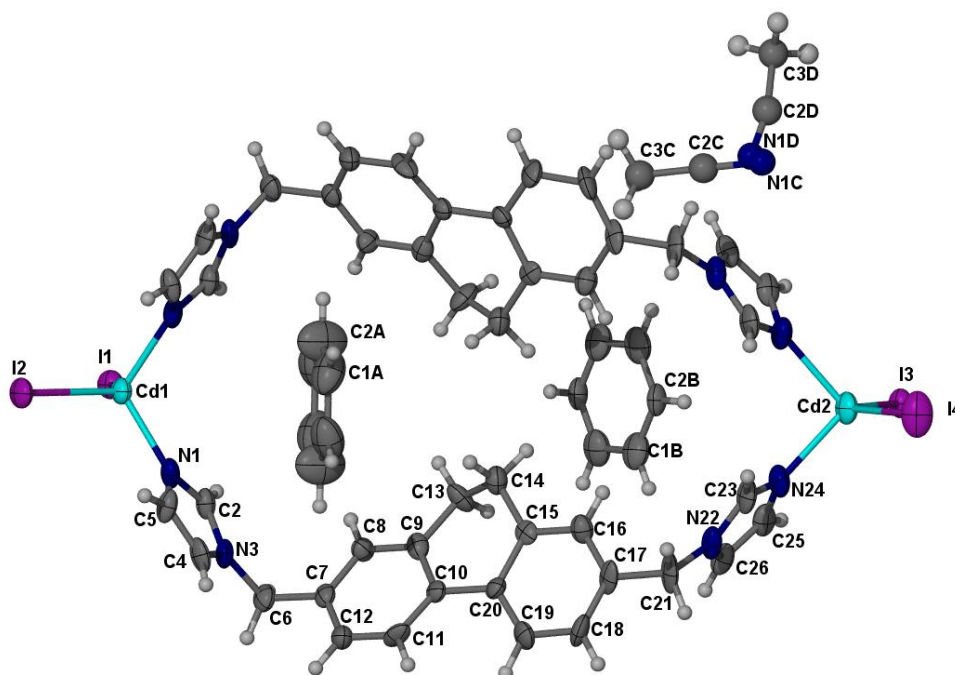


Figure 6.7 Thermal ellipsoid (50% probability) plot of MC22. The MeCN molecules are represented as ball and stick models and the ASU is appropriately labelled.

The ligand (**L3**) moiety is coordinated to the Cd cation in an approximately C-shaped conformation but is slightly twisted such that the metallocycle adopts a chair-shaped conformation. The imidazole moieties of each ligand molecule are in an up-down orientation (i.e. anti-parallel) in relation to each other. Both dihydrophenanthrene moieties are tilted towards the centre of the metallocycle such that they are almost co-planar in relation to each other. Because the bridging methylene carbon atoms (C13 and C14, Figure 6.7) are not aromatic, they have more freedom of motion and, in this instance, are positioned in an up-down (buckled) arrangement to facilitate optimal orientation of the hydrogen atoms attached to the bridge. This means that the two opposing methylene carbon atoms (i.e. C13 and C14) of separate ligand molecules are in close proximity to each other across the metallocycle (3.61(3) Å). This distance is sufficiently close that the metallocycle is divided into two unequal parts. Figure 6.8 clearly demonstrates how this contact results in the creation of two distinct pores or apertures. Owing to this division, the guest molecules are too large to fit inside the confines of the metallocycles and are rather located in the recesses of the metallocycles.

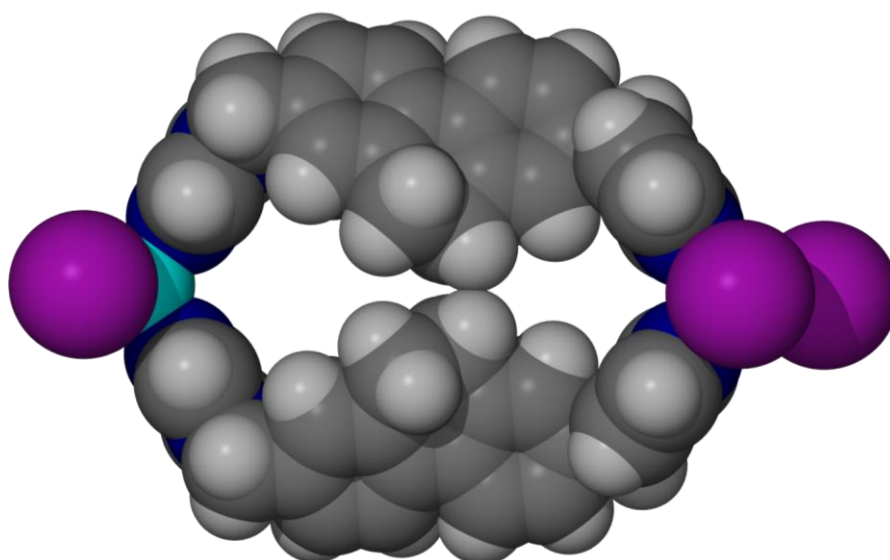


Figure 6.8 Space-filling representation of the metalloporphyrin in MC22 depicting the closure of the metalloporphyrin aperture to create two small, distinct pores.

The metalloporphyrins are organised in layers that propagate parallel to the (001) plane. The layers are maintained by weak $\pi\cdots\pi$ interactions between the imidazole moieties of adjacent metalloporphyrins. These interactions are more pronounced between the imidazole rings labelled N22-C26 (3.576 Å, red fragmented lines in Figure 6.9) than between those labelled N1-C5 (3.781 Å). The imidazole moieties involved in these interactions are aligned 180° in relation to each other to maximise $\pi\cdots\pi$ stabilisation. These $\pi\cdots\pi$ interactions allow the metalloporphyrins to fit together in a “head-to-head” (interdigitating) manner in the individual layers such that the layer resembles a set of stairs when viewed parallel to (010). Within the individual layers the metalloporphyrins are arranged in rows with the methylene bridge carbon atoms of the dihydrophenanthrene moieties pointed either upwards (red shaded region, Figure 6.9) or downwards (blue shaded region). These layers stack in an offset manner such that the dihydrophenanthrene moieties are directed towards (referred to here as “face-to-face”) or away from each other (“back-to-back”) in an alternating fashion (Figure 6.10). This arrangement allows the formation of two different solvent-accessible spaces (Figure 6.11). The “back-to-back” arrangement results in the formation of a small solvent-filled pocket whereas the “face-to-face” arrangement creates a larger space, which is filled with benzene and MeCN guest molecules.

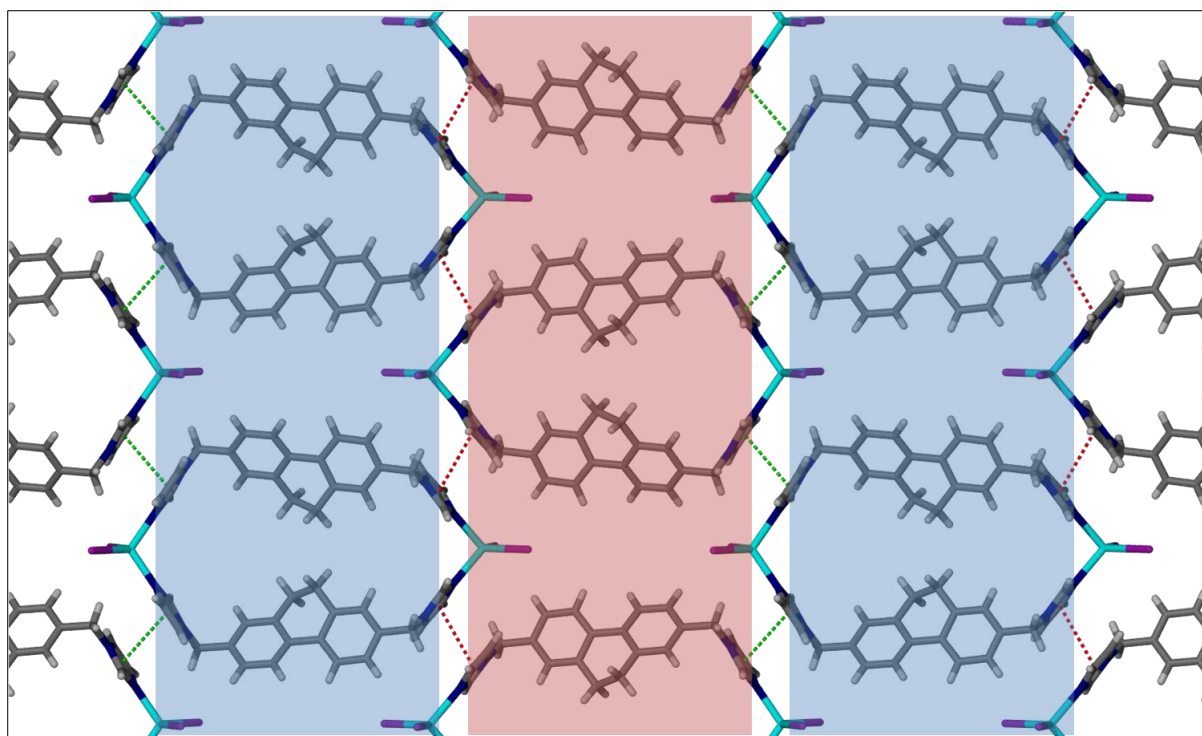


Figure 6.9 Single layer of MC22 stabilised by $\pi\cdots\pi$ interactions between imidazole moieties. The red fragmented lines indicate the closer interactions whereas the green fragmented lines indicate those that are slightly longer. The blue shaded area indicates the metalloacycles whose dihydrophenanthrene moieties are directed out of the plane whereas the red area indicates those directed into the plane. Guest molecules included in the structure have been omitted for clarity.

The intriguing aspect of this metalloacycle is that the two dissimilar pores of the metalloacycle extend into two dissimilar solvent-filled cavities. One extends into a continuous channel-like cavity that contains benzene and MeCN guest molecules and the other into a discrete pocket that houses a single benzene molecule. The inclusion and location of the guest molecules in this structure appear to be partially responsible for the unusual conformation of the metalloacycles.

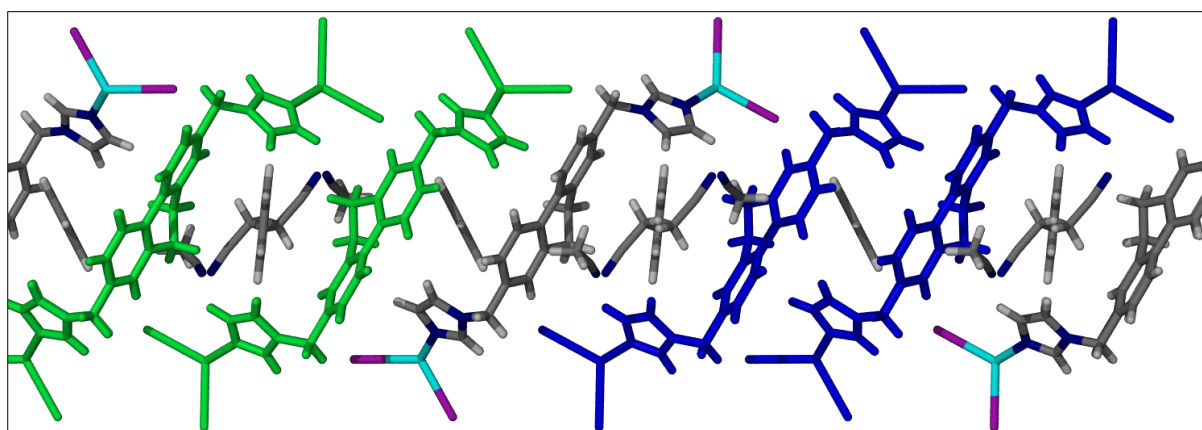


Figure 6.10 Column of metalloacycles of MC22 showing the face-to-face (green) and back-to-back (blue) arrangement of the dihydrophenanthrene moieties in separate layers.

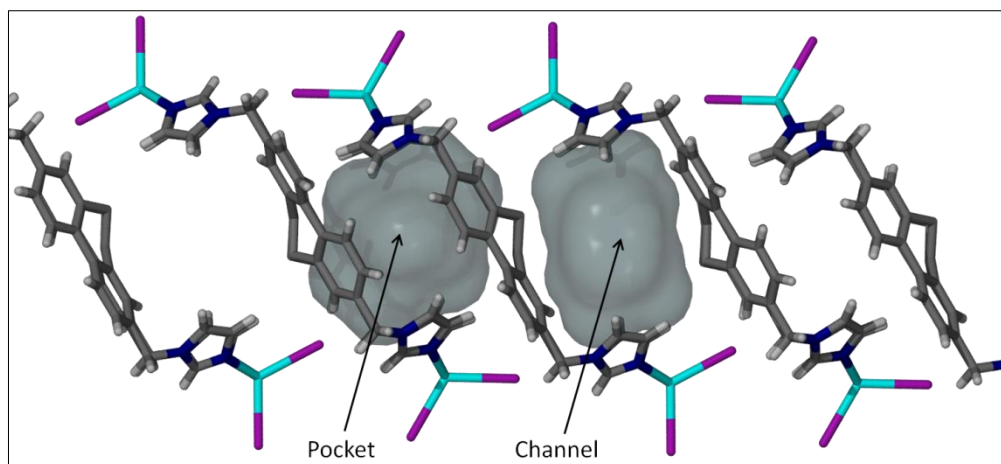


Figure 6.11 Metalloccycles of MC22 viewed side-on to demonstrate the two solvent-accessible voids. When the metalloccycles are arranged “back-to-back” a discrete pocket is formed, whereas if they are organised “face-to-face” a larger channel is formed.

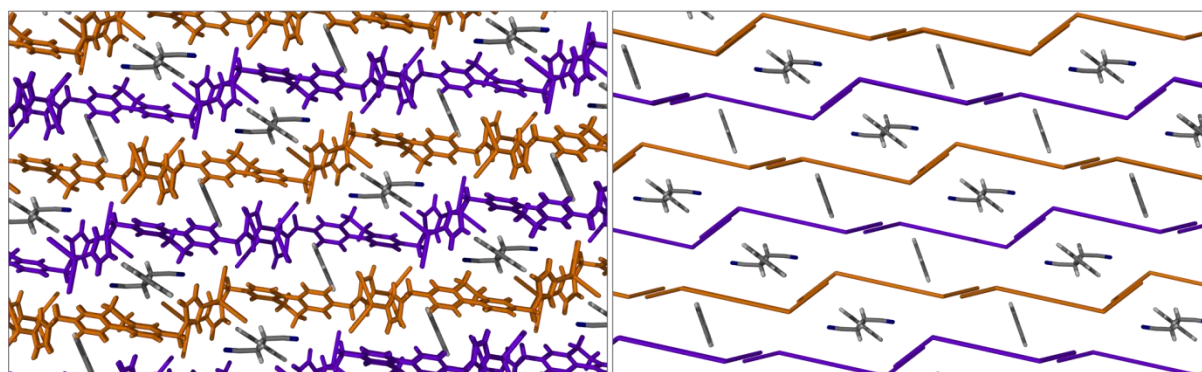


Figure 6.12 Packing arrangement of the metalloccycles of MC22 viewed down the channels (left). Simplified representation of the metalloccycles arranged to form two different solvent-accessible void spaces (right). The metalloccycle layers are coloured orange or purple for clarity.

Four molecules of MeCN are located in the channel space between the metalloccycles, positioned in such a way that they encircle the iodide counter ions of nearby complexes. Because the MeCN molecules are each disordered over two positions of equal occupancy, there is more than one possible packing arrangement of these guest molecules. Because of very weak C–H \cdots N/C interactions between the neighbouring molecules, they follow in a circular weakly hydrogen-bonded pattern rotating in either a “clockwise” (green molecules in Figure 6.13) or “anti-clockwise” (yellow) manner about the iodide anions. In this way, the MeCN molecules also appear to mimic the conformation of the metalloccycles and adopt a chair-shaped conformation around the iodide anions (Figure 6.14).

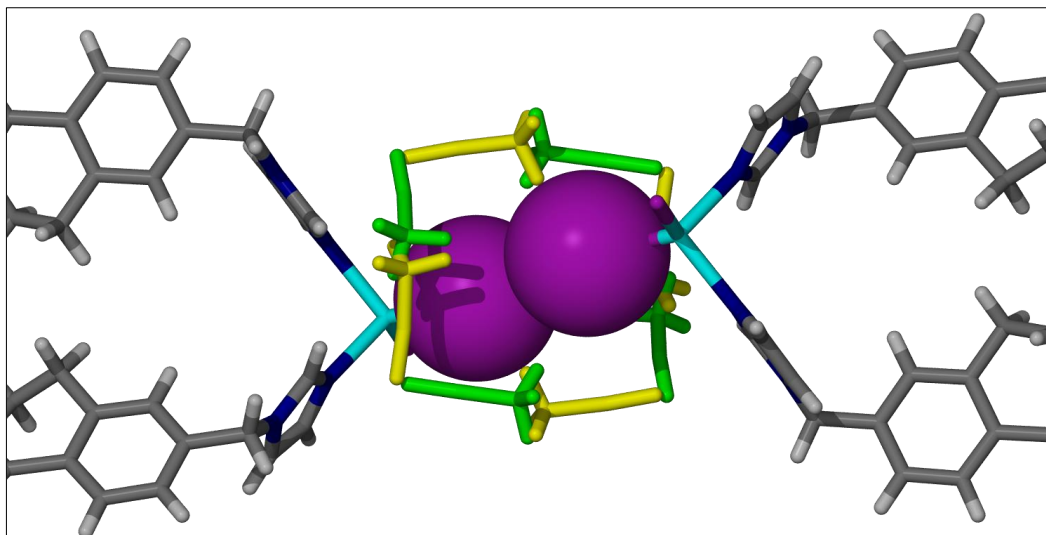


Figure 6.13 The MeCN molecules included in the structure of **MC22** are arranged around the interacting I...I anions in either a “clockwise” (green) or “anti-clockwise” (yellow) manner.

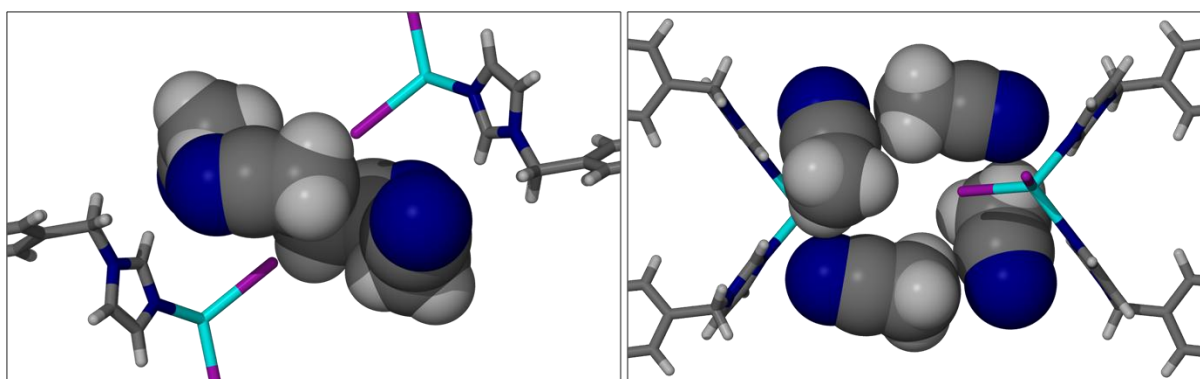


Figure 6.14 Space-filling representation of the MeCN molecules arranged around the iodide anions of nearby metalloccycles in **MC22**, viewed from two different perspectives. The figure on the left shows the approximate chair-shaped conformation of the MeCN guests. Only one of the possible arrangements is shown for clarity.

As in the previous structure there are only a few intermolecular interactions. The host metalloccycles are arranged in layers, which are stacked on top of one another in an offset manner (Figure 6.12). These stacks are stabilised by C–H... π interactions between carbon atoms of the imidazole rings and the phenyl moieties of the metalloccycles in adjacent layers (3.542 Å). Weak lone-pair... π interactions occur between aryl moieties of the host metalloccycles and the nitrile groups of MeCN guest molecules. The nitrile groups of the MeCN molecules are also involved in C–H... π interactions with the imidazole moieties of the hosts. The fingerprint plot (Figure 6.15) confirms the lack of strong interactions in the structure, with the primary contribution to the plot being from van der Waals interactions.

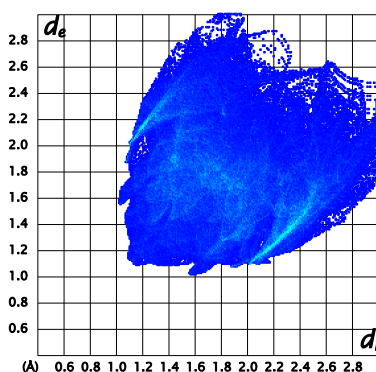


Figure 6.15 Fingerprint plot of the metallocycle in MC22.

Thermal analysis of MC22 shows a stepwise weight loss (Figure 6.16). The first step commences at approximately 30 °C, leading directly into the broader second step. The thermogram is then stable until decomposition, which has a slight inflection in the trace, at approximately 350 °C. The percentage weight loss that occurs with each step could not be attributed unambiguously to the removal of the four guest molecules. However, it is thought that the first step corresponds to the loss of one benzene and two MeCN molecules, which reside in the channel-like cavity, whereas the second step corresponds to the removal of the benzene molecule from the small pockets. Attempts were made to remove only the guest molecules situated in the channel spaces as a single-crystal to single-crystal transformation. Unfortunately, this process proved extremely difficult because crystals of this compound tend to grow in clusters and single crystals are difficult to separate. Therefore, X-ray intensity data for the desolvated crystals could not be collected.

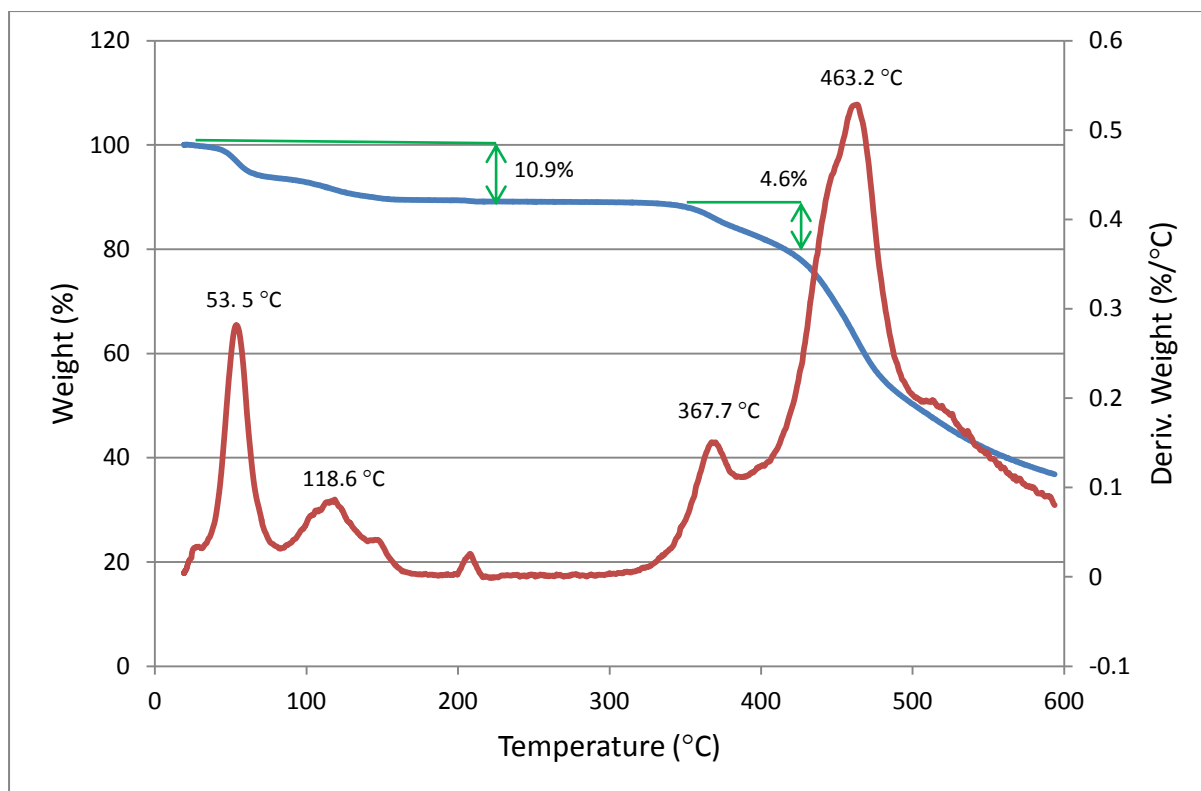


Figure 6.16 TG trace of MC22. The blue trace shows the percentage weight loss as a function of temperature (°C) and the red trace represents the first derivative of the same weight loss.

6.2.1.3 MC23 – $[\text{Cd}_2\text{I}_4\text{L}_3] \cdot 3\text{MeCN} \cdot 2\text{C}_7\text{H}_8$

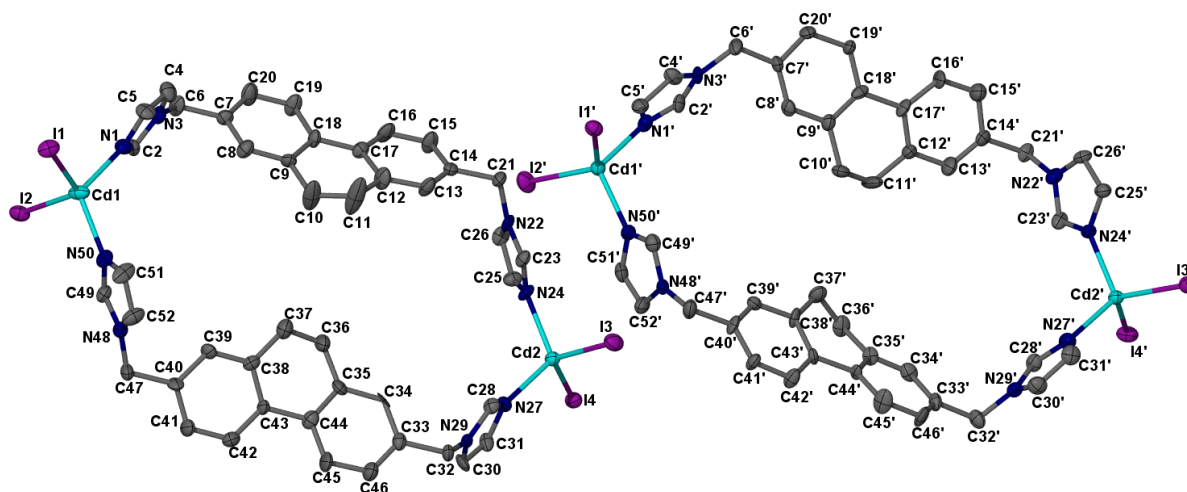


Figure 6.17 Thermal ellipsoid plot (50% probability) of the metallocycles in the ASU of MC23. Metallocycles are labelled MC, on the left, and MC' is on the right. The included solvent molecules, as well as the hydrogen atoms, have been omitted for clarity.

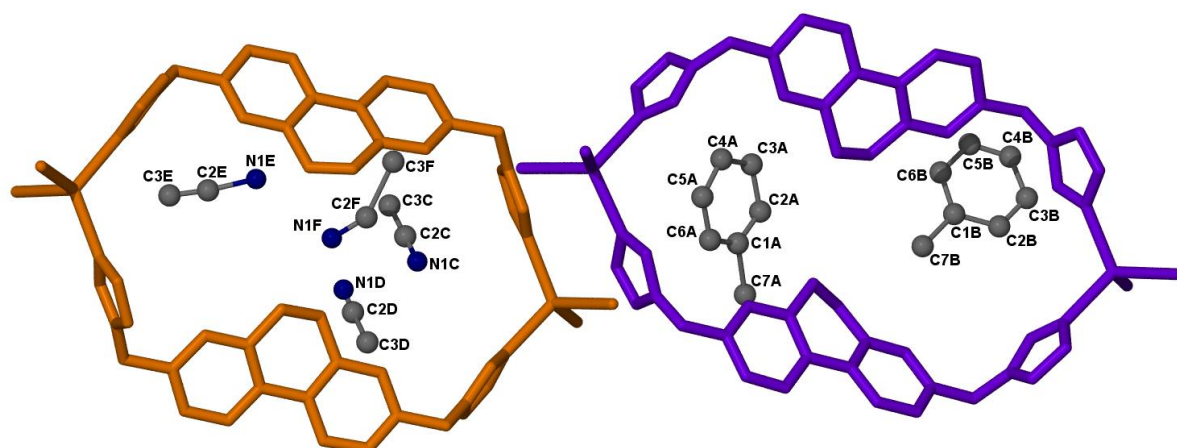


Figure 6.18 The asymmetric unit of **MC23**, with the included toluene and MeCN guest molecules labelled. The guest molecules are labelled A-F. MeCN molecules E and F each have a site occupancy of 0.5. Hydrogen atoms have been omitted for clarity. The metalloccycle **MC** is shown in orange and that labelled **MC'** is depicted in purple.

A structure similar to **MC22** was obtained from the combination of **L3** and CdI_2 in a solvent mixture of toluene and MeCN. Although the structures share similarities in their arrangements, they cannot be considered isostructural since both the crystal systems and unit cell parameters are different. For the toluene-included structure the space group is Cc , rather than $C2/m$, as in the benzene structure. The structure was checked for missed symmetry to ensure that the space group choice is indeed correct. Structure solution was attempted in $C2/c$, $C2/m$ as well as Cc with the best refinement obtained in Cc . Visual inspection of the structure also indicated that Cc is indeed the correct space group. Two complete metalloccycles are included in the ASU of **MC23** (Figure 6.17); small conformational differences are observed in the ligand molecules as well as for each metalloccycle, even though they appear almost identical. The guest molecules included in the structure are not all well resolved and so there is some residual electron density that could not be modelled (Figure 6.18). The SCD model suggests that there are three molecules of toluene and at least another three of MeCN in the ASU. However, only two toluene guests could be modelled adequately. Two MeCN molecules (labelled **A** and **B**, Figure 6.18) are fully occupied while those labelled **E** and **F** are disordered over two possible positions with approximately equal occupancies.

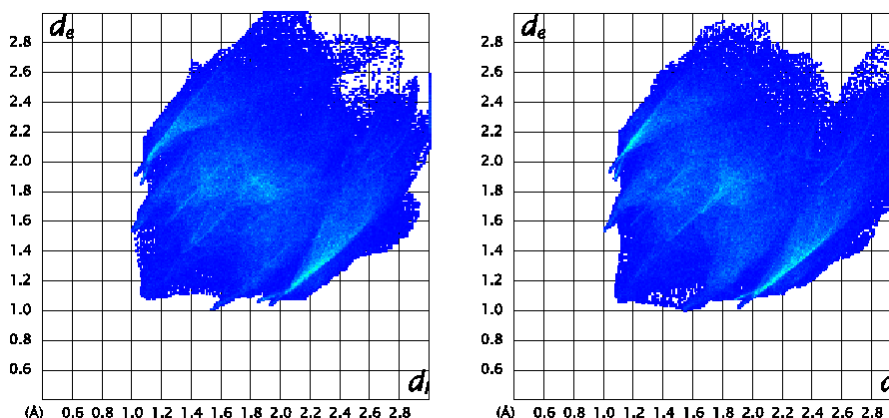


Figure 6.19 Fingerprint plots of the metalloccycles labelled **MC** (left) and **MC'** (right) in the ASU of **MC23**

The ligand molecules (**L3**) are coordinated to the cadmium cation in a C-shaped conformation, with the metalloccycles each adopting approximate chair-shaped conformations. The nonaromatic carbon atoms of the dihydrophenanthrene moieties are out of the plane defined by the aromatic atoms, as in the structure of **MC22**. However, in **MC23** the relative atomic positions of these carbon atoms are slightly different in each of the four ligand molecules in the ASU, bringing about a lowering of the symmetry of the structure. The fingerprint plots for the independent metalloccycles (**MC** and **MC'**) show only small differences in the intermolecular interactions experienced by each of them (Figure 6.19).

The symmetry-independent metalloccycles are organised into separate layers, which are stabilised by $\pi \cdots \pi$ interactions between imidazole moieties of neighbouring metalloccycles (Figure 6.20). Each layer is constructed from one or the other of the symmetry-independent metalloccycles (depicted in orange or purple). These two independent layers align “back-to-back” (i.e. concavities towards each other) to form a type of bilayer. This arrangement includes MeCN molecules, aligned as anti-parallel dimers within small one-dimensional channels (Figure 6.21). The bilayers are aligned in a “face-to-face” (i.e. convex dihydrophenanthrene moieties towards each other) manner and are separated by the other guest molecules – two toluene molecules and a MeCN molecule.

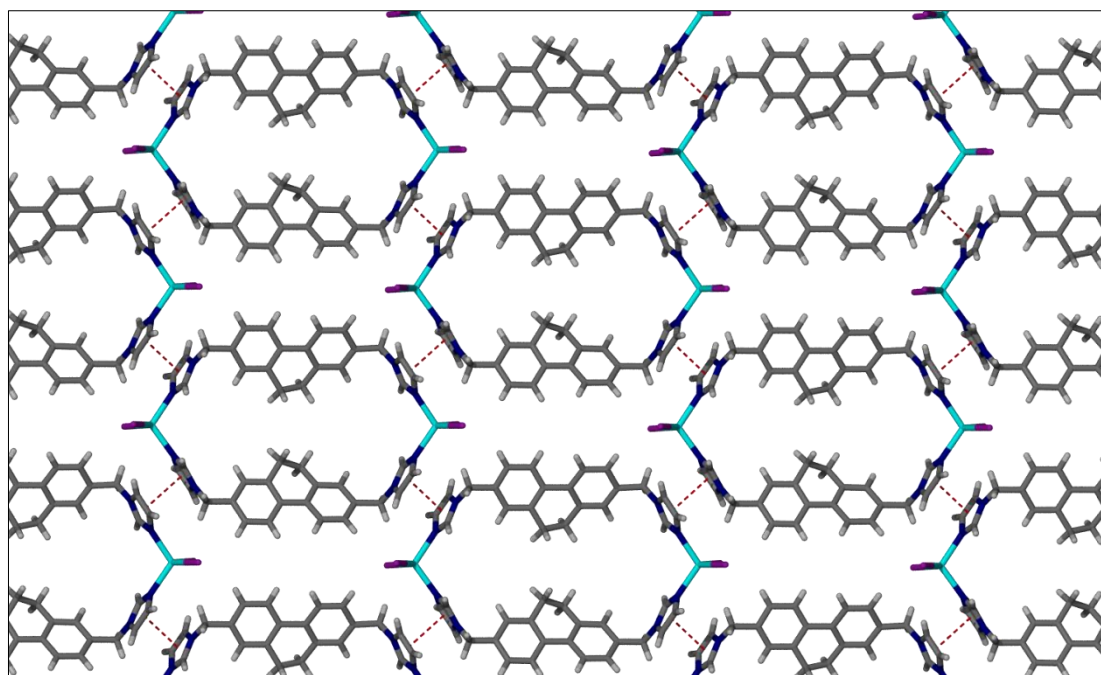


Figure 6.20 Single layer of metalloccycle **MC'** in **MC23** involving $\pi\cdots\pi$ stacking between adjacent imidazole moieties. Interactions are shown by the fragmented red lines.

Analogous to the benzene structure (**MC22**), the orientation of the dihydrophenanthrene moieties is such that the methylene bridges (C10 and C11; C36 and C37) are directed towards the centre of the metalloccycle and divide the aperture of the metalloccycle in two. In this instance, the two small pores of each of the unique metalloccycles appear to be similar in size and shape. However, the conformation of the dihydrophenanthrene moieties, together with the organisation of the two unique metalloccycles, gives rise to two distinct guest-filled spaces (Figure 6.22).

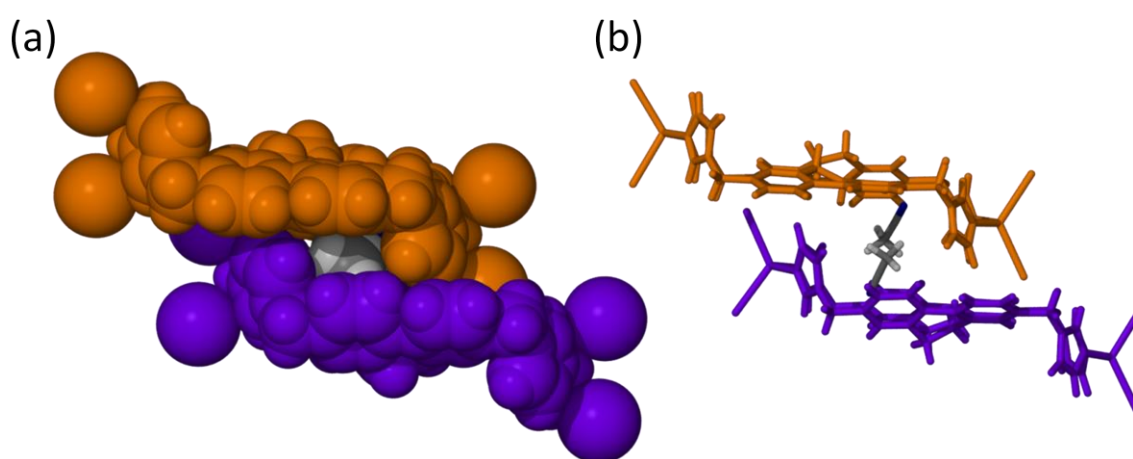


Figure 6.21 (a) Space-filling representation of two symmetry-independent metalloccycles of **MC23**, which form the bilayers, and which encapsulate two MeCN molecules. (b) "Back-to-back" alignment of the symmetry-independent metalloccycles **MC** (orange) and **MC'** (purple) shown in capped-stick representation.

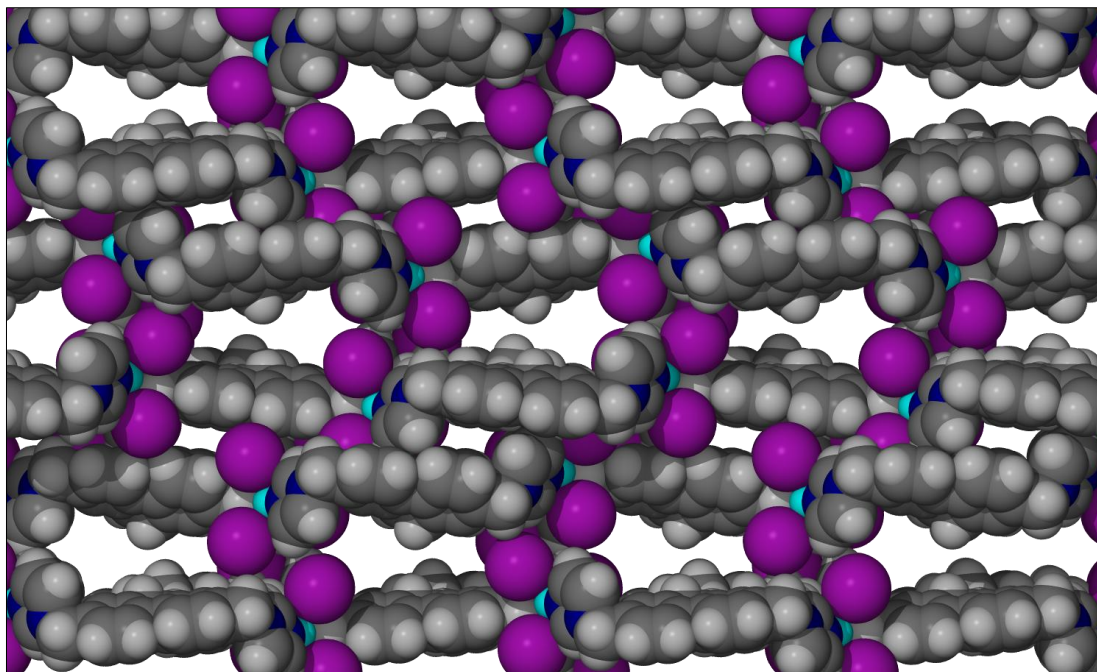


Figure 6.22 Space-filling representation of metalloporphyrins of **MC23** showing the two different solvent-accessible channels viewed along [100]. Guest molecules have been omitted to show the different solvent-filled spaces.

The smaller cavities are each filled with two MeCN molecules, which are arranged as head-to-tail dimers stabilised by C–H···N interactions (3.47(2) Å). Two symmetry-independent metalloporphyrins associate in an offset manner and encapsulate these MeCN dimers in these cavities (Figure 6.21). Viewing the structure down the channels (crystallographic *a* axis), it appears that each cavity is continuous; however, the MeCN guests are too large to traverse from one pocket through the small pores into a neighbouring pocket. The larger channels, formed between metalloporphyrin bilayers, accommodate the toluene guests along with the partially occupied MeCN molecules.

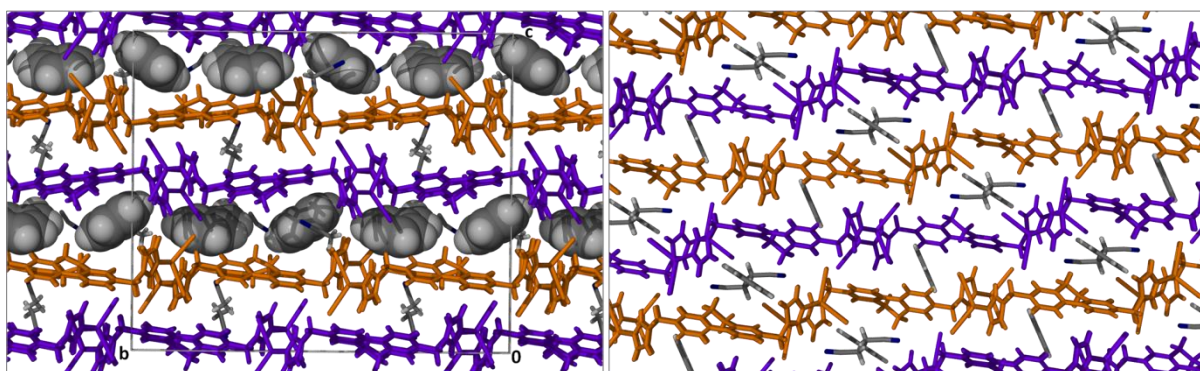


Figure 6.23 Comparison of the packing arrangements of the metalloporphyrins in the structures of **MC23** (left) and **MC22** (right).

On first assessment the structure of **MC23** appears highly similar to that of **MC22**, which includes benzene and MeCN guest molecules. However, inclusion of toluene, which is larger than benzene, appears to alter the symmetry of the structure (Figure 6.23). The metalloporphyrin

layers in MC22 are organised in a slightly offset manner, whereas the bilayers in MC23 are stacked one on top of the other in an anti-parallel arrangement (Figure 6.24).

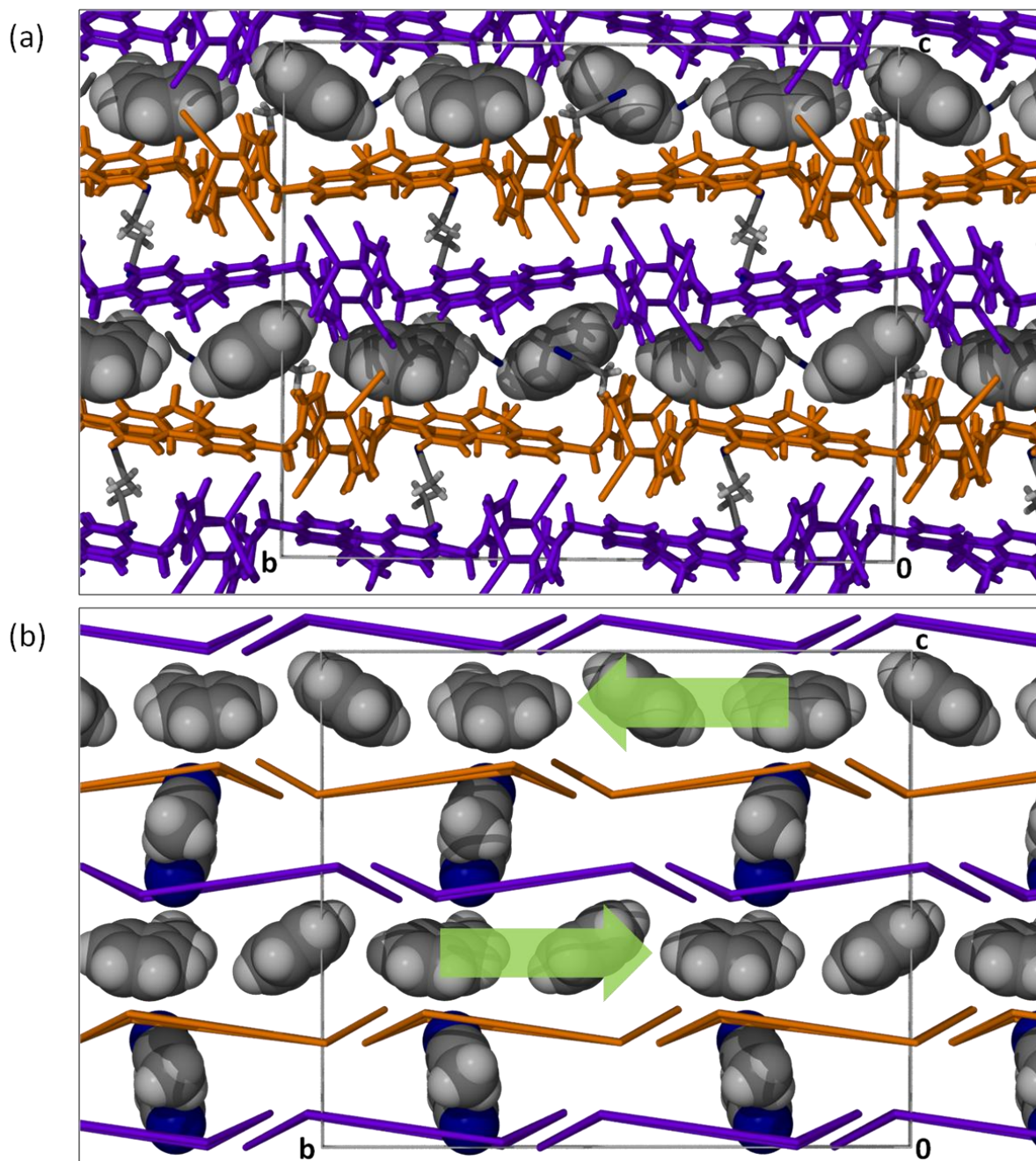
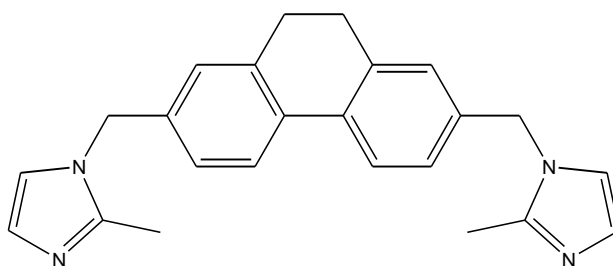


Figure 6.24 Packing arrangement of MC23 viewed along [100] (a) and a simplified representation (b). Green arrows in (b) indicate the anti-parallel alignment of the bilayers stacked along [001]. The two symmetry-independent metalloporphyrins are coloured orange and purple and have been reduced to their simplest representation, whereas the guest molecules are depicted in van der Waals representation. The MeCN molecules in the toluene channels have been omitted for clarity.

6.2.2 STRUCTURES OBTAINED WITH 2-METHYLIMIDAZOLE COORDINATING GROUPS



Scheme 6.2 Ligand **L4**, 1,1'-(9,10-dihydrophenanthrene-2,7-diyl)bis(2-methyl-1*H*-imidazole)

6.2.2.1 MC24 – [Cd₂L₄L₄]₂·DCM·MeCN

Crystals of **MC24** were obtained by the combination of **L4** (Scheme 6.2) with CdI₂ in a solvent mixture of DCM and MeCN. Ligand **L4** is analogous to **L3**, but the imidazole moiety is substituted with an 2-methylimidazole coordinating group. **MC24** crystallises in the monoclinic space group *C2/c*, with a cadmium cation coordinated to half a ligand molecule (**L4**) and two iodide counter ions in the ASU (Figure 6.25).

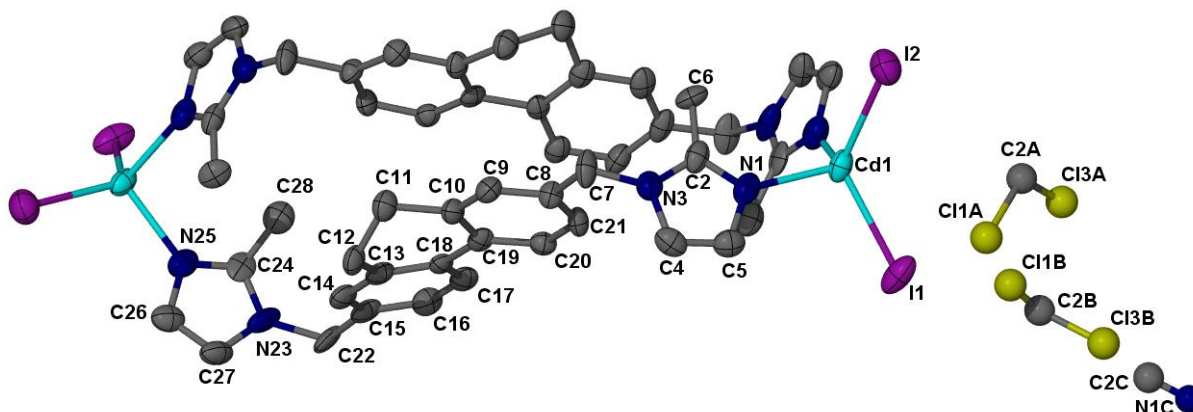


Figure 6.25 Thermal ellipsoid plot (50% probability) of **MC24**. The DCM molecules and partial MeCN are shown in ball-and-stick representation. Only the ASU has been labelled and hydrogen atoms have been omitted for clarity.

A DCM molecule, disordered over two positions of unequal occupancy, is also included in the ASU. The DCM molecule labelled **B** (Figure 6.25) constitutes the position of approximately 65% occupancy, whereas that labelled **A** is the position of 35% occupancy. A MeCN molecule is incorporated in the ASU, although this molecule could not be modelled completely. These guest molecules are situated in interstitial spaces between the metalloccycles.

The metalloccycles in this crystal structure are unlike the others previously discussed. The ligand molecules assume a divergent (*S*-shaped) conformation, twisting in order to facilitate

coordination to the cadmium cations. The imidazole moieties are positioned approximately perpendicular to the dihydrophenanthrene spacer. It is presumed that the substituted 2-methyl groups of the 2-methylimidazole moieties contribute to this conformation. Both methyl groups of the 2-methylimidazole moieties of each of the **L4** ligand molecules are directed towards the interior of the metalloccycles. These ligand molecules are, in turn, orientated such that they fit into each other, similarly to $\pi\cdots\pi$ embrace interactions (Figure 6.26). Or more simply, the metalloccycle has collapsed (imploded) in on itself. Also noteworthy is that the methylene bridges of the dihydrophenanthrene moieties (C11 and C12) are located on the same side of the plane of the metalloccycle.

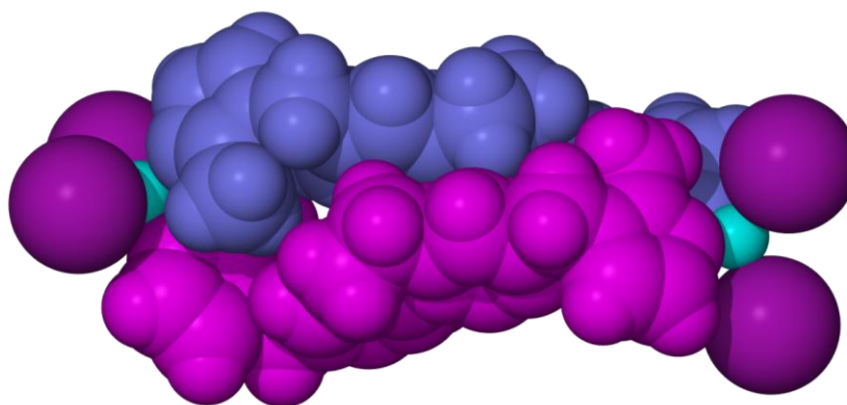


Figure 6.26 Space-filling representation of the metalloccycle of **MC24**. Opposing ligand molecules are coloured blue and pink to indicate the embrace of the two molecules.

The metalloccycles are stabilised by a number of weak C–H \cdots C contacts with neighbouring metalloccycles. These interactions occur between the imidazole moieties and the methylene bridging carbon atoms (C11 and C12) as well as between the methylene carbon atoms and the dihydrophenanthrene biphenyl moieties. Weak intermolecular interactions also occur between the chlorine atom of the DCM guest (higher-occupancy position) and the carbon atoms (C9) of the dihydrophenanthrene moieties (3.69(2) Å). These are accompanied by weak C–H \cdots π contacts between the methylene linker carbon atoms (C7) and the nitrile moieties of the MeCN guest molecules (3.488 Å). Apart from these few weak interactions, it appears that the packing arrangement of these metalloccycles is governed by close packing.

The packing arrangement is such that guest molecules occupy the spaces created by four adjacent metalloccycles and extend between the layers of metalloccycles (Figure 6.27). Specifically, the disordered DCM molecules are located in the spaces between cadmium iodide centres of neighbouring metalloccycles arranged in two-dimensional layers, whereas the MeCN molecules reside in the spaces between these layers.

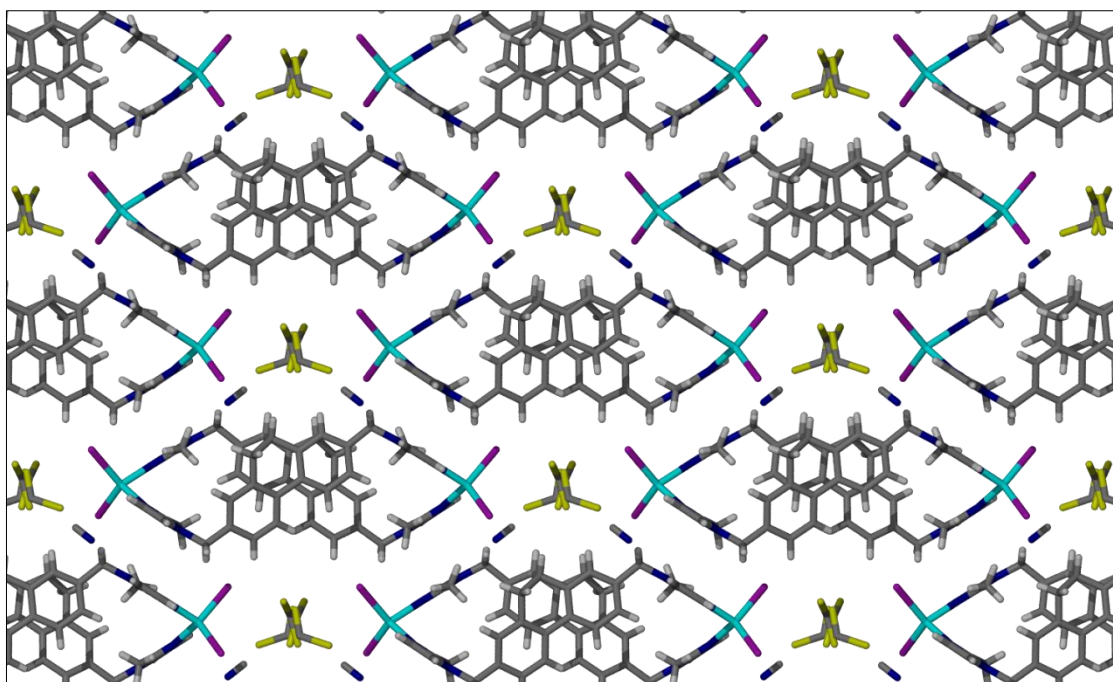


Figure 6.27 Packing arrangement of MC24 viewed perpendicular to (001).

The fingerprint plot of the metallocycle in MC24 (Figure 6.28) indicates that there are indeed only weak intermolecular interactions. The plot is dominated by weak van der Waals interactions with some characteristic tails indicating C–H...C contacts.

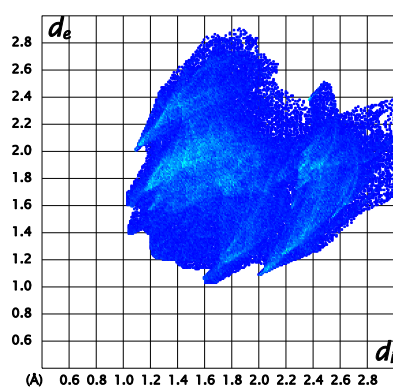


Figure 6.28 Fingerprint plot generated for the metallocycle of MC24

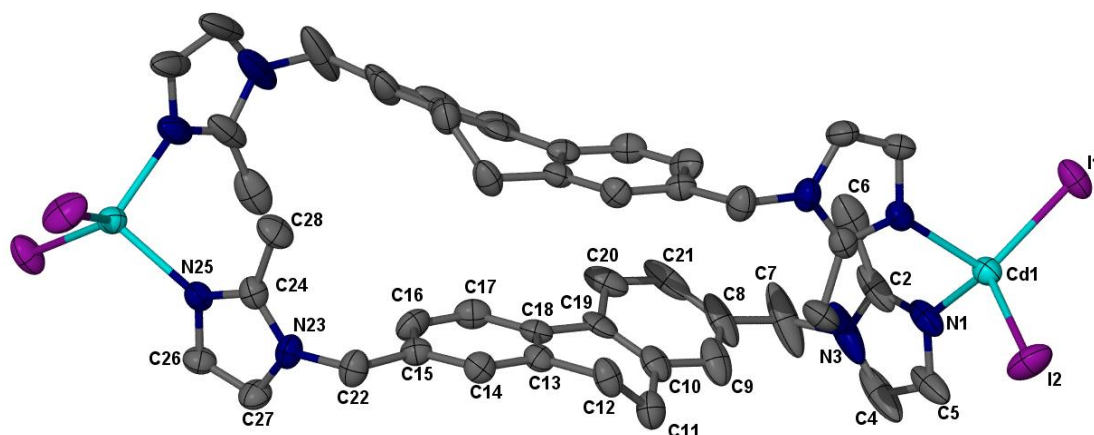
6.2.2.2 $\text{MC24}_{\text{vac}} - [\text{Cd}_2\text{I}_4\text{L}_4\text{2}]$ 

Figure 6.29 Thermal ellipsoid (50% probability) representation of MC24_{vac} . Only atoms of the ASU have been labelled and the hydrogen atoms have been omitted for clarity.

Crystals of MC24_{vac} were prepared by placing a few single crystals of **MC24** under vacuum at room temperature for approximately 5 hours and subsequently collecting the X-ray intensity data. The desolvation process occurs as a single-crystal to single-crystal transformation. The structure of MC24_{vac} is much the same as that of the DCM solvate, maintaining the $C2/c$ symmetry with comparable unit cell parameters. The ASU is composed of a single ligand molecule, in a divergent (S-shaped) conformation, coordinated to CdI_2 (Figure 6.29).

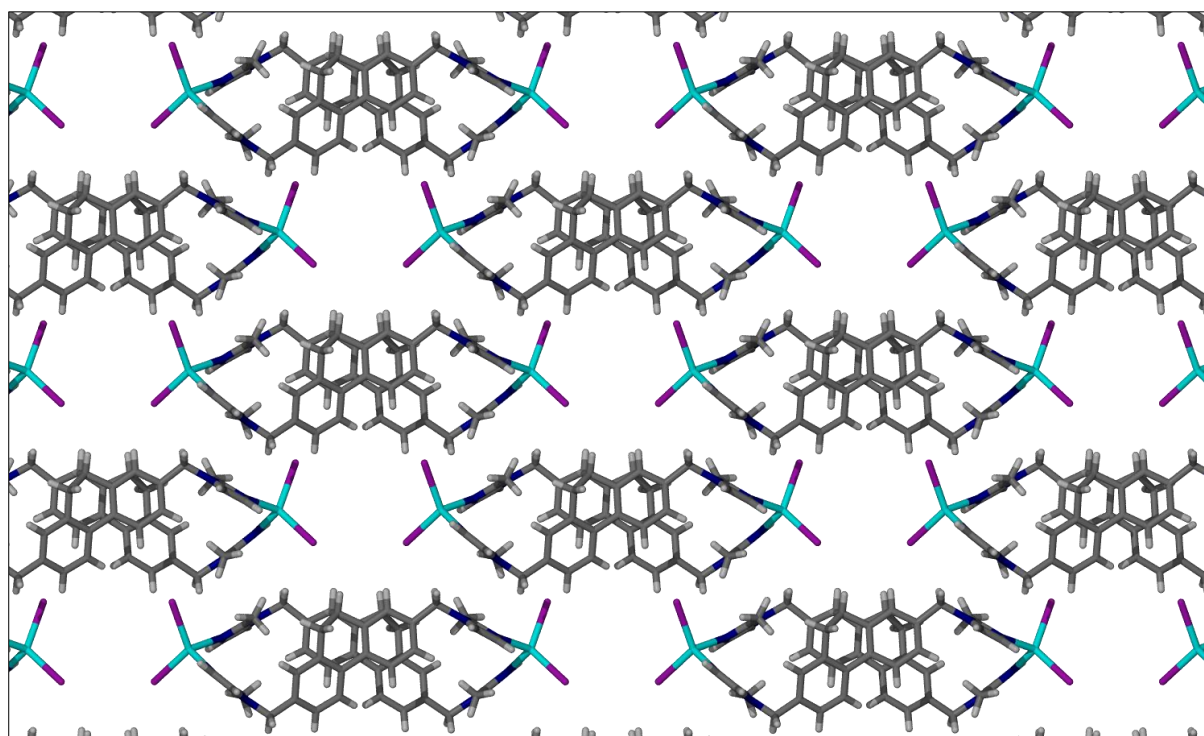


Figure 6.30 Packing arrangement of MC24_{vac} viewed perpendicular to (001).

Removal of guest molecules results in a closer packing arrangement of the metalloccycles in **MC24_{vac}** compared to the parent structure **MC24** (Figure 6.30). Accompanying this slight rearrangement is an increased number of intermolecular interactions between the host molecules. Neighbouring metalloccycles pack such that there are weak C–H...C contacts between the 2-methyl groups of the 2-methylimidazole moieties of one host and the 2-methylimidazole *ipso*-carbon atom (C2 or C24) of a neighbouring metalloccycle (3.546(9) Å). C–H...C contacts also occur between the methylene carbon atoms and neighbouring imidazole moieties (3.53(1) Å). Further stabilisation is facilitated by interaction of iodide counter ions of one metalloccycle with methylene carbon atoms of another (3.882(7) and 4.043(6) Å). These interactions occur between metalloccycles, which are stacked along the *b* axis. Packing of the metalloccycles along [001] is maintained primarily by C–H... π interactions between imidazole carbon atoms and the π -delocalised electrons of the dihydrophenanthrene moieties. Apart from these interactions, the metalloccycles appear to associate in the solid state by means of close packing and this is confirmed by the lack of strong interactions observed in the fingerprint plot (Figure 6.31). Owing to the awkward shape of the metalloccycles they are unable to pack efficiently and small void spaces are therefore present in the structure. However, these spaces are much smaller than those observed in the structure that includes DCM and MeCN (**MC24**).

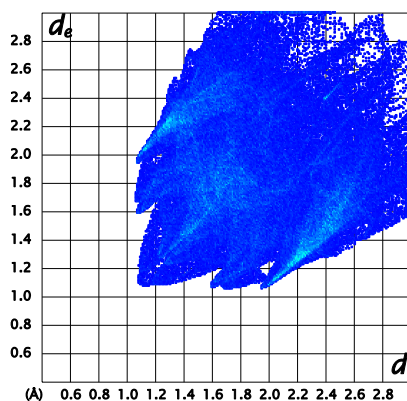


Figure 6.31 Fingerprint plot of the metalloccycle of **MC24_{vac}**.

6.2.2.3 **MC25** – [Cd₂L₄L₂]·C₆H₆

Observing that neither DCM nor MeCN are included within the cavities of the metalloccycles in **MC24**, it was postulated that crystallisation from a different solvent system may template the metalloccycle in the desired manner – i.e. an “open” metalloccycle. Benzene and toluene were selected because of their molecular shapes and volumes, as well as their potential to participate in π ... π interactions with the aromatic moieties of the host metalloccycle.

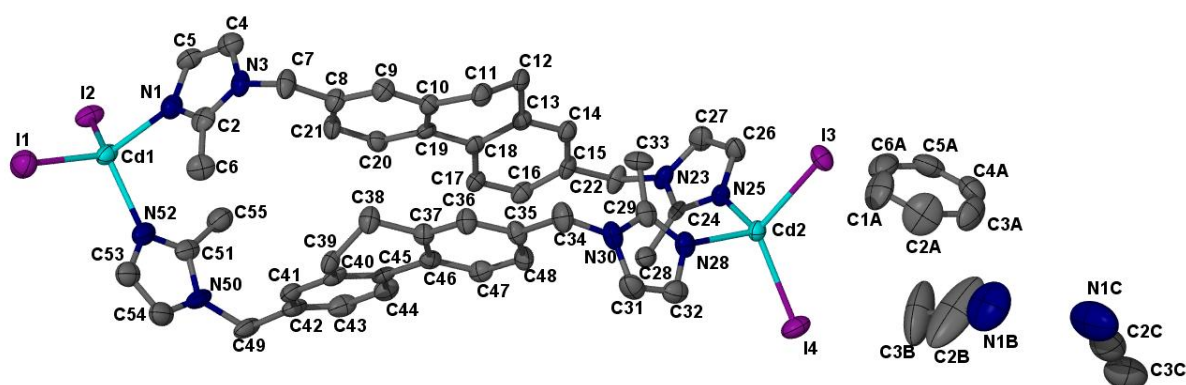


Figure 6.32 Asymmetric unit of **MC25** represented as 50% probability thermal ellipsoids. Hydrogen atoms have been omitted for clarity.

Upon first inspection, the structure of **MC25** bears remarkable resemblance to the structure of **MC24**, but the structure is actually quite different. The complex crystallises in the space group $P2_1/c$ with unit cell parameters only slightly dissimilar to those of **MC24**. The slight decrease in symmetry of the structure compared to **MC24** is presumably due to the arrangement of the included guest molecules. The ASU consists of one entire metallocycle – two ligand molecules (**L4**) ditopically coordinated to two cadmium cations, each coordinated to two iodide counter ions – as well as one molecule of benzene and two molecules of MeCN (Figure 6.32). The packing arrangement of **MC25** is comparable to that observed in **MC24**. Adjacent metallocycles are stabilised through a number of weak intermolecular interactions, the majority of which are C–H \cdots π contacts.

The guest molecules in the structure associate as a six-membered adduct – four MeCN molecules arranged in an offset head-to-tail tetramer – with benzene molecules at either extremity of the adduct (Figure 6.33). The tetramer arrangement is stabilised by C–H \cdots π (3.589 Å) as well as lone-pair \cdots π interactions (3.520 Å) between the two symmetry-independent MeCN guest molecules. The outermost MeCN molecules (labelled **B**) of the adduct are involved in C–H \cdots π interactions with the methyl group of the 2-methylimidazole moieties in the host metallocycle. The fingerprint plot of the metallocycle indicates the absence of any strong intermolecular interactions in the structure (Figure 6.34).

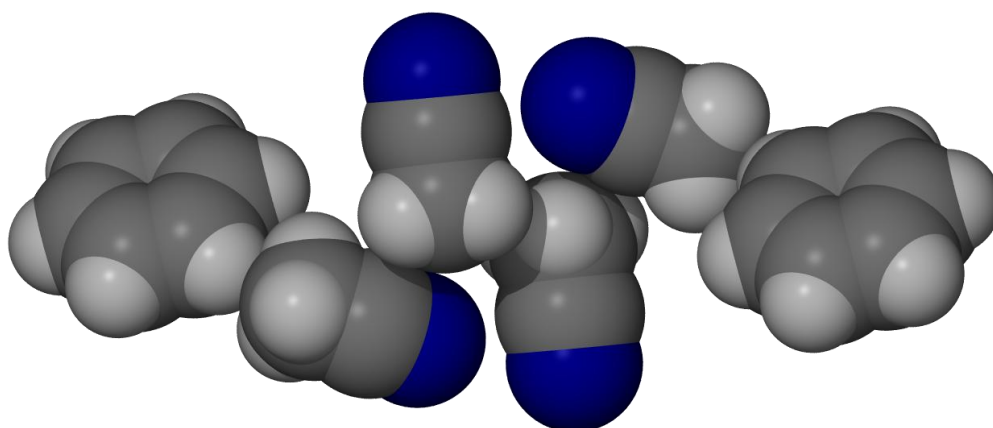


Figure 6.33 Space-filling representation of the six-member adduct of the guest molecules in MC25

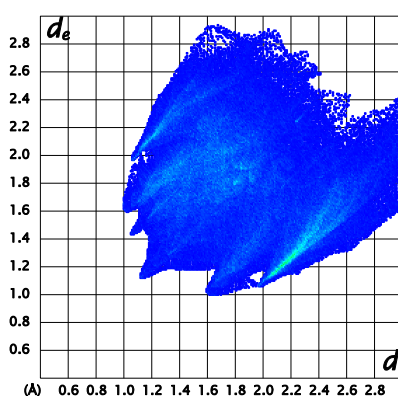


Figure 6.34 Fingerprint plot of the metallocycle in MC25.

6.2.2.4 MC26 – $[\text{Cd}_2\text{I}_4\text{L}_4] \cdot \text{C}_7\text{H}_8$

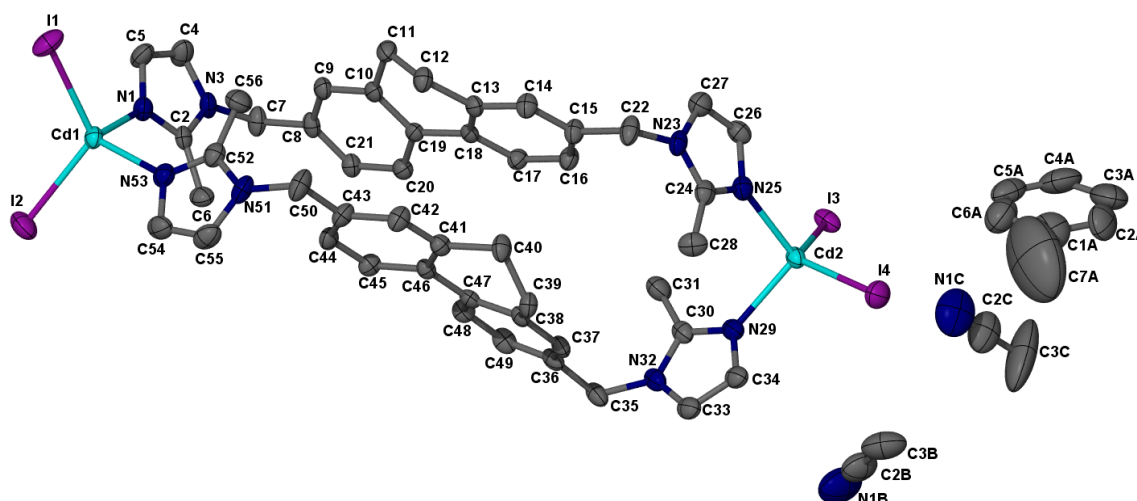


Figure 6.35 Thermal ellipsoid plot (50% probability) of the ASU of MC26. Hydrogen atoms have been omitted for clarity.

MC26 was prepared by reacting L4 with CdI_2 in a solvent system consisting of toluene and MeCN. The ASU comprises an entire metallocycle, one toluene molecule and two MeCN

molecules (Figure 6.35). The crystal structures **MC25** and **MC26** can be classified as isoskeletal and are solvatomorphs of **MC24**. Both **MC25** and **MC26** crystallise in the space group $P2_1/c$ and possess similar unit cell parameters. The ligand molecules in **MC26** are in a divergent (S-shaped) conformation and are twisted to coordinate to the cadmium cations. The rotation angle (Figure 6.36) between the dihydrophenanthrene units is 80.3° , which is slightly smaller than the 83.5° rotation observed for the benzene structure. The anisotropic displacement ellipsoid of the methyl carbon atom of the toluene guest is large and this can be ascribed to the movement of the molecule in the interstitial space, rather than disorder of this atom.

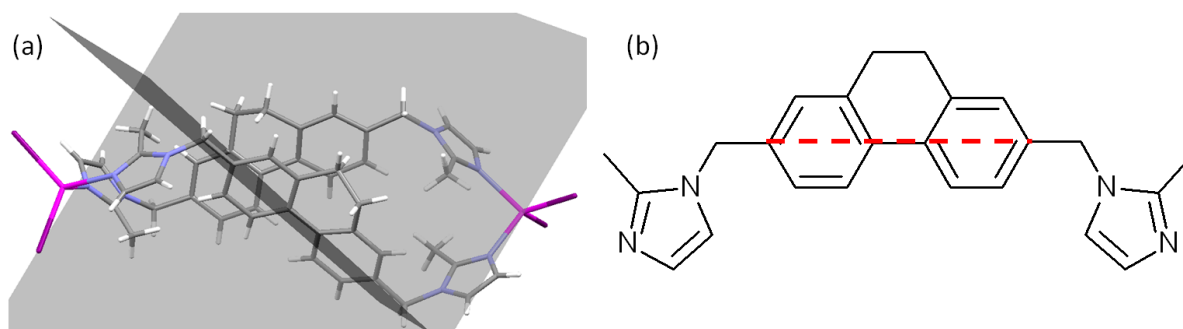


Figure 6.36 Least-squares planes defined by the central carbon atoms of the biphenyl moiety of the 9,10-dihydrophenanthrene moieties of the organic spacers in **MC26**. (a) The angles between planes in the metallocycles, (b) a schematic of the plane through the dihydrophenanthrene moieties.

The structure of **MC26** is similar to that of **MC25** and will therefore not be discussed in great detail. The primary difference in the structure is the inclusion of toluene, rather than benzene, in the interstitial spaces along with MeCN. These guest molecules are arranged in much the same way as the benzene and MeCN molecules in the structure of **MC25**.

A number of C–H \cdots π interactions exist between neighbouring metallocycles, as well as a few between the metallocycles and nearby MeCN guest molecules. The three guest molecules associate with one another to form a six-membered adduct (Figure 6.37) analogous to that observed in the structure of **MC25**. This association is maintained by C–H \cdots π interactions between symmetry-independent MeCN molecules, together with lone-pair \cdots π interactions between MeCN guests aligned in a head-to-head T-shaped contact (3.538 \AA). The fingerprint plot (Figure 6.38) confirms the absence of strong intermolecular interactions in the structure.

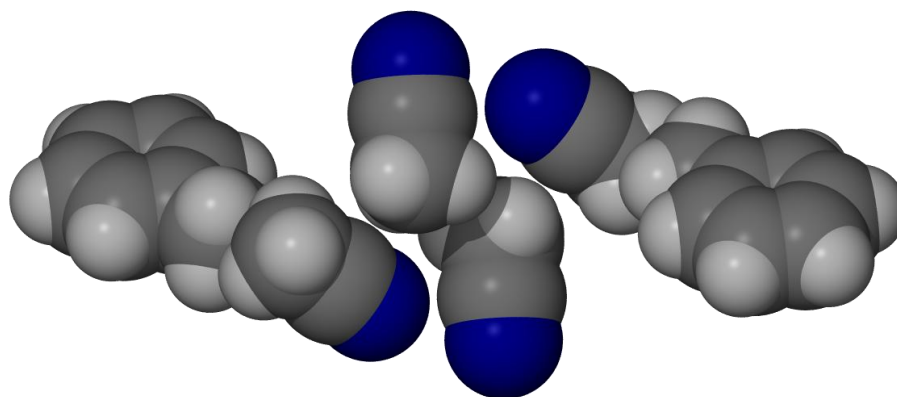


Figure 6.37 Van der Waals representation of the six-membered adduct of guest molecules in MC26

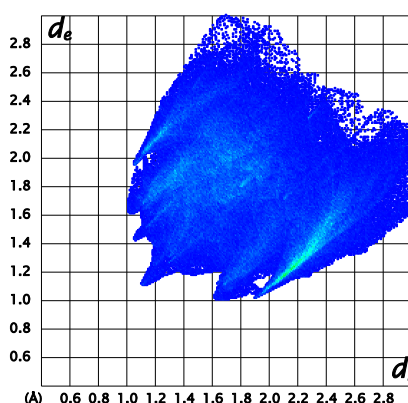


Figure 6.38 Fingerprint plot of MC26

The structures obtained with the 2-methylimidazole-functionalised ligands demonstrate that the formation of discrete metallocyclic complexes is still possible even if the ligand adopts a divergent (S-shaped) conformation rather than the anticipated C-shaped (convergent) conformation. The 2-methyl substituent groups on the imidazole moieties most probably contribute to the collapsed conformation since they increase the steric bulk and/or contribute to the awkward shape of the metallocycle.

Of more interest is the comparison of the structures obtained using the different ligand molecules. If we compare the structures of MC25 and MC26 to those of MC22 and MC23, where the unsubstituted imidazole ligand is used, it is clear that there are significant differences in the conformations of the metallocycles. For the imidazole-functionalised metallocycles the dihydrophenanthrene moieties are arranged in an approximately co-planar manner compared to the parallel arrangement of the corresponding moieties in the 2-imidazole-functionalised metallocycles (Figure 6.39).

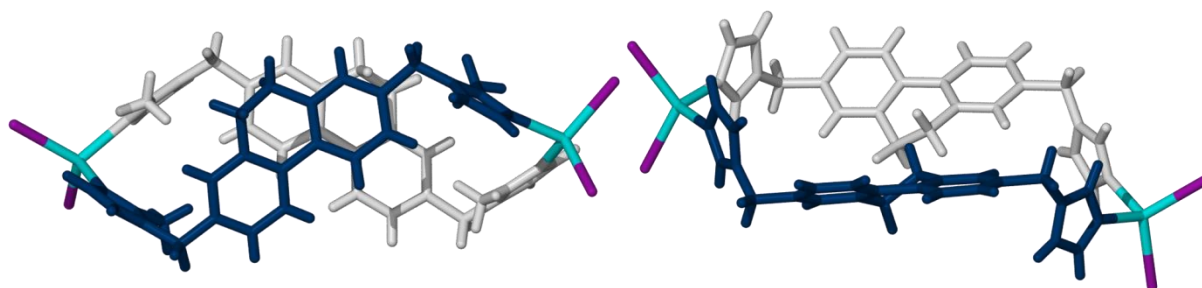
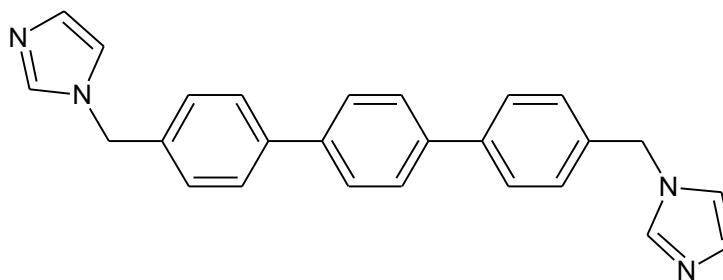


Figure 6.39 Comparison of the different conformations of the metallocycles of **MC25** (left) and **MC22** (right).

6.2.3 STRUCTURES WITH A TERPHENYL SPACER

To further expand the study of imidazole-based metallocycles, a ligand spacer that is longer than the others already investigated was prepared. This terphenyl-derived spacer (Scheme 6.3) is also similar to a biphenyl spacer, which has been used extensively in areas of supramolecular chemistry and crystal engineering.



Scheme 6.3 Ligand **L5**, 1,1'-(terphenyl-2,7-diyl)dimethanediylbis(1*H*-imidazole)

6.2.3.1 MC27 – [Cd₂I₄L₅]₂·Guest

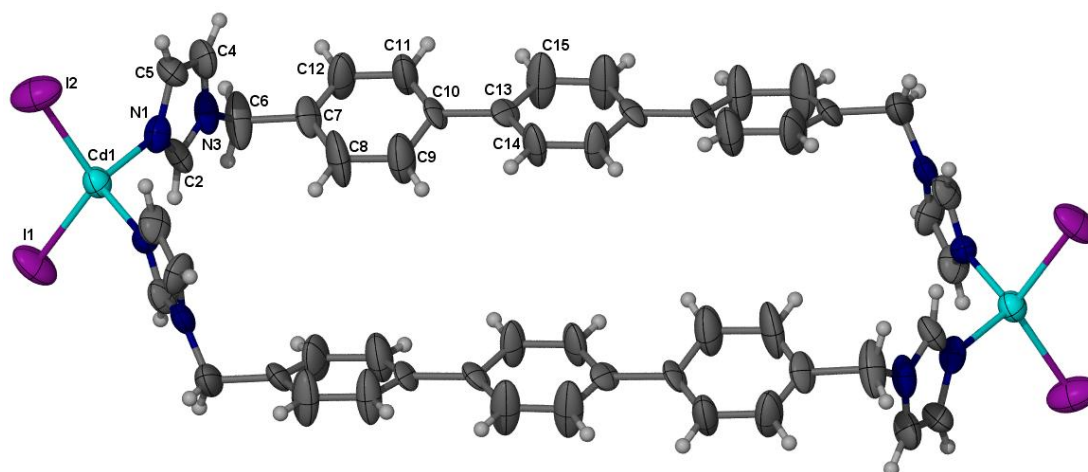


Figure 6.40 Thermal ellipsoid (50% probability) plot of the metallocycle of **MC27**. Only the atoms of the ASU are labelled.

A combination of **L5** (Scheme 6.3) and cadmium iodide in a mixture of DCM and MeCN yielded the zero-dimensional metallocycle of **MC27**. The complex crystallises in the monoclinic space group *C2/m*, with half a ligand molecule coordinated to CdI₂ in the ASU

(Figure 6.40), and with the cadmium cation adopting a tetrahedral coordination geometry. There is some unresolved electron density within the confines of the metalloccycle, but the identity of this guest could not be determined since its site occupancy is too low to model adequately. The ligand molecule of the metalloccycle assumes an approximate C-shaped conformation and the metalloccycle adopts a chair-shaped conformation much like that observed in the structures of **MC22** and **MC23**. It is interesting that the aryl moieties of each of the **L5** ligand molecules are orientated approximately planar relative to one another. A slight rotation of the ring orientations compensates somewhat for steric hinderance from hydrogen atoms of the neighbouring ring in the same ligand molecule.

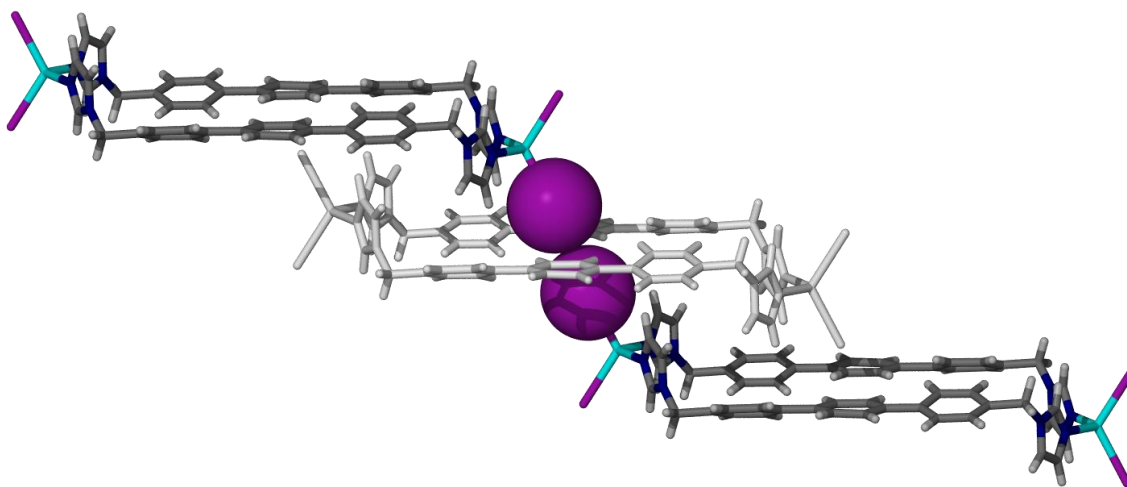


Figure 6.41 I...I interaction between adjacent metalloccycles. Two iodide ions involved in the interaction are depicted in space-filling representation to indicate the proximity of the ions. The metalloccycles are represented as capped-sticks. The complex represented in white demonstrates how the interior space of the metalloccycle is divided by the halogen bond.

Only a few intermolecular interactions occur between the metalloccycles and it appears that their solid-state arrangement is primarily due to close packing. The only noteworthy intermolecular interaction is the weak halogen bonding (I...I) between iodide counter ions of nearby metalloccycles (3.906(4) Å, Figure 6.41).

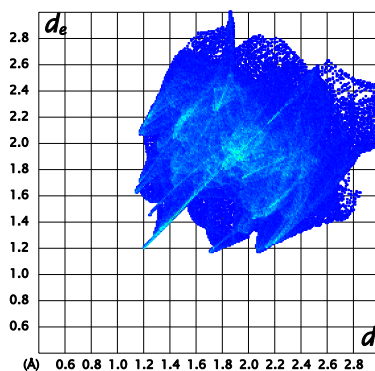


Figure 6.42 Fingerprint plot of the metalloccycle in **MC27**

The fingerprint plot (Figure 6.42) generated from the Hirshfeld surface of the metalloporphyrin of **MC27** confirms the lack of strong interactions in the structure (the majority of the plot is due to van der Waals interactions). The metalloporphyrins associate by means of weak $\pi\cdots\pi$ interactions between the imidazole moieties of adjacent metalloporphyrins, which are aligned in an anti-parallel manner with respect to each other (Figure 6.43). These associations direct the organisation of metalloporphyrins into layers. These layers then stack on top of one another in an offset manner such that one of the iodide counter ions of the metalloporphyrin bisects the metalloporphyrin in an adjacent layer. The iodide ions (I1) not involved in halogen bonding are directed towards the space between metalloporphyrins in adjacent layers. This arrangement facilitates formation of solvent-filled cavities (or pockets), which traverse through the interior of two metalloporphyrins. The pockets are “capped” (above and below in Figure 6.44) by the side-by-side arrangement of two terphenyl moieties of adjacent metalloporphyrins. Iodide counter ions of neighbouring metalloporphyrins are also involved in confining the cavity.

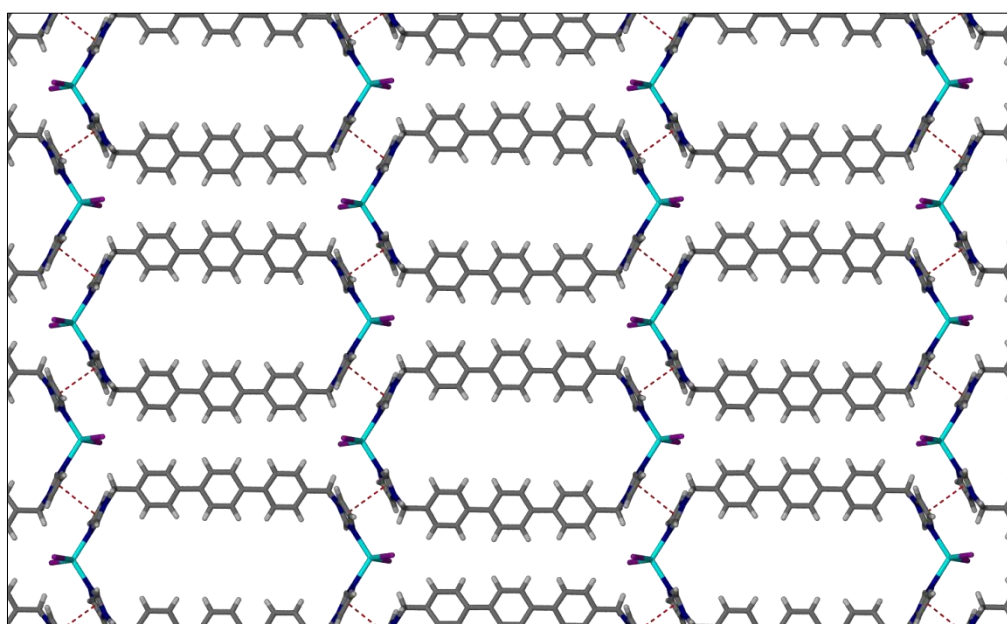


Figure 6.43 Single layer of metalloporphyrins of **MC27** maintained by $\pi\cdots\pi$ interactions between the imidazole moieties (indicated by the fragmented red lines)

The unresolved electron density in the structure resides within the confines of the cavities (Figure 6.44). Efforts to model this residual electron density as both MeCN and DCM yielded an unsatisfactory model owing to very low occupancy of these guests and/or disorder of these guests. A number of methods (e.g. TGA, PXRD, NMR, IR, and TGA-MS) are available, which may be used, in conjunction with SCD data, to characterise the guest molecules. However, owing to a number of complications, including small sample size, phase impurity, the use of a binary solvent system and deterioration of the sample once removed from the

mother liquor, these techniques could not be effectively implemented. A SQUEEZE electron count reveals that there are 79 residual electrons accommodated within the solvent-accessible voids, which correlates to at least one molecule each of DCM and MeCN (64 electrons), although it is assumed that a second molecule of DCM is also included in the cavities. The structure described in the section below (**MC27**_{CCl₄}) suggests that these assumptions are correct – i.e. at least one molecule each of DCM and MeCN is included.

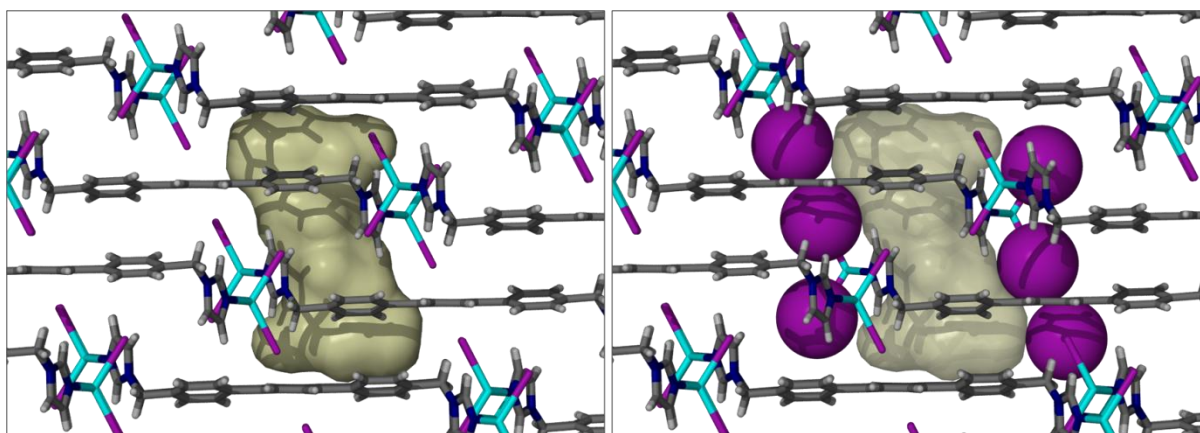


Figure 6.44 Guest-accessible pocket shown as a light yellow surface traversing two metalloccycles of **MC27**. The cavity is “capped” by the side-by-side association of two metalloccycles. Iodide ions (shown in space-filling representation on the right) of neighbouring metalloccycles are also involved in confining the space. The pockets are mapped using a probe with a radius of 1.3 Å.

6.2.3.2 **MC27**_{CCl₄} – [Cd₂I₄L₅]₂·MeCN·DCM

A few single crystals obtained from the DCM/MeCN crystallisation – i.e. **MC27** – were selected and immersed in a small amount of CCl₄ in a capped vial. After approximately one month a suitable crystal was selected for X-ray intensity data collection. The data obtained suggests that the crystals undergo a single-crystal to single-crystal phase transformation with the space group of the crystal converting from monoclinic *C2/m* to triclinic *P* $\bar{1}$. The ASU of **MC27**_{CCl₄} consists of one entire ligand molecule coordinated to CdI₂, one molecule of MeCN disordered over two positions of equal occupancy, and a DCM molecule, which is only 20% occupied, can also be modelled (Figure 6.45). We assume that the lowering of symmetry from a monoclinic to a triclinic crystal system is brought about by minor changes in the conformation of the metalloccycle, particularly the rotation of the phenyl moieties in the terphenyl spacer.

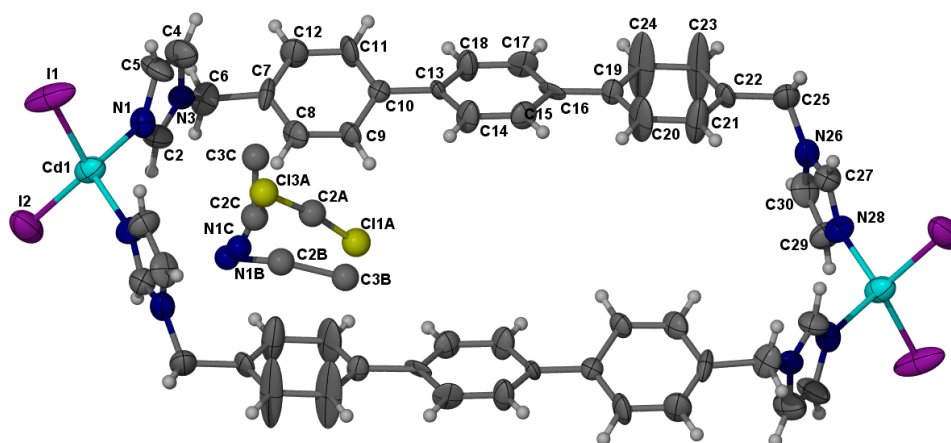


Figure 6.45 Thermal ellipsoid plot (50% probability) of **MC27**_{CCl₄}. The atoms of the ASU are labelled. The disordered MeCN molecules are labelled as **B** and **C**.

$\pi \cdots \pi$ Interactions are responsible for maintaining the metalloccycles in layers, as in **MC27**. However, because there is an entire ligand molecule present in the ASU, in this instance there are two slightly dissimilar interactions. The interactions indicated as red fragmented lines in Figure 6.46 are slightly shorter (3.796 Å) than those indicated in green (3.864 Å). The primary differences between the structures of **MC27** and **MC27**_{CCl₄} are the orientations of the phenylene rings of the ligand moiety and the size of the pockets, which accommodate the guest molecules. The phenylene rings of the metalloccycle of **MC27**_{CCl₄} are rotated such that one distal ring (C19-C24) as well as the central ring are approximately planar relative to each other, while the third ring is rotated slightly out of this plane (26.2°). The cause of these changes is not known but it is noted that the atoms of the distal ring (C19-C24) have large thermal ellipsoids, which indicate some motion of this ring. It is possible that this ring undergoes dynamic tilting as guest molecules move through the system. If this is the case, it is interesting that only one of these phenylene rings is involved and not both phenylene moieties that surround the pockets.

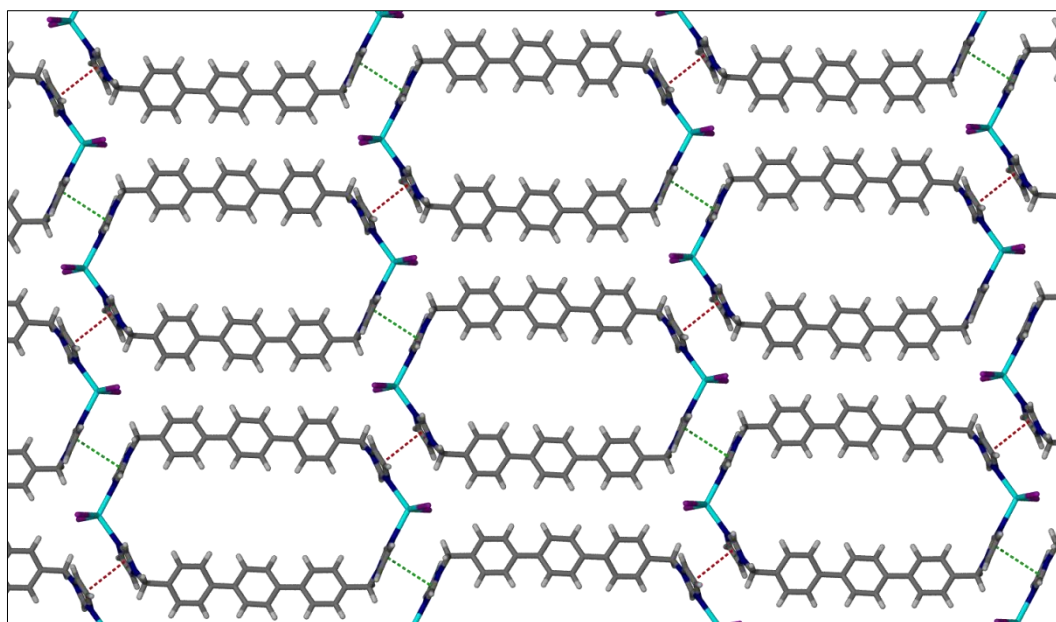


Figure 6.46 Single layer of metallocycles of **MC27**_{CCl₄} maintained by $\pi\cdots\pi$ interactions between imidazole moieties of adjacent metallocycles. The interactions are indicated by the green and red fragmented lines. The interactions shown in red are slightly shorter than those in green. Guest molecules have been omitted for clarity.

The suspected movement of guest molecules out of the pockets could account for the decrease in the volume observed for the pocket-shaped voids (270 \AA^3 in **MC27** to 237 \AA^3 in **MC27**_{CCl₄}). SQUEEZE analysis confirms the release of some of the guest molecules since the residual electron count decreases from 79 in **MC27** to 55 in the pockets of **MC27**_{CCl₄} (Figure 6.47). In this instance, it is possible to partially model the guests included within the metallocycles. From this model, it appears that there is a MeCN molecule, disordered over two positions of equal occupancy. A single DCM molecule can also be modelled within the cavity, though it has a very low occupancy (approximately 20%). The SQUEEZE electron count correlates well with these findings.

At first it was thought that the structure had undergone a solvent-exchange and therefore contained CCl₄ molecules (CCl₄ = 74 electrons) within the pockets. It was later realised that the crystals had simply experienced partial desolvation by immersion of the fully solvated crystals in a CCl₄ solution. If CCl₄ had indeed been included in the voids it is suspected that the void volume would have increased with the inclusion of the larger CCl₄ molecule.

Because only a few crystals were treated in this manner, there was too little sample to perform TG analysis to verify the identity of the guests. From the SCD and squeeze analysis it is reasonable to assume that the structure of **MC27** probably contains at least one MeCN molecule and possibly a partially- or fully-occupied DCM molecule positioned on the mirror plane through the metallocycles.

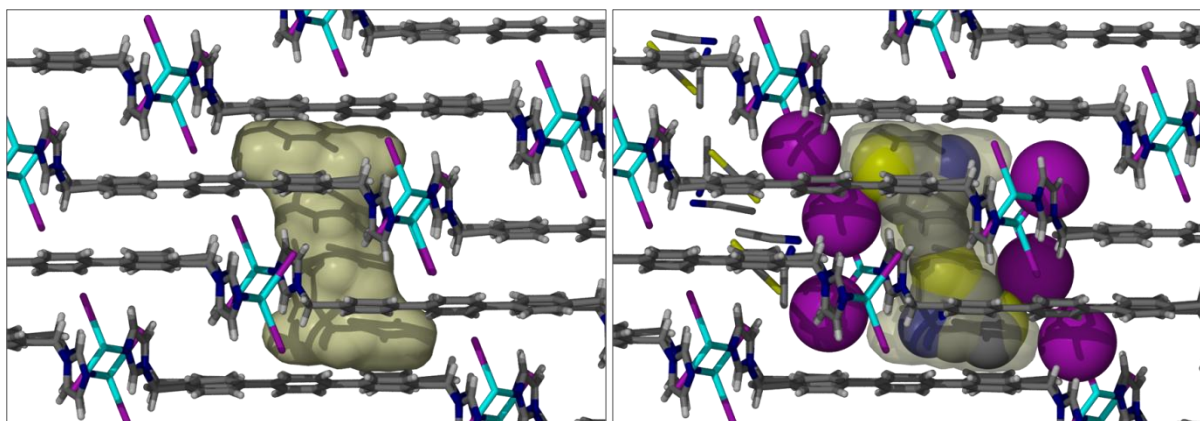


Figure 6.47 Guest-accessible pocket traversing two metalloCycles (left) of **MC27_{CCl4}**. The cavity is “capped” by the side-by-side association of two metalloCycles. Iodide ions (shown in space-filling representation of neighbouring metalloCycles) are also involved in confining the space (right). Surfaces are mapped using a probe of radius 1.3 Å. The DCM and MeCN guests are depicted in the figure on the right in space-filling representation, showing how they occupy the space of the mapped surface.

As observed in the previous structure of **MC27**, there are only weak intermolecular interactions between the host molecules. I···I interactions are still responsible for division of the apertures in neighbouring metalloCycles into two parts, and the distance between the ions is only slightly longer than in **MC27** (3.967(3) Å). Other host-host interactions are weak C–H··· π interactions between the methylene carbon atoms of one metalloCycle and the central phenyl moiety (4.330 Å) in another. C–H··· π interactions also occur between an imidazole moiety of one metalloCycle and a phenylene ring located in an adjacent layer (3.972 Å). Offset π ··· π interactions between the distally located phenylene moieties of metalloCycles (3.986 Å) of different layers are also observed. The fingerprint plot (Figure 6.48) generated from the Hirshfeld surface of the metalloCycle indicates that there are no strong interactions in the structure, but rather that packing is governed by weak van der Waals contacts.

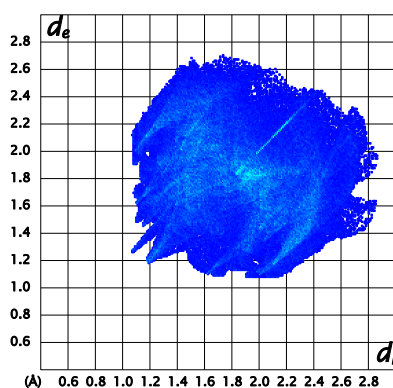


Figure 6.48 Fingerprint plot of metalloCycle of **MC27_{CCl4}**

6.2.3.3 MC27_{vac} – [Cd₂I₄L₅]

An evacuated structure was obtained by heating a few single crystals of **MC27** to 30 °C under vacuum for approximately 5 hours. A suitable crystal was immediately selected for analysis by SCD. Although the crystal was highly fractured, the data were adequate for structure solution when treated as a non-merohedral twin or split crystal. The poor quality of the data should be taken into account when analysing the structural aspects of **MC27_{vac}** since the accuracy of the atomic coordinates will be poor. However, it is possible to discern the dramatic adjustments that the atoms undergo upon complete removal of the guest molecules. This rearrangement can account for the increase in mosaicity of the crystals as the guest molecules are removed from the discrete pockets described in the previous two structures, **MC27** and **MC27_{CCl4}**.

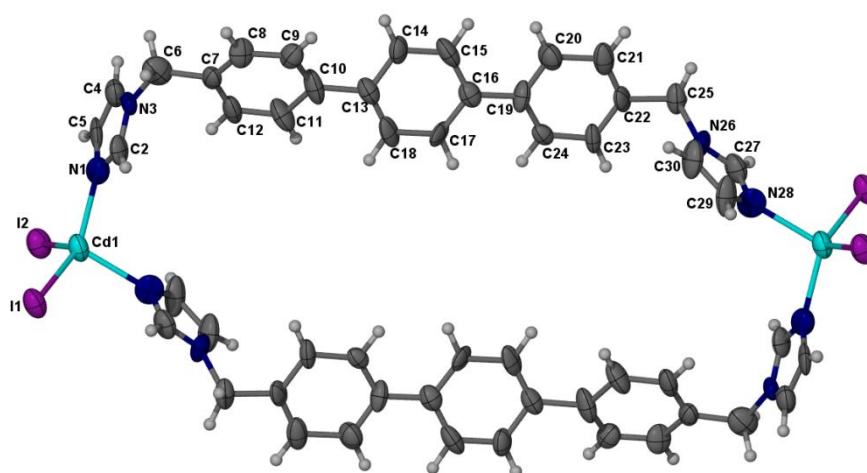


Figure 6.49 Thermal ellipsoid plot of the evacuated structure of **MC27_{vac}** with the atoms of the ASU labelled.

The complex crystallises in the triclinic space group $P\bar{1}$, with an ASU that consists of an entire ligand molecule coordinated to CdI₂ (Figure 6.49). The metallocycle is similar to that observed in the structure of **MC27_{CCl4}**. The ligand molecule still coordinates to the cadmium cation in a C-shaped conformation. However, the ligand is highly deformed. It is plausible that this conformational distortion imposes tremendous strain on the crystals, causing them to fracture.

The orientation of the phenylene moieties in the *p*-terphenyl spacer is similar to that observed in the metallocycle of **MC27_{CCl4}** (Figure 6.51). However, the terphenyl spacer, in this instance, appears to bend, compensating somewhat for the structural rearrangement of the metallocycle. The evacuated structure exemplifies a similar situation to that observed in the CCl₄ structure, with little change in the dihedral angle between two of the phenylene rings (6.5°). However, there is a major distortion of the bond (C10-C13) between the central ring

(C13-C18) and the neighbouring aryl ring (C7-C12). These rings are rotated by an angle of 26.3° relative to each other, which is nearly identical to that observed in the structure of **MC27**_{CCl₄}. The movement of one imidazole moiety (buckling), however, causes the bond (C10-C13) between the phenyl rings to bend. The large conformational changes in the metallocycles are observed in the structure overlay of the three structures of **MC27** shown in Figure 6.50. The structures of **MC27** and **MC27**_{CCl₄} show only slight differences in conformation, whereas **MC27**_{vac} is dramatically different.

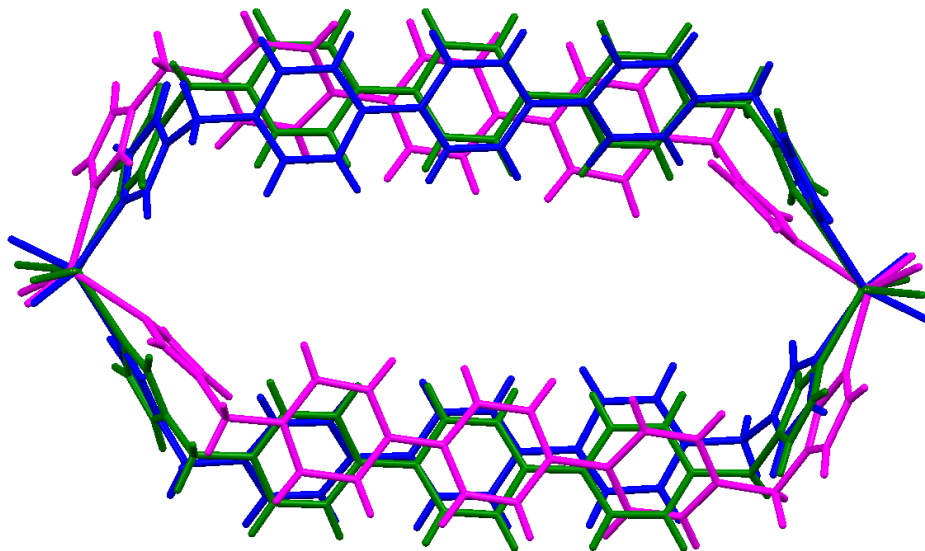


Figure 6.50 Structure overlay of the metallocycles of **MC27** (blue), **MC27**_{CCl₄} (green) and **MC27**_{vac} (pink).

The coordination geometry about the cadmium cation of **MC27**_{vac} also undergoes a dramatic change as the crystal converts from the monoclinic crystal system (**MC27**) to a triclinic one (**MC27**_{vac}). Specifically, the N–Cd–N angle changes from $115.7(6)^\circ$ in the DCM solvate to $107.3(7)^\circ$ in the evacuated structure ($116.5(4)^\circ$ in CCl₄). The angle of the methylene bridge (C6 and C25) also changes during the rearrangement. In both the DCM and CCl₄ solvates this angle is approximately $111(1)^\circ$, whereas in the evacuated structure one bridge becomes more acute $109(2)^\circ$ while the other expands to $115(2)^\circ$. These observations demonstrate the relative flexibility of these metallocycles, even in the solid state. Since the structural data are poor in quality, residual electron density is still present. However, according to SQUEEZE, several voids with volumes of only 7 \AA^3 are present, each apparently containing a single electron in its void. From this it can be assumed that the crystal is fully evacuated. This also appears to indicate that the metallocycle is indeed templated by the included solvent molecules. However, the structure of the metallocycle is too “flexible” to withstand the removal of the guest template molecules. Because of the packing arrangement of these molecules in the solid state it may be difficult to obtain a solvent template that

renders the structure more stable, but which can also be successfully removed without disrupting the integrity of the crystals.

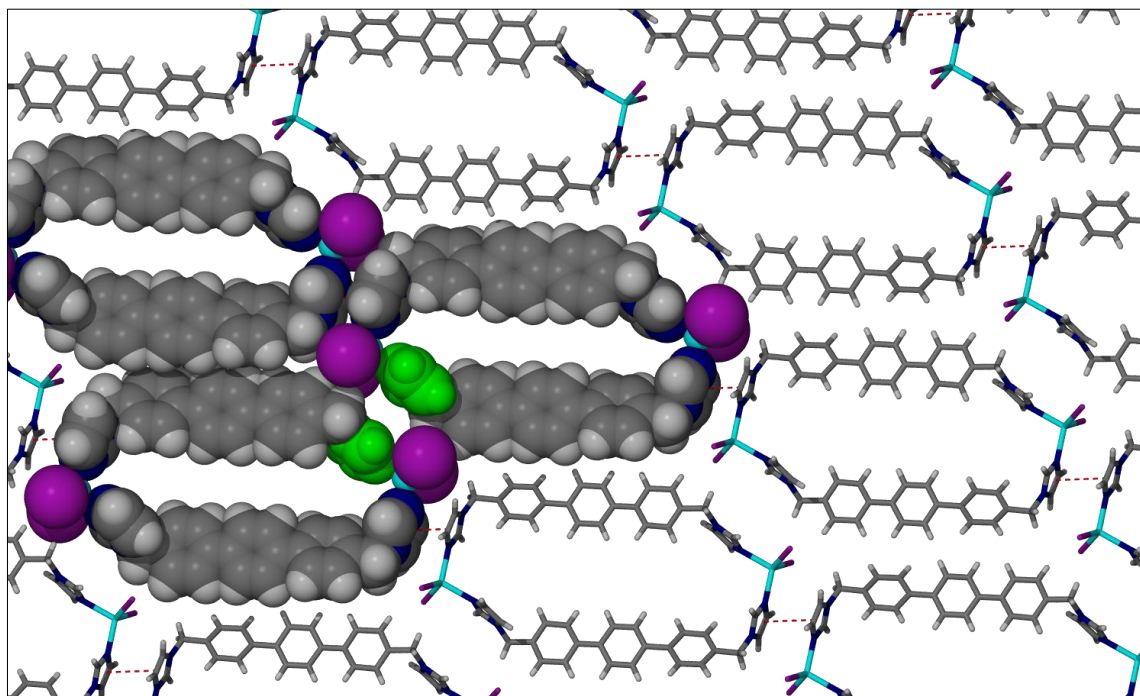


Figure 6.51 A single layer of metalloccycles of MC27_{vac} . The $\pi\cdots\pi$ interactions between imidazole moieties are depicted by the red fragmented lines. The imidazole moieties that buckle into the metalloccycles are depicted in green space-filling representation.

A number of $\text{C-H}\cdots\pi$ contacts between neighbouring metalloccycles appear to stabilise the structure. The distortion of the metalloccycles results in $\pi\cdots\pi$ interactions (3.794 \AA) between only two of the imidazole moieties (N1-C5) (Figure 6.51). Also owing to the changes in conformation of the metalloccycles, the I \cdots I interactions between neighbouring layers of metalloccycles, as highlighted in the previous structures (MC27 and $\text{MC27}_{\text{CCl4}}$), are no longer observed in the structure MC27_{vac} . The fingerprint plot of the metalloccycle of MC27_{vac} confirms the absence of strong intermolecular interactions in the crystal structure (Figure 6.52).

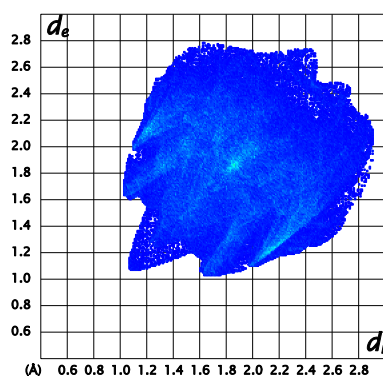


Figure 6.52 Fingerprint plot of MC27_{vac}

6.2.3.4 MC28 – [Cd₂I₄L₅]₂·C₆H₆

The crystals of **L5** with CdI₂ grown from benzene and MeCN are only slightly different from those obtained from the DCM-MeCN solution, **MC27**. The complex also crystallises in the space group *C2/m*, but with slightly dissimilar unit cell parameters such that the two structures cannot be described as isostructural or even isoskeletal. The metallocycles of **MC28** appear similar to those in **MC27**, with a quarter of the cycle forming part of the ASU. In this instance an entire molecule of benzene is also included in the ASU (Figure 6.53). The ligand molecules assume an approximately C-shaped conformation and the phenyl rings of the terphenyl moieties are twisted slightly out of the metallocycle plane, orientated 20.8° relative to each other. The metallocycles assume a chair-shaped conformation as in the structure of **MC27**.

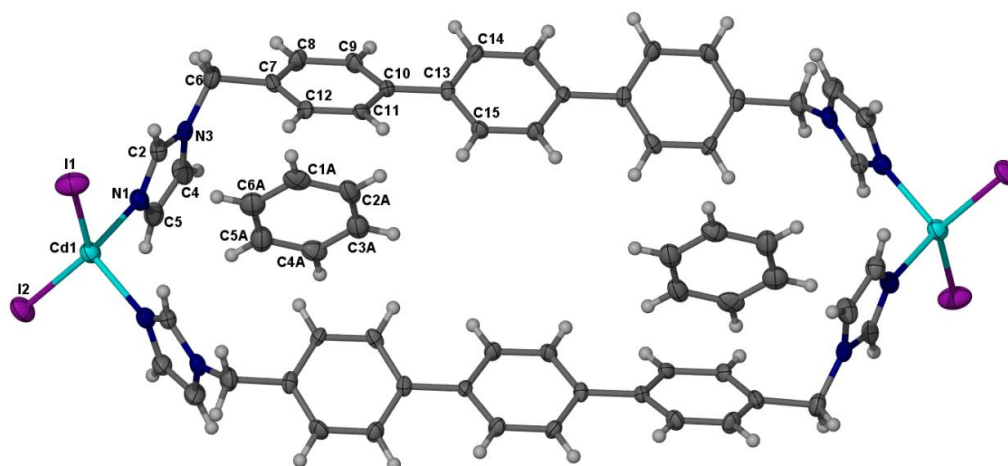


Figure 6.53 Thermal ellipsoid (50% probability) plot of **MC28**. Only the atoms of the ASU have been labelled.

The included benzene molecules reside within the confines of the metallocycles and are positioned perpendicular to the terphenyl rings of the host. These molecules are located on a special position (mirror plane) such that the atoms are all half occupied. The benzene molecules are positioned such that they interact with the distally located phenylene rings of the host by way of weak C–H⋯π interactions.

The packing arrangement of the metallocycles is analogous to that observed in **MC27**, with small differences in the placement of the metallocycles relative to one another. Unlike the previous three structures (**MC27**, **MC27**_{CdI₄} and **MC27**_{vac}), layers of the metallocycles are not maintained by π⋯π interactions between adjacent imidazole moieties, but the metallocycles are rather shifted such that C–H⋯π interactions between the methylene carbon atom (C6) and the adjacent imidazole moieties are responsible for stabilising the layers (3.696 Å). This shift is due to the benzene guest molecules that separate the terphenyl

moieties of metalloccycles arranged side-by-side, since the benzene molecules protrude out of the metalloccycles and into adjacent layers. The distance between side-by-side metalloccycles is thus comparable to the distance between terphenyl moieties of individual complexes (Figure 6.54). The alteration in the layer stabilisation brings about a slightly different offset in the stacking of the layers compared to that observed in **MC27** such that the terphenyl moieties of neighbouring layers are aligned though they are too distant for $\pi\cdots\pi$ interactions.

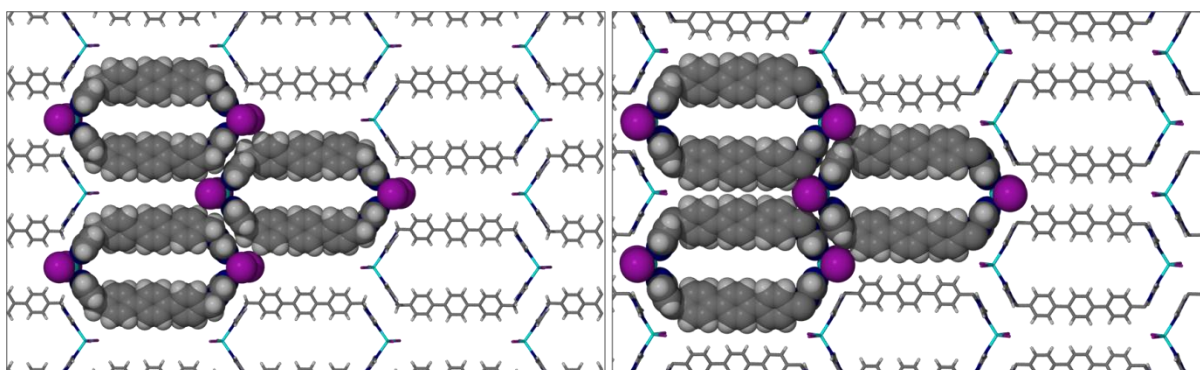


Figure 6.54 Single layer of metalloccycles in **MC28** maintained C–H $\cdots\pi$ interactions between adjacent metalloccycles (left). A few of the metalloccycles are represented as space-filling models to demonstrate the proximity of the metalloccycles. On the right is a similar representation of the DCM-included structure **MC27** for comparison.

The two-dimensional layers are stabilised by a number of weak interactions between the metalloccycles. The methylene linkages (C6) are sufficiently close for C–H $\cdots\pi$ interactions with the central phenylene ring of the terphenyl moiety (3.578 Å) of neighbouring layers. C–H $\cdots\pi$ interactions also occur between carbon atoms of the imidazole groups and the π -electrons of the distal phenylene rings (3.588 Å). I \cdots I intermolecular contacts (4.091(2) Å) are more distant than observed in the structures of **MC27** and **MC27**_{CCl4}. It is assumed that the inclusion of the larger benzene molecules in the cavities results in this slight separation of the iodide ions. Instead there are C–H \cdots I interactions between phenyl ring carbon atoms and an iodide counter ion of metalloccycles in a separate layer (3.771(7) Å).

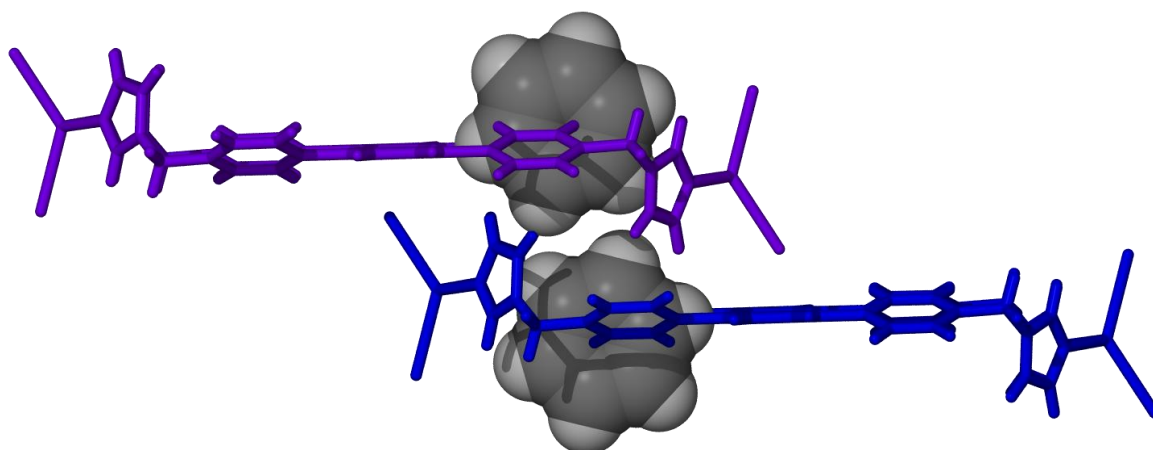


Figure 6.55 Two benzene molecules are included in the pockets formed by two metalloporphyrins of **MC28** in adjacent layers. The guest molecules are favourably positioned for C–H... π interactions with the host.

The solvent-filled pockets are formed by two metalloporphyrins that are partially eclipsed (Figure 6.55); these two metalloporphyrins accommodate two benzene molecules in each of the pockets. These pockets protrude slightly into the space between two metalloporphyrins in the adjacent layers as shown in Figure 6.56. Thus, the inclusion of benzene in the metalloporphyrins brings about a shift in the layer arrangement of the host in order to facilitate guest inclusion. The volume of the guest-filled cavities is expected to be larger than in the structure of **MC27** and this is indeed the case. The solvent-accessible void volume calculated using SQUEEZE is 292 \AA^3 , compared to 270 \AA^3 in **MC27**.

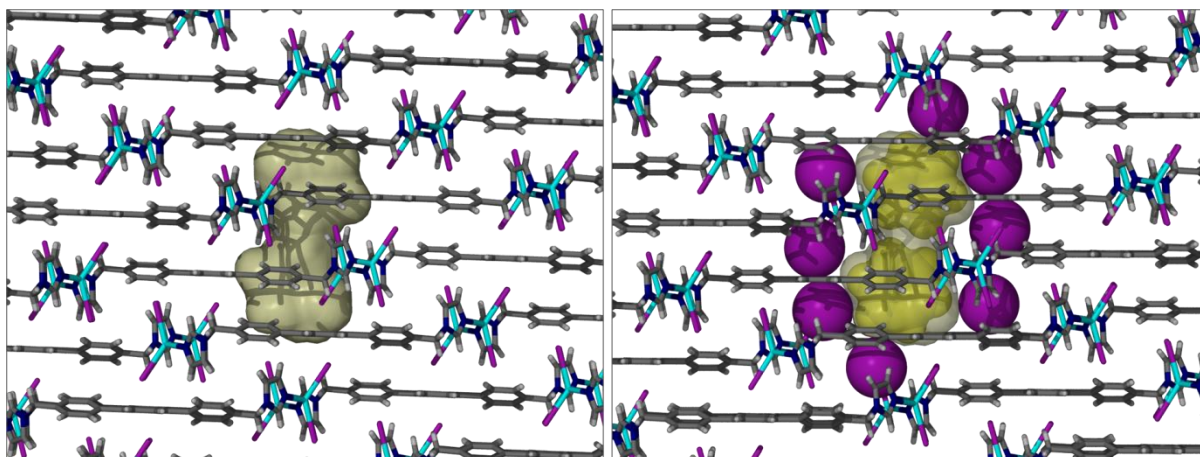


Figure 6.56 Packing arrangement of **MC28** showing the guest-accessible pocket, which traverses two metalloporphyrins and protrudes slightly into the space between two metalloporphyrins in adjacent layers (left). The cavity is confined at the top and bottom by the side-by-side association of two metalloporphyrins. Iodide ions of neighbouring metalloporphyrins are also involved in confining the space (right). Surfaces are mapped using a probe of radius 1.5 \AA . The benzene guests are depicted in the figure on the right in space-filling representation to show how they fill the cavities.

The included benzene molecules form weak C–H... π contacts with the nearby distally located phenylene ring (3.583 \AA) and these interactions presumably render the compound thermally more stable than the structures containing DCM – **MC27** and **MC27**_{CCl₄} – in which

no host-guest interactions occur. The fingerprint plot confirms the lack of strong intermolecular interactions in the crystal structure (Figure 6.57).

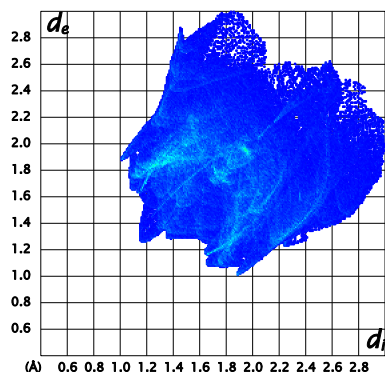


Figure 6.57 Fingerprint plot of MC28

6.2.3.5 MC29 – $[\text{Cd}_2\text{I}_4\text{L}_5_2]\cdot\text{C}_7\text{H}_8$

Crystals of **MC29** were obtained by the reaction of **L5** with cadmium iodide in a mixture of toluene and MeCN. The complex crystallises in the monoclinic space group $C2/m$ with unit cell parameters corresponding to those of **MC28**. The ASU consists of a half-occupied cadmium cation, which is coordinated to a quarter ligand molecule (**L5**) and two iodide counter ions (Figure 6.58). A single molecule of toluene is situated on a mirror plane within the metallocycle such that its atoms are only half occupied.

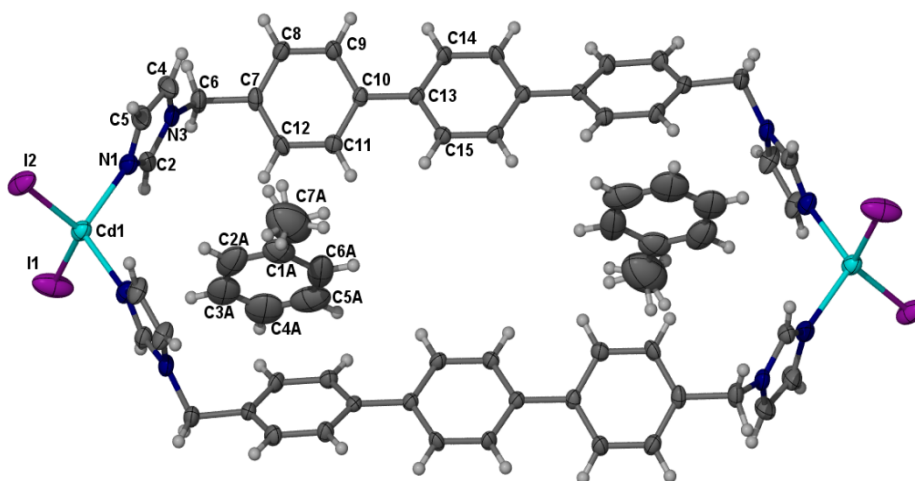


Figure 6.58 Thermal ellipsoid (50% probability) plot of **MC29**. The atoms of the ASU are labelled. The hydrogen atoms of the methyl groups of the toluene molecules are disordered over two positions owing to the location of the molecule on a mirror plane.

The packing arrangement of the metallocycles is analogous to that observed in **MC28** and will therefore not be discussed in detail. The metallocycles also assume a chair-shaped conformation and are organised in a step-like manner along $[100]$. As in the previous structure of **MC28**, the imidazole moieties are shifted away from each other such that they

are too distant for $\pi\cdots\pi$ interactions, and adjacent metalloporphyrins are instead involved in C–H $\cdots\pi$ interactions (3.741 Å) between the methylene linkages (C6) and the imidazole rings (Figure 6.59). These interactions organise the metalloporphyrins into two-dimensional layers. Metalloporphyrins in adjacent layers communicate through C–H $\cdots\pi$ interactions between imidazole carbon atoms and the π -electrons of the distally-located phenylene ring (3.777 Å). C–H \cdots I interactions occur between the distally-located phenyl carbon atoms (C9) and the iodide counter ions (I1) of a nearby metalloporphyrin (3.882(5) Å). The toluene guest molecules are positioned within the metalloporphyrins and are orientated perpendicularly to the terphenyl moieties. This orientation is favourable for C–H $\cdots\pi$ interactions with the distally-situated phenylene rings (3.646 Å) of the host. The I \cdots I distances between anions of nearby metalloporphyrins are slightly more distant (4.162(2) Å) than in the structure of **MC28** (4.091(2) Å) and cannot be considered to have a substantial effect on the packing arrangement. It is believed that the inclusion of the toluene molecules is responsible for this shift in the I \cdots I interaction. The methyl groups of the toluene molecules are located at a distance of 3.60(5) Å from one another such that toluene molecules are aligned in a head-to-head manner within the cavities of the metalloporphyrins (Figure 6.60).

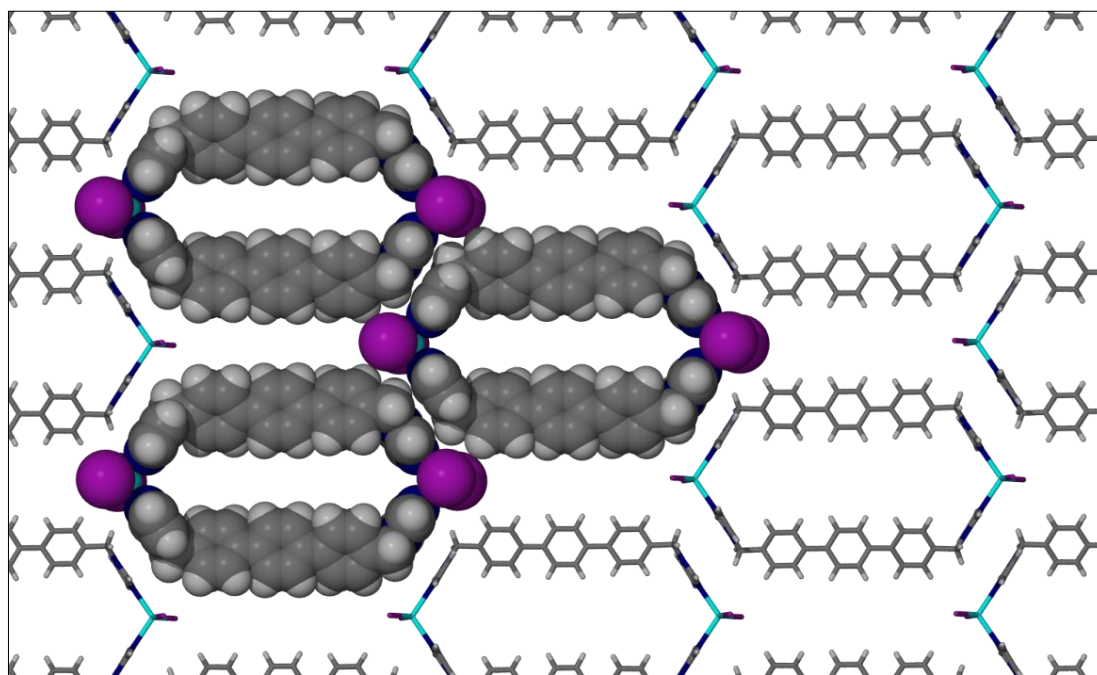


Figure 6.59 Single layer of metalloporphyrins of **MC29**.

SQUEEZE electron density analysis confirms that there are indeed solvent-accessible voids in the crystal structure (occupied by the toluene guest) and these voids have an approximate volume of 335 Å³, which is substantially larger than those observed in the structures of **MC27** (270 Å³) and **MC28** (292 Å³). The residual electron density count in

these voids accounts for two toluene molecule per void (per unit cell), which correlates well with the crystal structure analysis.

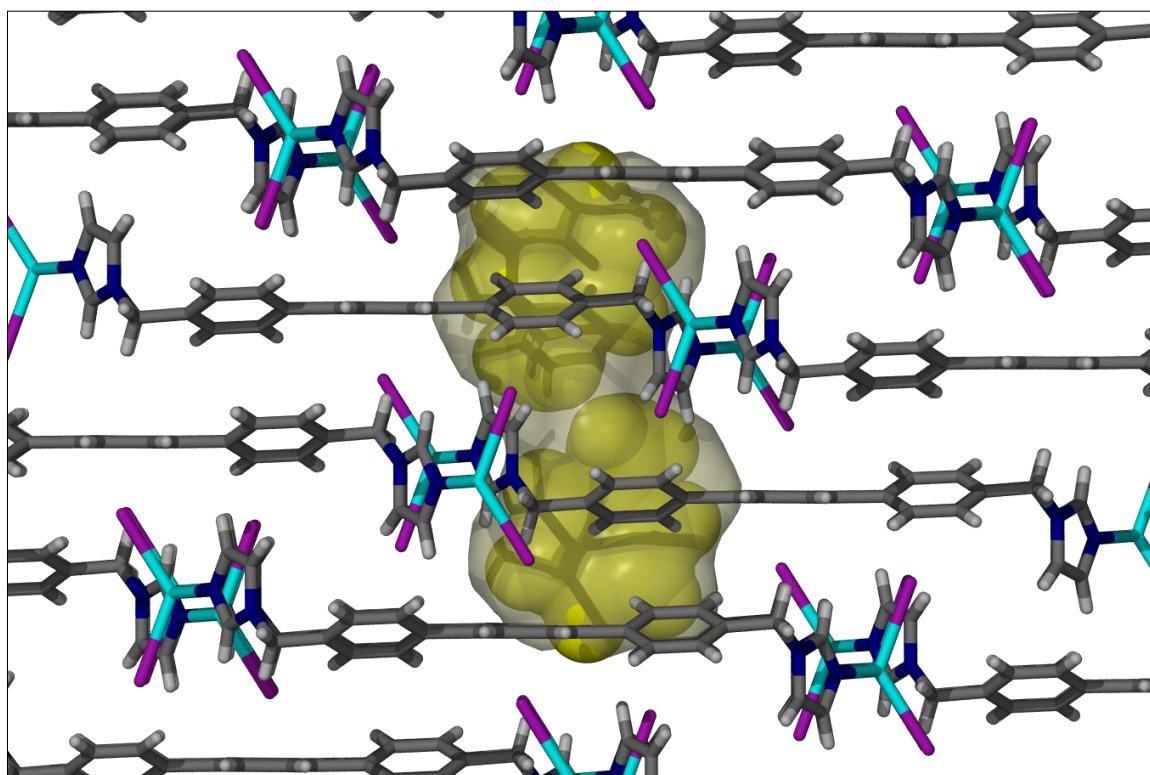


Figure 6.60 Solvent-accessible void in **MC29** is shown as a semi-transparent yellow surface. The surface has been mapped with a 1.4 Å probe, and toluene guest molecules (coloured yellow) are shown in van der Waals representation.

6.3 DISCUSSION AND CONCLUDING REMARKS

The packing arrangement of the terphenyl-derived metalloccycles is quite similar to that of the dihydrophenanthrene-derived metalloccycles (benzene and toluene). The spacing between the layers is different but this can be ascribed to the fact that for the dihydrophenanthrene-derived metalloccycles the guest molecules reside between the layers owing to the pinching of the metalloccycles. It therefore appears that the dihydrophenanthrene-based metalloccycles are not templated by the guest molecules since they would then be expected to include the guests in the resulting cavities. The metalloccycles in all these structures (**MC22**, **MC23** and **MC27-29**) assume chair-shaped conformations and associate in layers maintained by weak interactions between the imidazole moieties. These layers pack on top of one another in an offset manner in most instances

It is quite remarkable that the DCM-included (**MC27**), partially desolvated (**MC27_{CCl4}**) as well as the evacuated (**MC27_{vac}**) structures of **MC27** were obtained since the partially desolvated structure may be viewed as an intermediate between the solvated and evacuated structures. Because desolvation of **MC27** occurs readily under ambient conditions, the

structure of a transition phase is not trivial to obtain by SCD analysis. It appears that the immersion of the **MC27**_{DCM} crystals into CCl₄ slows the desolvation process sufficiently for the crystals to be analysed. While this finding is serendipitous, it is nonetheless remarkable and it is clear that the crystals convert from one form to the other in a single-crystal to single-crystal transformation. This result gives an indication of how the structure of the metalloacycle adapts upon guest removal to eventually yield the guest-free phase.

The layer arrangements in the majority of the metalloacycles discussed are governed by weak $\pi\cdots\pi$ interactions between anti-parallel arranged imidazole moieties of adjacent metalloacycles. Interestingly, these crystals were found to be relatively unstable under ambient conditions. Other structures, **MC28** and **MC29**, which make use of C–H $\cdots\pi$ interactions to maintain layers of metalloacycles, appear to be slightly more stable than those held together by $\pi\cdots\pi$ interactions. Depending on the size and overall shape of the metalloacycles, the layers pack either directly on top of one another or, in most instances, are arranged in a slightly offset manner. The type of guest molecules (template molecules) included in the structure also influences the overall organisation of the structure in the solid state, with the larger molecular volume of benzene and toluene being able to disturb the arrangement of the metalloacycles slightly. The inclusion of benzene and/or toluene (**MC28** and **MC29**) also rendered the respective crystals thermally more stable than those of the DCM-included structures (**MC27**). However, the extent of this stability could not be quantified by TG analysis owing to the small quantity of sample obtained. It is not certain if the increased thermal stability of the crystals is due to the included guests or if it is the host-host and/or host-guest interactions induced by these included guests that are responsible for the increase in thermal stability.

Small modifications to the organic linker can result in large differences in the resulting metalloacycle structures. Although we were unable to prepare structures that are able to withstand the removal of the guest molecules in a single-crystal to single-crystal transformation, we were able to establish a crystallisation technique that reliably produced crystals containing discrete metalloacycles. That we were able to prepare a number of these structures from a variety of organic solvents demonstrates the propensity for metalloacycle structures to form with ligands containing imidazole functionalities. By varying a few of the experimental conditions, as well as the design of the organic linker, it may be plausible to eventually engineer metalloacycles that are more robust.

The terphenyl-derived ligand was synthesised with the intention of producing metalloCycles with large solvent-accessible voids, and this goal was achieved. However, this did not occur in a predictable manner. Comparing the terphenyl-based structures to those of the two dihydrophenanthrene-derived metalloCycles (imidazole-functionalised, **MC22** and **MC23**), the metalloCycles are analogous in conformation – i.e. the chair conformation. The packing arrangement of the metalloCycles is also remarkably similar; it is thought that the flexibility of the dihydromethylene bridge is primarily responsible for the difference in the overall packing and guest arrangement between the layers. This flexible bridge obstructs the aperture of the metalloCycles, **MC22** and **MC23**, such that guest molecules cannot be occluded within the metalloCycles. The elongated terphenyl-based ligand appearing in **MC27-29** cannot block this space in the same manner, thus allowing passage of the guest molecules.

Comparison of the benzene- and toluene-included structures obtained for the imidazole (**MC22-23**) and 2-methylimidazole (**MC25-26**) dihydrophenanthrene ligands reveals remarkable differences. Firstly, the incorporation of the substituted methyl group results in a collapse of the metalloCycles. The aromatic spacers in **MC25** and **MC26** are offset but aligned in a parallel manner relative to each other, whereas in the imidazole-functionalised structures, **MC22** and **MC23**, the aromatic spacers are approximately co-planar relative to each other so that the metalloCycles assume a chair conformation. In all four instances the solvent guest molecules are not confined within the metalloCycles, but rather occupy the surrounding spaces.

From these observations, it is clear that there are some preferences in the formation of metalloCycles. In the instances of the collapsed metalloCycles it seems that templation around a guest molecule does not occur. Whether or not it is possible to acquire a more suitable template for “open” metalloCycles (uncollapsed) remains to be seen. Of course, the structures reported here are those that were successfully obtained using a limited number of techniques and conditions, and it is plausible that other metalloCycle structures can be obtained by other methods or by using other metal salts.

From the twelve metalloCyclic structures obtained in this investigation it is clear that formation of these complexes is indeed possible and that there is a propensity for these structures to form reliably. Though, it is thought that most of these structures are formed by the template effect, it appears that the formation of some of the metalloCycles is not exceptionally sensitive to the nature of the template (solvent guest), but rather the size and shape of the guest (at least in the instances reported here). It has been clearly demonstrated

that these imidazole-based aromatic ligands are reliable options in the preparation of metalloacycles, even though their conformations are flexible and therefore somewhat unpredictable. In future studies it would be appropriate to investigate analogous ligands that incorporate different substituents on either the imidazole moieties or the aromatic spacers.

6.4 EXPERIMENTAL

CRYSTALLISATIONS

All crystallisations were carried out using the same layering technique where a solution of the metal salt is slowly layered on top of a solution of the organic ligand, and the two layers are allowed to slowly diffuse into each other, resulting in the formation of single crystals at the interface of the two layers.

MC21_{Benz}

CoBr₂ (0.024 mmol) was dissolved in methanol and slowly layered onto a solution of **L3** (0.024 mmol) in benzene, which afforded blue plate-shaped crystals.

MC22 and MC23

Single crystals were obtained by the slow diffusion of a MeCN solution of CdI₂ (0.025 mmol) into a solution (benzene or toluene) of **L3** (0.025 mmol).

MC24, 25, 26

A MeCN solution of CdI₂ (0.025 mmol) was slowly layered onto a solution of **L4** (0.025 mmol) in DCM, benzene or toluene to afford colourless needle-shaped crystals.

MC24_{vac}

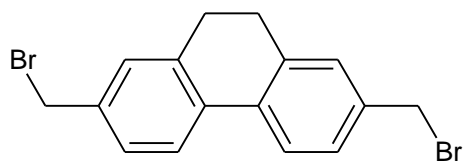
Single crystals of **MC24_{vac}** were obtained by placing a few crystals of **MC24** in a vacuum oven at room temperature for 5 hours.

MC27

Single crystals suitable for X-ray diffraction were obtained by the slow diffusion of CdI₂ (0.022 mmol in acetonitrile) into a solution (DCM, benzene, toluene) of **L5**. Crystals of **MC27_{CCl4}** were obtained by selecting single crystals of **MC27** and immersing them in a small quantity of CCl₄ for 4 weeks. The evacuated structure **MC27_{vac}** was prepared by removing a few crystals of **MC27** from the mother liquor (DCM/MeCN) and placing them in a vacuum oven at 30 °C for 5 hrs and collecting the SCD data immediately thereafter.

LIGAND SYNTHESSES

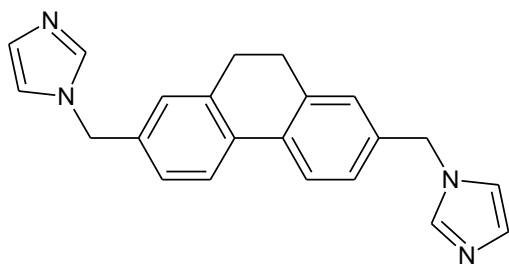
PRECURSOR (P3) 2,7-bis(bromomethyl)-9,10-dihydrophenanthrene



The procedure for the synthesis of precursor (**P3**) was followed as described in the literature.² 9,10-Dihydrophenanthrene (29 mmol, 5.3 g), paraformaldehyde (128 mmol, 3.9 g), hydrogen bromide (48%), phosphoric acid (85%) and hydrogen bromide (33% in HOAc) were placed in a round-bottom flask and heated to 80 °C under an inert atmosphere. The mixture was stirred for approximately 24 hours, after which the temperature was increased to 120 °C for a further 12 hours (monitoring the reaction with TLC). Once the solution had cooled, the solid was filtered, washed with acetone and recrystallised from benzene to yield fine white needle-shaped crystals.

Yield: 40-45%, ¹H NMR (400 MHz, CDCl₃) δ ppm 2.88 (s, 4 H) 4.53 (s, 4 H) 7.28 (d, *J*=1.75 Hz, 2 H) 7.34 (dd, *J*=7.99, 1.95 Hz, 1 H) 7.71 (d, *J*=7.99 Hz, 2 H); ¹³C NMR (400 MHz, CDCl₃) δ ppm 28.74, 33.56, 124.22, 127.74, 128.86, 134.17, 137.03, 137.91

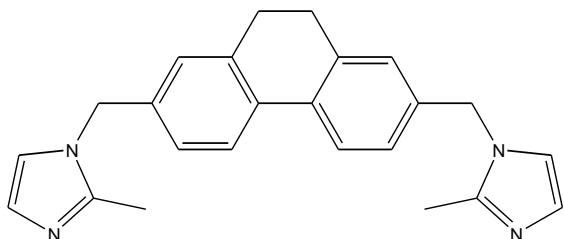
LIGAND (L3) 1,1'-(9,10-dihydrophenanthrene-2,7-diyl)dimethanediylbis(1*H*-imidazole)



The synthesis of **L3** was adapted from literature procedures.³⁻⁶ An aqueous solution of sodium hydroxide (25%, 40 ml) was added to imidazole (14 mmol, 0.98 g) dissolved in acetonitrile (20 ml). The suspension was stirred at 25 °C for 2 hours after which time an acetonitrile solution (100 ml) of 2,7-bis(bromomethyl)-9,10-dihydrophenanthrene (6.8 mmol, 2.5 g) was added. This solution was stirred for 4 days at 30 °C (monitored by TLC). A sticky yellow solid formed in the clear solution. Excess solvent was removed under reduced pressure, affording a light yellow solid. This solid was dissolved in chloroform and washed with water until the washings were pH-neutral. The organic layer was then extracted and the solvent removed under reduced pressure, yielding an orange coloured oil. The oil was taken up in a minimum of chloroform and added dropwise to *n*-hexane, affording a white precipitate.

Yield: 52%; ^1H NMR (300 MHz, $\text{DMSO}-d_6$) δ ppm 2.75 (s, 4 H), 5.18 (s, 4 H), 6.91 (t, $J=1.17$ Hz, 2 H), 7.15 (s, 2 H), 7.18 (d, $J=1.76$ Hz, 2 H), 7.21 (t, $J=1.17$ Hz, 2 H), 7.77 (dd, $J=5.06, 2.71$ Hz, 2 H), 7.77 (s, $J=1.17, 1.17$ Hz, 2 H); ^{13}C NMR (300 MHz, $\text{DMSO}-d_6$) δ ppm 28.21, 49.26, 119.65, 124.04, 126.24, 127.29, 128.71, 132.96, 137.07, 137.25, 137.45.

LIGAND (L4) 1,1'-(9,10-dihydrophenanthrene-2,7-diyl)dimethanediylbis(2-methyl-1H-imidazole)

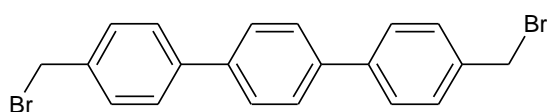


Ligand **L4** was synthesised by following a procedure set out by Rajakumar *et al.*³⁻⁵ In this method, an aqueous solution of NaOH (7 ml, 25%) was added to acetonitrile (20 ml) along with 2-methylimidazole and stirred for approximately 30 min at room temperature, forming an emulsion. The precursor (**P3**) was then added to the mixture to form a suspension that was left to stir vigorously overnight. The solution went from a white suspension to a yellow solution after approx 12 hrs. After a further 6 hrs a bright yellow solid had formed in a colourless solution. This mixture was allowed to stir for a further 24 hrs, after which the solvent was removed *in vacuo*, leaving a green and white solid. The solid was taken up in CHCl_3 (5×50 ml) and washed with brine (2×50 ml). The CHCl_3 layer was extracted and dried overnight on anhydrous MgSO_4 . The solution was then filtered and reduced on a rotary evaporator to leave an orange oil. The orange oil was taken up into a minimum of CHCl_3 and added dropwise to *n*-hexane, immediately forming an off-white precipitate that was collected by filtration.

Yield = 1.022 g, 68%; ^1H NMR (300 MHz, $\text{DMSO}-d_6$) δ ppm 2.25 (s, 6 H) 2.75 (s, 4 H) 5.12 (s, 4 H) 6.77 (d, $J=1.32$ Hz, 2 H) 7.04 (dd, $J=2.05, 1.76$ Hz, 4 H) 7.13 (d, $J=1.17$ Hz, 2 H) 7.77 (d, $J=8.66, 2.79$ Hz, 2 H); ^{13}C NMR (300 MHz, $\text{DMSO}-d_6$) δ ppm 12.79, 28.21, 48.38, 120.30, 123.98, 125.66, 126.45, 126.73, 132.76, 136.76, 137.23, 143.89.

PRECURSOR (P5) 4,4''-bis(bromomethyl)-1,1':4',1''-terphenyl

L5 was prepared in a two step process following literature procedures.^{2,7}

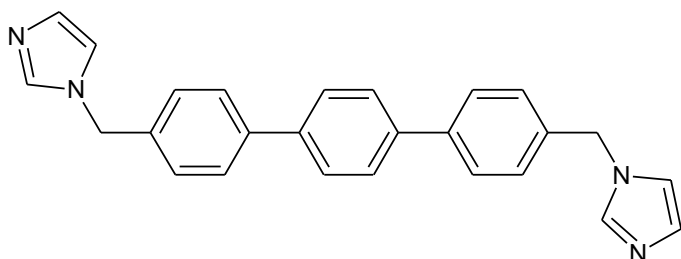


p-Terphenyl (20 mmol, 5.00 g) and paraformaldehyde (90 mmol, 2.9 g) were placed in a round-bottom flask, to which hydrogen bromide (33% in HOAc) and phosphoric acid (75 mmol, 4.35 ml) were added. The mixture was

heated to 80 °C under nitrogen for between 16 to 48 hrs (monitored by TLC), after which the temperature was increased to 125 °C for a further 5 hours. The mixture was cooled to room temperature before the off-white solid was filtered and washed with copious amounts of acetone. The desired product was extracted from the solid material with hot benzene, and the solvent removed under reduced pressure. The solid was then recrystallised from boiling chloroform to yield a white crystalline product.

Yield: 14-18%, ^1H NMR (300 MHz, CDCl_3) δ ppm 4.57 (s, 4 H), 7.49 (dt, $J=8.36$, 1.91 Hz, 4 H), 7.63 (dt, $J=8.36$, 1.91 Hz, 4 H), 7.67 (s, 4 H) ^{13}C NMR (300 MHz, CDCl_3) δ ppm 33.31, 127.42, 127.51, 129.58, 136.94, 139.62, 140.72.

LIGAND (L5) 1,1'-(terphenyl-2,7-diyl)dimethanediylbis(1*H*-imidazole)



An aqueous solution of sodium hydroxide (25%, 30 ml) was added to imidazole (7.7 mmol, 0.52 g) dissolved in acetonitrile (50 ml) and stirred at room temperature. After 2 hours, 4,4''-bis(bromomethyl)-*p*-

terphenyl was added to the suspension and allowed to stir for approximately 5 days at 30 °C, constantly monitoring the reaction progress by TLC. Solvent was removed and the resultant precipitate washed with water until a neutral pH was obtained. The precipitate was then dissolved in chloroform and washed again with water. The organic layer was extracted and the solvent removed to afford an off-white powder.

Yield: 54%; ^1H NMR (300 MHz, $\text{DMSO}-d_6$) δ ppm 5.24 (s, 4 H), 6.93 (t, $J=1.03$ Hz, 2 H), 7.22 (t, $J=1.17$ Hz, 2 H), 7.35 (d, $J=8.36$ Hz, 4 H), 7.70 (d, $J=8.36$ Hz, 4 H), 7.73 (s, 4 H), 7.80 (d, $J=1.03$ Hz, 2 H); ^{13}C NMR (300 MHz, $\text{DMSO}-d_6$) δ ppm 49.19, 119.66, 126.89, 127.21, 128.16, 128.77, 137.17, 137.49, 138.75, 139.00.

Table 6.1 Selected crystallographic data for metalloacycles formed with the 9,10-dihydrophenanthrene linker (**MC21-26**)

	MC21	MC22	MC23	MC24	MC24_{vac}	MC25	MC26
Molecular, Empirical formula	C ₁₄ H ₁₃ N ₂ Co _{0.5} Br	C ₂₇ H ₂₆ N ₅ CdI ₂	C ₂₇ H _{26.25} CdI ₂ N _{4.75}	C ₂₄ H ₂₄ N ₄ CdI ₂ · CH ₂ Cl ₂	C ₂₄ H ₂₆ CdI ₂ N ₄	C ₂₉ H ₃₀ CdI ₂ N ₅	C _{29.5} H ₃₁ CdI ₂ N ₅
M_r/ g.mol⁻¹	315.61	786.73	780.67	836.12	734.67	814.78	821.79
Crystal System	Monoclinic	Monoclinic	Monoclinic	Monoclinic	Monoclinic	Monoclinic	Monoclinic
Space Group	<i>C2/m</i>	<i>C2/m</i>	<i>Cc</i>	<i>C2/c</i>	<i>C2/c</i>	<i>P2₁/c</i>	<i>P2₁/c</i>
a/Å	13.515(9)	21.517(8)	15.848(3)	26.663(9)	25.261(2)	22.535(5)	22.615(2)
b/Å	29.712(2)	16.439(6)	30.277(7)	13.662(5)	13.932(1)	13.656(3)	13.6894(9)
c/Å	8.090(5)	16.350(6)	26.258(6)	19.184(6)	18.868(2)	20.058(5)	20.106(1)
α/°	90	90	90	90	90	90	90
β/°	118.261(7)	99.521(5)	104.034(3)	123.278(4)	129.696(1)	102.074(4)	102.274(1)
γ/°	90	90	90	90	90	90	90
Z	8	8	16	8	8	8	8
V/Å³	2861(3)	5704(4)	12223(4)	5842(3)	5109.3(8)	6036(2)	6082.3(7)
T/K	100	100	100	100	100	100	100
D_{calc}/g cm⁻³	1.465	1.832	1.697	1.901	1.910	1.793	1.795
N-total	6506	16892	38538	11485	14868	36032	35993
N-independent	2132	6354	17717	3613	5523	13280	13260
N-observed	1403	3542	14558	2832	4060	9417	11060
R₁ [I>2σ(I)]	0.0570	0.0725	0.0434	0.0498	0.0440	0.0465	0.0405
wR₂	0.1516	0.1687	0.1163	0.1180	0.0973	0.1028	0.0995
GOF	1.018	0.978	1.038	1.035	1.041	1.042	1.034

Table 6.2 Selected crystallographic data for the metallocycles constructed with the *p*-terphenyl linker (MC27-29)

	MC27	MC27 _{CCl4}	MC27 _{vac}	MC28	MC29
Molecular, Empirical formula	C _{26.75} H ₂₂ N ₄ CdCl _{0.75} I ₂	C ₂₇ H ₂₆ N ₅ CdI ₂	C ₂₆ H ₂₂ CdI ₂ N ₄	C ₃₂ H ₂₈ N ₄ CdI ₂	C ₃₃ H ₃₀ CdI ₂ N ₄
M_r/ g.mol⁻¹	857.34	808.98	756.68	834.78	848.81
Crystal System	Monoclinic	Triclinic	Triclinic	Monoclinic	Monoclinic
Space Group	<i>C2/m</i>	<i>P</i> $\bar{1}$	<i>P</i> $\bar{1}$	<i>C2/m</i>	<i>C2/m</i>
a/Å	17.18(1)	11.497(9)	10.096(3)	16.497(4)	16.917(4)
b/Å	16.00(1)	11.698(5)	12.087(3)	18.400(5)	18.054(5)
c/Å	13.166(9)	13.113(5)	12.116(3)	12.641(6)	12.778(3)
α/°	90	115.454(5)	109.881(4)	90	90
β/°	125.533(7)	110.763(7)	107.661(4)	128.827(3)	127.321(8)
γ/°	90	93.355(7)	95.868(5)	90	90
Z	4	2	2	4	4
V/Å³	2945(4)	1442(1)	1289.7(6)	2989(2)	3104(1)
T /K	100	100	100	100	100
D_{calc} /g cm⁻³	1.934	1.864	1.949	1.855	1.816
N-total	8559	6124	10443	6434	9354
N-independent	1418	1740	5248	2744	3491
N-observed	1226	1401	2452	2145	2820
R₁ [I>2σ(I)]	0.0639	0.0485	0.1429	0.0474	0.0469
wR₂	0.1551	0.1235	0.3236	0.1134	0.1247
GOF	1.136	1.041	1.043	1.059	1.028

6.5 REFERENCES:

1. S. J. Lee and W. Lin, *Acc. Chem. Res.*, 2008, **41**, 521-537.
2. A. Helms, D. Heiler and G. McLendon, *J. Am. Chem. Soc.*, 1992, **114**, 6227-6238.
3. P. Rajakumar and S. Raja, *Tetrahedron Lett.*, 2009, **50**, 223-227.
4. P. Rajakumar, S. Selvam and M. Dhanasekaran, *Tetrahedron Lett.*, 2005, **46**, 6127-6130.
5. P. Rajakumar and M. Dhanasekaran, *Tetrahedron*, 2002, **58**, 1355-1359.
6. P. Rajakumar, A. Senthilmurugan and K. Srinivasan, *J. Chem. Res.*, 2006, **6**, 359-361.
7. S. Ghosh, R. Chakrabarty and P. S. Mukherjee, *Dalton Trans.*, 2008, 1850-1856.

CHAPTER 7

SUMMARY AND CONCLUDING REMARKS

One must appreciate the almost endless number of possible combinations when it comes to the construction of supramolecular materials. To be able to design materials with desired properties and functions is both an accomplishment and an enigma. For this to become an everyday reality it is of utmost importance that the underlying principles that govern the association and packing of molecules in the solid state are well understood. The difficulty in achieving this outcome lies in the fact that the interactions between molecules, particularly in the solid-state, are often the result of some compromise to achieve the most favourable arrangement. The arrangement that is observed, however, is not necessarily the most stable form and there may in fact be many possible forms for the same components. Taking these facts into consideration it is not surprising that the endeavour to manipulate molecules into a desired 3D arrangement is still far from being realized.

During the course of this study a new method for identifying and classifying packing motifs was developed and is discussed in *Chapter 3*. It was shown that this method is effective in the classification of a number of known polyaromatic hydrocarbons and can be extended to the analysis of simple heteroaromatic molecules as well. Analysis of a few cocrystal compounds indicates that, with some fine-tuning, it may be possible to utilise this method in the motif analysis of a number of simple compounds of this type. It is postulated that this method is relatively robust in the analysis of simple aromatic compounds and future work would incorporate the investigation of a number of other simple aromatic compounds as well as cocrystal compounds that will be synthesised in an attempt to extend the array that already exists.

Chapter 4 introduced a series of 17 homeotypic metallocyclic inclusion compounds. These metallocycles were all prepared from the same ligand (**L1**) and transition-metal salts containing bromide counter ions. The structural analysis of these compounds revealed that the coordinative bond is the most robust interaction present in the formation of the metallocycles. Only weaker $\pi \cdots \pi$ interactions appear to stabilise the packing of these metallocycles in the formation of layers. The most remarkable feature that spans the entire series of homeotypic structures is the inclusion of acetonitrile molecules in the interstitial spaces between the metallocycle layers. These molecules are integral in the formation of the crystals and removal of these guests is presumed to cause a structural collapse. The removal of these and other guests included in the cavities of the metallocycles occurs readily under ambient conditions. The only sample in the series that did not conform to these observations was that of the dioxane-included structure. It is thought that the weak C–H \cdots O host-guest interactions that are present in this structure are enough to stabilise this compound to a greater extent compared to the other structures in the series. From these observations it also appears that the guests in the

cavities and the interstitial acetonitrile guests interact such that, as one guest is released from the structure, the other is no longer obstructed and is also easily removed, thus causing the structure to collapse.

It was shown that the metallocyclic structure could be grown from a variety of solvent systems as long as acetonitrile is present in the solvent mixture. It was also observed that the metallocycles have a size-inclusion limit for the guests contained within their cavities. Toluene, ethyl acetate and *p*-xylene all appear to be too large; however the more interesting aspect of these structures is the inclusion of an acetonitrile molecule in the cavity. This demonstrates the reliability of the components to form metallocycle structures rather than other possible architectures. It also suggests that the cavities are selective towards the solvent molecules that are slightly larger than acetonitrile and only include acetonitrile as a last resort.

The metallocycles have similar thermal profiles as well as highly similar PXRD patterns; discrepancies in these patterns can be attributed to the conformational changes that the metallocycles undergo in response to the guest molecules included in the cavities.

Future work on this series should include obtaining the crystal structures of the nickel and zinc metallocycles that have already been obtained in the cobalt series. Experiments should be carried out with different solvent systems to possibly obtain structures that can withstand desolvation as a single-crystal to single-crystal process. With the very recent acquisition of hotstage-DSC and pressure-DSC instruments, these compounds should be analysed with these techniques. The hotstage-DSC should confirm the presumed packing rearrangement that the structures undergo during guest removal, whereas the pressure-DSC analysis may provide information regarding the possible porosity of these compounds in their guest-free state. Competition experiments can also be carried out in an attempt to elucidate any selectivity that the metallocycles may have for one guest over another.

A second series of isoskeletal structures was prepared from the same ligand and copper bromide. These metallocycles pack in a more efficient manner so that there are no interstitial spaces in the packing arrangement. Guest molecules are confined within the cavities of the metallocycles and can be removed without collapsing the structure. Guest removal occurs as a single-crystal to single-crystal transformation. Regrettably, all attempts to resolvate these crystals failed. These samples should also be analysed by DSC (hotstage and pressure).

The unprecedented concomitant formation of an infinite catenane and its topological isomer – unlinked metallocycles – is reported in *Chapter 5*. The formation of the catenane is governed by the infinite $\pi\cdots\pi$ stack involving the phenanthrenyl moieties of the metallocycles. These moieties arrange in an offset twist to maximize stabilization between the similar components. This aromatic $\pi\cdots\pi$ stack is speculated to be the major contributing factor to the

luminescence exhibited by these crystals on exposure to UV light. Crystals of the topological isomer of the catenane were obtained concomitantly. The packing arrangement of these metallocycles is considerably different to that of the catenane, being maintained primarily through C–H... π interactions. It is assumed that the catenane crystals are the thermodynamic product of the reaction while the unlinked metallocycles are the kinetic products. The possibility of seeding a solution to obtain the desired crystals should also be investigated.

Future work on this system would include solid-state fluorescence spectroscopy to quantify the observed luminescence and potentially determine the source of the luminescence i.e. ligand-localised, ligand-to-metal charge transfer (LMCT) or metal-to-ligand charge transfer (MLCT) etc. Also solvent exchange experiments should be attempted to ascertain if the luminescence or other properties of the catenane can be tuned. Further crystallizations of **L2** with other transition-metal salts should be conducted to ascertain if catenanes can be constructed containing other metal centres and whether these catenanes have different properties to that already obtained. This may lead to a series of catenane structures with tunable properties that could lead to various applications.

Chapter 6 reports a number of metallocyclic structures obtained by crystallisation of three related imidazole-functionalised ligands with a variety of transition-metal halide salts. Although crystallisations were set up with a variety of transition-metal halide salts, only cadmium iodide and cobalt bromide salts were incorporated in the crystal structures for this series of ligands. The ligands employed in this study were varied in the composition of the aromatic spacer moieties so that comparisons and conclusions could be made. However, because only a limited number of metallocyclic compounds were obtained during this study, it is difficult to make any broad assumptions. The assumption that the ligand must coordinate in a fixed C-shaped conformation in order to facilitate metallocycle formation is not necessarily true, as shown in the examples of the collapsed metallocycles. In these instances, it is thought that the 2-methyl substituents of the imidazole groups are responsible for the collapse of the metallocycles. These metallocycles are remarkably different from their imidazole-based analogues in which the ligand moieties of the metallocycles are arranged co-planar rather than in a parallel fashion.

It is interesting to note that the metallocycles prepared with **L3** and **L5** and cadmium iodide are remarkably similar. The metallocycles in these structures assume a chair conformation and their packing arrangements are remarkably similar. The additional bridging carbon atoms of **L3** are assumed to prevent the inclusion of guest molecules within the confines of the metallocycles as they are in the metallocycles of **L5**. One of the most remarkable outcomes of this study was the single-crystal to single-crystal transformation of

the terphenyl-based metallocycle from the DCM structure (**MC27**) to the intermediate structure (**MC27_{CCl4}**) and finally the guest-free metallocycle (**MC27_{vac}**).

Because of the exploratory nature of a project like this there is still much work that can be done with these systems, both with the existing metallocycles that have been obtained as well as with the organic ligands that have been synthesized during the course of this study. Firstly crystallisations should be attempted with other transition-metal salts with larger counter ions, particularly those of silver. The ligand series could also be extended with the use of a meta-terphenyl spacer (as well as a number of other possible spacers) to assess if the ligands can be preorganised in a suitable conformation for metallocycle synthesis. Of course modifications to the imidazole moieties can also be assessed, such as the benzimidazole and 2-methylimidazole moieties as well as other substituents. Other metal-to-ligand ratios should also be tested.

As much as we aspire to be able to predict and engineer crystal structures to fit with our requirements there are still many unanswered questions regarding the conditions (and interactions) responsible for the final outcome. Therefore, this study is meaningful in the bigger scheme of things to be able to understand how molecules arrange by self-assembly to form discrete architectures.

“In many areas of chemistry, an X-ray single-crystal structure determination of a novel compound represents the solution to a particular problem, or the end of a specific project: the cynosure is usually the identity of the molecule itself, or some particular feature within its molecular structure. An alternative view, however, would be to treat the structural information as the beginning of a new venture, leading to questions of far reaching and fundamental importance regarding the interrelationships between molecules and ions in the solid state. Since the crystal structure represents a situation where all the bonding and non-bonding forces are poised at an energetic minimum (not necessarily a global minimum!), it contains all the information regarding the importance of, and balance between, intermolecular forces. If this information could be extracted and deconvoluted, then prospects of designing materials with specific properties would be vastly enhanced. Consequently, it is of great importance to improve our understanding of the forces that determine the structures of crystalline materials, and single-crystal data provide a natural starting point.” Aakeröy and Seddon¹

REFERENCES

1. C. B. Aakeröy and K. R. Seddon, *Chem. Soc. Rev.*, 1993, **22**, 397-407.